NASA CR-159134

NASA Contractor Report 159134

Exploratory Studies of the Cruise Performance of Upper Surface Blown Configurations

Experimental Program - High - Speed Force Tests

J. A. Braden, J. P. Hancock,
K. P. Burdges, and J. E. Hackett

LOCKHEED-GEORGIA COMPANY
Marietta, Georgia 30063

NASA Contract NAS1-13871
OCTOBER 1979

National Aeronautics and
Space Administration

Langley Research Center
Hampton, Virginia 23665
AC 804 827-3966

FOREWORD

This document is submitted in accordance with the requirements of NASA Contract NAS1-13871, Exploratory Studies of the Cruise Performance of Upper Surface Blown Configurations. W. C. Sleeman, Jr. is the NASA-Langley Contract Monitor and J. A. Braden is the Lockheed-Georgia Project Manager.

The technical results under this contract are presented in five reports. For convenience, the overall program documentation is summarized below:

DOCUMENTATION SUMMARY

CR Number	Title
CR-3193	Summary Report
CR-3192	Experimental Program - Test Facilities, Model Design, Instrumentation, and Low-Speed, High-Lift Tests
CR-159134	Experimental Program - High-Speed Force Tests
CR-159135	Experimental Program - High-Speed Pressure Tests
CR-159136	Program Analysis and Conclusions

N80-15070 #

TABLE OF CONTENTS

TABLE OF CONTENTS (CONT'D)

LIST OF FIGURES

LIST OF FIGURES (CONT'D)

LIST OF FIGURES (CONT'D)

LIST OF FIGURES (CONT'D)

LIST OF FIGURES (CONT'D)

LIST OF FIGURES (CONT'D)

LIST OF FIGURES (CONT'D)

LIST OF FIGURES (CONT'D)

LIST OF FIGURES (CONT'D)

LIST OF FIGURES (CONT'D)

LIST OF FIGURES (CONT'D)

LIST OF FIGURES (CONT'D)

SUMMARY

The purpose and scope of the Cruise Performance Data Base Contract (NAS1-13871) are reviewed briefly in Section 1 of this document. Pertinent model and installation details are then described briefly. Objectives of the force test are discussed and the run schedule is outlined. Data are presented for testing performed in two separate facilities. These are the Lockheed-Georgia Compressible Flow Facility (CFF) and Lockheed California 4 x 4 Blowdown Tunnel. For this type of test, the primary difference between the two facilities is test section size. The CFF test section is 50.8 x 71.1 cm (20 x 28 in.) while the 4 x 4 test section is roughly a square 122 cm (48 in.) on a side. The effects of a wide range of nozzle geometric variations are covered by the data. Nozzle aspect ratio, boattail angle and chordwise position are among the more important parameters investigated. Both straight and swept wing aircraft configurations were simulated. Each of the study configurations was tested across a range of nozzle pressure ratios, lift coefficients and Mach numbers.

1.0 INTRODUCTION

In early 1975, the NASA awarded a contract (NAS1-13871) to the Lockheed-Georgia Company for the acquisition of a high-speed, experimental data base for aircraft configurations featuring nacelles mounted on the upper wing surface. This design concept, known as USB (upper-surface blowing), had received earlier, experimental endorsements as a viable means of achieving moderate-to-good powered lift performance along with beneficial noise reduction in the STOL environment. In the interest of further development of the USB-system, the contractual work performed by the Lockheed-Georgia Company emphasizes an exploratory investigation of the transonic cruise characteristics of USB nacelle-wing combinations. Included in the Program Plan is the commitment to perform three dimensional force tests of a selected range of nacelle/wing/fuselage combinations. This effort is an important part of the Task II, Cruise Performance Data Base, which is described in CR-3193. The force test results provide comparative values of total configuration performance parameters not readily obtained in any other way. They also provided a basis for correlation of the analytical and pressure data, as performed in CR-159136, Program Analysis and Conclusions.

2.0 SYMBOLS

Dimensional data are presented herein in both the International System of Units (SI) and the U. S. Customary Units. The measurements and calculations were made in the U. S. Customary Units.

A	area, cm^2 ($in.^2$)
A5	nozzle exit area, cm^2 (in^2)
AR	aspect ratio
BL	abbreviation for "boundary-layer"
b	model span, cm (in.)
c	local wing chord, cm (in.)
$\bar{c}$	mean aerodynamic chord, cm (in.)
CD	nozzle discharge coefficient
CDC	calculated nozzle discharge coefficient
C_{D_M}	measured drag coefficient, $D/q_\infty S_W$
CGS =	specific gross thrust coefficient $= (\frac{F_{g_M}}{W_{a_M}})/(\frac{F_{g_i}}{W_{a_i}})$
CGSC =	calculated specific thrust coefficient $= (\frac{F_{g_c}}{W_{a_c}})/(\frac{F_{g_i}}{W_{a_i}})$
C_{L_M}	measured lift coefficient, $L/q_\infty S_W$
C_{M_M}	measured pitching moment coefficient, $M_Y/q_\infty S_W$
C_μ	model gross thrust coefficient, $F_M/q_\infty S_W$
C_T	nozzle gross thrust coefficient, $F_{NZ}/q_\infty S_W$
CVE	effective nozzle velocity coefficient $= V_e/V_{G_i}$
CV5	nozzle throat velocity coefficient $= V_{S_M}/V_{S_i}$
D	drag, N(lb)
F_A	axial force, N(lb)
FGM	measured gross thrust, N (lb)

FGM/A5*PSO	isolated nozzle gross thrust parameter
F_M	nozzle gross thrust installed on wing, N(lb)
F_N	normal force, N(lb)
F_{NZ}	isolated nozzle gross thrust, N(lb)
H_j	jet nozzle total pressure, N/m^2 (lb/in.^{2})
H_j/p_∞,PT5M/PSO	measured jet nozzle exit pressure ratio
L	lift, N(lb)
M_Y	model pitching moment about quarter chard, m-N (in.-lb)
M_{Y_S},MYFS	model pitching moment about quarter chord measured statically, m-N (in.-lb)
M_∞	freestream (tunnel) Mach number
p_∞	freestream static pressure, N/m^2 (lb/in.^{2})
PSO	ambient static pressure, N/m^2 (lb/in.^{2})
PT4M/PSO	reference nozzle pressure ratio, based on nozzle internal rake
PT5I/PSO	ideal jet exit pressure ratio
q_∞	freestream dynamic pressure, N/m^2 (lb/in.^{2})
R_N	Reynolds number
R_{NC}	Reynolds number based on chord length
RPR	Ram pressure ratio
S_W	wing area, m^2(ft^2)
Wa	airflow, N/sec (lb/sec)
x	distance parallel to tunnel centerline, cm (in.)
z	vertical distance, cm (in.)
α	angle of attack, degrees
δ_j	jet deflection angle, degrees
η	percent semispan
η_t	jet turning efficiency, $\dfrac{\sqrt{F_N^2 + F_A^2}}{F_M}$

3.0 MODEL AND INSTRUMENTATION DETAILS

The basic objective of the model design effort was to develop a wing-nacelle arrangement which could accommodate a wide range of USB nozzle types for comparative evalution. An arrangement for metering smooth-profile, high-pressure air to the nozzle entrance was considered necessary. Means for obtaining force measurements with a high pressure air line bridging the balance were also required.

3.1 Model Design

To accomplish the desired objectives, the high-speed test configurations were developed around two wing-body combinations with untapered wings swept 0 and 25 degrees. These basic test vehicles could be combined in build-up fashion with a series of nacelle forebodies to form a wide range of powered or unpowered configurations. The choice of piped-in nozzle supply air over a powered simulator was made for simplicity and economy. A smooth flow profile at the nozzle entry was ensured by a choke plate with 0.159 cm (1/16 in.) diameter holes evenly distributed over the plate. The substitution of nacelles with other configuration designs, as well as conversion to the clean wing configurations, was made possible by the build-up design of the nacelle pylon, and nozzle mounting block.

Figure 1 shows an example of a 3-D swept wing force model installation in the CFF. Extensive filleting used to minimize the sharpness of the nacelle-wing junctures is evident in the photo. A 3-D straight wing force model installation in the Lockheed California 4 x 4 wind tunnel is pictured in Figure 2.

Subscripts

c	calculated
i	ideal
m	measured
STA 5	represents nozzle exit conditions
STA 6	represents fully-expanded flow

Figure 1. Dual D-duct installation on 3-D swept wing force model in CFF.

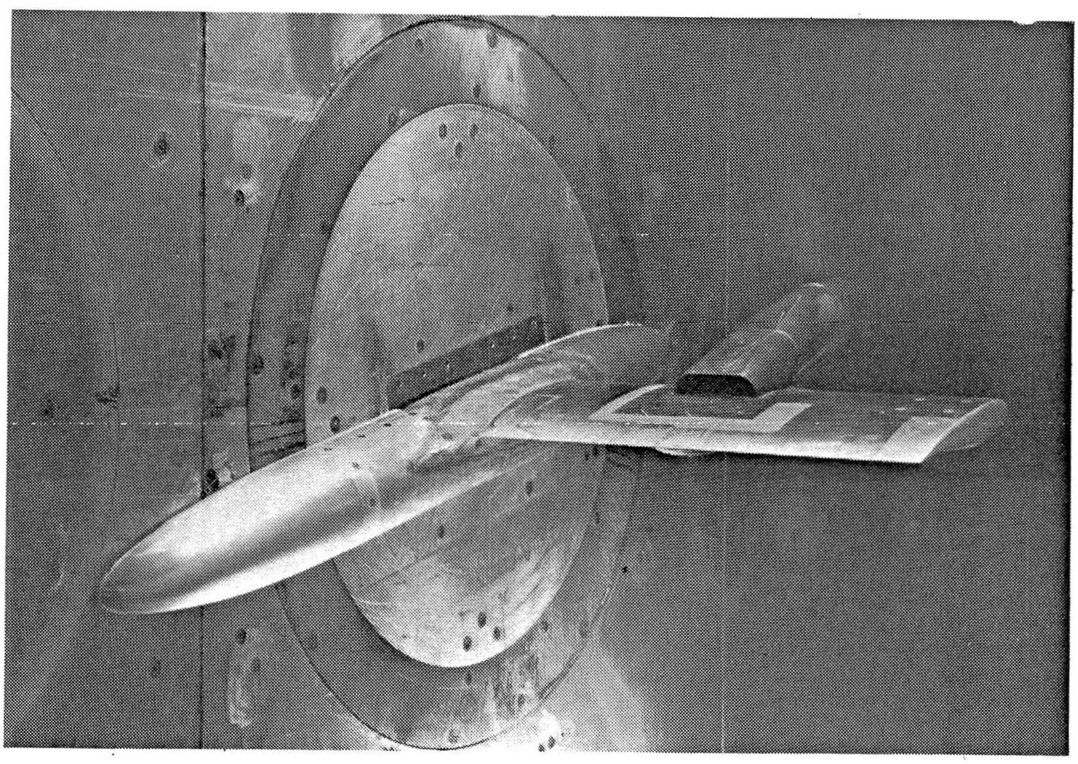

Figure 2. AR4 nozzle installation on 3-D straight wing force model in 4 x 4.

Except for the size of the test section, the setup was essentially the same here as for the CFF.

Basic planforms for the straight and swept wing models are shown in Figures 3 and 4. In both cases the planform area is 898 cm^2 (139.2 $in.^2$). Although locations of the surface static pressure rows are pictured, they were not hooked up during the force test phase of the program.

Details of the fuselage half-body installation are shown in Figure 5. The major portion of the fuselage, including forebody and afterbody, is identical for both straight and swept wings. A hollow center insert, however, as represented by the dashed line, is changed when a wing change is made. Spacing from the tunnel wall is set by a half-inch thick boundary layer plate represented by the section lines in A-A.

A table, shown in Figure 6, has been prepared to summarize the various model components and symbol designations. The symbol designations are used herein for defining configurations in run schedules and plot labels. Where practical, the designations selected are the first letters of the component names. For instance, F is for fuselage, W for wing, P for pylon, C for cowl (forebody), and N for nozzle. Subscripted numbers identify different variations of a given configuration type.

Key dimensions for all of the test nozzles are presented in the table of Figure 7. Four primary variables were used to establish the matrix of test nozzles. These were relative size, aspect ratio, discharge location, and

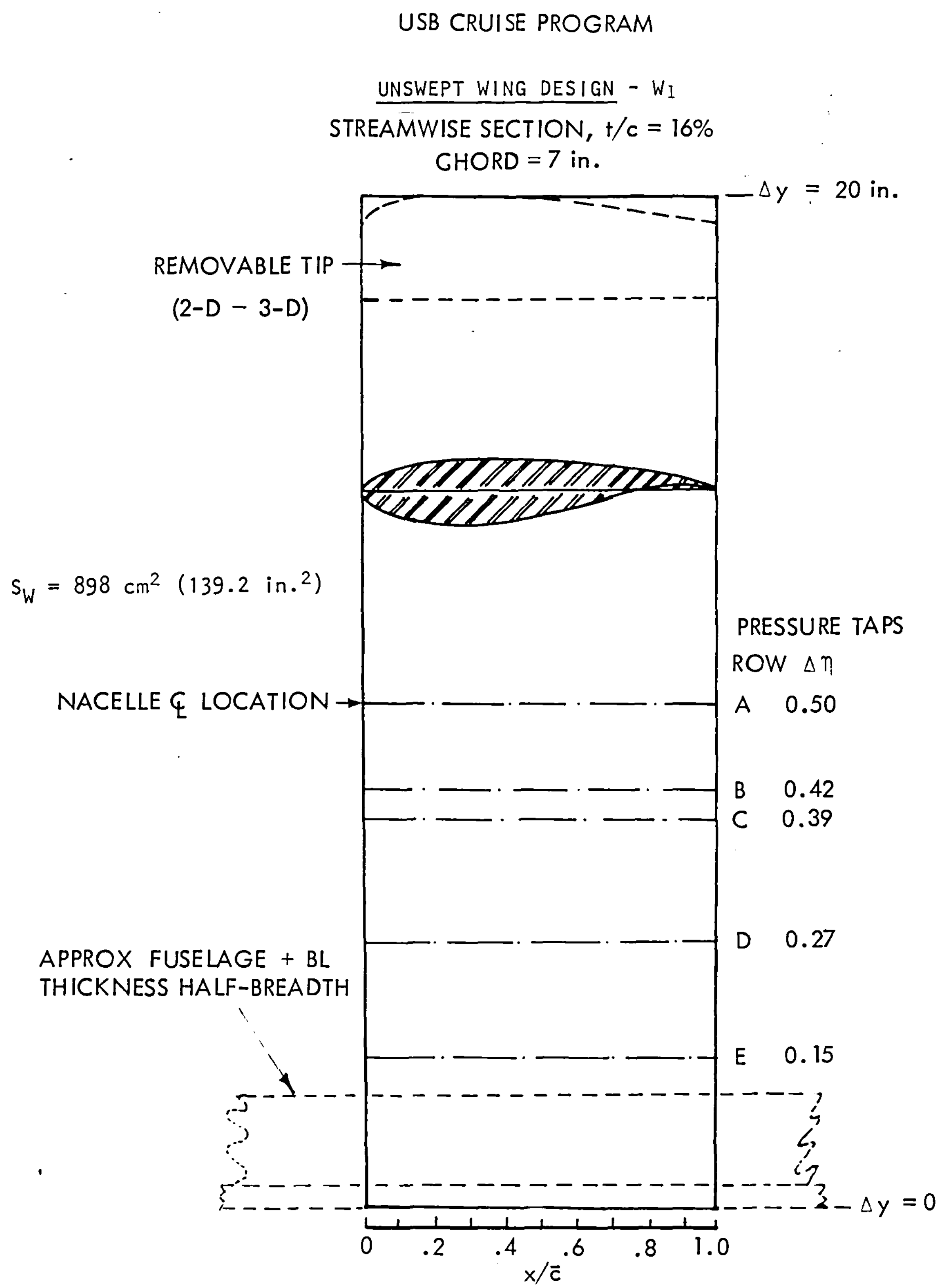

Figure 3. Straight wing planform and instrumentation layout

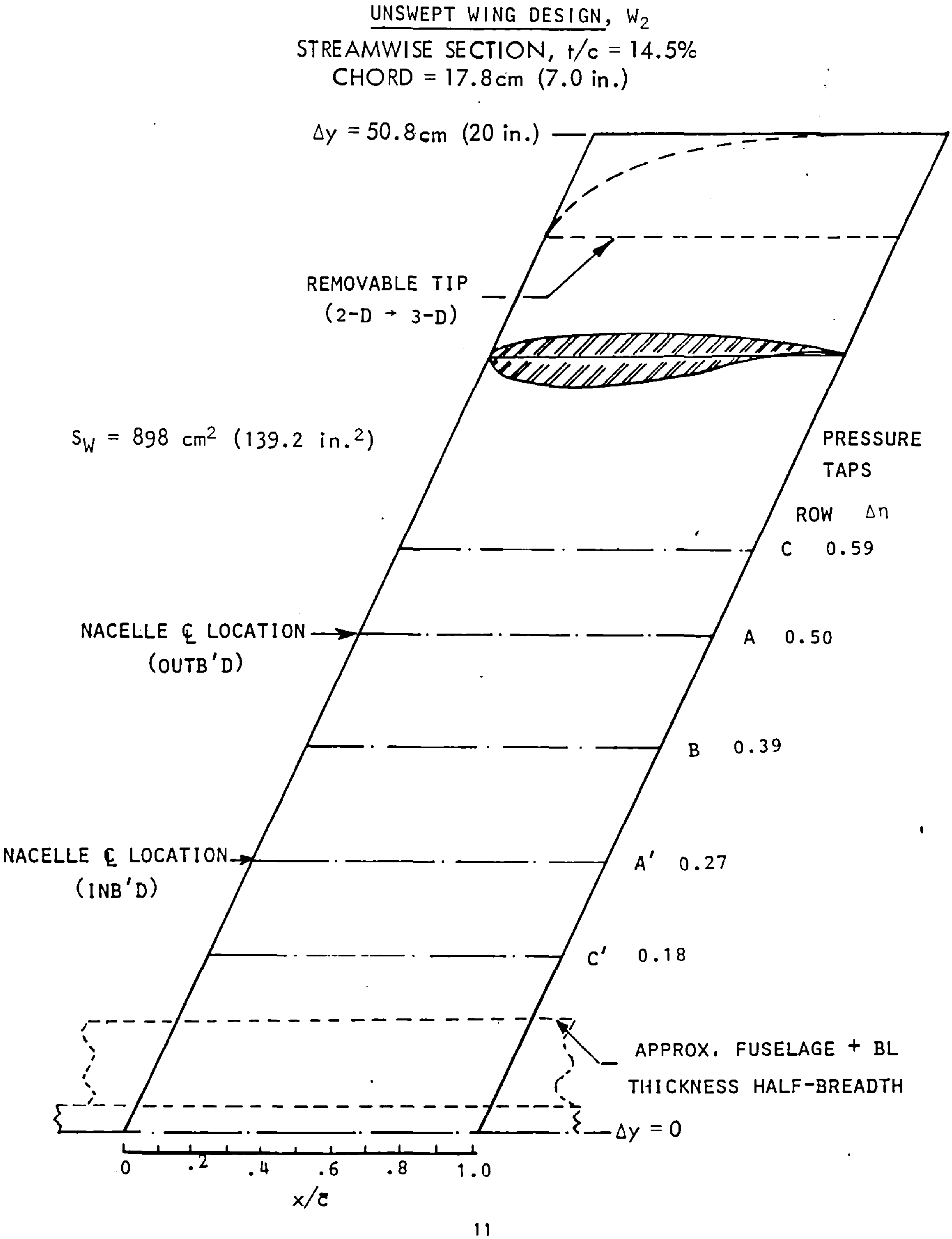

Figure 4. Swept wing planform and instrumentation layout

USB CRUISE PROGRAM

*FUSELAGE FINENESS RATIOS, ℓ/d

NOSE = 2.57
CENTERBODY = 4.14
AFT-BODY = 3.00
OVERALL = 9.71

*EXCLUDES B.L. PLATE

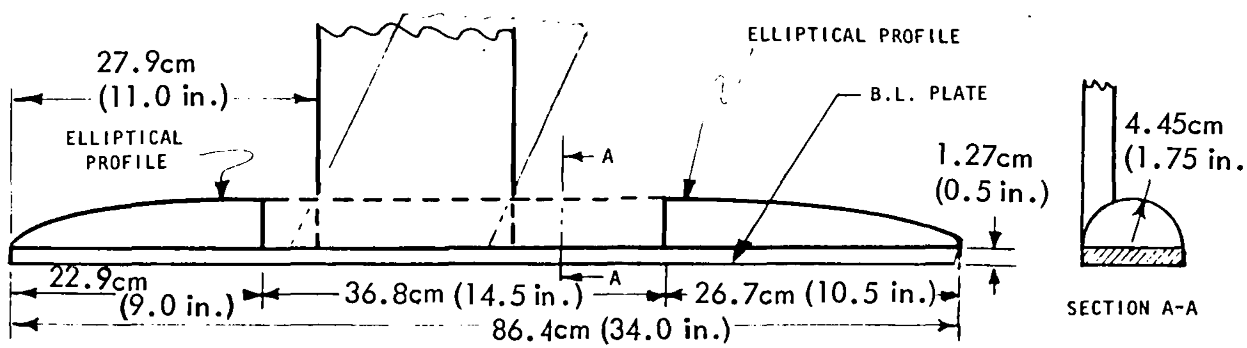

Figure 5. Force model fuselage with provision for mounting either straight wing or swept wing

USB CRUISE PROGRAM

COMPONENT TYPE	COMPONENT DESCRIPTION	NO. REQD.	NEW	EXISTING	DESIG-NATION
FUSELAGE	Nose	1	X		N_1
	Afterbody	1	X		A_1
	Center Section for High Existing Wing	1	X		F_1
	Center Section for High New Wing	1	X		F_2
WING	Straight Wing	1		X	W_1
	Swept Wing ($\Lambda = 25^{\circ}$)	1	X		W_2
	Straight Wing Tip Fairing	1	X		T_1
	Swept Wing Tip Fairing	1	X		T_2
	Instrumented T.E. for Swept Wing	1	X		E_1
	Segmented Flap for Swept Wing	1	X		S_1
	Straight Clean Wing Fairing Block	1		X	B_1
	Swept Clean Wing Fairing Blocks	2	X		B_2, B_3
	Straight Wing Nozzle Mounting Block	1		X	B_4
	Swept Wing Nozzle Mounting Blocks	3	X		B_5, B_6, B_7
PYLON	Straight Wing Short Pylon for Pipe Nacelles	1	X		P_1
	Straight Wing Long Pylon for Pipe Nacelles	2	X		P_2, P_3
	Swept Wing Short Pylon for Pipe Nacelles	1	X		P_4
	Swept Wing Long Pylon for Pipe Nacelles	2	X		P_5, P_6
	Straight Wing Short Pylon for Faired Nacelles	1		X	P_7
	Straight Wing Long Pylon for Faired Nacelles	1	X		P_8
	Swept Wing Long Pylon for Faired Nacelles	2	X		P_9, P_{10}
	Straight Wing Pylon for Flo-Thru Nacelles	1	X		P_{11}
	Straight Wing Long Pylon for Streamline Nacelles	1	X		P_{12}
	Swept Wing Long Pylon for Streamline Nacelles	1	X		P_{13}
	Straight Wing Pylon for Integr. Pipe Nacelles	1	X		P_{14}
	Swept Wing Pylon for Integr. Pipe Nacelles	1	X		P_{15}
NACELLE	Short Faired Forebody for Straight Wing	1		X	C_1
	Long Faired Forebody for Straight Wing	1	X		C_2
	Long Faired Forebody for Swept Wing	2	X		C_3, C_4
	Flow-Thru Forebody for Straight Wing	1	X		C_5
	Streamline Forebody for Straight Wing	1	X		C_6
	Streamline Forebody for Swept Wing	1	X		C_7
	Upstream Pipe Forebody for Large Nacelle	1	X		C_8
	Upstream Pipe Forebody for Intermediate Nacelle	1	X		C_9
NOZZLE	Large D-Duct Nozzle Pipe Mounted	1	X		N_1
	Intermediate Long Circular Nozzle, Wing & Pipe Mounted	1	X		N_2
	Intermediate Long D-Duct Nozzle, Wing & Pipe Mounted	1	X		N_3
	Intermediate Long High AR Nozzle, Wing & Pipe Mounted	1	X		N_4
	Intermediate Very High AR Nozzle, Wing & Pipe Mounted	1	X		N_5
	Small Streamline Nacelle Nozzle, Straight Wing	1	X		N_6
	Small Streamline Nacelle Nozzle, Swept Wing	1	X		N_7

Figure 6. Summary of model and test hardware components (Sheet 1)

USB CRUISE PROGRAM

COMPONENT TYPE	COMPONENT DESCRIPTION	NO. REQD.	NEW	EXISTING	DESIGNATION
NOZZLE (cont'd)	Small D-Duct Nacelle Nozzle, Swept Wing	2	X		N_8^1 & N_8^2
	Large Circular Nozzle, Pipe Mounted	1	X		N_9
	Large Very High AR Nozzle, Pipe Mounted	1	X		N_{10}
	Small Circular Nozzle, Swept Wing	1	X		N_{11}
	Small High AR Nozzle, Swept Wing	1	X		N_{12}
	Small Very High AR Nozzle, Swept Wing	1	X		N_{13}
	Intermediate Short Circular Nozzle, Discharge at 20% C	1		X	N_{1E}
	Intermediate Short Circular Nozzle, Discharge at 35% C	1		X	N_{2E}
	Intermediate Short D-Duct Nozzle, Discharge at 35% C	1		X	N_{3E}
	Intermediate Short High AR Nozzle, Discharge at 35% C	1		X	N_{4E}
	Intermediate Long D-Duct Nozzle Extension	3	X		X_1, X_2, X_3
	Intermediate Long Circular Nozzle Flow Deflector	1	X		D_1
	Large Spacers to Position Pipe Nozzles	3	X		L_1, L_2, L_3
	Intermediate Spacers to Position Pipe Nozzles	3	X		L_4, L_5, L_6
	Transition Adapter for Pipe Area Change	1	X		L_7
	Constant Area Adapter for Pipe Nozzle	1	X		L_8
	Choke Plates for Small Nozzles	2	X		K_5, K_6
	Choke Plate for Intermediate Nozzles	1		X	K_7
	Choke Plate for Large Nozzles	1	X		K_8
INSTRUMENTATION	3 Rows Additional Pressure Taps, Straight Wing	30	X		R_1, R_2, R_3
	3 Rows Basic Pressure Taps, Straight Wing	61		X	R_4, R_5, R_6
	6 Rows Pressure Taps, Swept Wing	91	X		$R_7 - R_{12}$
	Nozzle Afterbody Pressure Taps (5 Nozzle)	20		X	$R_{13} - R_{16}$
	Nozzle Afterbody Pressure Taps (5 Nozzle)	70	X		$R_{17} - R_{30}$
	Duct Plenum Pressure Taps (1 Wing Block)	1		X	pt_1
	Duct Plenum Pressure Taps (1 Wing Block)	2	X		pt_2, pt_3
	57 Tube Calibration Rake for All Nozzles	1	X		Q_1
	214 Tube Wake Rake for Drag Measurements	2	X		J_1
	Orifice Pressure Taps for Flow Measurements	3		X	pt_4, pt_5
TEST HARDWARE	Double Wall Upstream Pipe for Large Nozzles	1	X		Z_1
	Motor Driven Traverse for Wake Rakes	1	X		Y_1
	Wall Fitting for Straight & Swept Wings, Upper End	1	X		V_1, V_2
	Straight & Swept Wing-to-Floor Balance Adapters	1	X		ba_1, ba_2
	Floor Porosity Disc for Both Wings	1	X		pd_1
	Basic Wall Plates for Straight Wing	2		X	wp_1, wp_2
	Basic Wall Plates for Swept Wing	2	X		wp_3, wp_4
	Orifice Assembly & Air Supply Piping	1		X	as_1
	Orifice Plate for Intermediate & Small Nozzles	1		X	O_1
	Orifice Plate for Large Nozzles	1	X		O_2

Figure 6. Summary of model and test hardware components (Sheet 2)

USB CRUISE PROGRAM

GEOMETRIC		RELATIVE SIZE	ASPECT RATIO	DISCHARGE LOCATION	BOATTAIL ANGLE	NOZZLE LENGTH		MAXIMUM DIAMETER		NOZZLE AREA		WINGS		MOUNTING	
NO.	NOZZLE DESCRIPTION / PARAMETER	c^2/A_N	AR	$x/\bar{c}$	δ ~ DEG	cm	(in)	cm	(in)	cm^2	(in^2)	STRAIT	SWEPT	PIPE	WING
N_1	LARGE D-DUCT, LONG	12	2.5	0.1 - 0.5	9.0	28.915	11.384	9.088	3.578	26.923	4.173	X		X	
N_2	INTERMED. CIRCL., LONG	24	1.25	0.35	5.90	20.447	8.050	6.426	2.530	13.464	2.087	X	X	X	X
N_3	INTERMED. D-DUCT, LONG	24	2.5	0.35	9.0	20.447	8.050	6.426	2.530	12.935	2.005	X		X	X
N_4	INTERMED. HIGH AR, LONG	24	4.0$^{\Delta}$	0.35	11.0	20.447	8.050	6.426	2.530	13.464	2.087	X		X	X
N_5	INTERMED. VERY HI-AR, LONG	24	6.0$^{\Delta}$	0.35	12.5	20.447	8.050	6.426	2.530	13.464	2.087	X		X	X
N_6	SM. STRMLIN. D-DUCT, LONG	48	2.5	0.35	9.00*	14.458	5.692	4.544*	1.789*	6.729	1.043	X			X
N_8^1	SM. INBD. D-DUCT, LONG	48	2.5	0.20	9.50	11.791	4.642	4.544	1.789	6.729	1.043		X		X
N_8^2	SM. OUTBD. D-DUCT, LONG	48	2.5	0.20	9.50	11.791	4.642	4.544	1.789	6.729	1.043		X		X
N_9	LARGE CIRCULAR, SHORT	12	1.25	0.1 - 0.5	12.00	28.915	11.384	9.088	3.578	26.923	4.173	X	X	X	
N_{10}	LARGE VERY HI-AR, LONG	12	6.0$^{\Delta}$	0.1 - 0.5	12.50	28.915	11.384	9.088	3.578	26.923	4.173	X		X	
N_{11}	SMALL CIRCL., SHORT	48	1.25	0.10	12.00	10.013	3.942	4.544	1.789	6.729	1.043		X		X
N_{12}	SMALL HI-AR, LONG	48	4.0$^{\Delta}$	0.35	11.00	14.458	5.692	4.544	1.789	6.729	1.043		X		X
N_{13}	SMALL VERY HI-AR, LONG	48	6.0$^{\Delta}$	0.50	11.00	17.125	6.742	4.544	1.789	6.729	1.043		X		X
N_{1E}	INTERMED. CIRCL., SHORT	24	1.25	0.20	16.78	9.629	3.791	6.426	2.530	12.813	1.986	X			X
N_{2E}	INTERMED. CIRCL., SHORT	24	1.25	0.35	16.78	12.296	4.841	6.426	2.530	12.813	1.986	X			X
N_{3E}	INTERMED. D-DUCT, SHORT	24	2.5	0.35	24.52	12.296	4.841	6.426	2.530	13.464	2.087	X			X
N_{4E}	INTERMED. HI-AR, SHORT	24	4.0$^{\Delta}$	0.35	35.88	12.296	4.841	6.426	2.530	13.464	2.087	X			X

$^{\Delta}$ *THESE ASPECT RATIOS ARE EXPRESSED FOR EQUIVALENT RECTANGULAR NOZZLE CROSSECTIONS*

* APPROXIMATELY EQUIVALENT DIMENSIONS FOR NON-CIRCULAR, NON-SYMMETRIC NACELLES

Figure 7. Key dimensions for nozzles in test matrix

boattail angle. Relative size was expressed by the parameter c^2/A_N, which relates the square of the wing chord to the nozzle area. Three relative sizes, 12, 24 and 48, were included in the program. Nozzle aspect ratios varied from 1.25 (circular) to 6.0. Chordwise discharge positions varied from 10 to 50 percent, with 35% being the baseline value. For the nozzle designed with the combination circular-arc, straight line contours, boattail angles ranged from 6 to 13 degrees. Boattail angles for the "E" nozzles, however, ranged from 16 to 36 degrees. The wings to which each of the nozzles are matched and the applicable mounting arrangements are also presented in the table.

3.2 Data Acquisition System

Model forces were measured in the CFF by means of a 5-component, floor mounted balance. It could measure lift, drag, pitching moment, rolling moment, and yawing moment. High pressure air was provided to the model by means of a dual-opposed bellows arrangement.

A wall mounted 6-component balance was employed in the 4 x 4 for force measurement. Its basic design and air ducting arrangement was essentially similar to the system used in the CFF.

Airflow was metered by means of a calibrated rake installed in each nozzle just downstream of the choke plate. Calibration curves for each nozzle were developed in a separate test conducted earlier in the program.

4.0 TEST DESCRIPTION

Both the pressure and force test phases of the USB Cruise Program were formulated around the use of minimum-cost, powered models in a porous wall, blowdown test facility. This combination permitted a test program covering a comprehensive series of test configurations and parameter variations over an extensive range of test conditions. Tests were conducted in both the Lockheed-Georgia CFF and the Lockheed-California 4x4 blowdown tunnels. A facility description is contained in Reference 2.

4.1 Test Objectives

The principal objective of the force test program was to generate a lift/drag data base sufficiently broad to accurately evaluate the potential of USB systems for cruise propulsion. In cases where a decision has been made to employ USB for its terminal area performance benefits, the data would need to be suitable for designing an installation with low cruise drag. An important goal was to obtain data which can be used to generate parametric curves describing the effects of systematic changes in key design variables.

4.2 Run Schedule Summary

The USB force test program can be broken down into two major efforts. The first of these, which is summarized in Figure 8, was conducted in the Lockheed-Georgia CFF and consisted of tests 20 and 21 covering the straight and swept wing configurations, respectively. All configurations were included in this part of the program. In the second effort, which is summarized in Figure 9, selected configurations from the first were tested in the Lockheed California

USB CRUISE PROGRAM

TEST DESCRIPTION	CONFIGURATION DESCRIPTION	CONFIGURATION DEFINITION	TEST NO.	TEST SERIES	RUN NOS.	MACH NO. M_∞	ANGLE OF ATTACK α~ DEG	NOZZLE PRES. RATIO, H/P_∞	REMARKS
Wall Interference, Lift & Drag Forces Plus Moments	3-D, Clean Swept Wing-Body	$F_2 W_2$	20	0	1 - 569	0.5 - 0.82	-1 to 5		R_N from 3.5 to 7.0 x 10^6/c Porosities from 2 to 5%
Lift & Drag, Forces & Moments	3-D Swept Wing-Body								
	+ Outbd. D-Duct Nacelle	$F_2 W_2 B_5 P_9 C_3 N_8^1$	20	1	1 - 171	Static + 0.6 - 0.82	1 to 5	1.0 - 3.0	Run No. 171 is Oil Flow
	+ 2D-Duct Nacelles	$F_2 W_2 B_{5,6} P_{9,10} C_{3,4} N_8^1, N_8^2$		2	172 - 255	Static + 0.6 - 0.75	1 to 5	1.0 - 2.9	Run Nos. 254 & 255 are Oil Flow
	+ Inbd. D-Duct Nacelle	$F_2 W_2 B_6 P_{10} C_4 N_8^2$		3	256 - 335	Static + 0.6 - 0.75	1 to 5	1.0 - 3.0	
	+ Circular Nacelle	$F_2 W_2 B_5 P_9 C_3 N_{11}$		4	336 - 453	Static + 0.6 - 0.8	1 to 5	1.0 - 3.5	Run No. 453 is Oil Flow
	+ AR 4 Nacelle	$F_2 W_2 B_5 P_9 C_3 N_{12}$		5	454 - 538	Static + 0.6 - 0.75	1 to 5	1.0 - 3.2	Run No. 538 is Oil Flow
	+ AR 6 Nacelle	$F_2 W_2 B_5 P_9 C_3 N_{13}$		6	539 - 647	Static + 0.6 - 0.75	1 to 5	1.0 - 3.3	
	+ AR 6 Nac. & Mid-Flap 5° Down	$F_2 W_2 B_5 P_9 C_3 N_{13A}$		7	648 - 687	Static + 0.6 - 0.78	1 to 5	1.0 - 3.4	
	+ AR 6 Nac. & Mid-Flap 5° Up	$F_2 W_2 B_5 P_9 C_3 N_{13B}$		8	688 - 754	Static + 0.6 - 0.78	1 to 5	1.0 - 3.4	
	+ Short Pylon & Flow-Thru Nac.	$F_2 W_2 B_2 P_5 C_5 N_2$		9	755 - 810	0.6 - 0.8	1 to 5		Run Nos. 809 & 810 are Oil Flow
	+ Long Pylon & Flow-Thru Nac.	$F_2 W_2 B_2 P_6 C_5 N_2$		10	811 - 857	0.6 - 0.8	1 to 5		
	+ D-Duct Nacelle, Inboard	$F_2 W_2 B_6 P_{10} C_4 N_8^2$		11	858 - 971	Static + 0.6 - 0.75	1 to 5	1.0 - 3.2	
	+ 2D-Duct Nacelles	$F_2 W_2 B_{5,6} P_{9,10} C_{3,4} N_8^1 N_8^2$		12	1 - 132	Static + 0.6 - 0.78	1 to 5	1.0 - 3.1	
	+ D-Duct Nacelle, Outboard	$F_2 W_2 B_5 P_9 C_3 N_8^1$		13	133 - 165	0.6 - 0.8	1 to 5	2.6 - 3.6	
	+ D-Duct Nac. with Fillet Reshaped	$F_2 W_2 B_5 P_{9A} C_3 N_8^1$		14	166 - 185	0.77	1 to 4	1.0 - 3.6	Run No. 166 is Oil Flow
Lift & Drag, Forces & Moments	3-D, Clean Straight Wing-Body	$F_1 W_1$	21	0	1 - 60	0.5 - 0.76	1 to 5		
	+ Short D-Duct Nacelle	$F_1 W_1 B_4 P_7 C_1 N_{3E}$		1	61 - 186	Static + 0.5 - 0.72	1 to 4	1.0 - 3.2	Run No. 115 is Oil Flow
	+ AR 4 Nacelle	$F_1 W_1 B_4 P_7 C_1 N_{4E}$		2	187 - 306	Static + 0.5 - 0.72	1 to 4	1.0 - 3.2	
	+ Circular Nacelle	$F_1 W_1 B_4 P_7 C_1 N_{2E}$		3	307 - 416	Static + 0.6 - 0.72	1 to 4	1.0 - 3.2	
	+ Short Circular Nacelle	$F_1 W_1 B_4 P_7 C_1 N_{1E}$		4	417 - 524	Static + 0.6 - 0.72	1 to 4	1.0 - 3.2	Run Nos. 523 & 524 are Oil Flow
	+ Long D-Duct & Deflector	$F_1 W_1 B_7 P_8 C_2 N_{3A}$		5	525 - 629	Static + 0.6 - 0.72	1 to 4	1.0 - 4.0	Run No. 666 is Oil Flow
	+ Long D-Duct without Deflector	$F_1 W_1 B_7 P_8 C_2 N_{3B}$		6	630 - 744	Static + 0.6 - 0.72	1 to 4	1.0 - 3.2	Run No. 665 is Oil Flow
	+ Long AR 4 Nacelle	$F_1 W_1 B_7 P_8 C_2 N_4$		7	745 - 845	Static + 0.6 - 0.72	1 to 4	1.0 - 3.0	
	+ Long AR 4 Nac. with Fillet Removed	$F_1 W_1 B_7 P_8 C_2 N_{4A}$		8	846 - 851	0.70	1	1.0 - 2.8	
	+ Long AR 6 Nacelle	$F_1 W_1 B_7 P_8 C_2 N_5$		9	852 - 961	Static + 0.6 - 0.72	1 to 4	1.0 - 3.0	Run No. 961 is Oil Flow
	+ Long AR 6 Nac. with Fillet Removed	$F_1 W_1 B_7 P_8 C_2 N_{5A}$		10	962 - 981	0.68	1 to 4	1.0 - 2.6	
	+ Long Circular Nacelle	$F_1 W_1 B_7 P_8 C_2 N_2$		11	1 - 92	Static + 0.6 - 0.72	1 to 4	1.0 - 3.0	
	+ Flo-Thru Inlet	$F_1 W_1 B_7 P_8 C_5 N_2$		12	93 - 128	0.50 - 0.75	1 to 4		Run No. 128 is Oil Flow
	+ Flo-Thru Inlet + Short Pylon	$F_1 W_1 B_1 P_1 C_5 N_2$		13	129 - 158	0.50 - 0.75	1 to 4		Run No. 158 is Oil Flow
	+ Flo-Thru Inlet + Long Pylon	$F_1 W_1 B_1 P_2 C_5 N_2$		14	159 - 194	0.50 - 0.75	1 to 4		Run No. 159 is Oil Flow
	+ Streamlined Nacelle	$F_1 W_1 B_9 P_{12} C_6 N_6$		15	195 - 257	Static + 0.6 - 0.72	1 to 4	1.0 - 4.0	
	+ Streamlined Nac. + Pylon Fillet	$F_1 W_1 B_9 P_{12} C_6 N_6$		16	258 - 370	Static + 0.6 - 0.72	1 to 4	1.0 - 3.2	
	+ Long Circular Nacelle	$F_1 W_1 B_7 P_8 C_2 N_2$		17	371 - 385	Static	0		

NOTES: (1) R_N = 3.5 X 10^6/c, except where noted. (2) Wall porosity = 5% for force tests and 4% for pressure tests, except as noted.

Figure 8. Run schedule summary for CFF force tests.

USB CRUISE PROGRAM

TEST DESCRIPTION	CONFIGURATION DESCRIPTION	CONFIGURATION DEFINITION	TEST NO.	TEST SERIES	RUN NOS.	MACH. NO. M_∞	ANGLE OF ATTACK α - DEG.	NOZZLE PRESS. RATIO H_j/P_∞	REMARKS
Calibration & Tares	3-D Clean Straight Wing-Body + Short D-Duct Nacelle	$F_1W_1B_4P_7C_1N_{3E}$	345	I	1 - 58	Static	0	1.4 - 3.0	Static & Flow Tares Investigated
Lift & Drag, Forces & Moments	3-D Clean Straight Wing-Body	F_1W_1			82 - 88	0.6 - 0.72	0 to 5		
	+ Short Pyl. & Flo-Thru Cir. Nac.	$F_1W_1B_1P_1C_5N_2$			89 - 96	0.6 - 0.74			
	+ Integr. Flo-Thru Cir. Nac.	$F_1W_1B_7P_{16}C_5N_2$			125 - 132	0.6 - 0.72			
Calibration & Tares	3-D Clean Straight Wing-Body + Long Circular Nacelle	$F_1W_1B_7P_8C_2N_2$	345	II	1 - 84	Static	0	1.4 - 3.0	Runs 70 & 73 -81 were made using nozzle isolation rig
Lift & Drag, Forces	3-D Clean Straight Wing-Body	F_1W_1			85 - 97	0.6 - 0.72	0 to 5		
	+ Long Circular Nacelle	$F_1W_1B_7P_8C_2N_2$			98 - 124	Static + 0.6-0.72		1.4 - 3.0	
	+ Long AR 4 Nacelle	$F_1W_1B_7P_8C_2N_4$			125 - 142			1.4 - 3.0	
	+ Long AR 6 Nacelle	$F_1W_1B_7P_8C_2N_5$			143 - 164			1.4 - 3.0	
	+ Short D-Duct Nacelle	$F_1W_1B_4P_7C_1N_{3E}$			165 - 186			1.4 - 3.0	
	+ Streamlined Nacelle	$F_1W_1B_9P_{12}C_6N_6$			187 - 206			1.4 - 3.0	
	+ Short AR 4 Nacelle	$F_1W_1B_4P_7C_1N_{4E}$			207 - 213	Static + 0.68		1.4 - 3.0	
	+ Short D-Duct Nacelle	$F_1W_1B_4P_7C_1N_{3E}$			214 - 217	Static	0	1.4 - 3.0	Static Re-check
Lift & Drag, Forces & Moments	2 D-Duct Nacelles +	$F_2W_2B_{5,6}P_{9,10}C_{3,4}N_8^{1,2}$			218 - 246	Static + 0.6-0.73	0 to 5	1.4 - 3.0	
	3-D Clean Swept Wing-Body	F_2W_2			247 - 255	0.6 - 0.81	0 to 5		
	+ Null Thrust Rig	$F_2W_2B_5P_9C_3N_{14}$			256 - 271	Static	0	1.4 - 3.0	Additional Tare Study
	+ AR 4 Nacelle	$F_2W_2B_5P_9C_3N_{12}$			272			1.4 - 3.0	
	+ Outb'd D-Duct Nacelle	$F_2W_2B_5P_9C_3N_8^1$			273			1.4 - 3.0	
	+ AR 6 Nacelle	$F_2W_2B_5P_9C_3N_{13}$			274 - 285			1.4 - 3.0	

NOTES: (1) $R_N = 3.5 \times 10^6/c$, except where noted.

Figure 9. Run schedule summary for 4 x 4 force tests.

4 x 4 wind tunnel. This was also a two-part effort with test numbers assigned by the facility as 345-I and 345-II. Calibration and tare runs, plus clean wing and flow-through configuration tests were made in Part I. The selected power configurations were included in Part II.

5.0 STRAIGHT WING TEST RESULTS

The presentation of the straight wing force data is divided into 5 parts. The basic clean wing-body is presented first followed by special sets of data taken for comparisons of the integrated with the pylon mounted nacelles and the faired-over with the flow-through nacelles. Finally, the results of running the standard configurations for the basic parametric analyses are presented for the CFF and 4 x 4 tests in that order.

5.1 Clean Wing-Body

Basic data for the clean wing-body are presented in Figures 10 through 12. These include lift, drag and pitching moment. Curves are presented for 5 different Mach numbers to assure adequate coverage of the full test range.

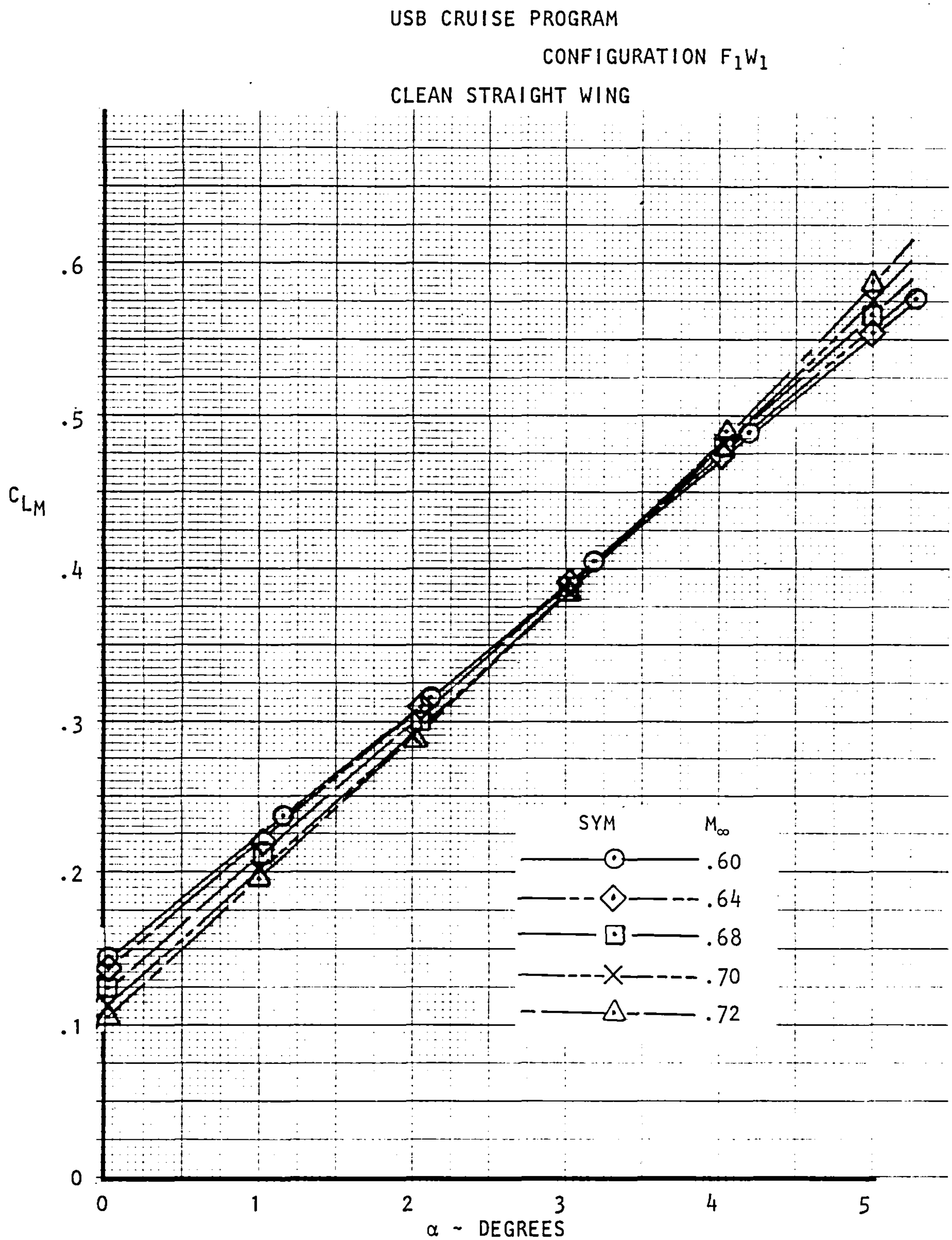

Figure 10. Variation of measured lift coefficient with angle of attack, $R_{NC} = 3.5 \times 10^6$.

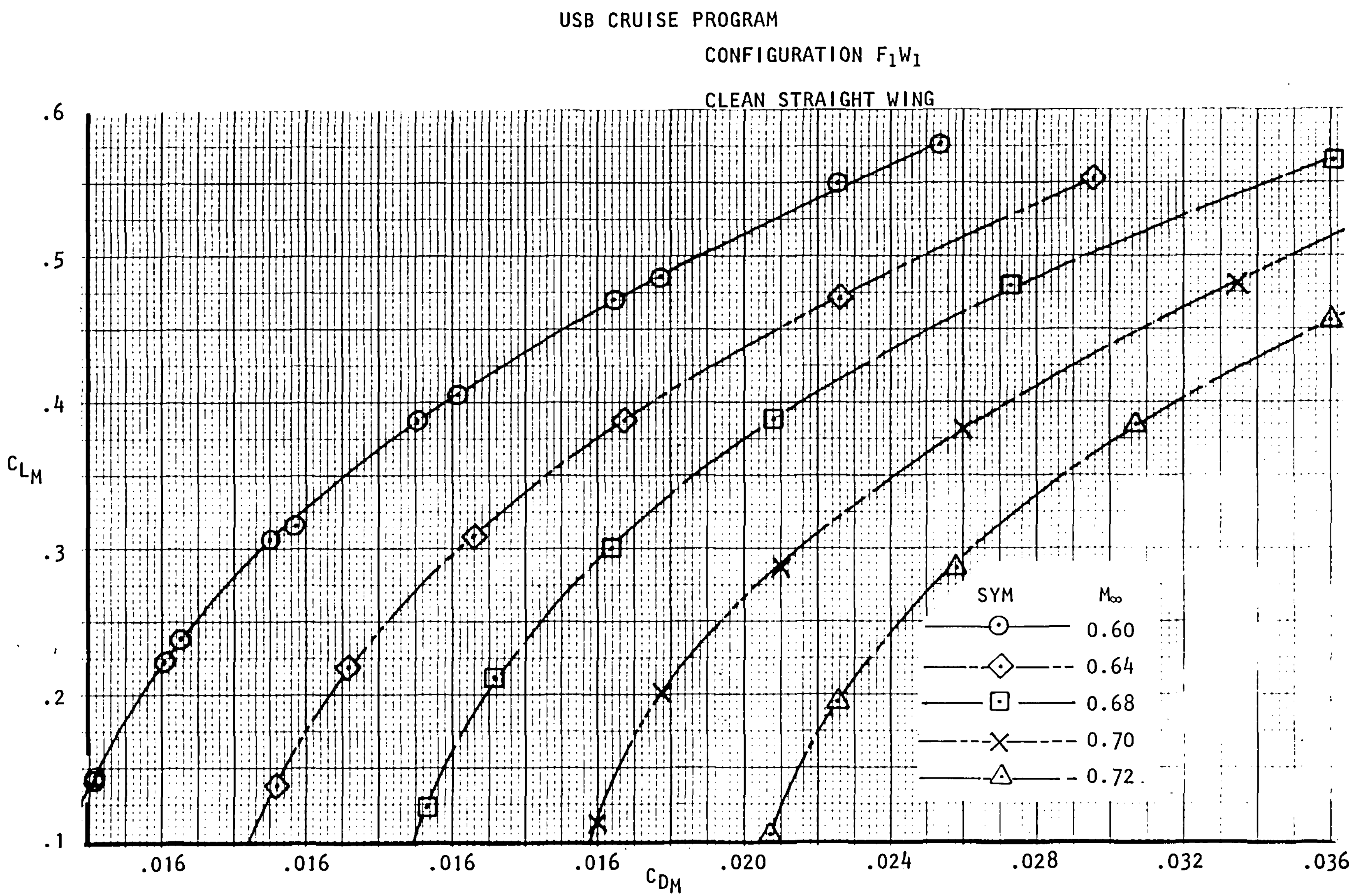

Figure 11. Variation of measured lift coefficient with measured drag coefficient, $R_{NC} = 3.5 \times 10^6$.

USB CRUISE PROGRAM

CONFIGURATION F_1W_1

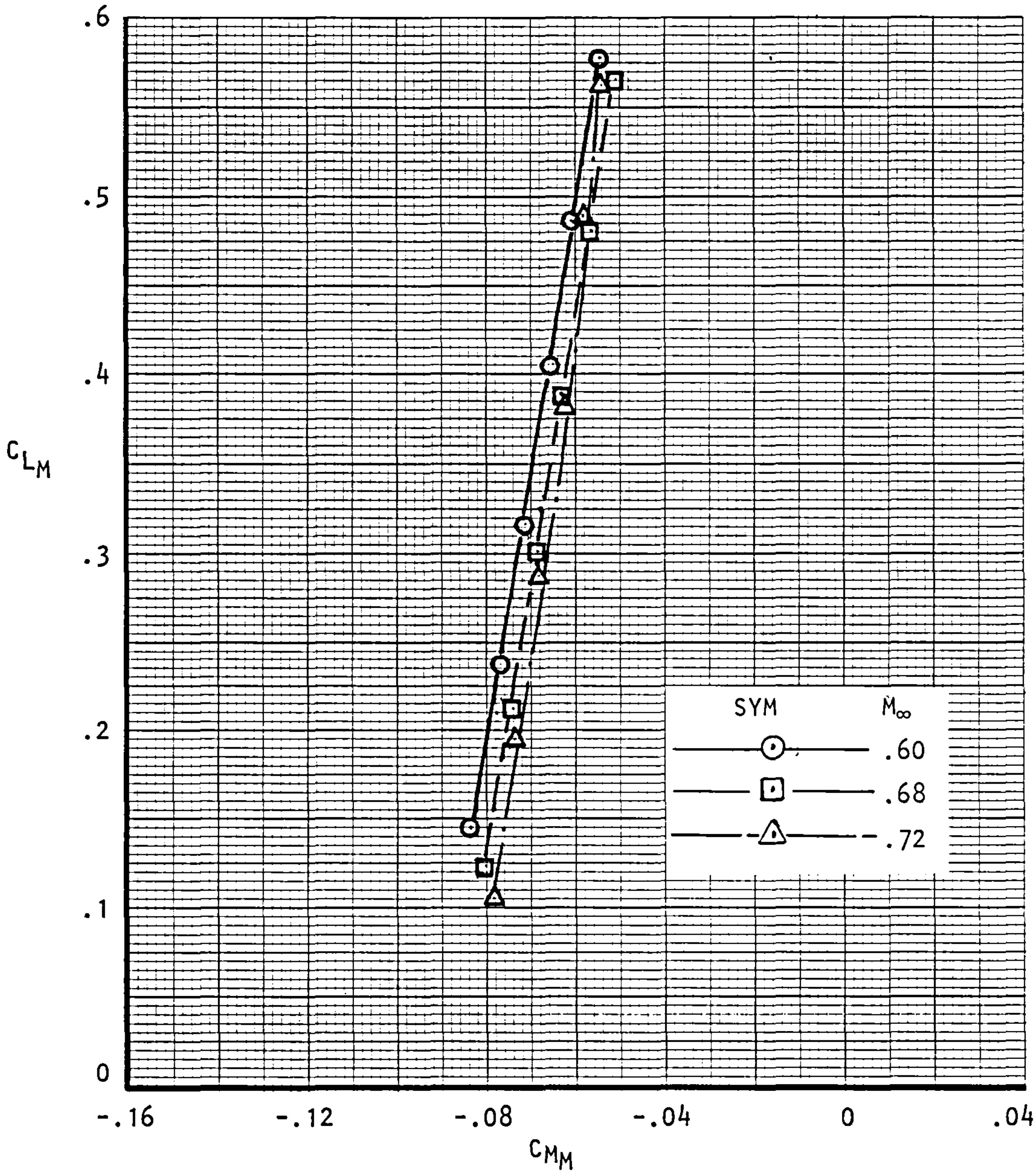

Figure 12. Variation of measured lift coefficient with measured moment coefficient, $R_{NC} = 3.5 \times 10^6$.

5.2 Data For Pylon Mounted Versus Integrated Nacelle Comparison

To perform a comparison of pylon mounted and integrated nacelle configurations, it was necessary to run the flow-through versions of these two installations. This was true because, in the pylon mounted configuration, it was not possible to supply the required high pressure air to the nozzle. The pylon mounted nacelle data are provided in Figures 13 and 14 while the integrated nacelle data are contained in 15 and 16.

5.3 Data For Faired-Over Versus Flow-Through Nacelle Comparison

In using the faired-over forebody nacelle configuration for power tests, it was assumed that the drag of this configuration would be essentially the same as that of a flow-through nacelle operating at design mass flow ratio. To prove this assumption, it was necessary to run the faired-over nacelle at flow-through pressure ratios and at least two Mach numbers for comparison with the identical configuration, but with an open forebody. Data for the faired forebody runs at flow-through pressure ratios are presented in Figures 17 and 18.

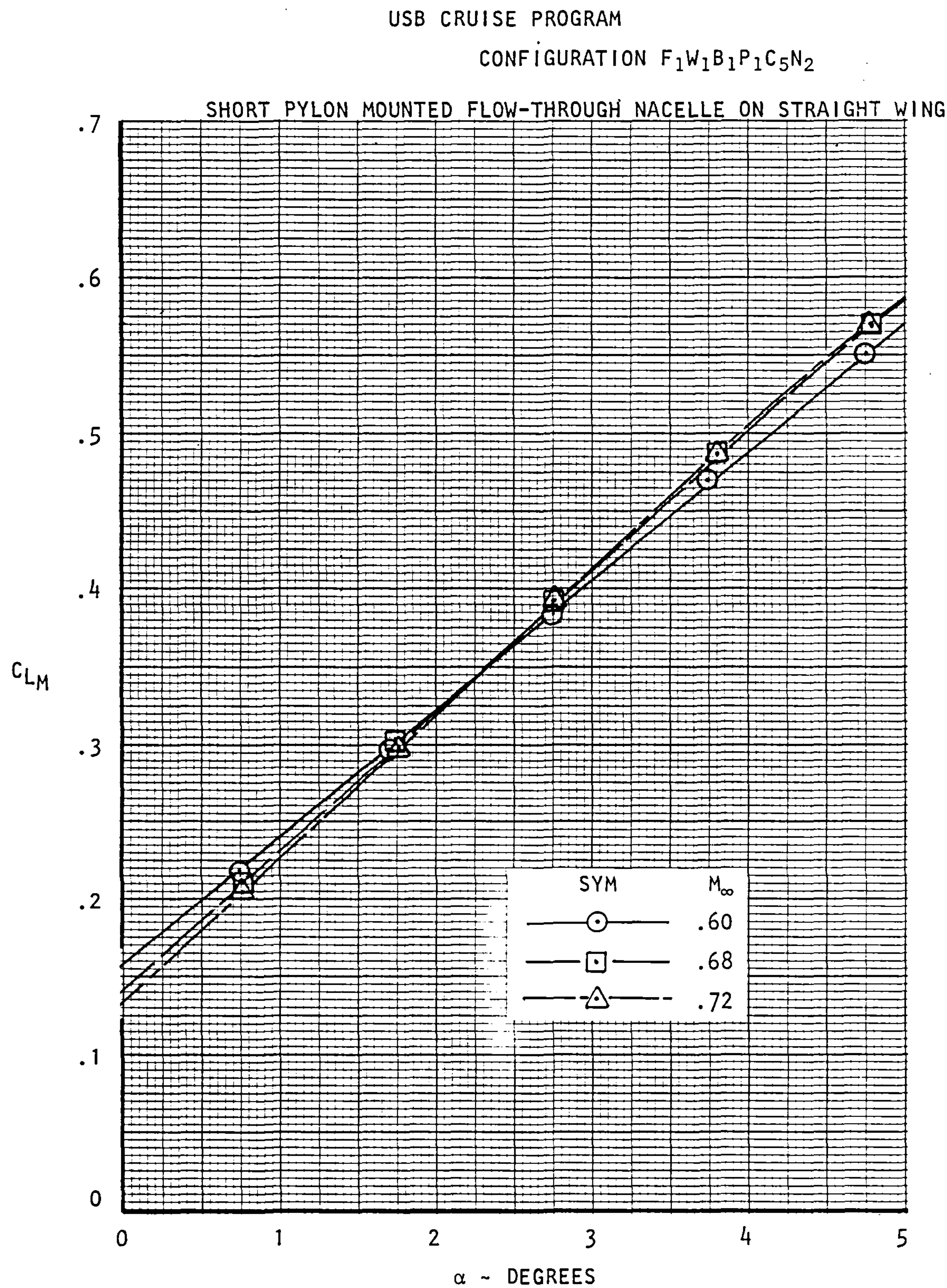

Figure 13. Variation of measured lift coefficient with angle of attack, $R_{NC} = 3.5 \times 10^6$, $H_j/p_\infty = RPR$.

USB CRUISE PROGRAM

CONFIGURATION $F_1W_1B_1P_1C_5N_2$

SHORT PYLON MOUNTED FLOW-THROUGH NACELLE ON STRAIGHT WING

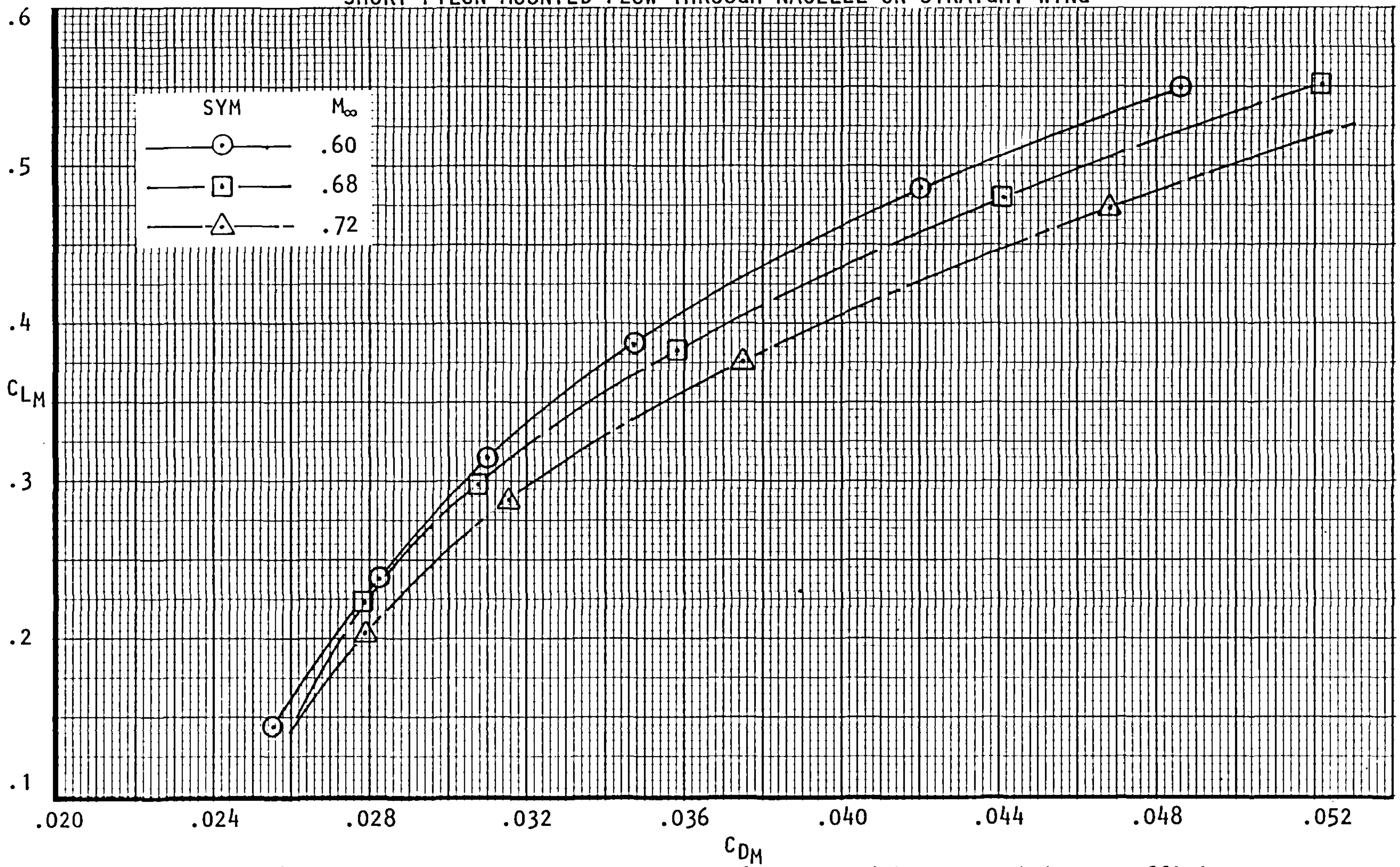

Figure 14. - Variation of measured lift coefficient with measured drag coefficient, $R_{NC} = 3.5 \times 10^6$, H_j/p_∞ = RPR.

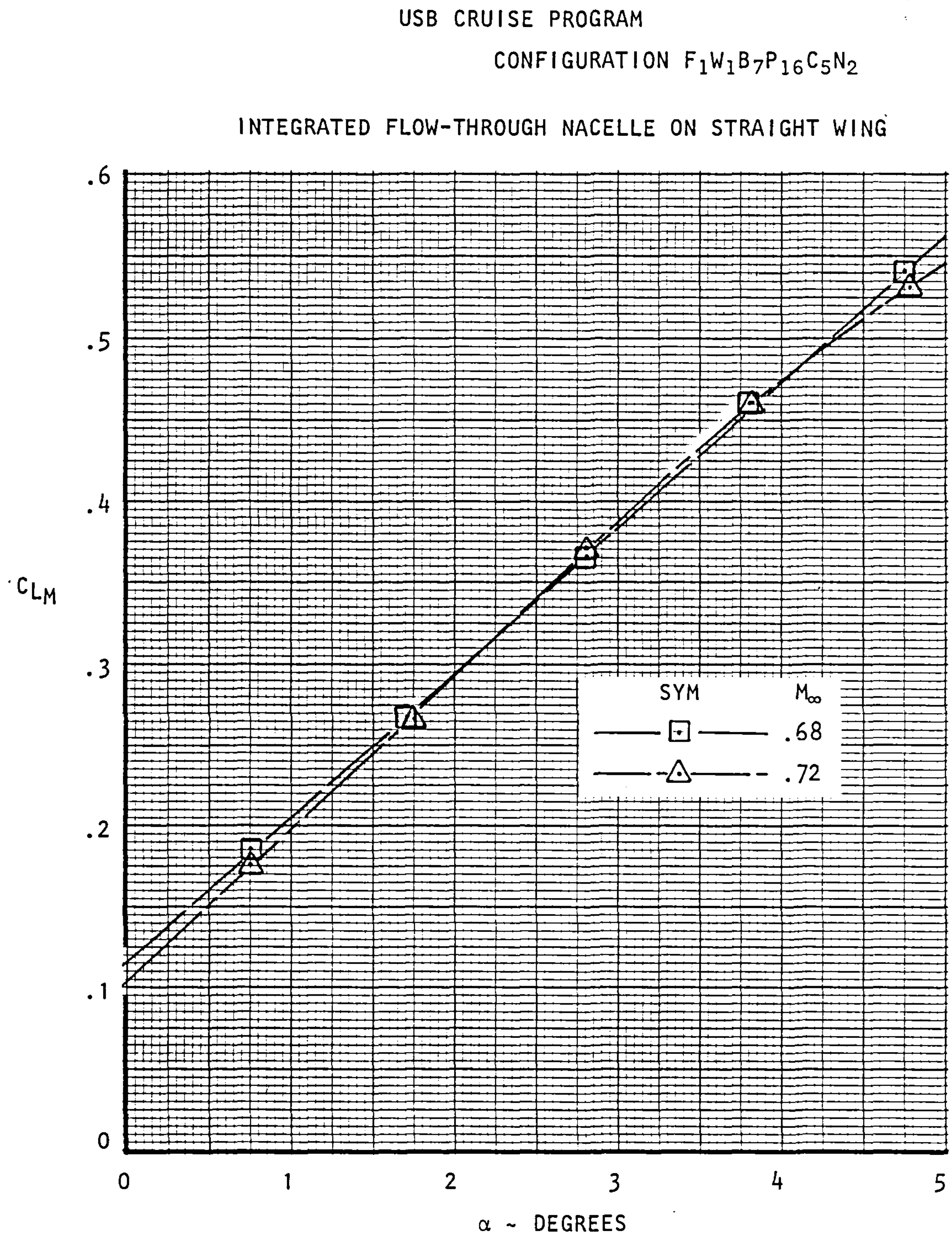

Figure 15. - Variation of measured lift coefficient with angle of attack, $R_{N_C} = 3.5 \times 10^6$, $H_j/p_\infty = RPR$.

USB CRUISE PROGRAM

CONFIGURATION $F_1W_1B_7P_{16}C_5N_2$

INTEGRATED FLOW-THROUGH NACELLE ON STRAIGHT WING

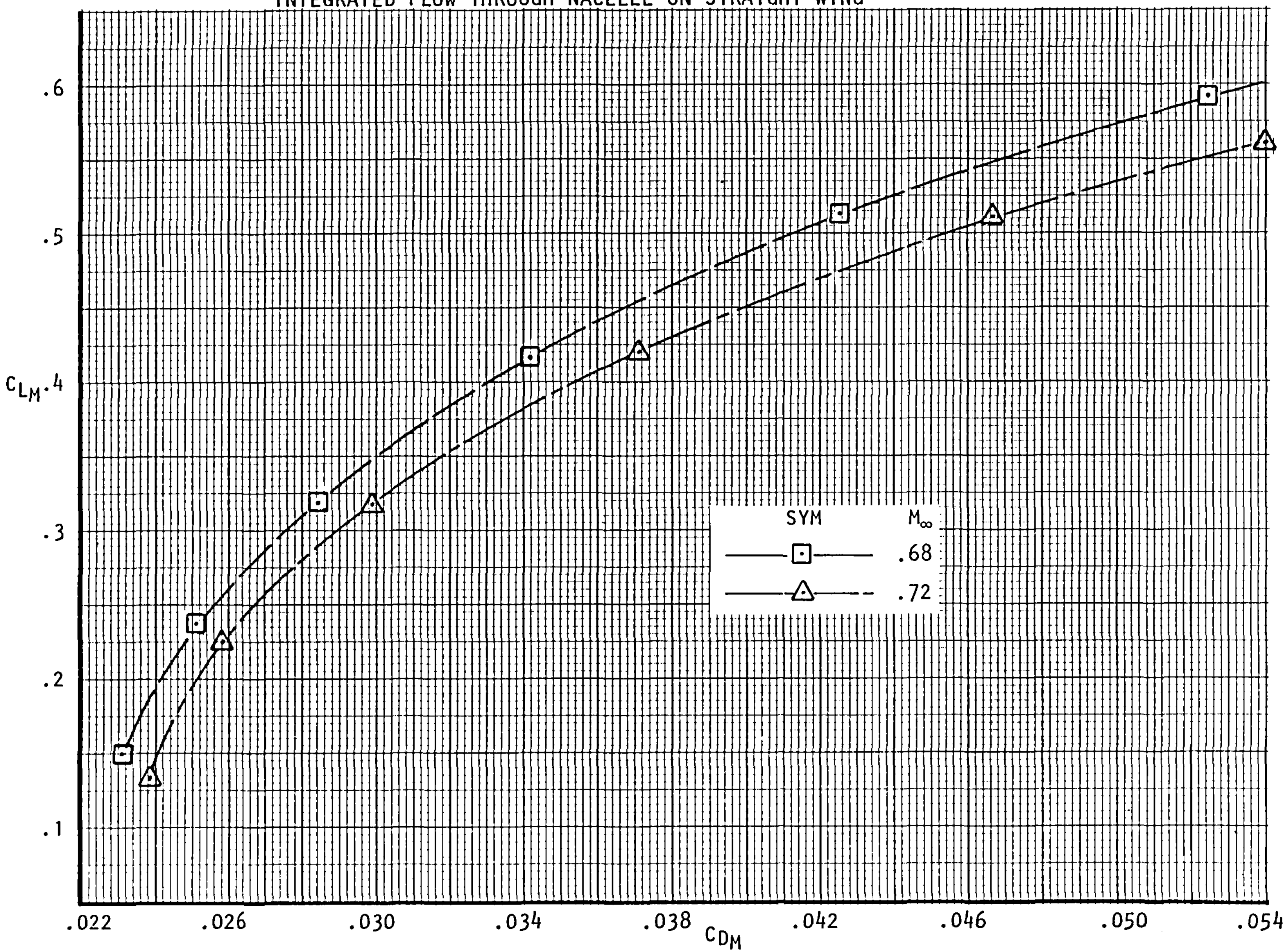

Figure 16. - Variation of measured lift coefficient with measured drag coefficient, $R_{NC} = 3.5 \times 10^6$, $H_j/p_\infty = RPR$.

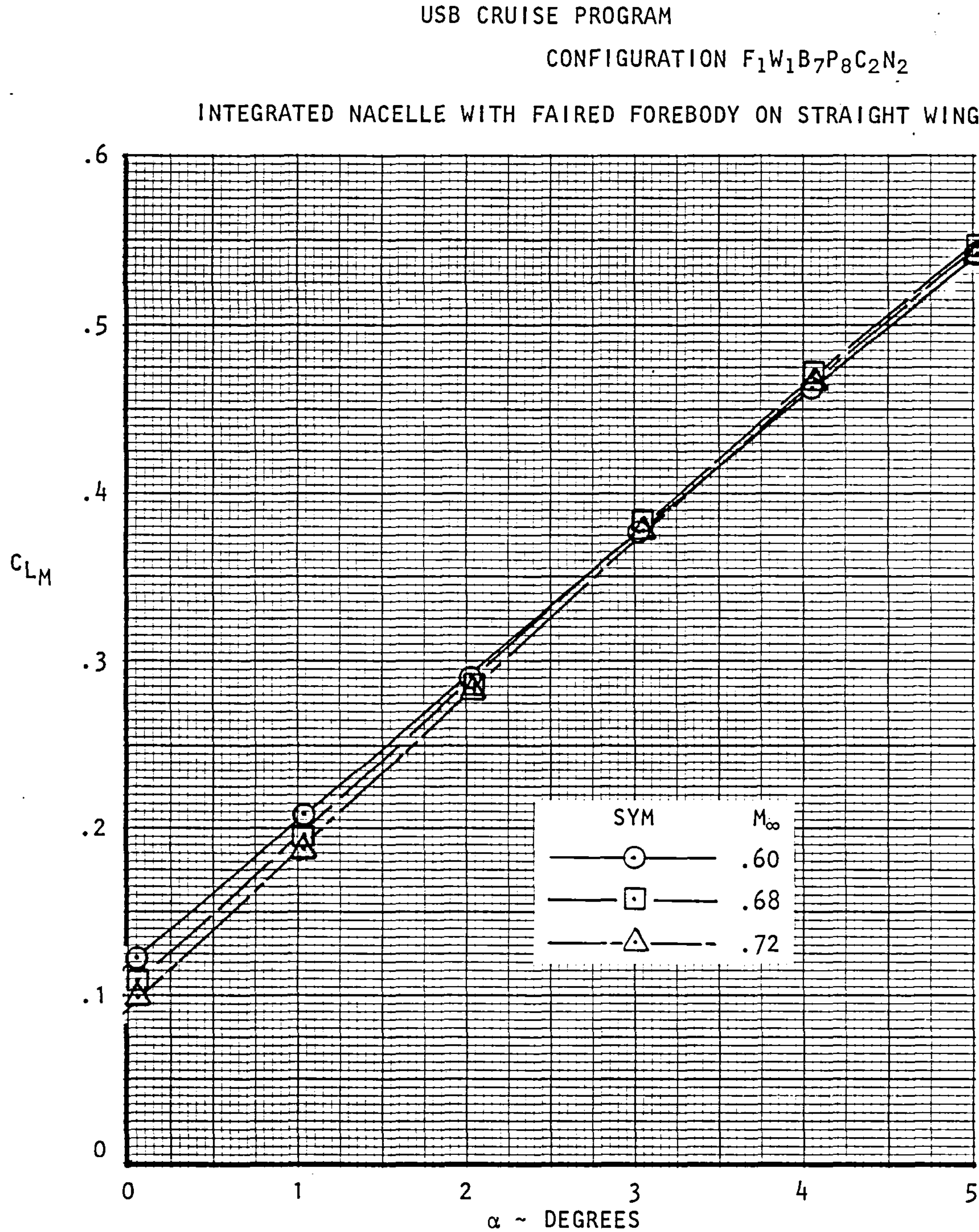

Figure 17. - Variation of measured lift coefficient with angle of attack, $R_{NC} = 3.5 \times 10^6$, $H_j/p_\infty = RPR$.

USB CRUISE PROGRAM

CONFIGURATION $F_1W_1B_7P_8C_2N_2$

INTEGRATED NACELLE WITH FAIRED FOREBODY ON STRAIGHT WING

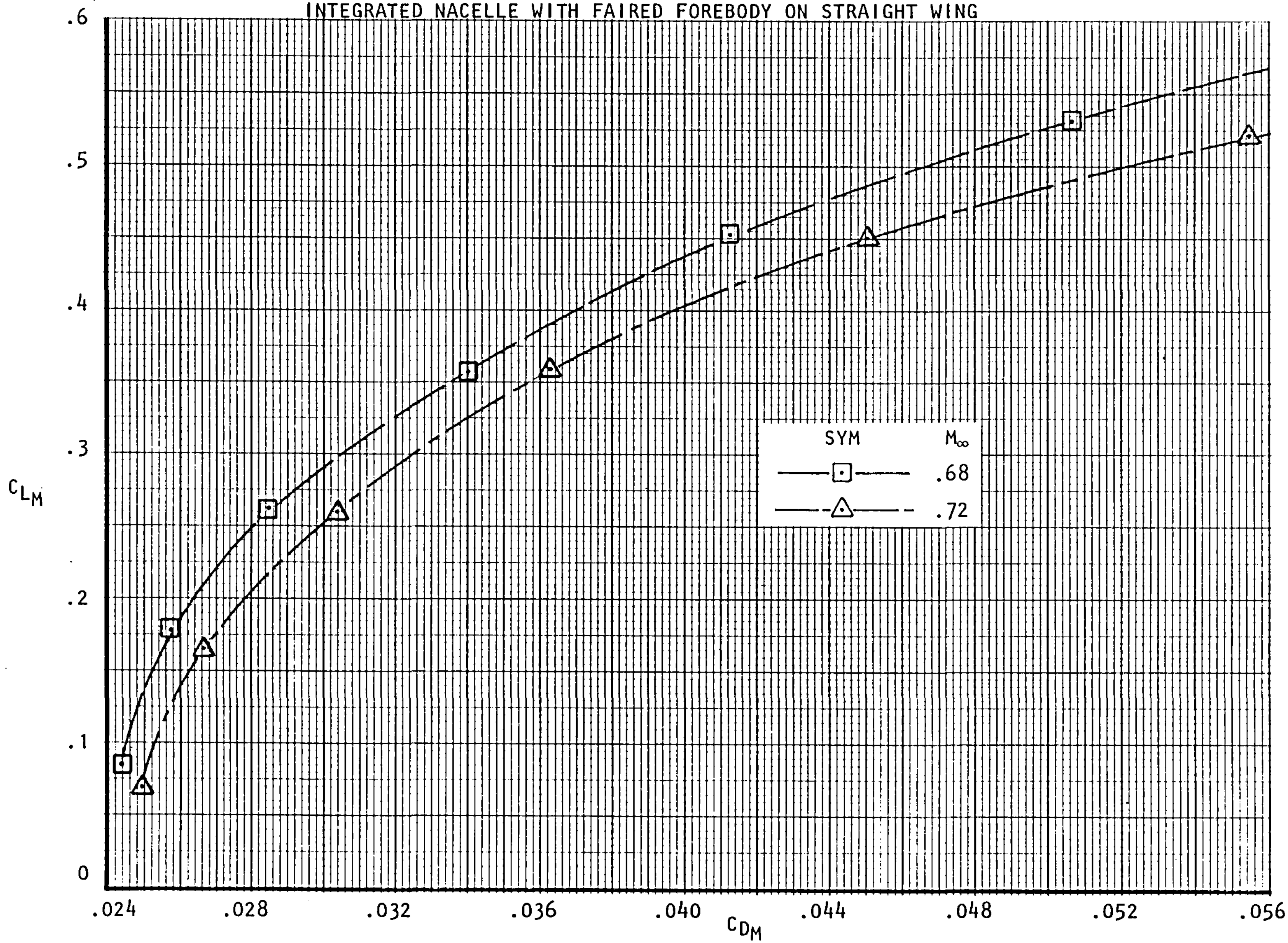

Figure 18. - Variation of measured lift coefficient with measured drag coefficient, $R_{NC} = 3.5 \times 10^6$, $H_j/p_\infty = RPR$.

5.4 Results From CFF Tests, Standard Configurations

Data for those straight wing configurations tests in the CFF only are presented in Figures 19 through 34. The data are presented as measured and contains nozzle thrust forces. Nozzle pressure ratios typically range from 1.4 to 2.6 and, in some cases, up to 3.0. A complete discussion of how these data have been reconciled with that obtained from the 4 x 4 is contained in Reference 3.

5.5 Results From 4 x 4 Tests, Standard Configurations

Data for all straight wing configurations tested in the 4 x 4 are presented in Figures 35 through 102. Ranges of variables are essentially the same as those obtained for the CFF data.

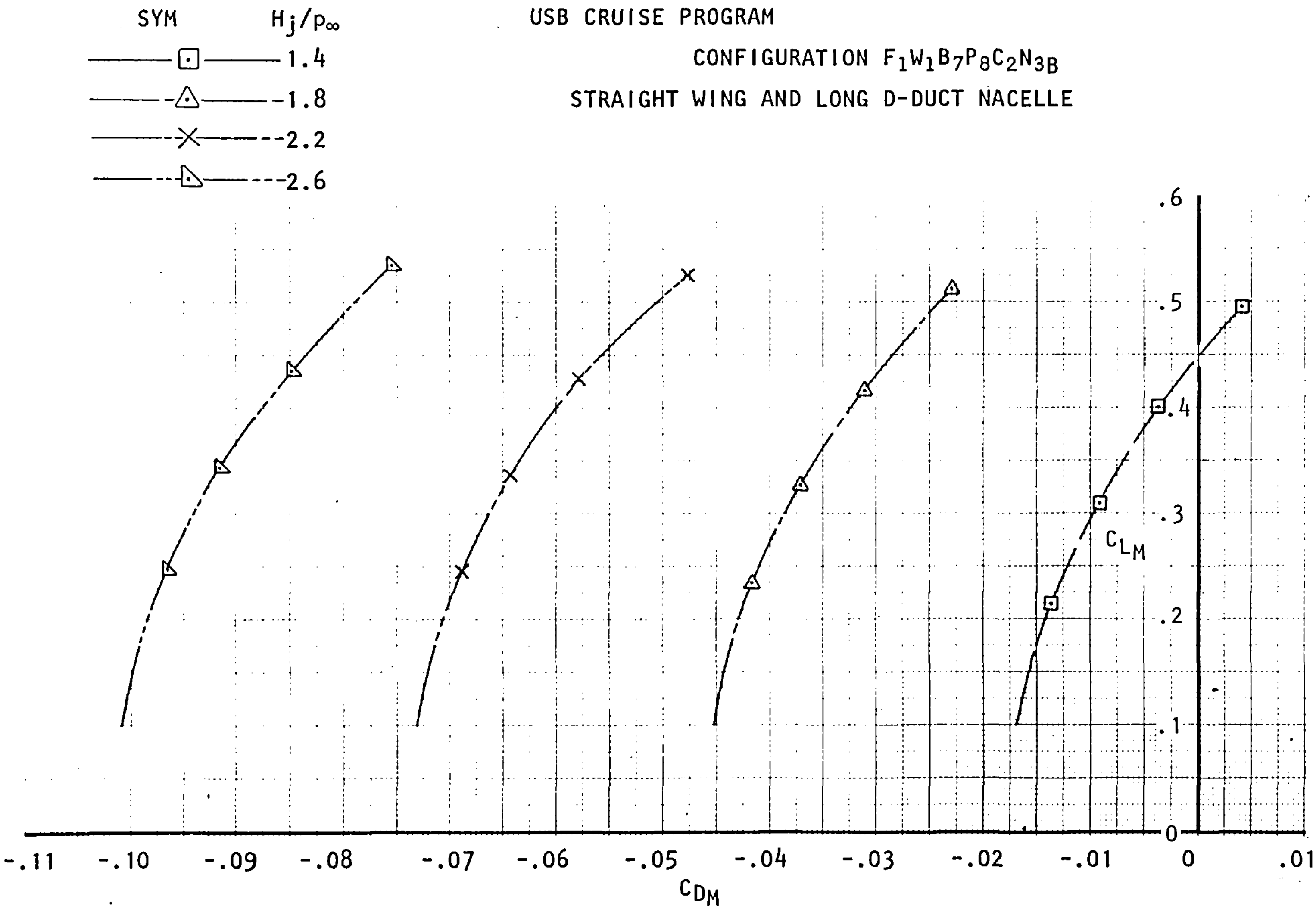

Figure 19. Variation of measured lift coefficient with measured drag coefficient and nozzle pressure ratio, $R_{NC} = 3.5 \times 10^6$, $M_\infty = 0.60$.

USB CRUISE PROGRAM

CONFIGURATION $F_1W_1B_7P_8C_2N_{3B}$

STRAIGHT WING AND LONG D-DUCT NACELLE

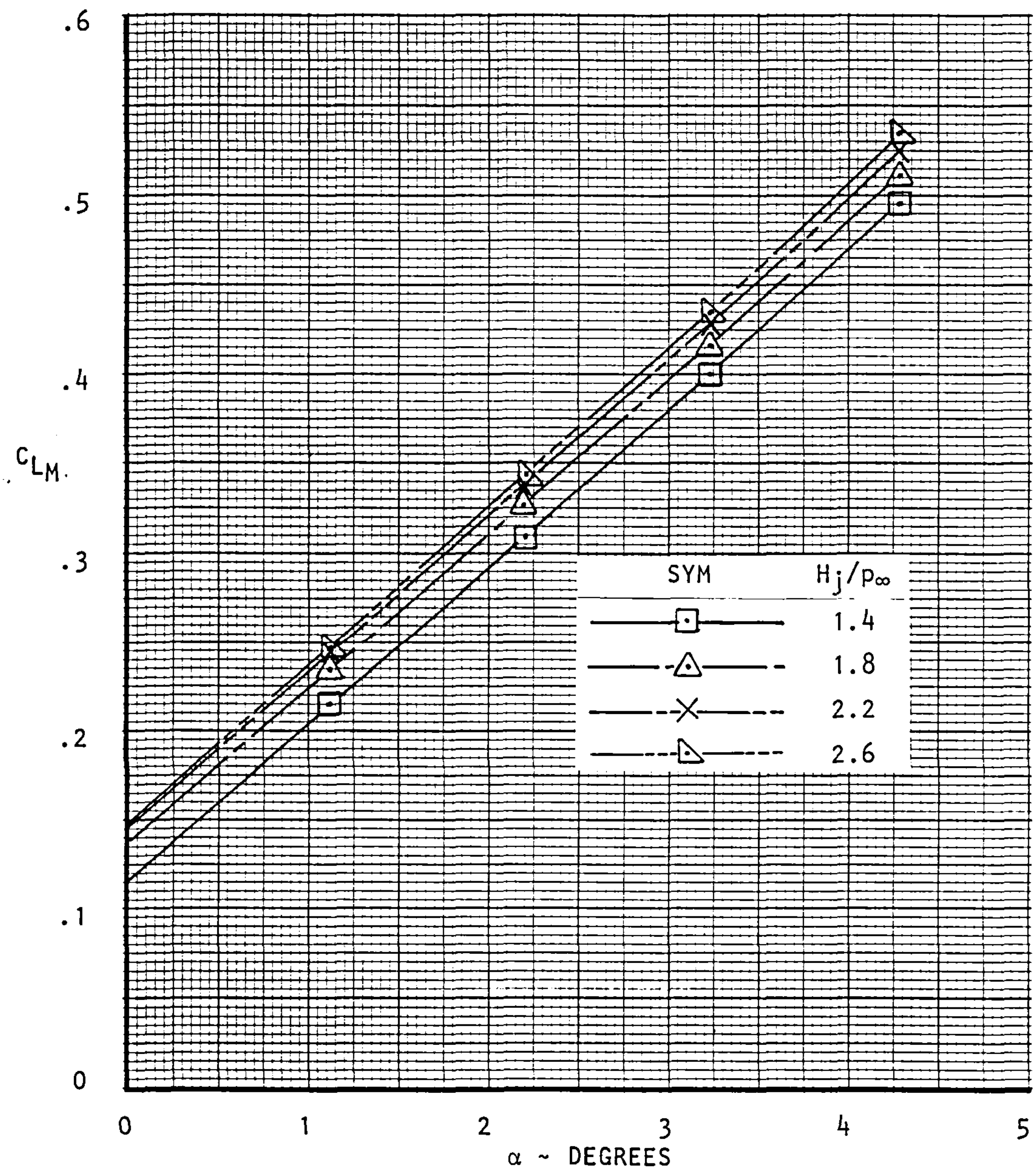

Figure 20. - Variation of measured lift coefficient with angle of attack, $R_{NC} = 3.5 \times 10^6$, $M_\infty = 0.60$.

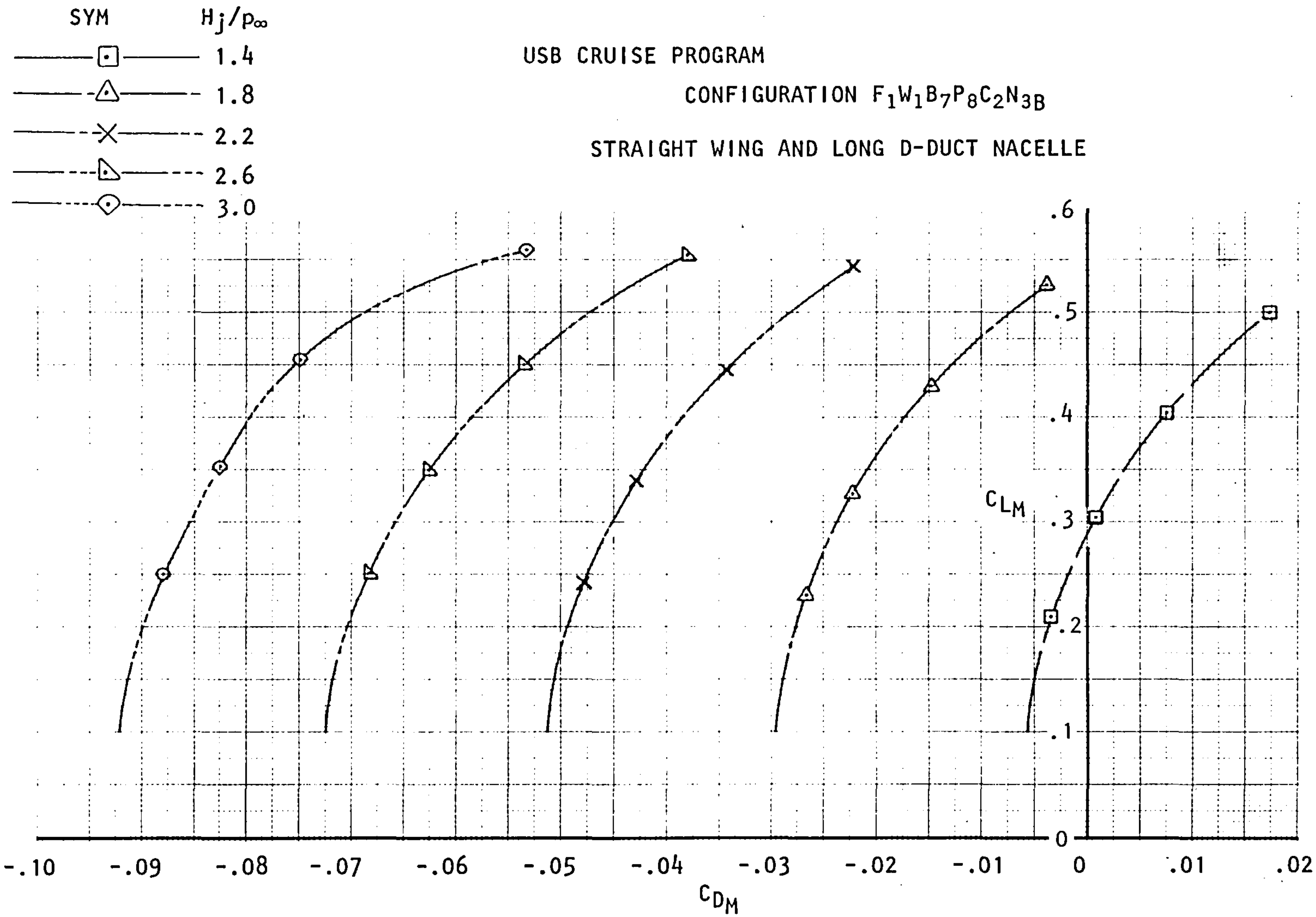

Figure 21. Variation of measured lift coefficient with measured drag coefficient and nozzle pressure ratio, $R_{NC} = 3.5 \times 10^6$, $M_\infty = 0.68$.

USB CRUISE PROGRAM

CONFIGURATION $F_1W_1B_7P_8C_2N_{3B}$

STRAIGHT WING AND LONG D-DUCT NACELLE

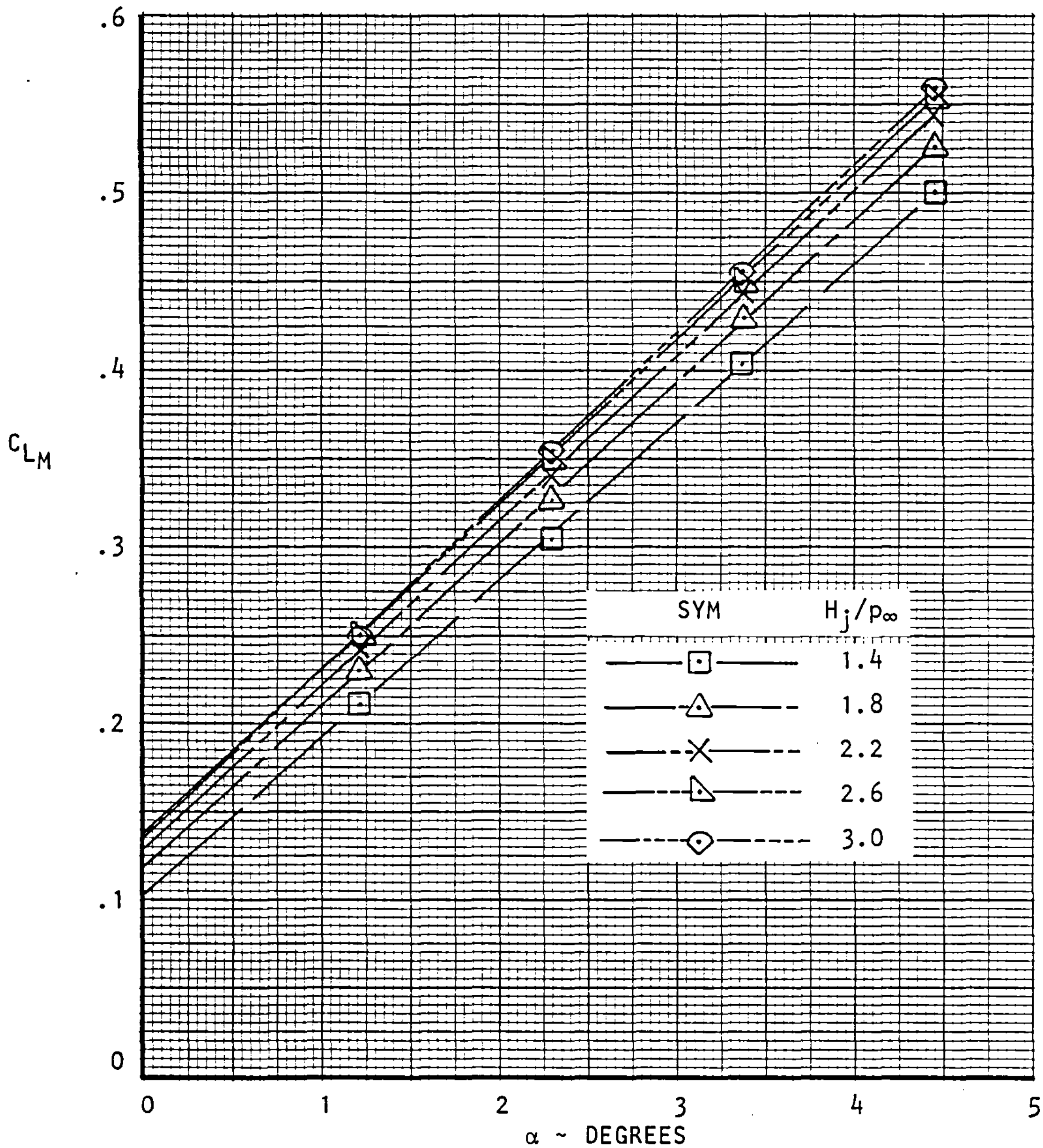

Figure 22. - Variation of measured lift coefficient with angle of attack, $R_{NC} = 3.5 \times 10^6$, $M_\infty = 0.68$.

USB CRUISE PROGRAM

CONFIGURATION $F_1W_1B_7P_8C_2N_{3B}$

STRAIGHT WING & LONG D-DUCT NACELLE

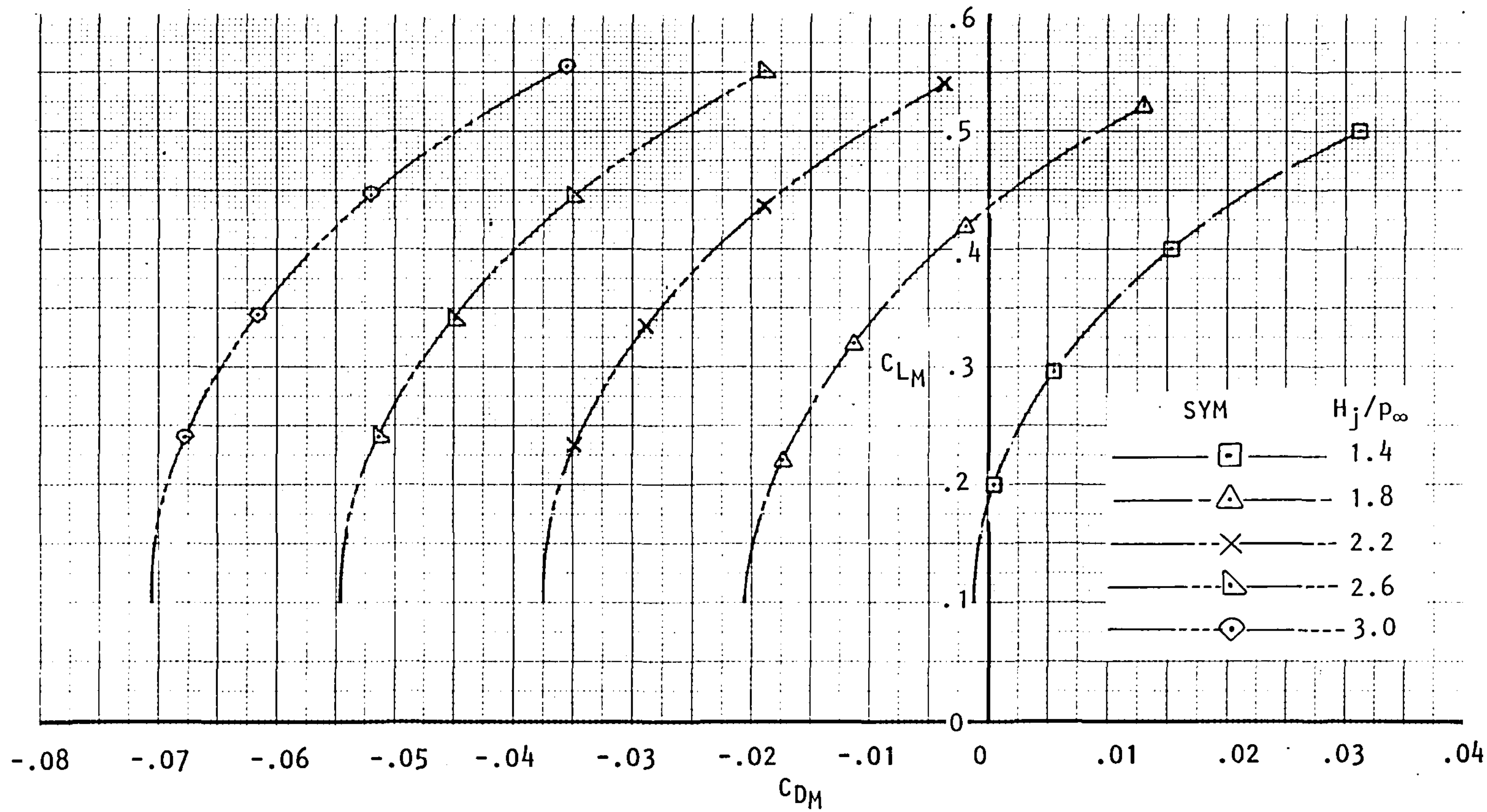

Figure 23. Variation of measured lift coefficient with measured drag coefficient. and nozzle pressure ratio, $R_{NC} = 3.5 \times 10^6$, $M_\infty = 0.72$.

USB CRUISE PROGRAM

CONFIGURATION $F_1W_1B_7P_8C_2N_{3B}$

STRAIGHT WING AND LONG D-DUCT NACELLE

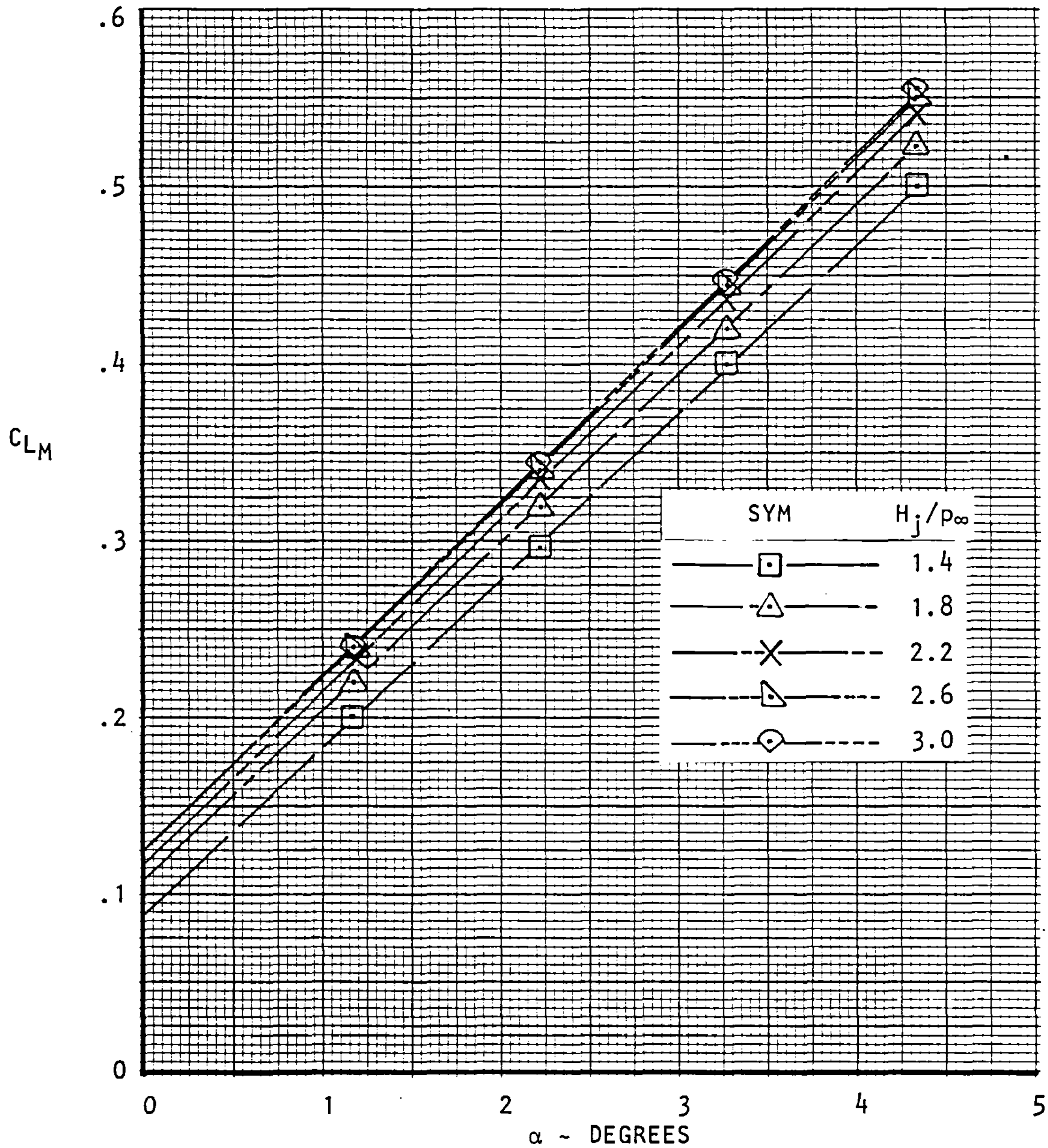

Figure 24. - Variation of measured lift coefficient with angle of attack, $R_{NC} = 3.5 \times 10^6$, $M_\infty = 0.72$.

USB CRUISE PROGRAM

CONFIGURATION $F_1W_1B_4P_7C_1N_{2E}$

STRAIGHT WING & SHORT CIRCULAR NACELLE @ x/c = 0.35

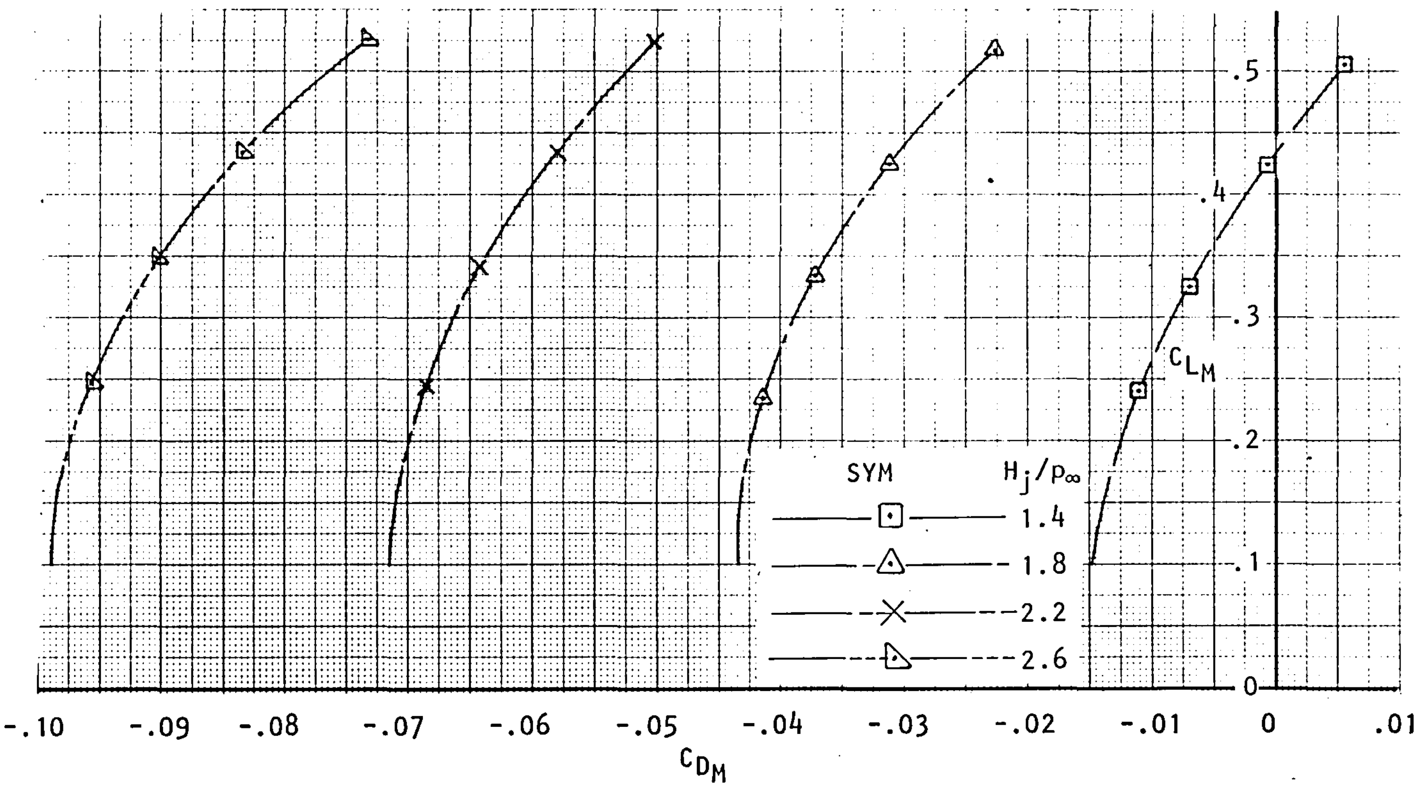

Figure 25. Variation of measured lift coefficient with measured drag coefficient and nozzle pressure ratio; $R_{NC} = 3.5 \times 10^6$, $M_\infty = 0.60$.

USB CRUISE PROGRAM

CONFIGURATION $F_1W_1B_4P_7C_1N_{2E}$

STRAIGHT WING AND SHORT CIRCULAR NACELLE @ x/c = 0.35

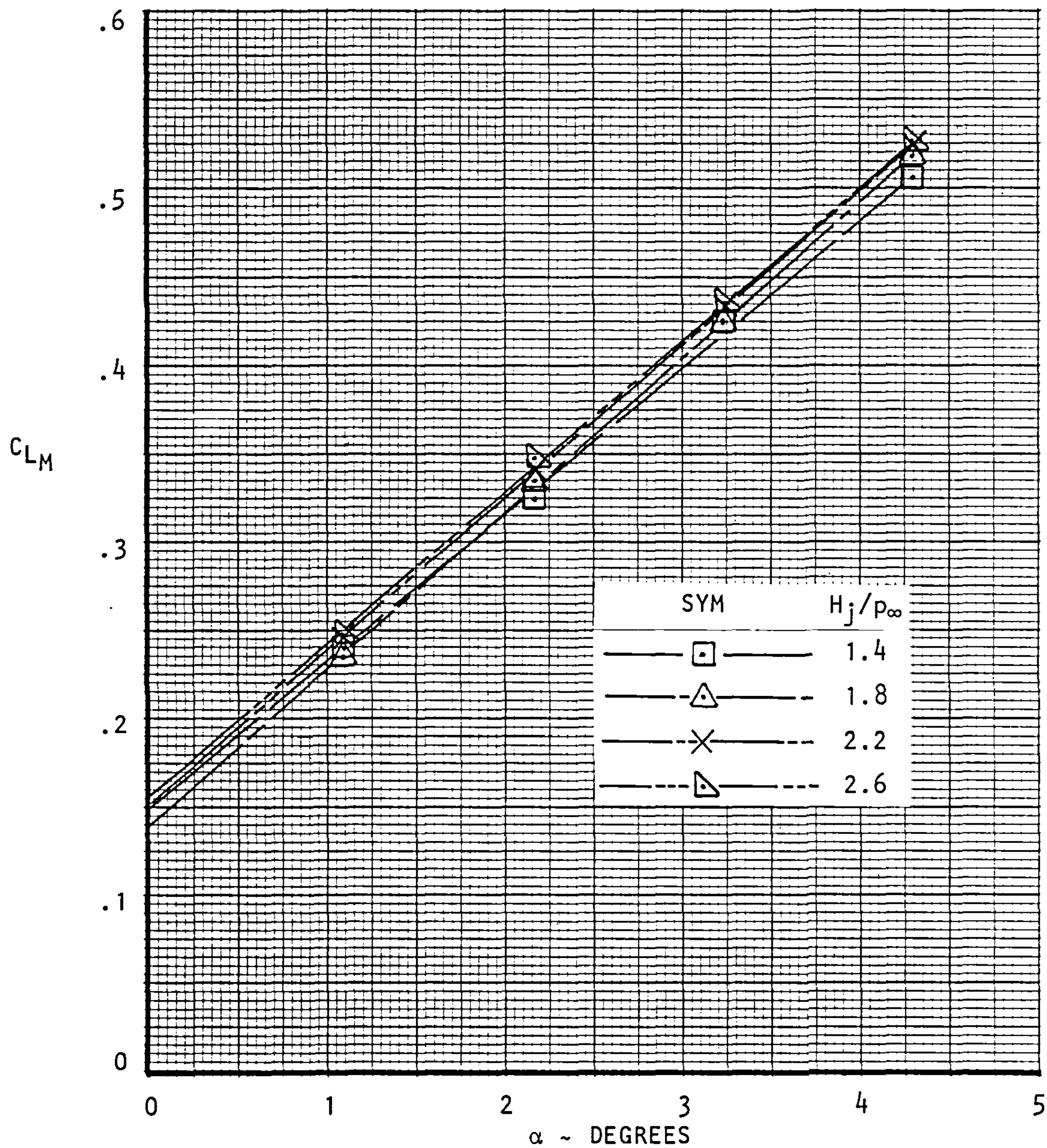

Figure 26. - Variation of measured lift coefficient with angle of attack, $R_{NC} = 3.5 \times 10^6$, $M_\infty = 0.60$.

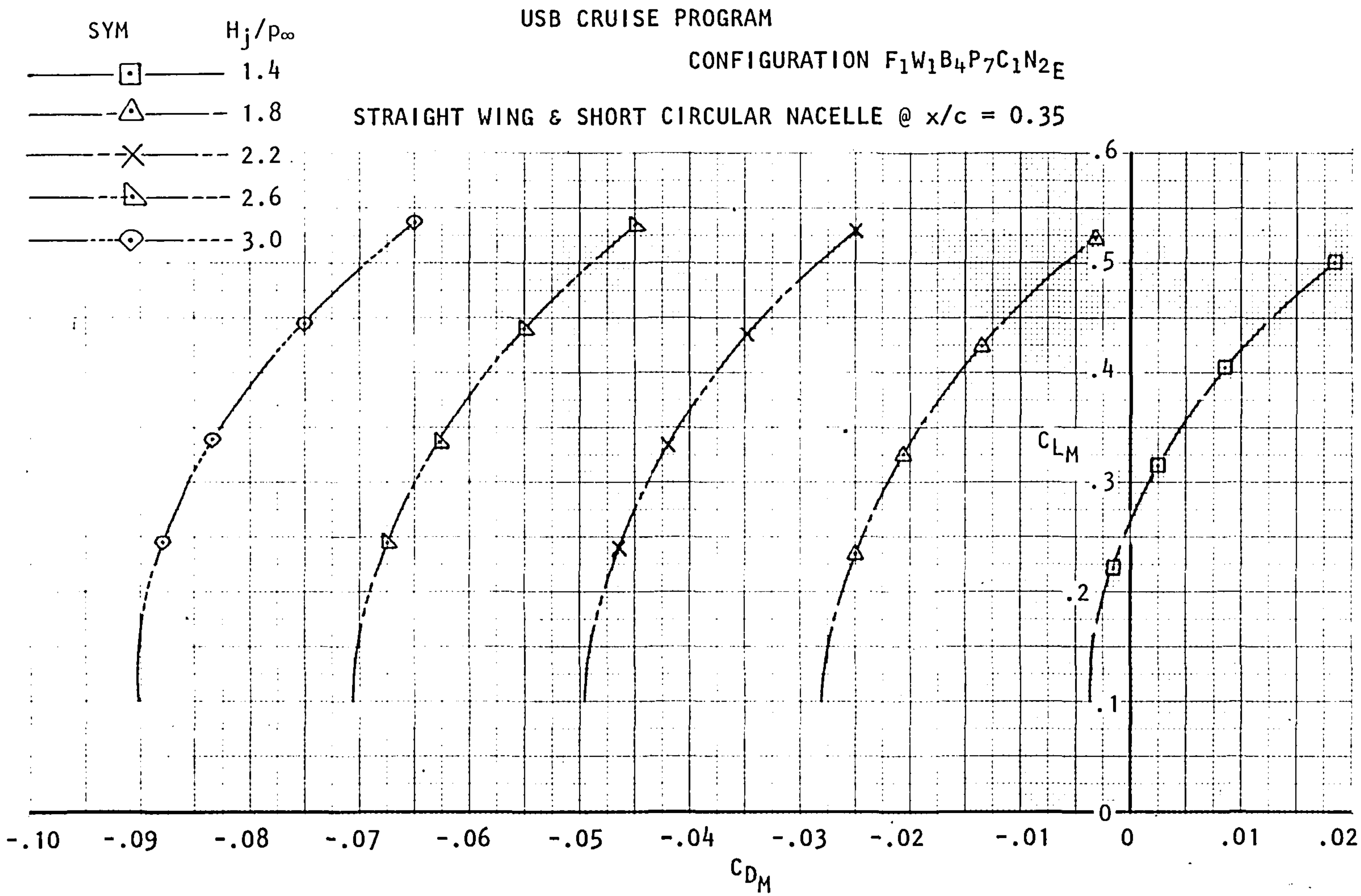

Figure 27. Variation of measured lift coefficient with measured drag coefficient and nozzle pressure ratio, $R_{NC} = 3.5 \times 10^6$, $M_\infty = 0.68$.

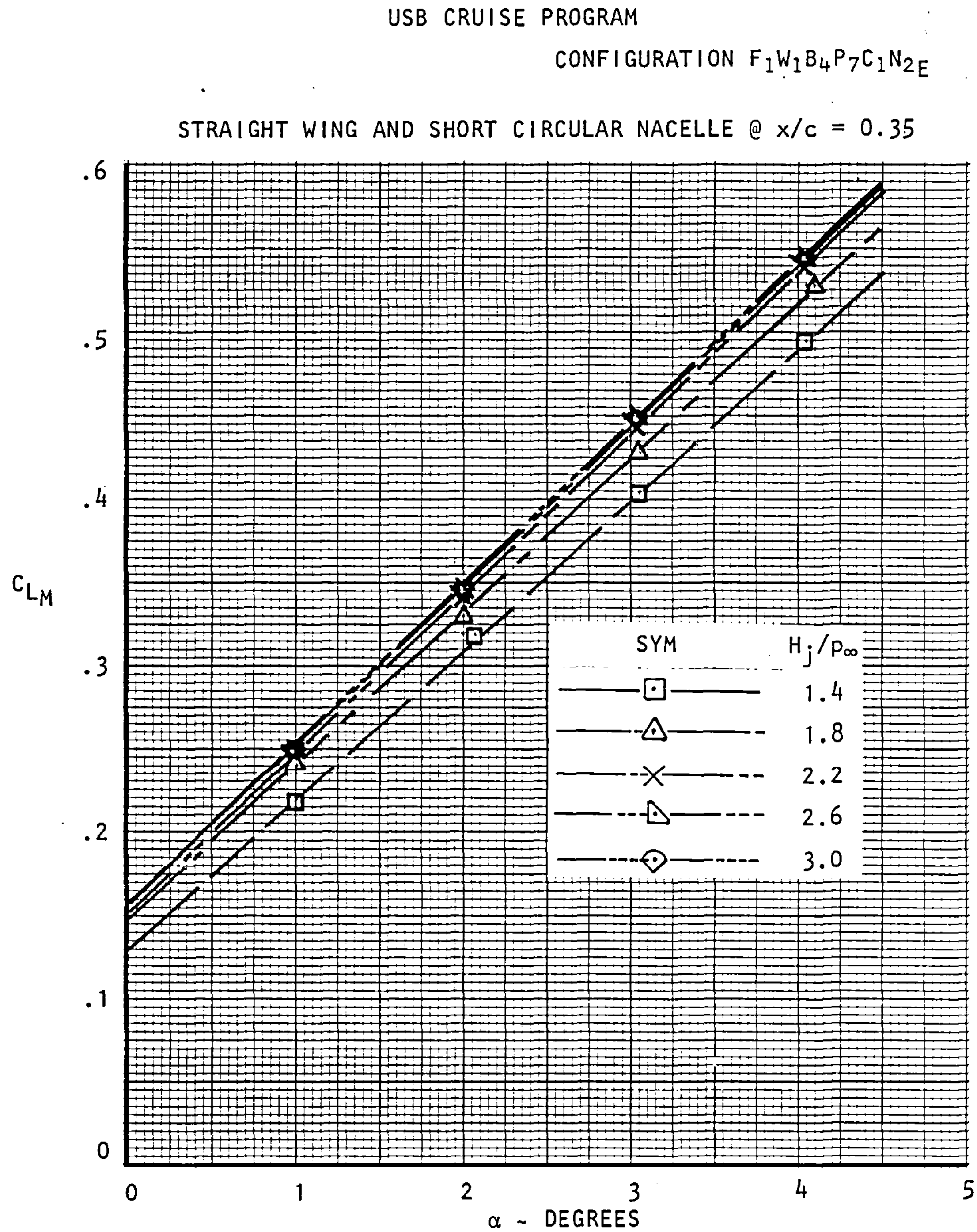

Figure 28. - Variation of measured lift coefficient with angle of attack, $R_{NC} = 3.5 \times 10^6$, $M_\infty = 0.68$.

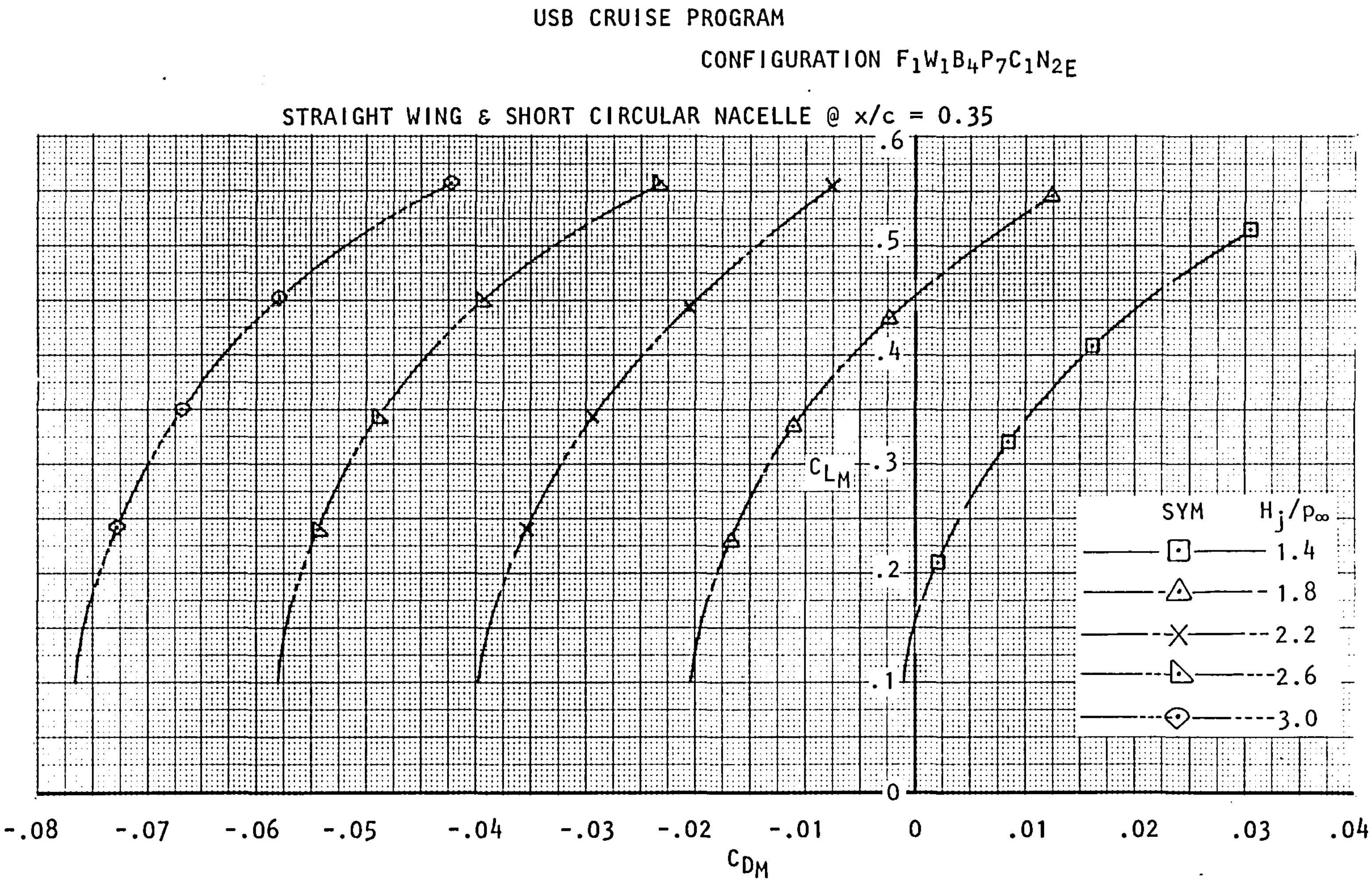

Figure 29. Variation of measured lift coefficient with measured drag coefficient and nozzle pressure ratio, $R_{NC} = 3.5 \times 10^6$, $M_\infty = 0.72$.

USB CRUISE PROGRAM

CONFIGURATION $F_1W_1B_4P_7C_1N_{2E}$

STRAIGHT WING AND SHORT CIRCULAR NACELLE @ x/c = 0.35

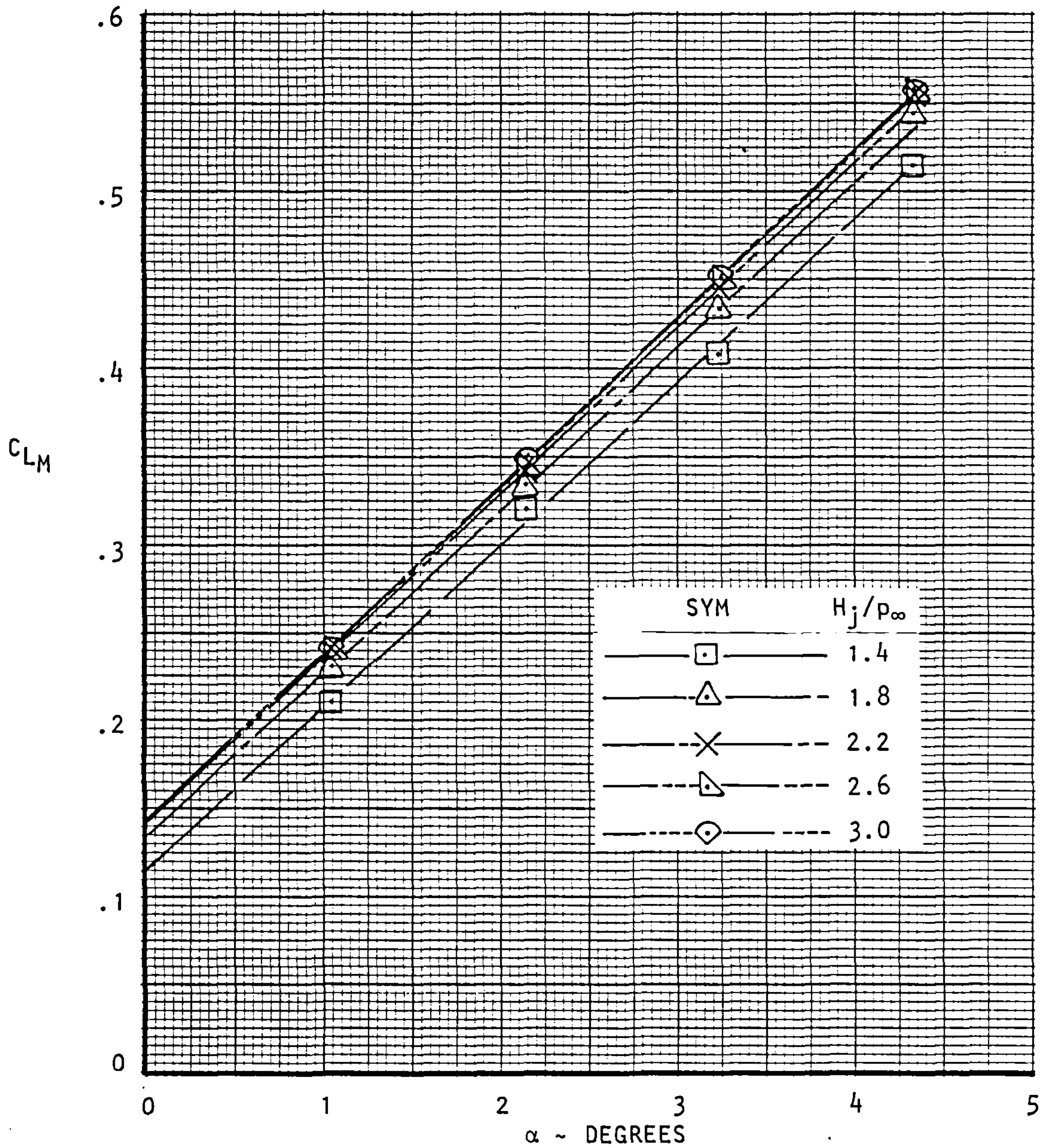

Figure 30. - Variation of measured lift coefficient with angle of attack, $R_{NC} = 3.5 \times 10^6$, $M_\infty = 0.72$.

USB CRUISE PROGRAM

CONFIGURATION $F_1W_1B_4P_7C_1N_4E$

STRAIGHT WING & SHORT AR4 NACELLE

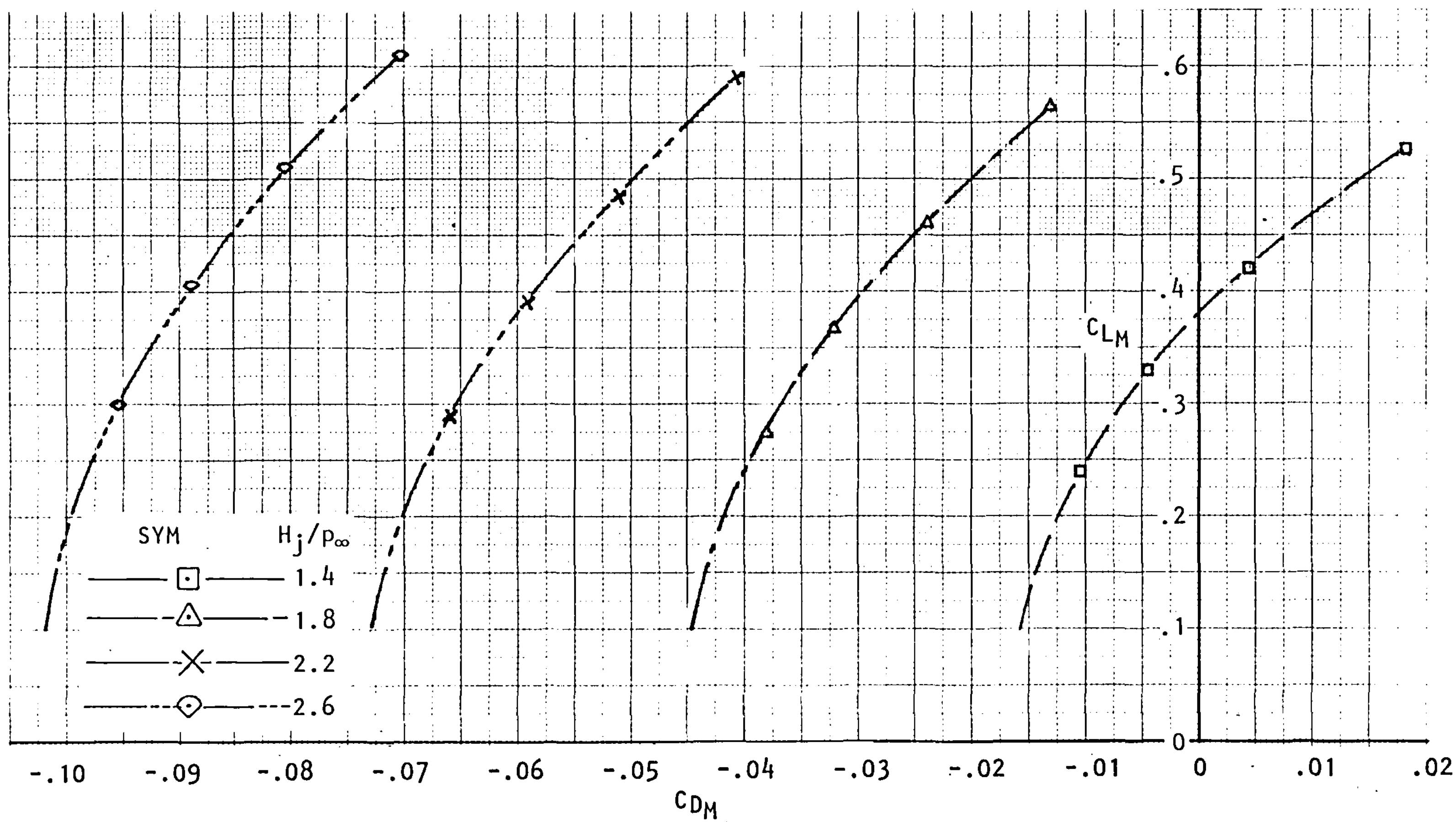

Figure 31. Variation of measured lift coefficient with measured drag coefficient and nozzle pressure ratio, $R_{NC} = 3.5 \times 10^6$, $M_\infty = 0.60$.

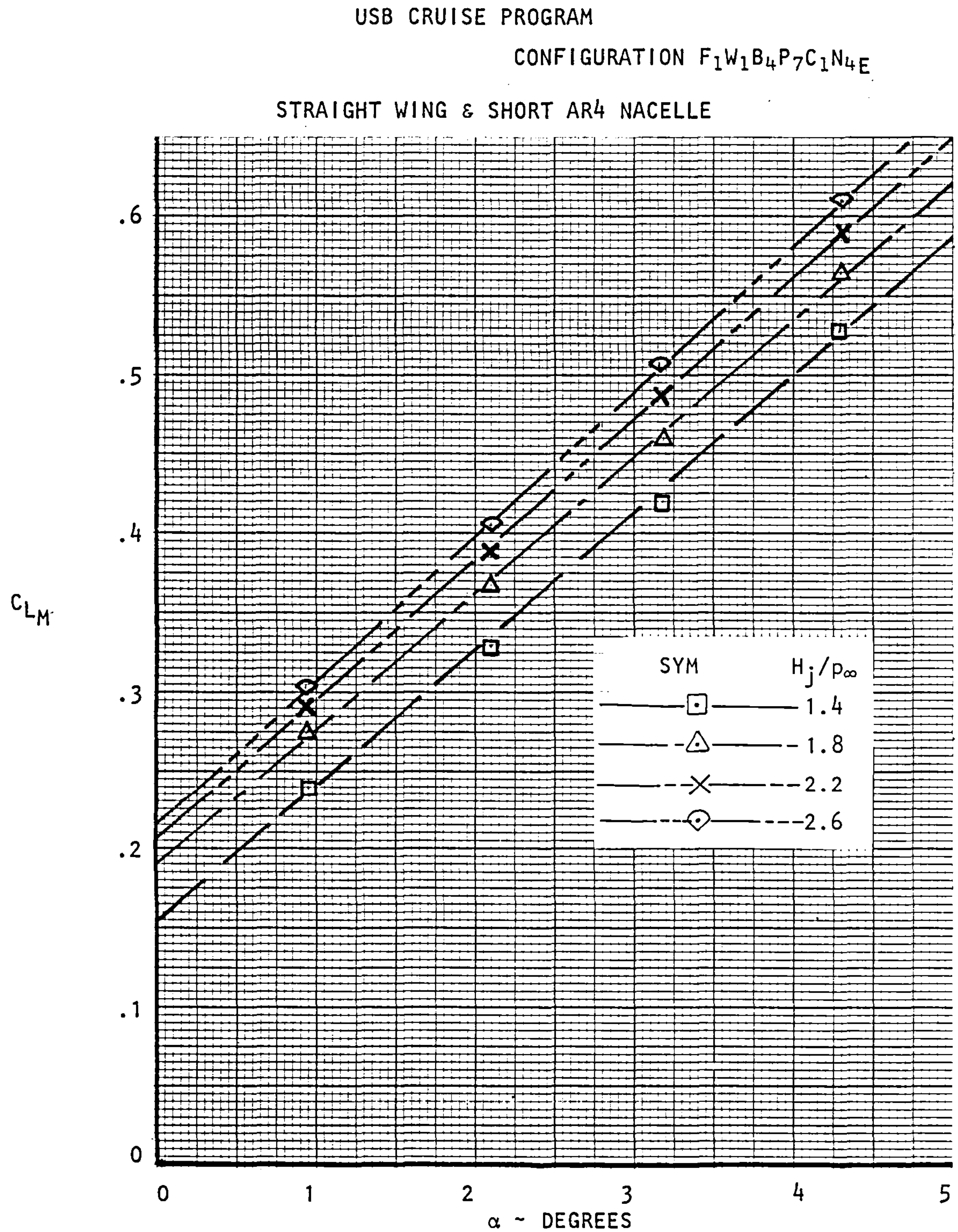

Figure 32. Variation of measured lift coefficient with angle of attack, $R_{NC} = 3.5 \times 10^6$, $M_\infty = 0.60$.

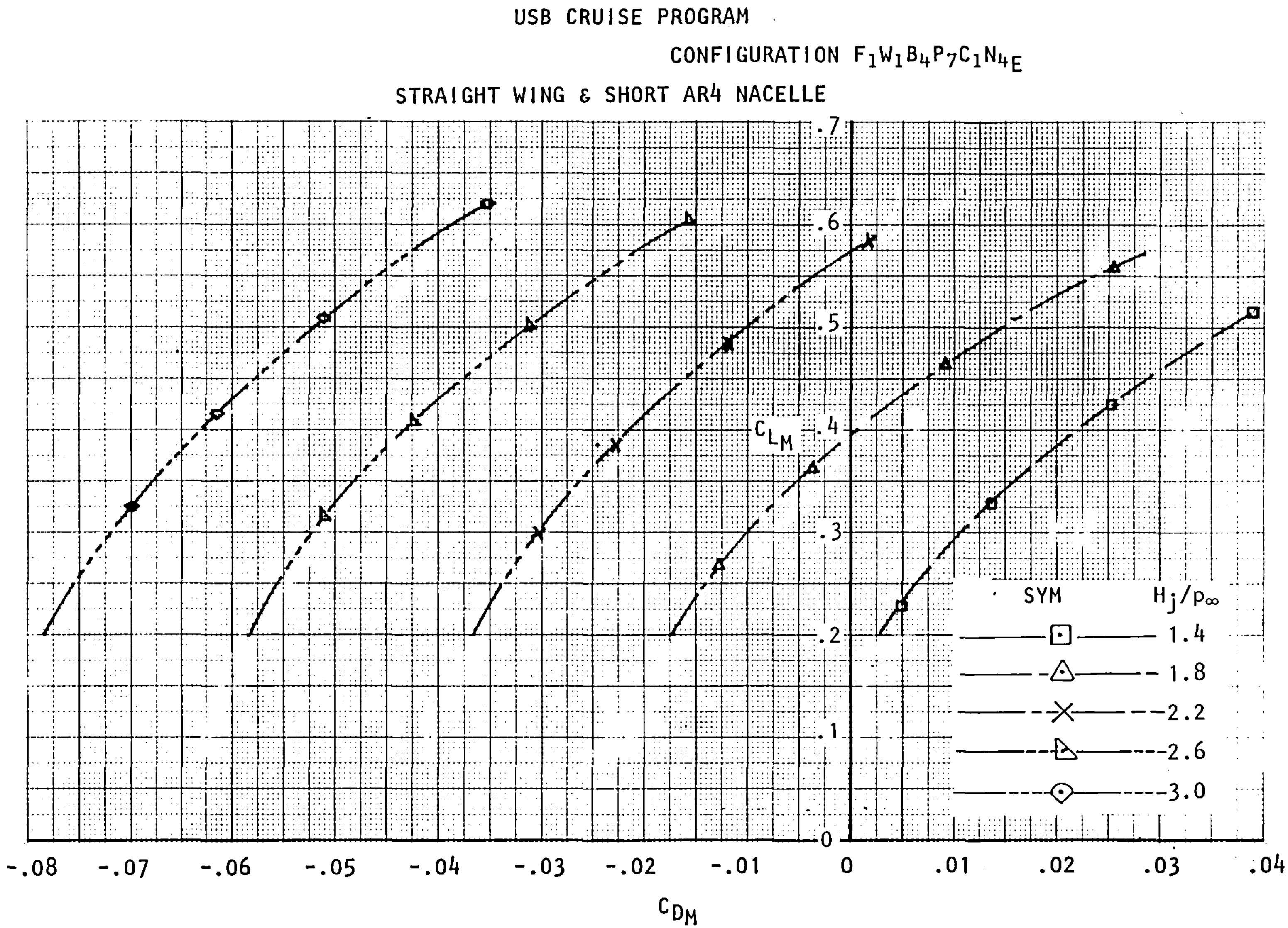

Figure 33. Variation of measured lift coefficient with measured drag coefficient and nozzle pressure ratio, $R_{NC} = 3.5 \times 10^6$, $M_\infty = 0.72$.

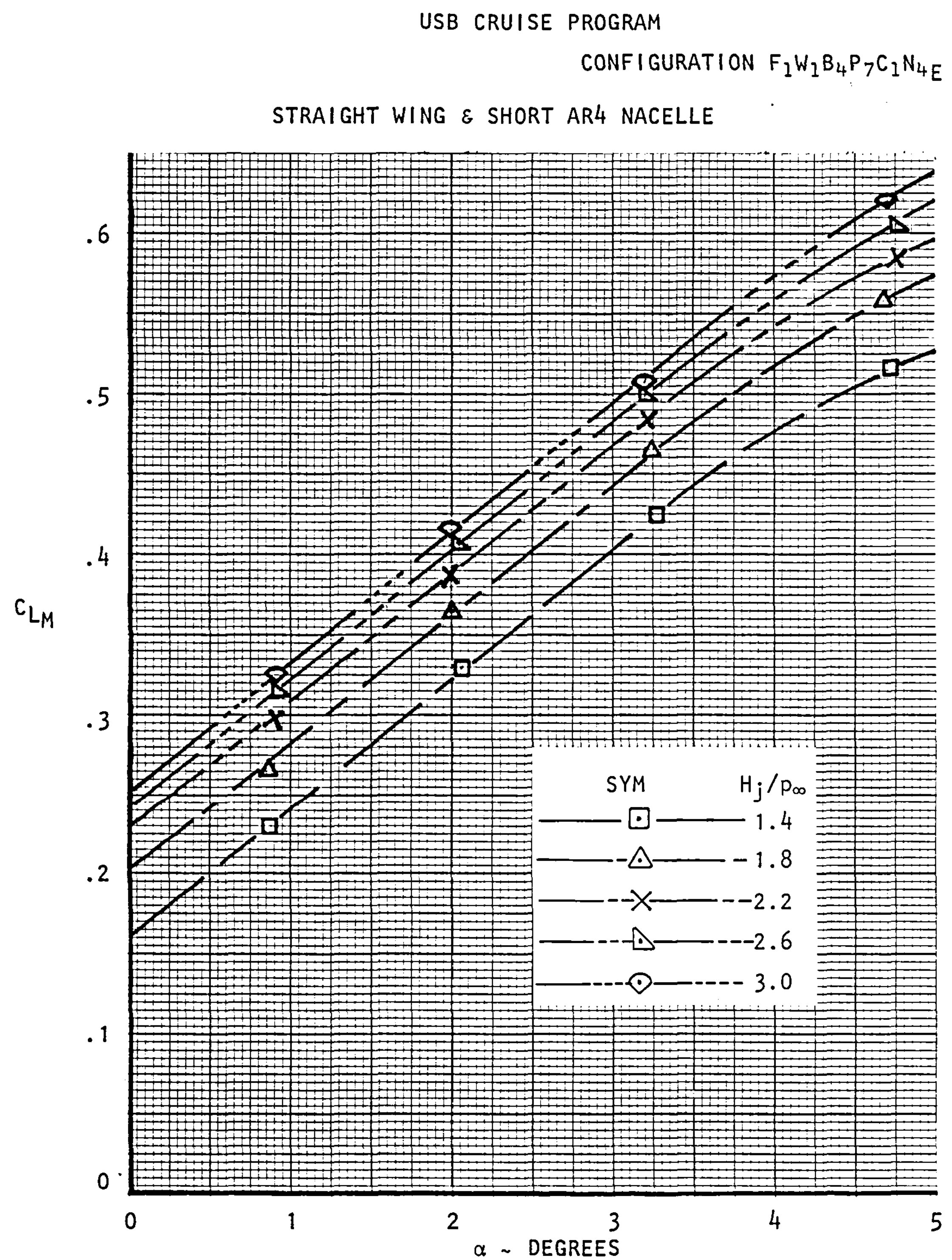

Figure 34. Variation of measured lift coefficient with angle of attack, $R_{NC} = 3.5 \times 10^6$, $M_\infty = 0.72$.

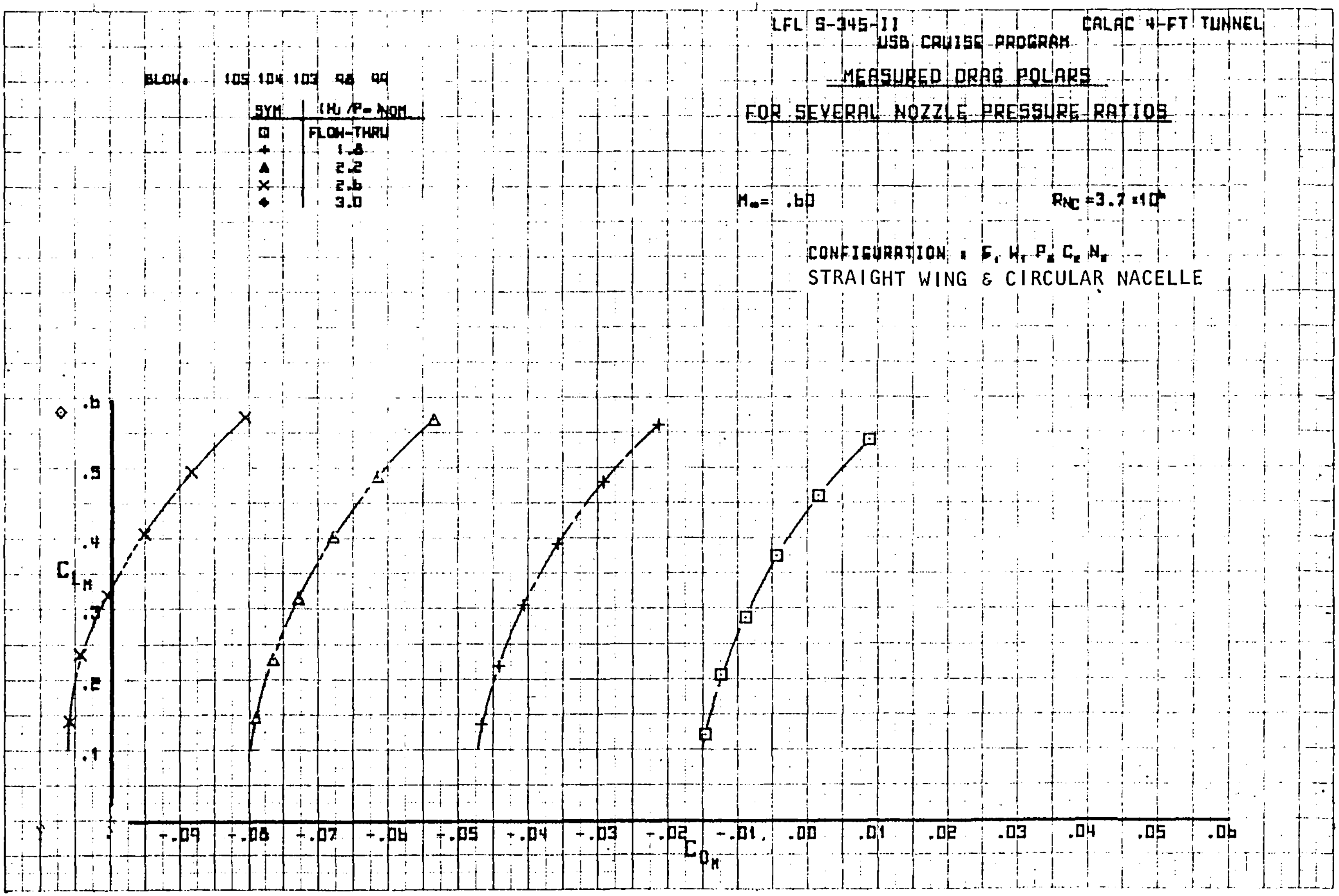

Figure 35. Variation of measured lift coefficient with measured drag coefficient and nozzle pressure ratio, $M_\infty = 0.60$.

USB CRUISE PROGRAM

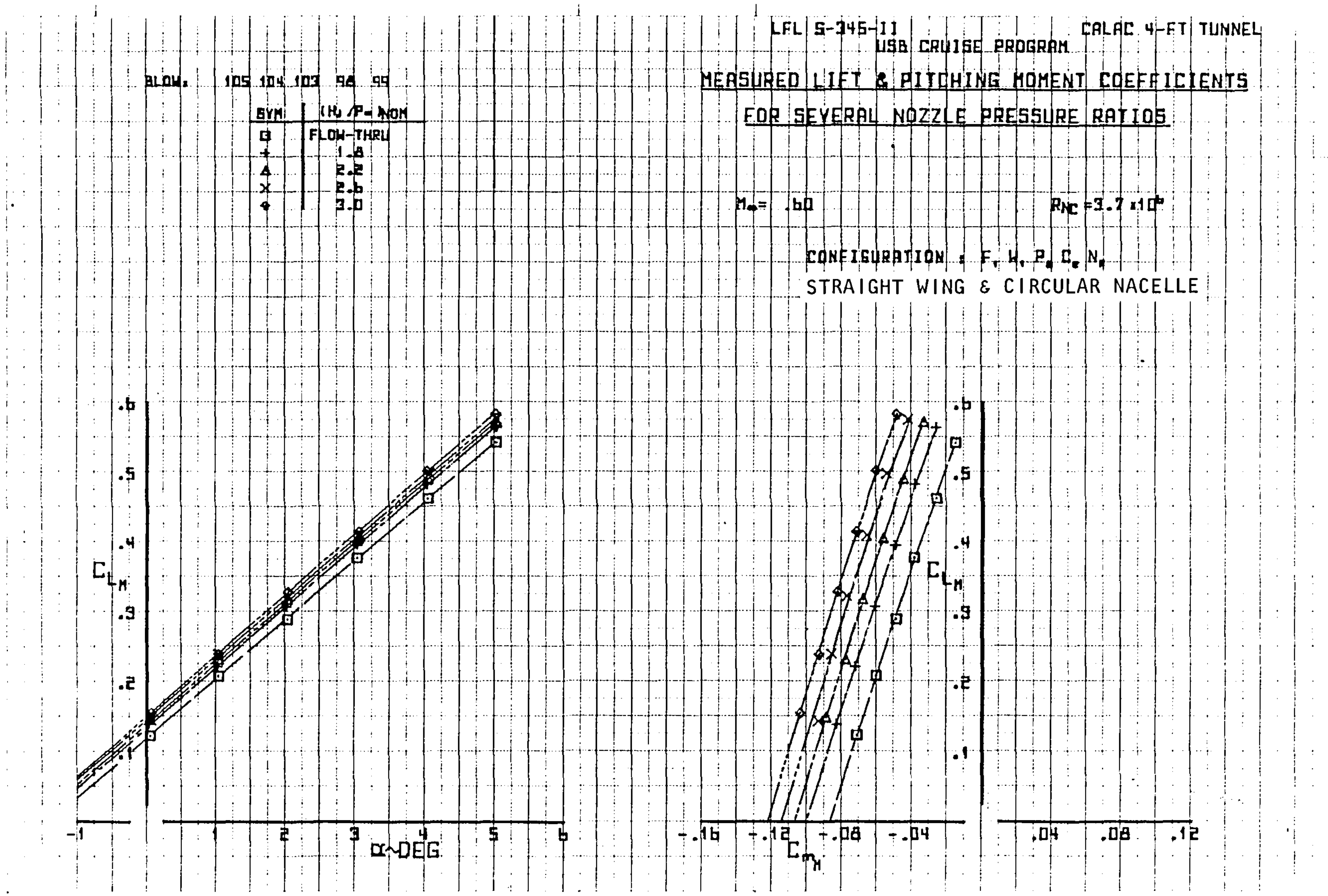

Figure 36. Variation of measured lift coefficient with angle of attack and moment coefficient, $M_\infty = 0.60$.

USB CRUISE PROGRAM

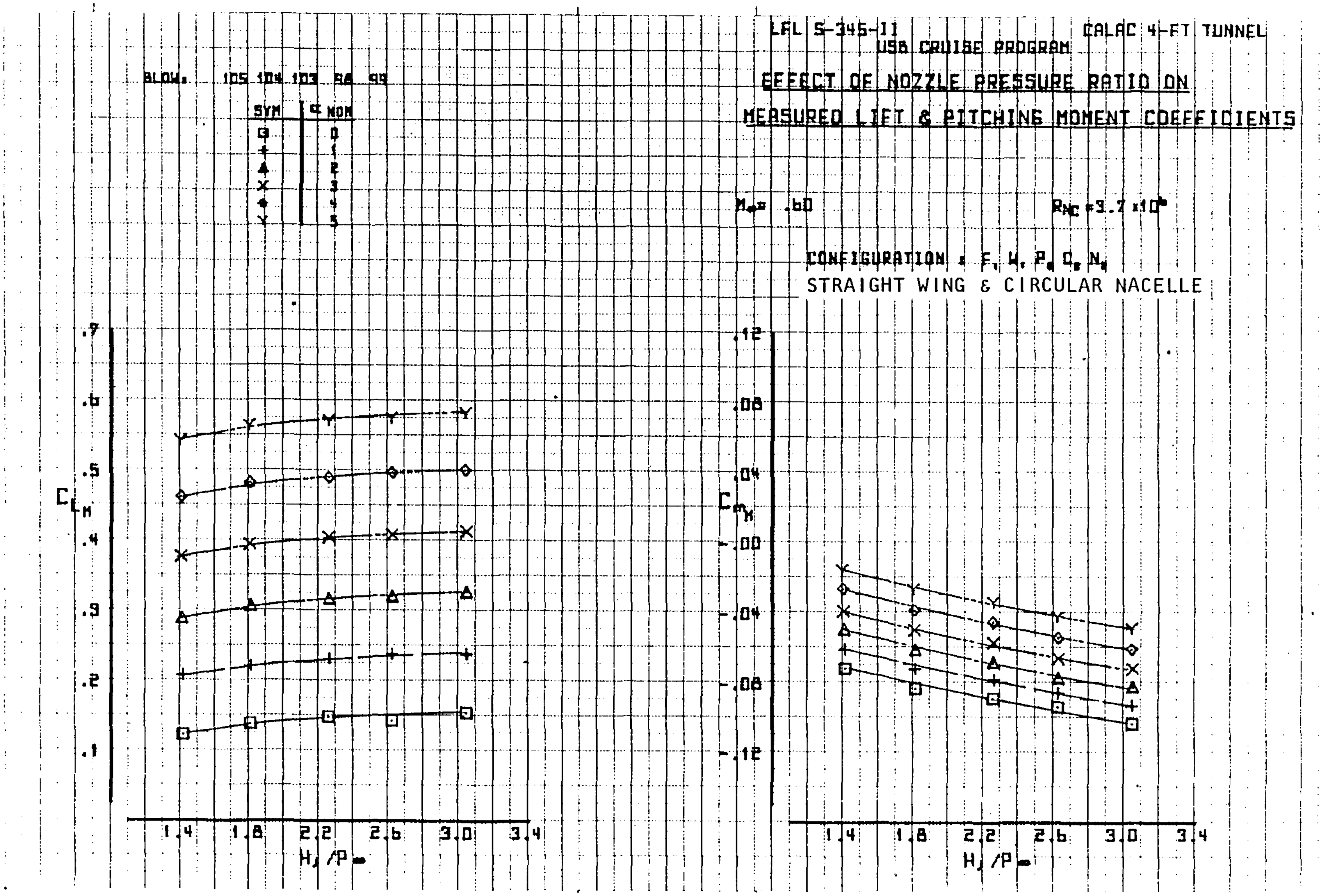

Figure 37. Variation of lift coefficient and moment coefficient with nozzle pressure ratio, $M_\infty = 0.60$.

USB CRUISE PROGRAM

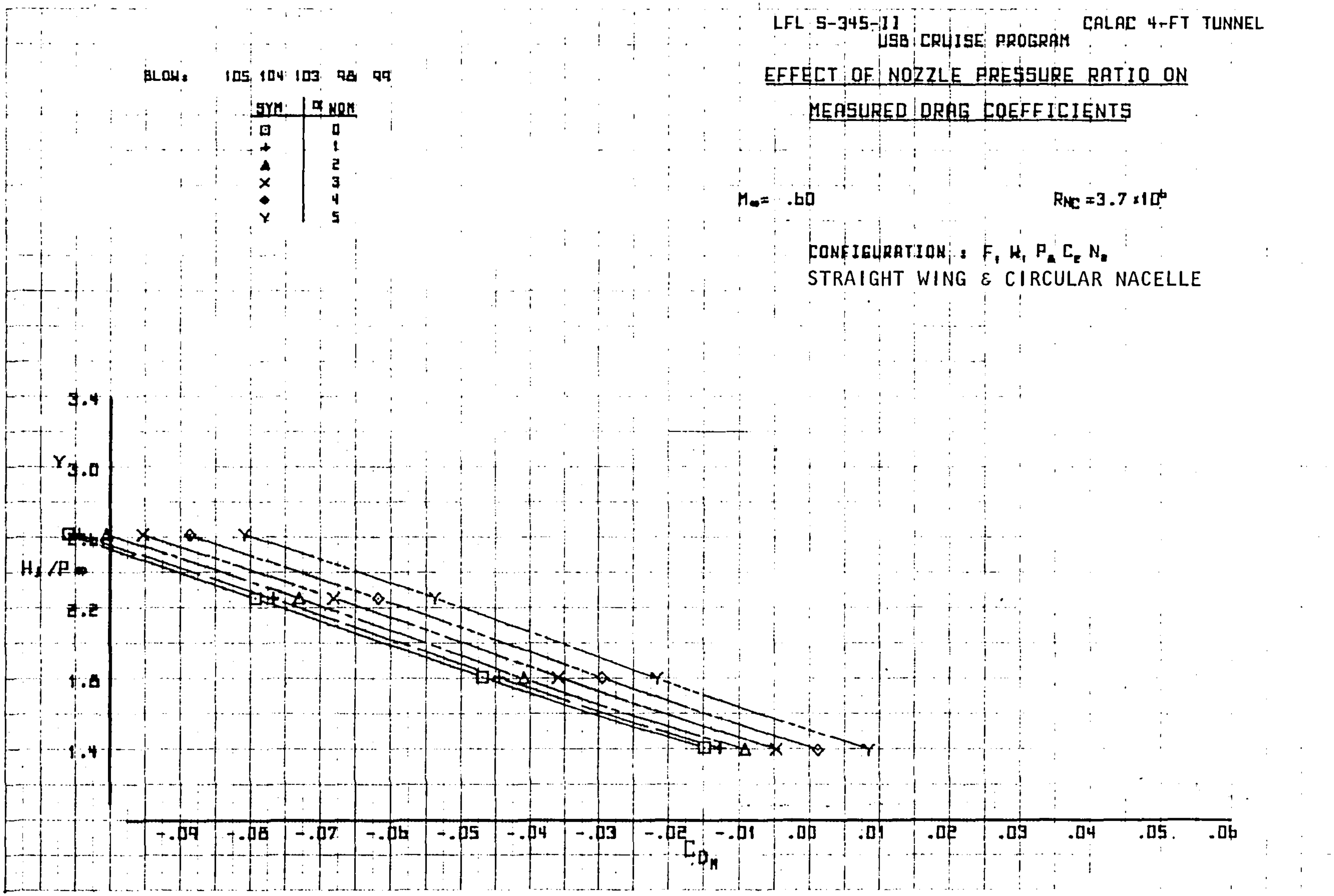

Figure 38. Variation of measured drag coefficient with nozzle pressure ratio, $M_\infty = 0.60$.

USB CRUISE PROGRAM

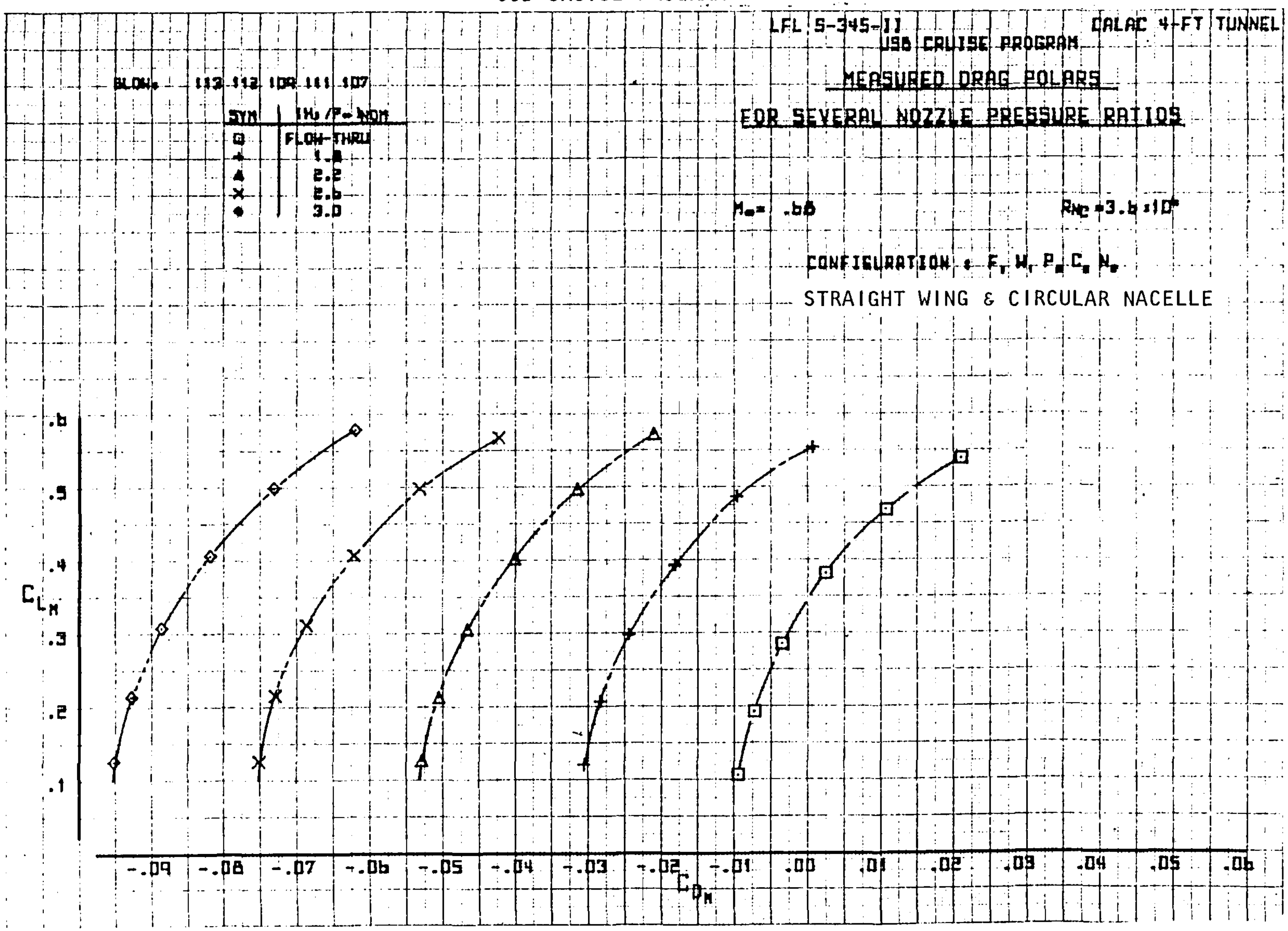

Figure 39. Variation of measured lift coefficient with measured drag coefficient and nozzle pressure ratio, $M_\infty = 0.68$.

USB CRUISE PROGRAM

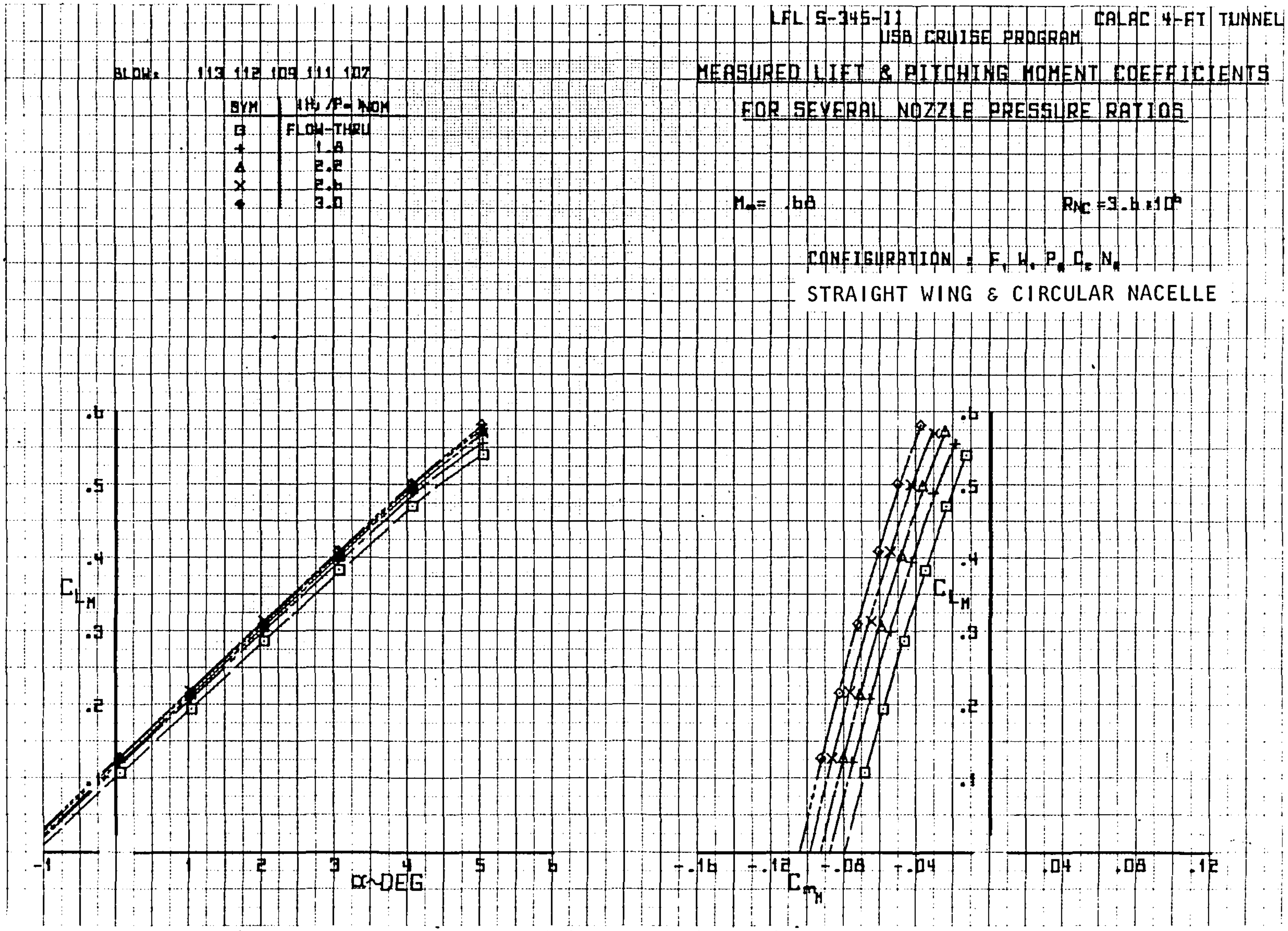

Figure 40. Variation of measured lift coefficient with angle of attack and moment coefficient, $M_\infty = 0.68$.

USB CRUISE PROGRAM

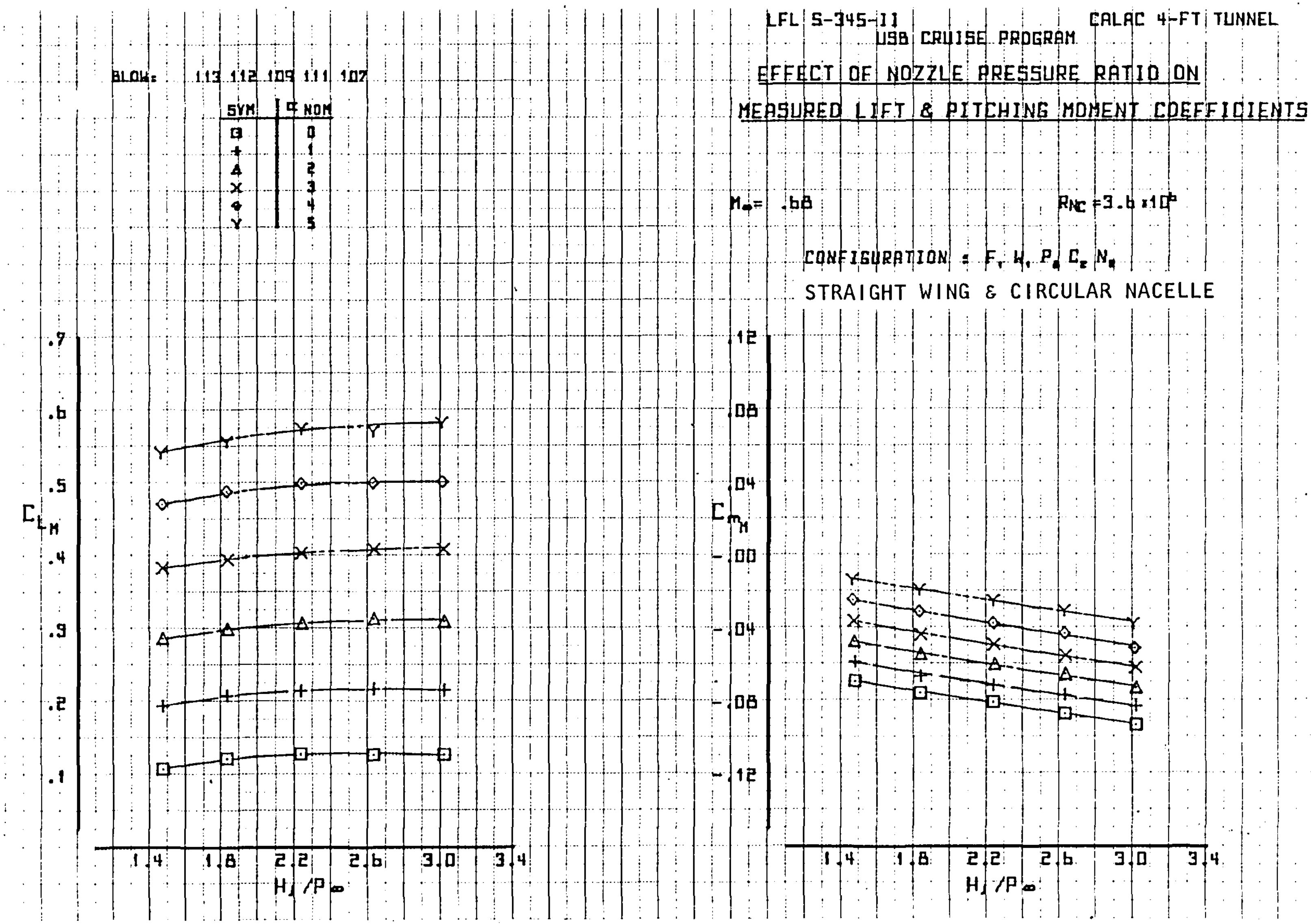

Figure 41. Variation of lift coefficient and moment coefficient with nozzle pressure ratio, M∞ = 0.68.

USB CRUISE PROGRAM

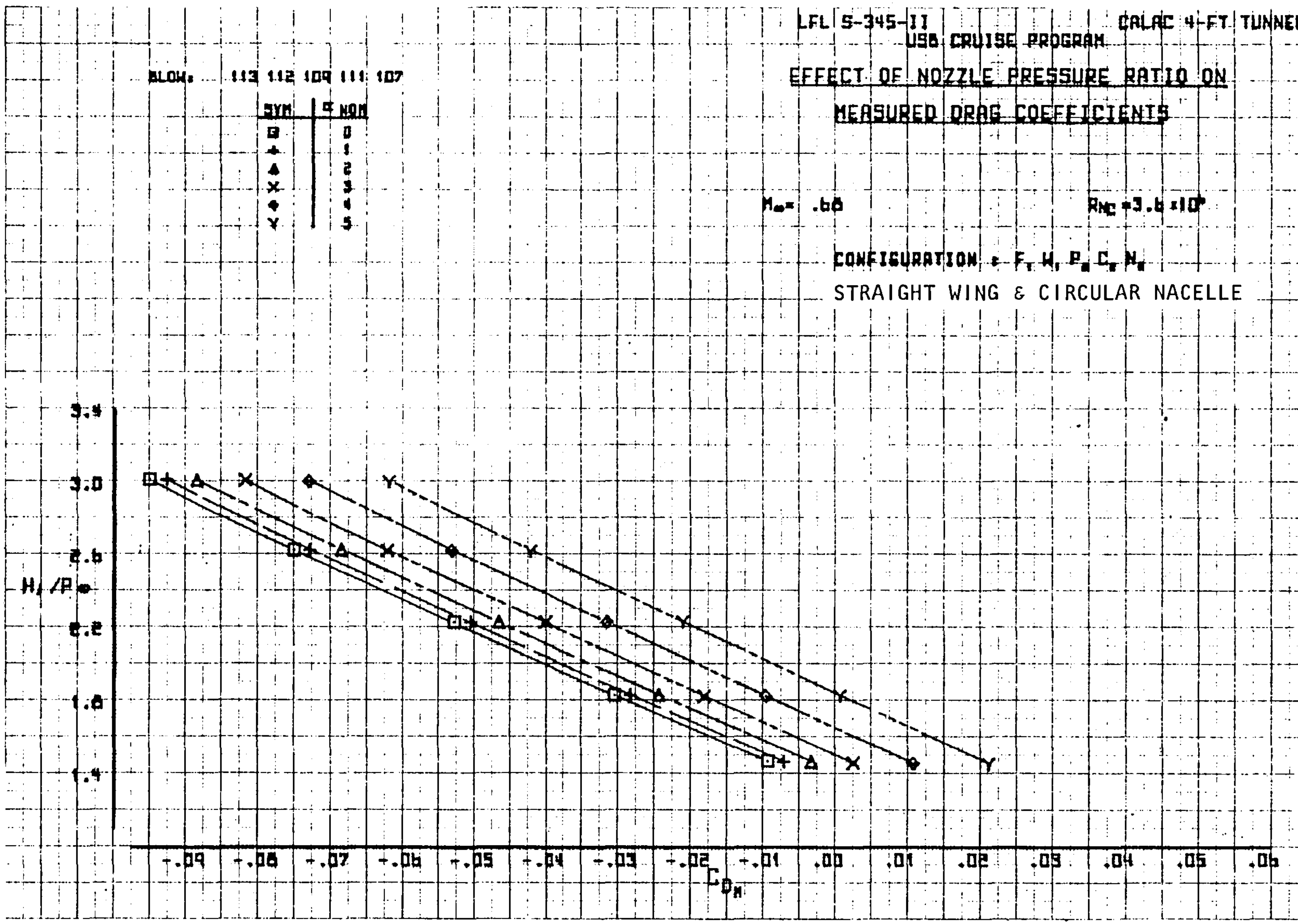

Figure 42. Variation of measured drag coefficient with nozzle pressure ratio, M_∞ = 0.68.

USB CRUISE PROGRAM

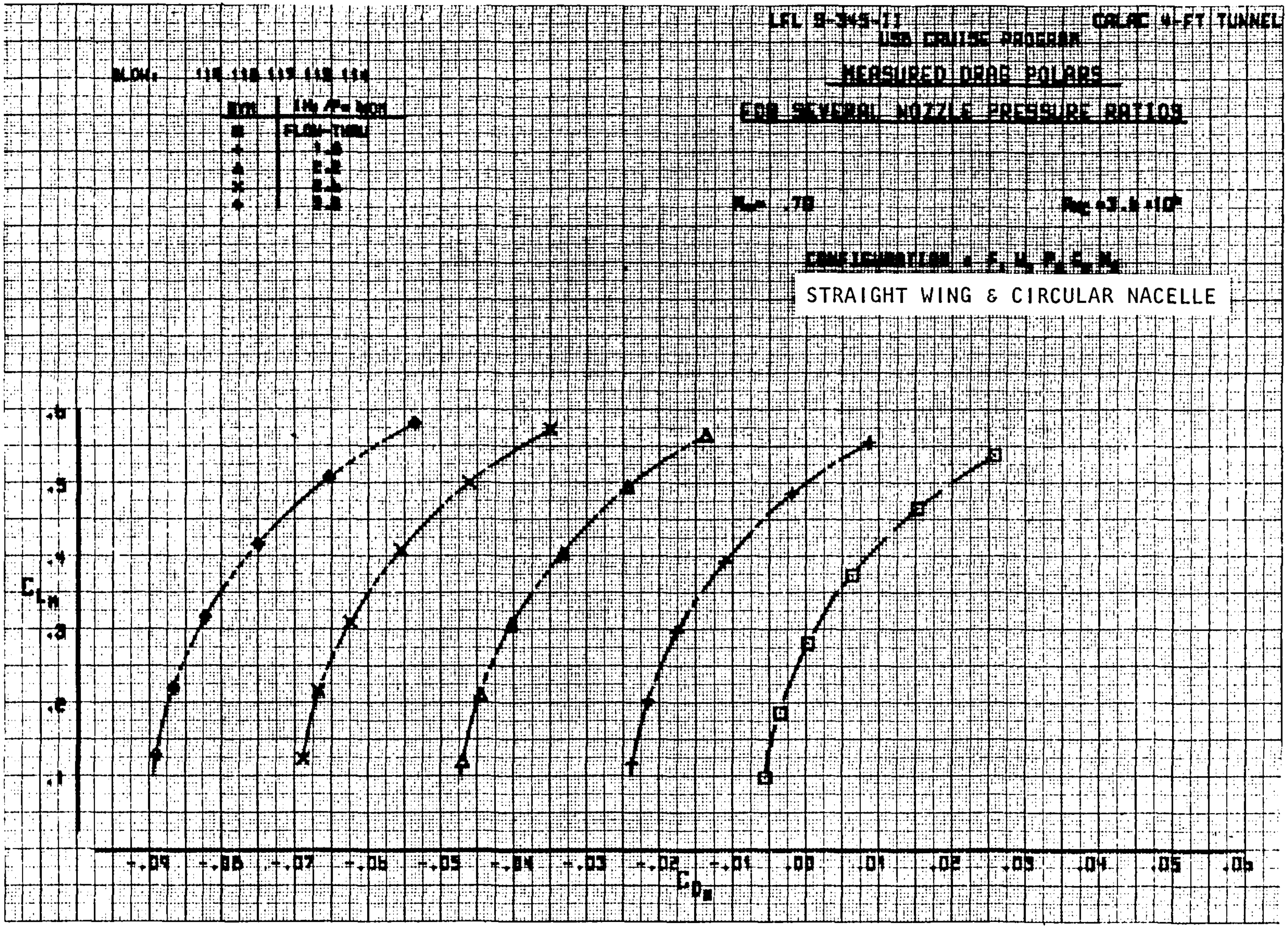

Figure 43. Variation of measured lift coefficient with measured drag coefficient and nozzle pressure ratio, $M_\infty = 0.70$.

USB CRUISE PROGRAM

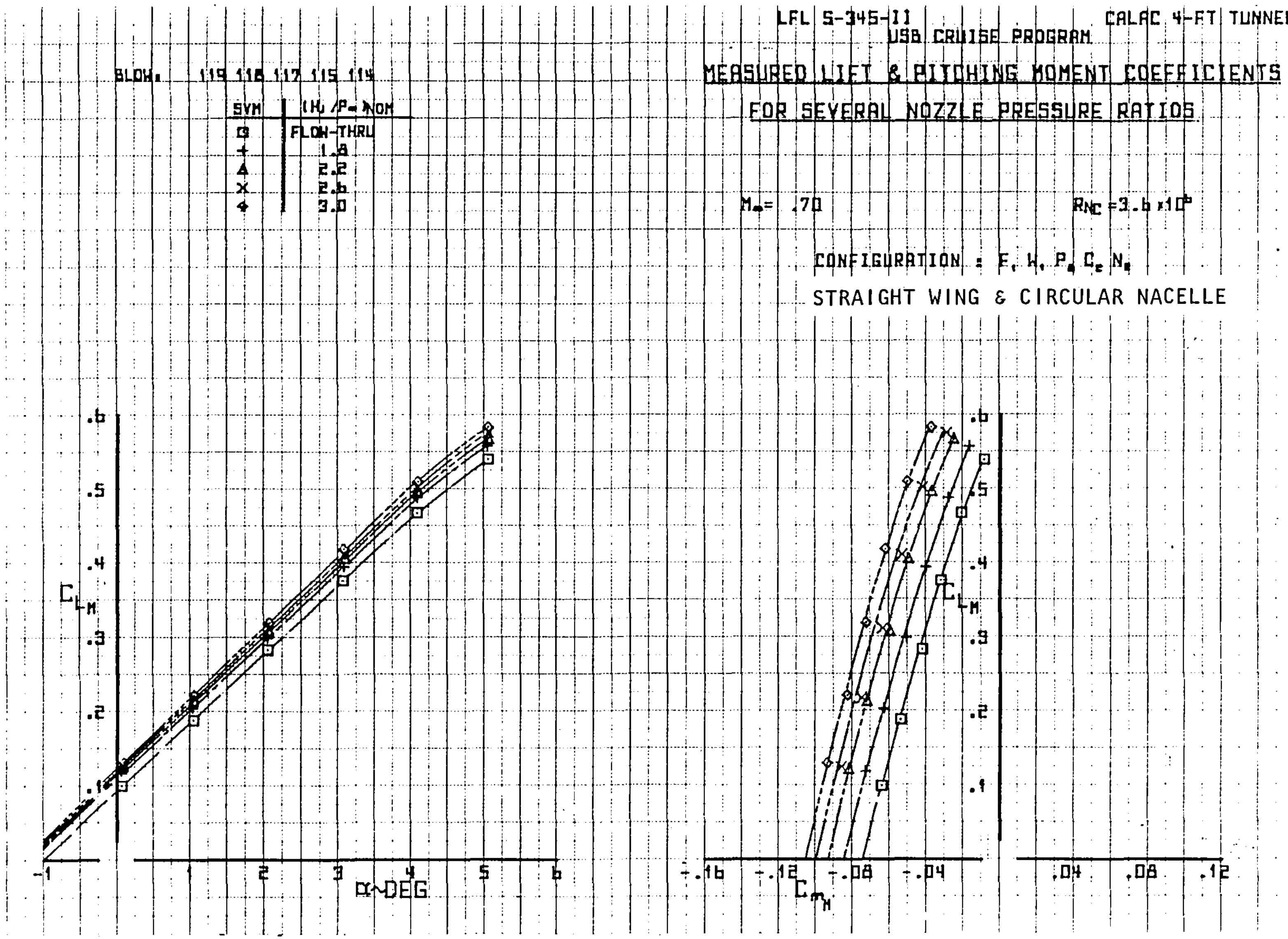

Figure 44. Variation of measured lift coefficient with angle of attack and moment coefficient, $M_\infty = 0.70$.

USB CRUISE PROGRAM

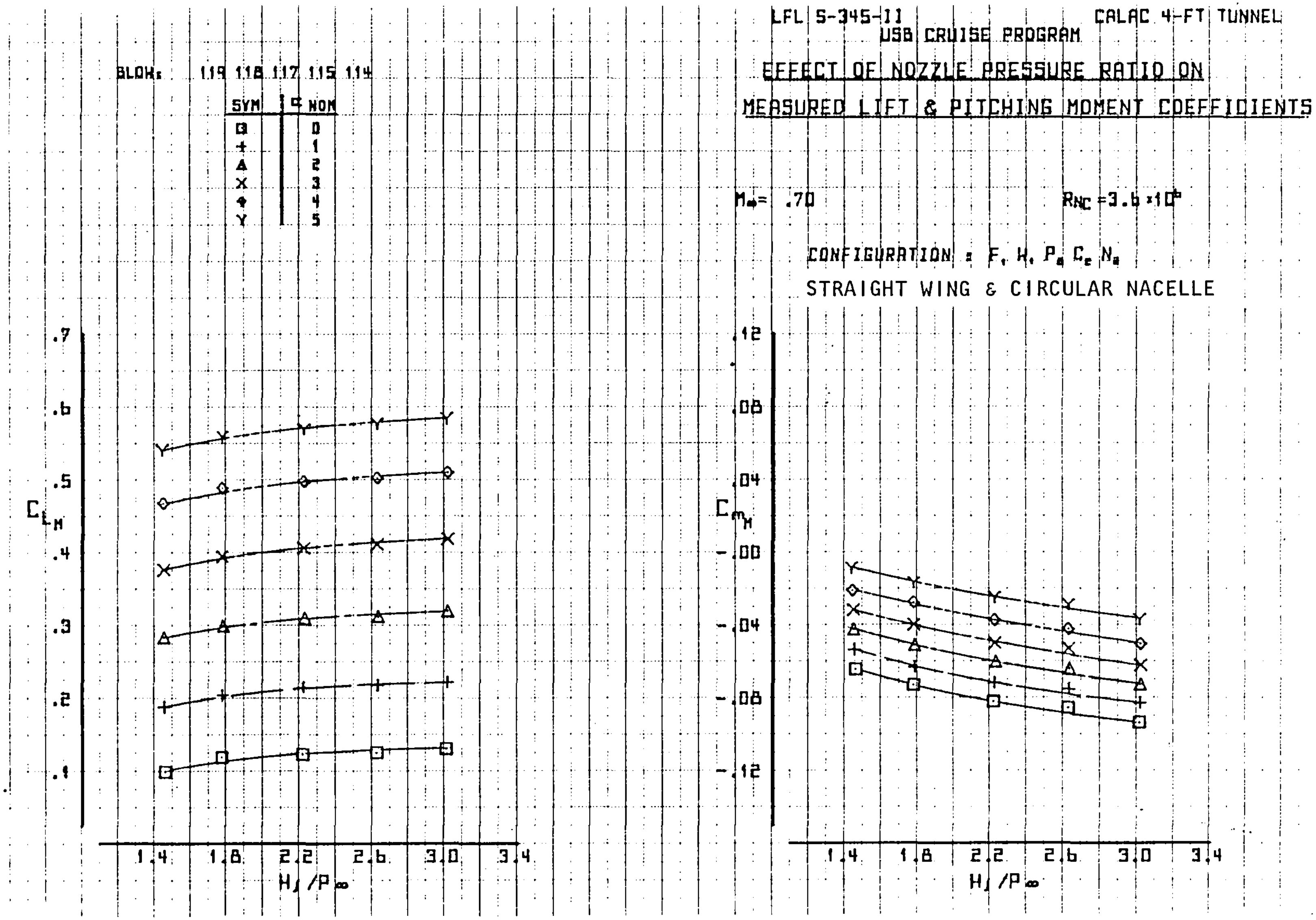

Figure 45. Variation of lift coefficient and moment coefficient with nozzle pressure ratio, $M_\infty = 0.70$.

USB CRUISE PROGRAM

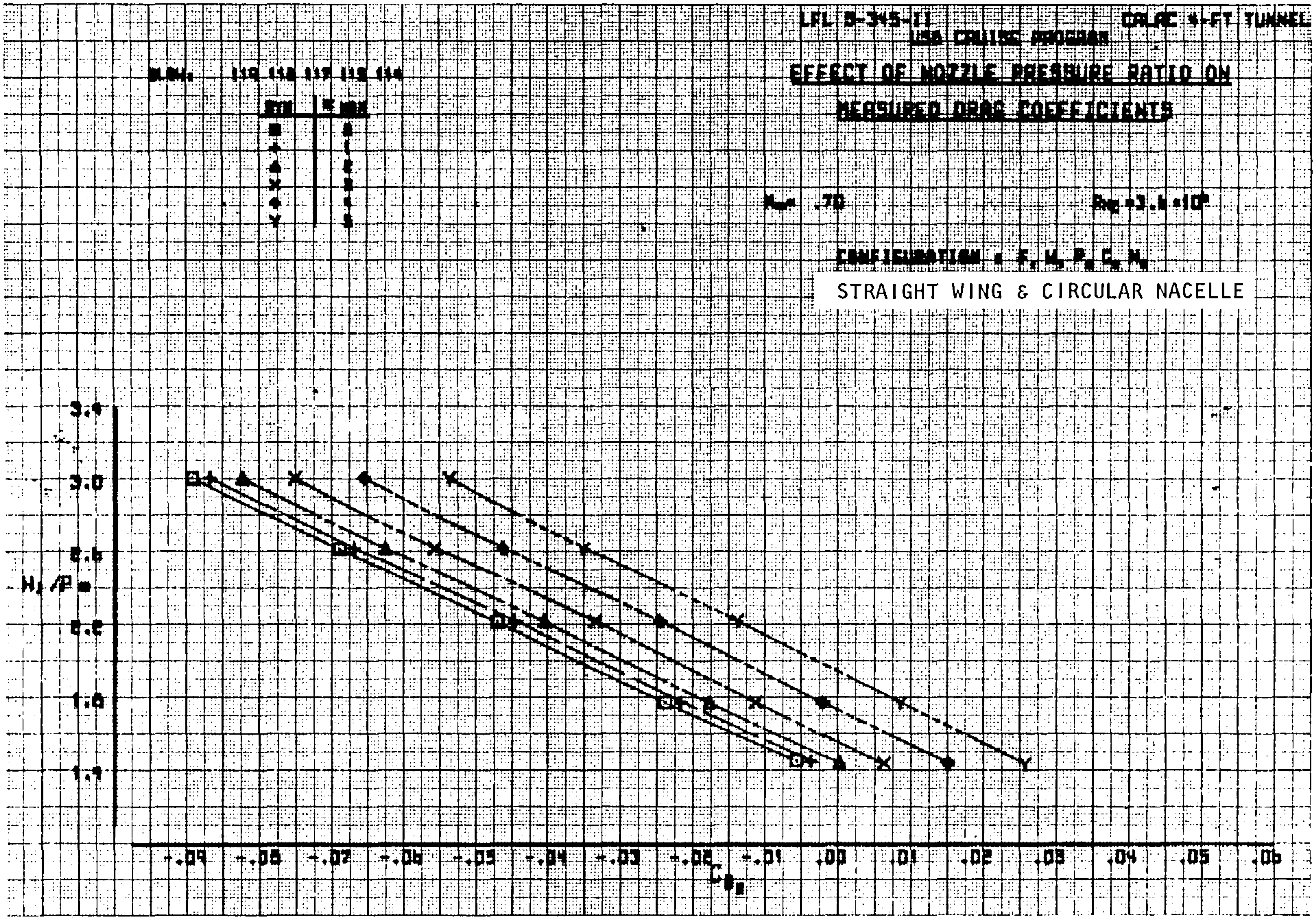

Figure 46. Variation of measured drag coefficient with nozzle pressure ratio, M_∞ = 0.70.

USB CRUISE PROGRAM

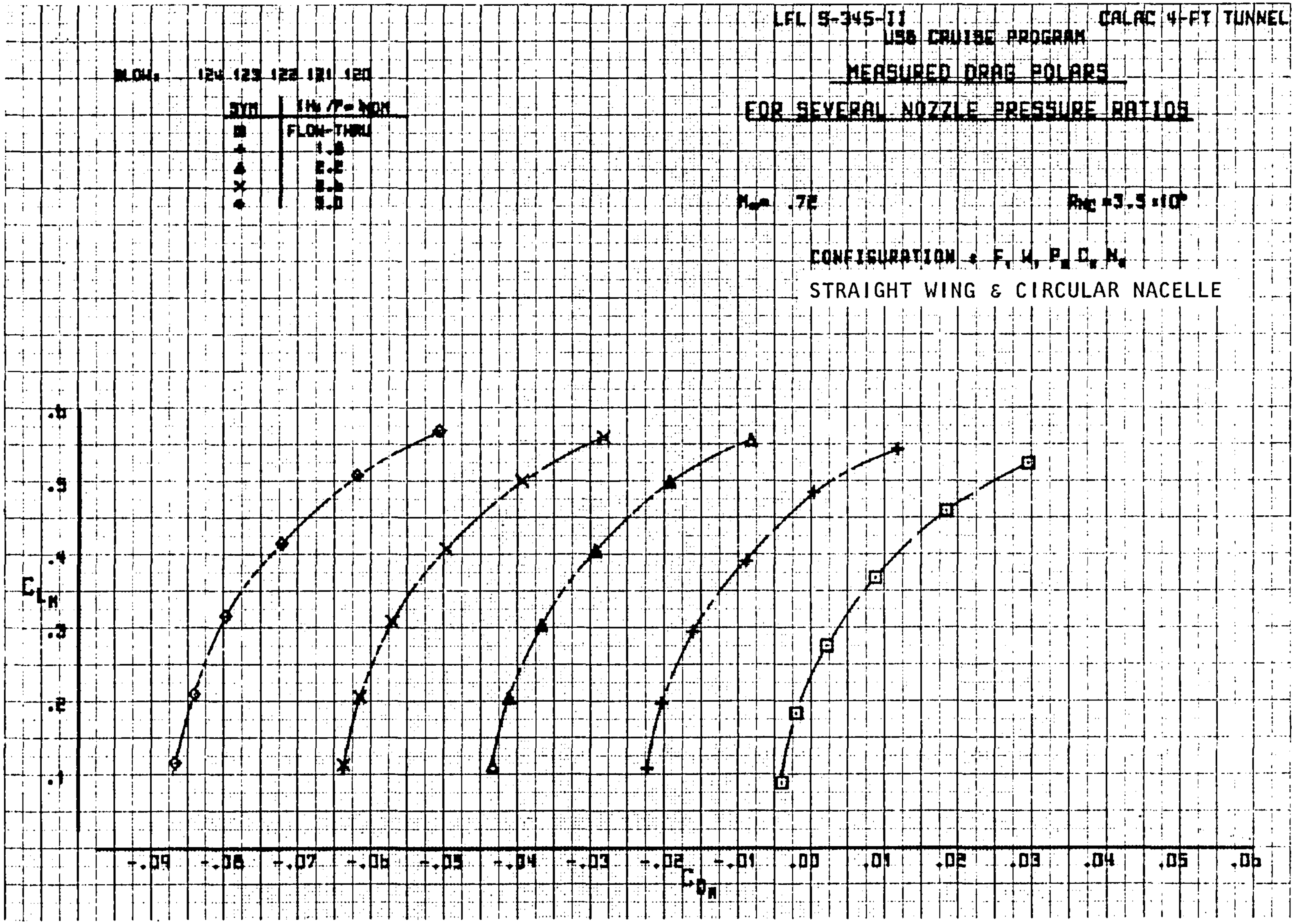

Figure 47. Variation of measured lift coefficient with measured drag coefficient and nozzle pressure ratio, M_∞ = 0.72.

USB CRUISE PROGRAM

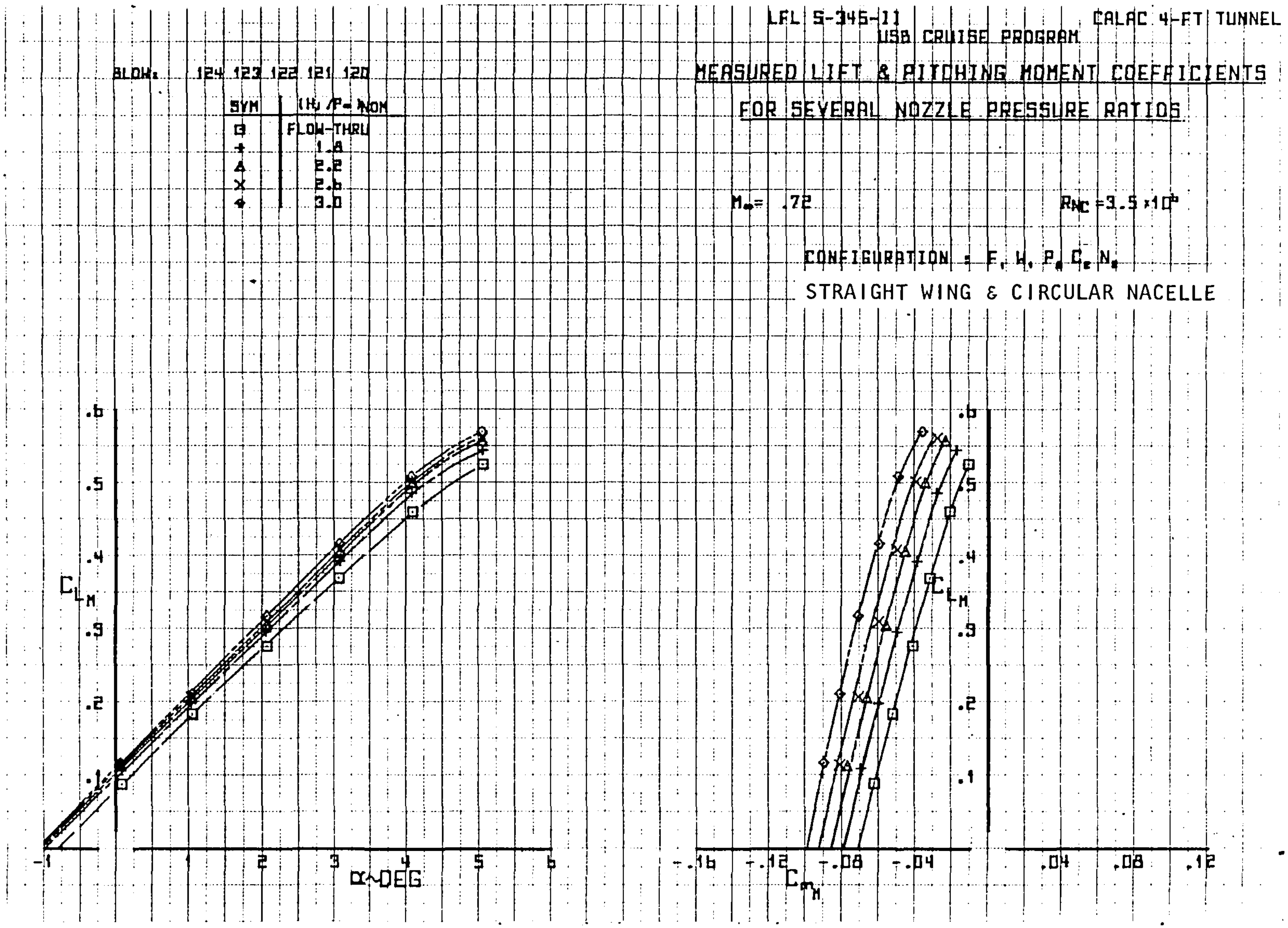

Figure 48. Variation of measured lift coefficient with angle of attack and moment coefficient, $M_\infty = 0.72$.

USB CRUISE PROGRAM

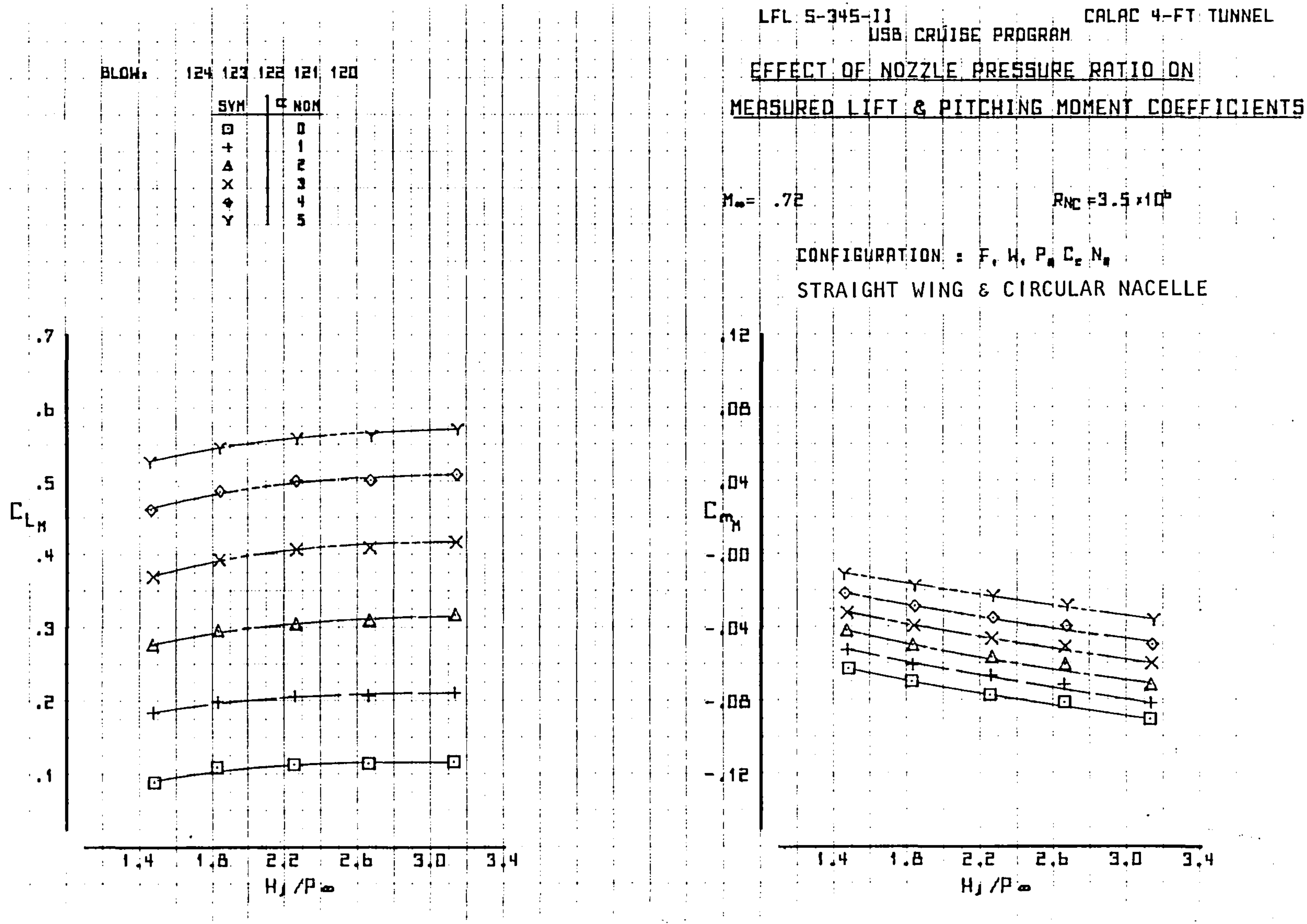

Figure 49. Variation of lift coefficient and moment coefficient with nozzle pressure ratio, $M_\infty = 0.72$.

USB CRUISE PROGRAM

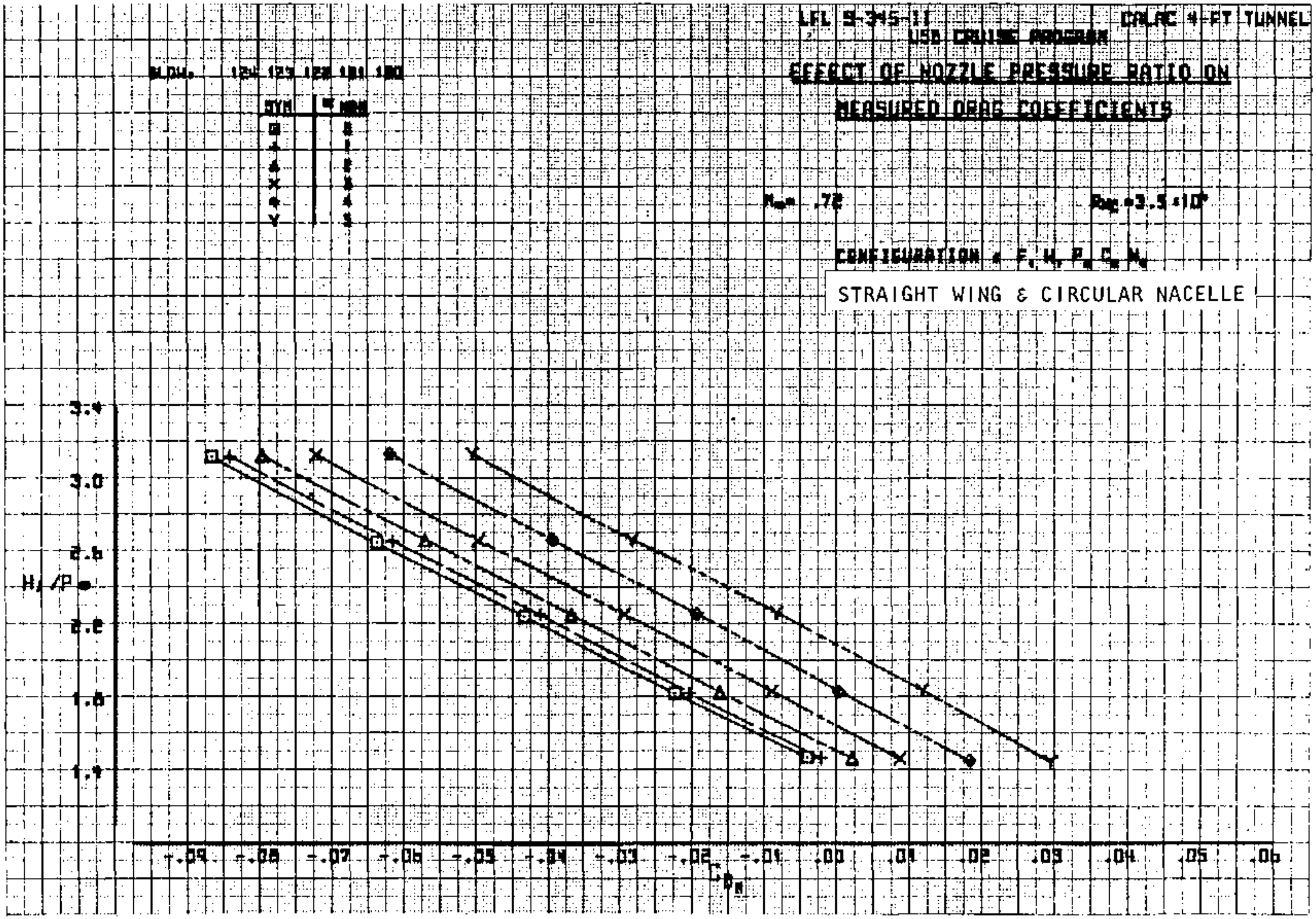

Figure 50. Variation of measured drag coefficient with nozzle pressure ratio, $M_\infty = 0.72$.

USB CRUISE PROGRAM

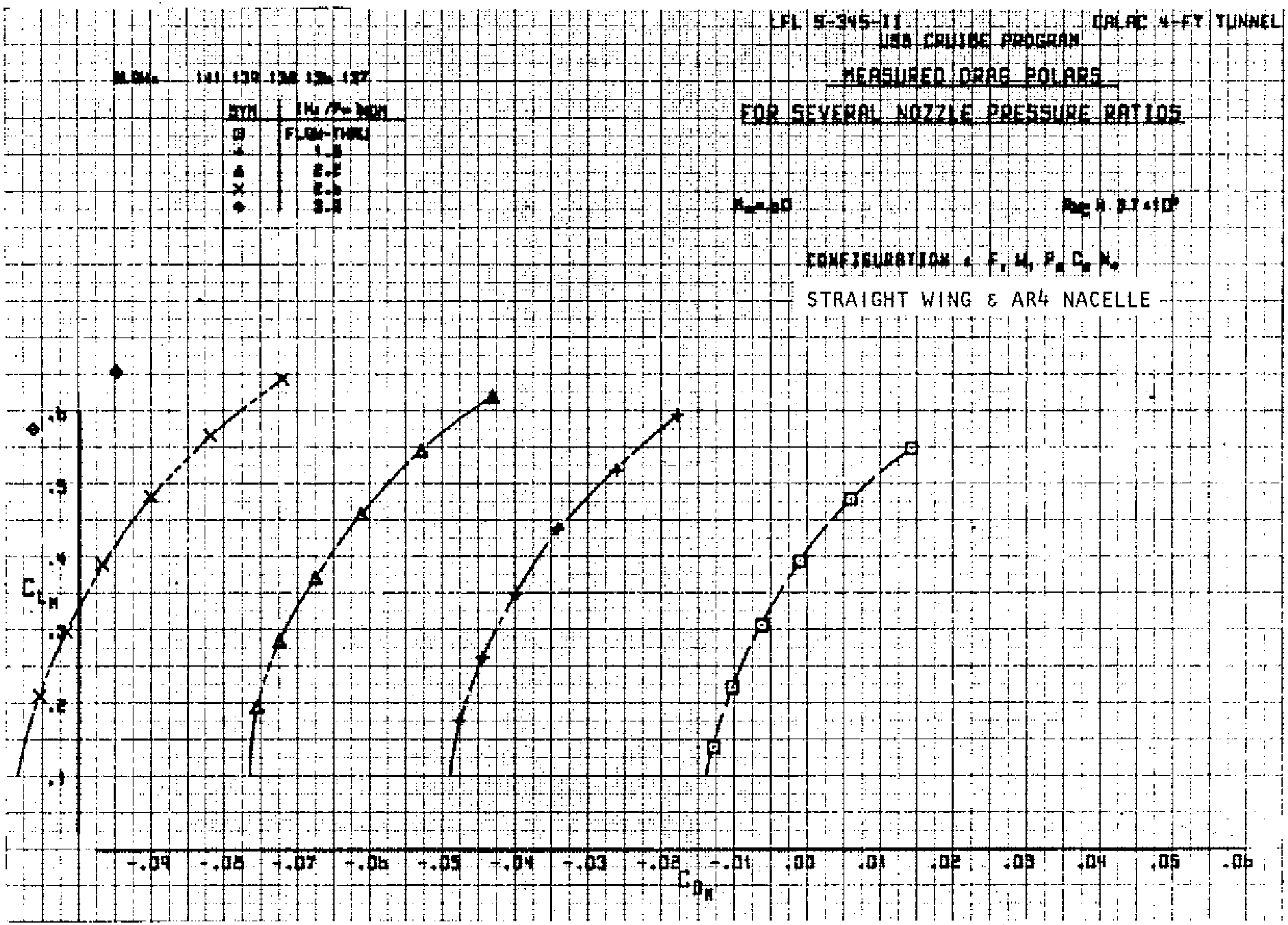

Figure 51. Variation of measured lift coefficient with measured drag coefficient and nozzle pressure ratio, $M_\infty = 0.60$.

USB CRUISE PROGRAM

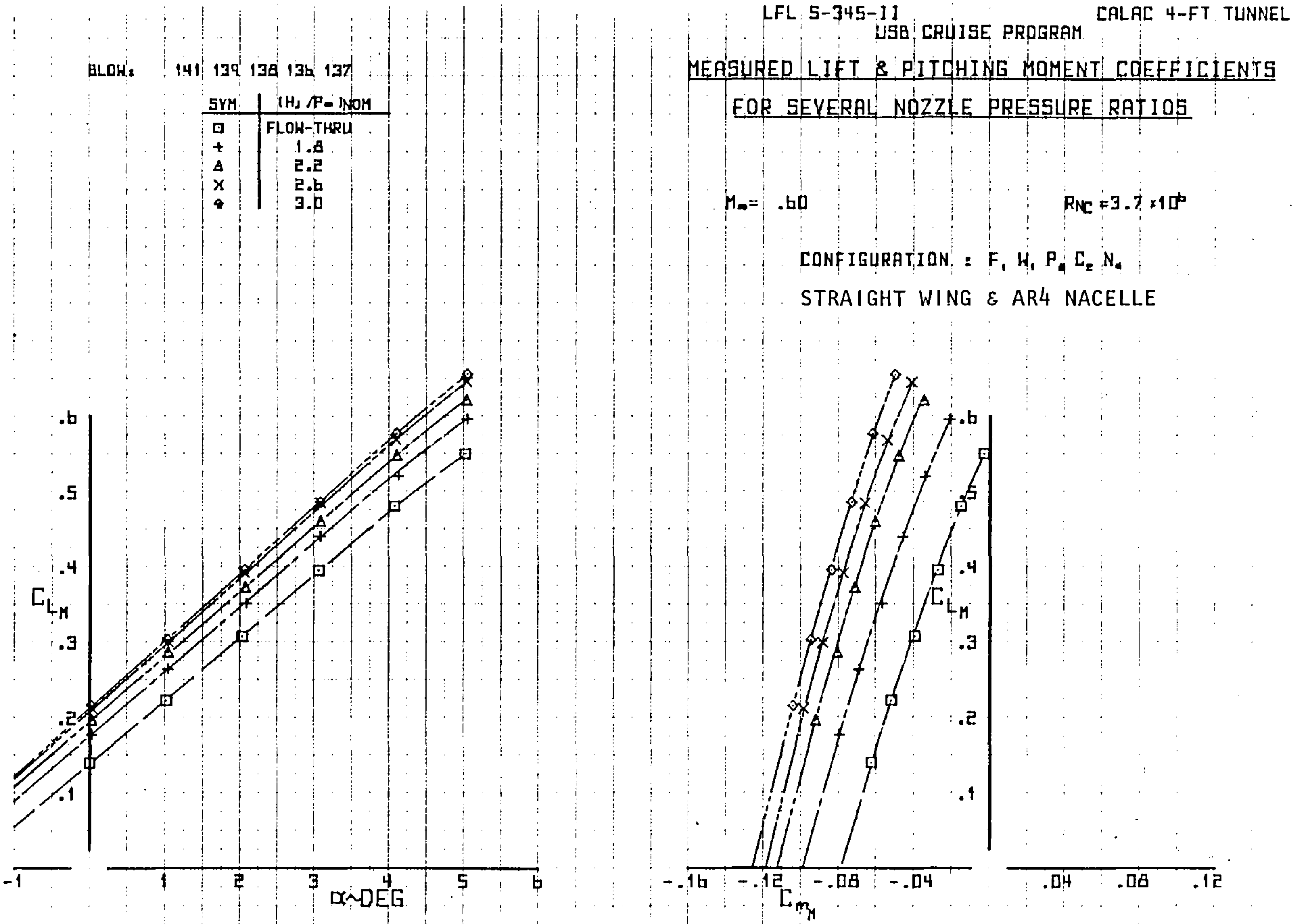

Figure 52. Variation of measured lift coefficient with angle of attack and moment coefficient, $M_\infty = 0.60$.

USB CRUISE PROGRAM

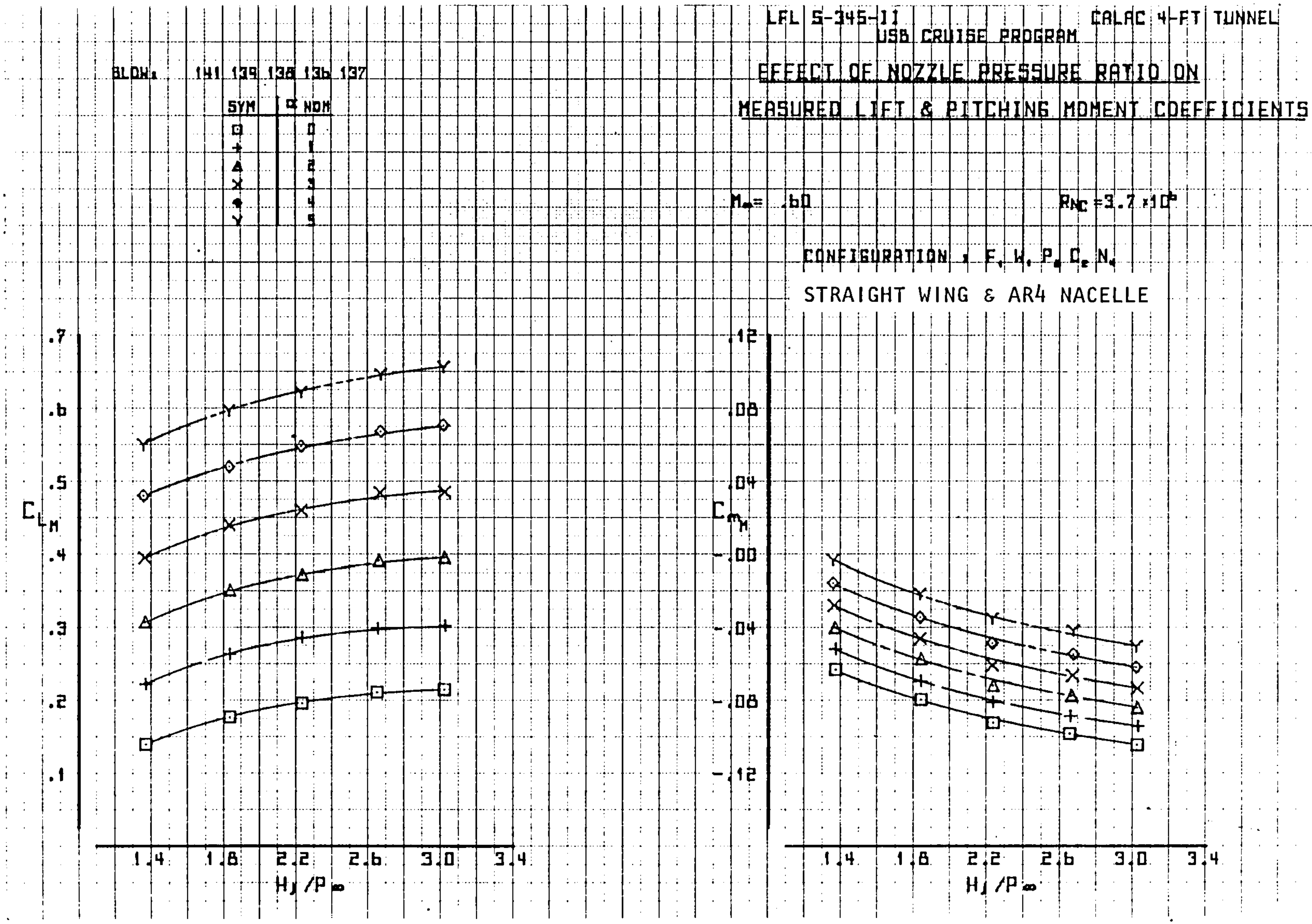

Figure 53. Variation of lift coefficient and moment coefficient with nozzle pressure ratio, $M_\infty = 0.60$.

USB CRUISE PROGRAM

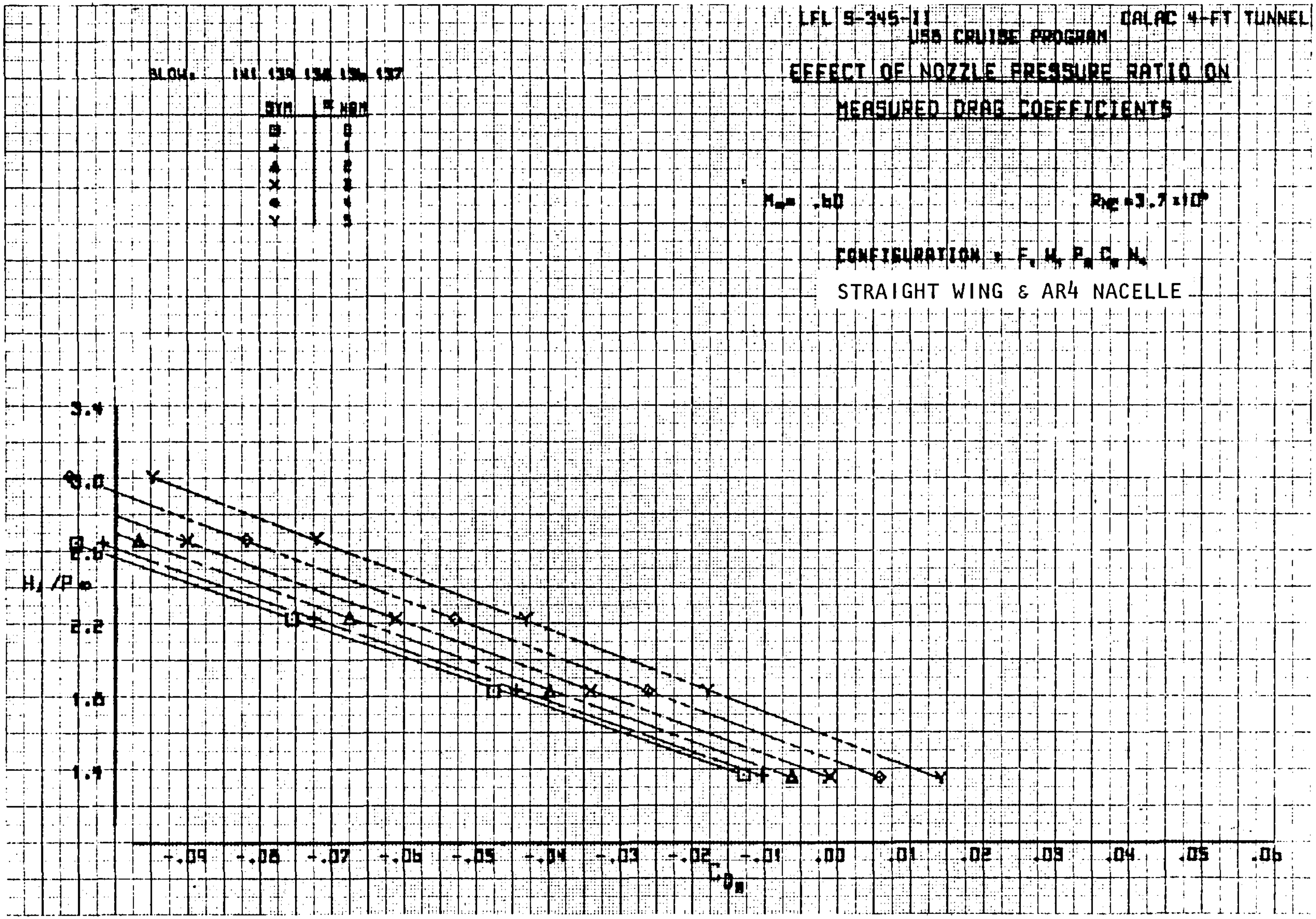

Figure 54. Variation of measured drag coefficient with nozzle pressure ratio, M_∞ = 0.60.

USB CRUISE PROGRAM

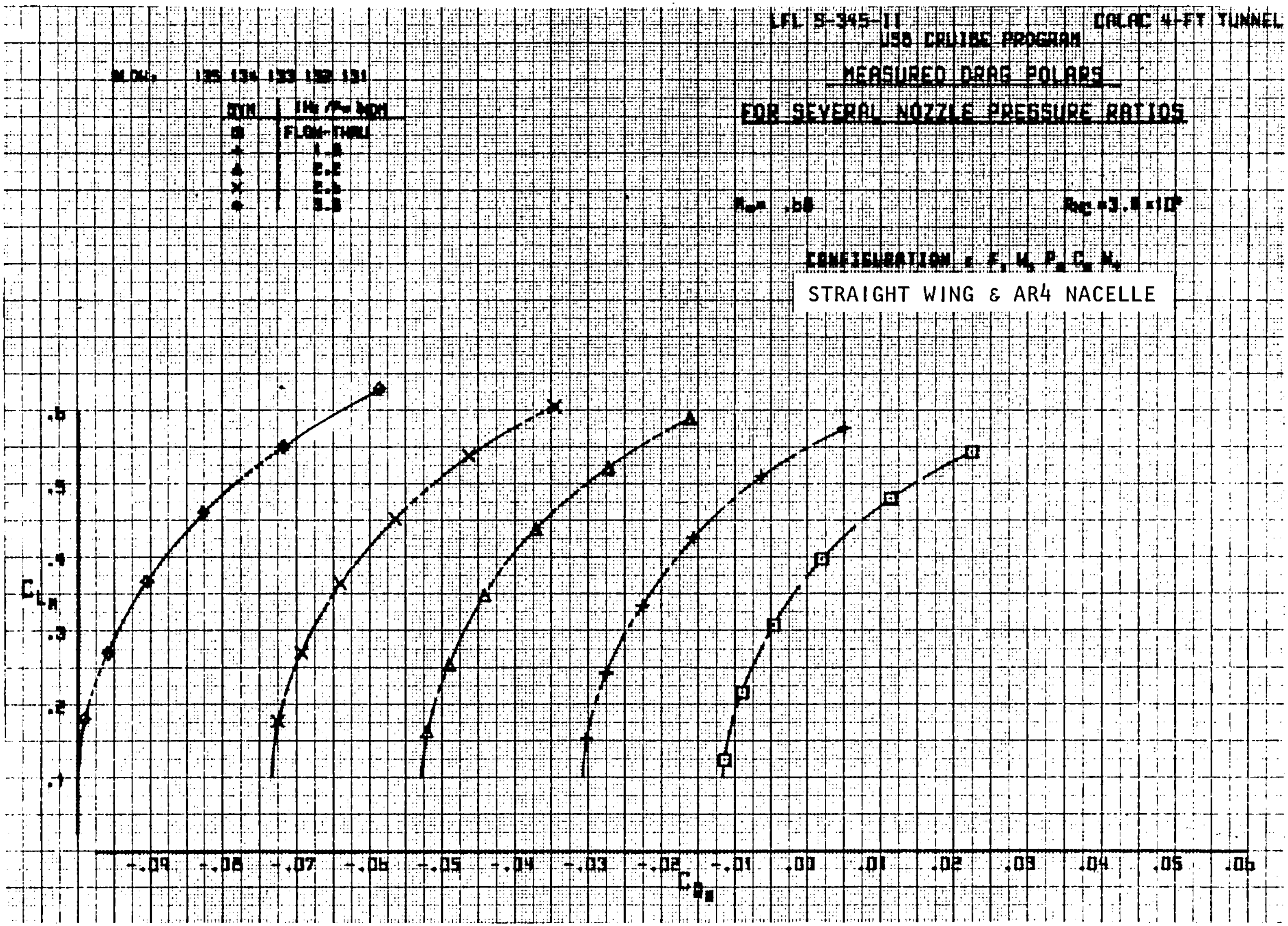

Figure 55. Variation of measured lift coefficient with measured drag coefficient and nozzle pressure ratio, $M_\infty = 0.68$.

USB CRUISE PROGRAM

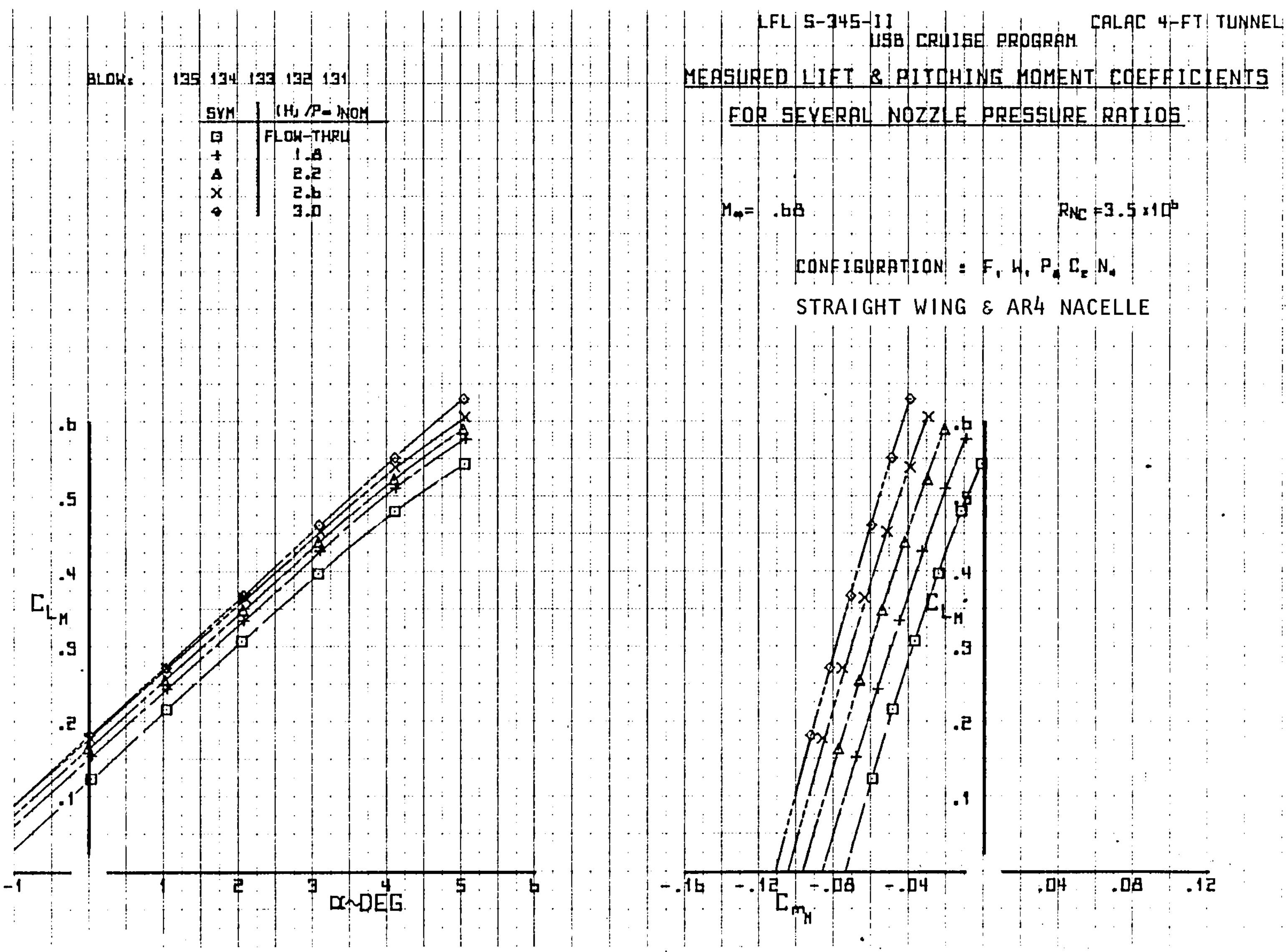

Figure 56. Variation of measured lift coefficient with angle of attack and moment coefficient, M_∞ = 0.68.

USB CRUISE PROGRAM

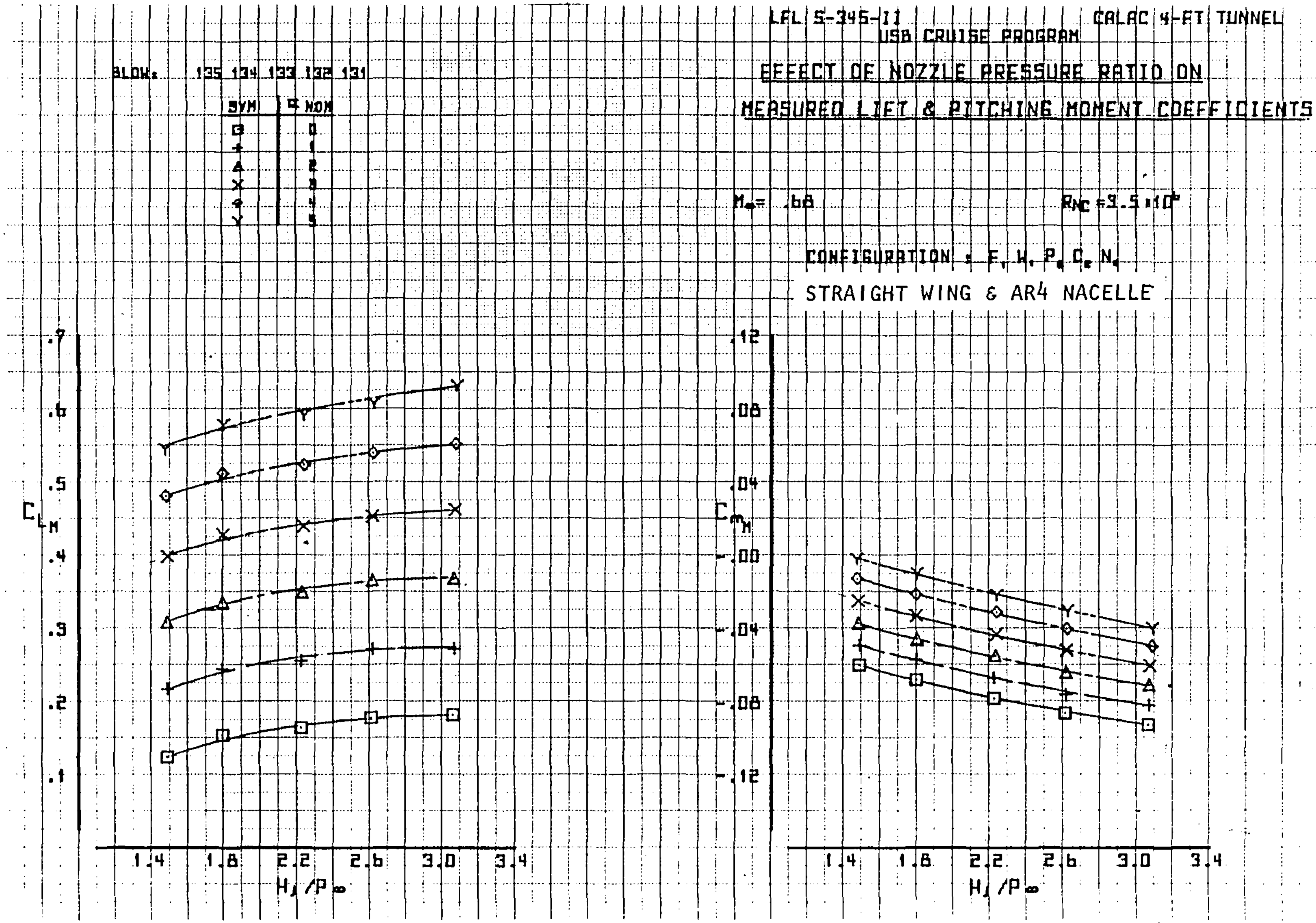

Figure 57. Variation of lift coefficient and moment coefficient with nozzle pressure ratio, $M_\infty = 0.68$.

USB CRUISE PROGRAM

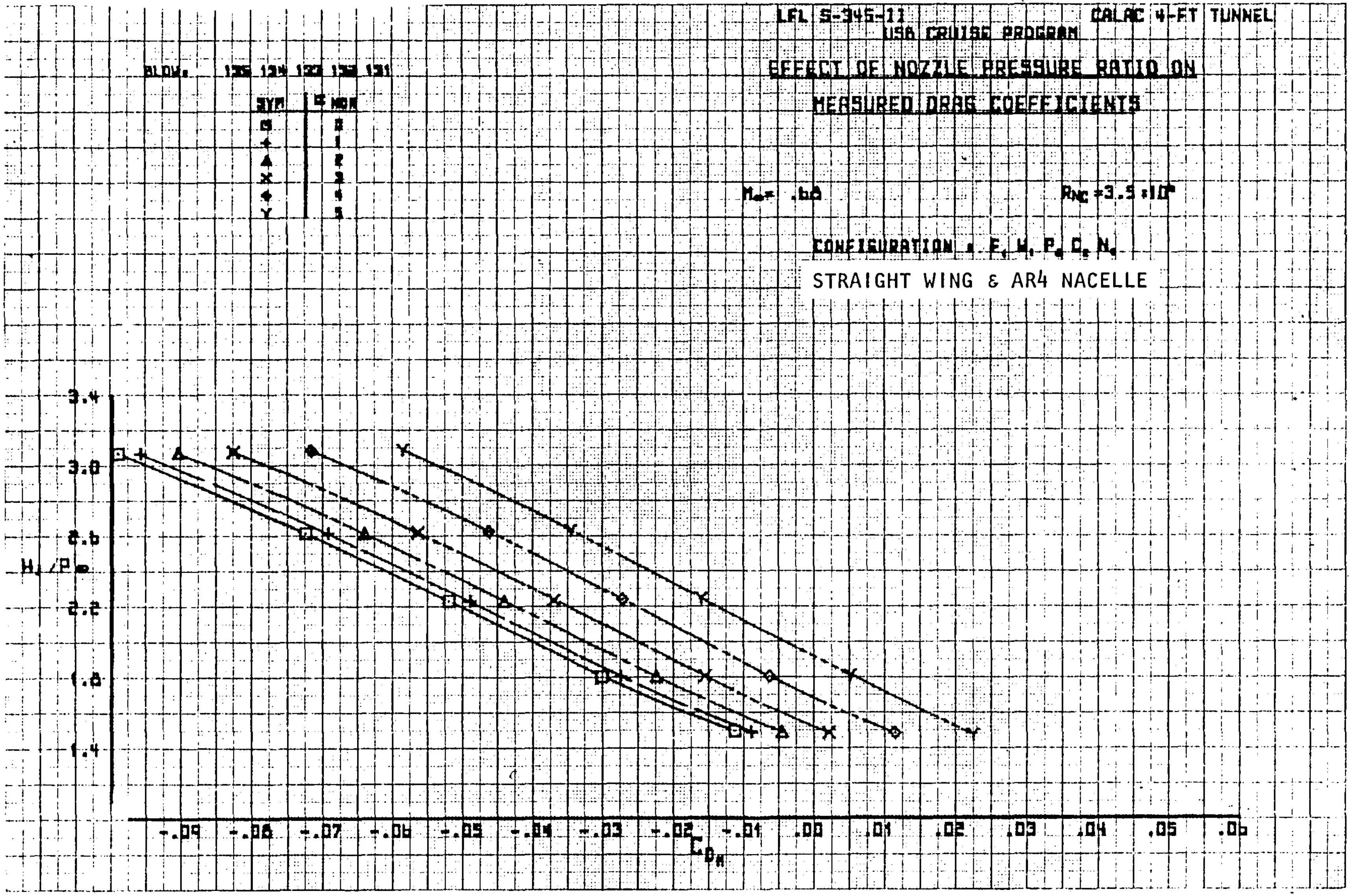

Figure 58. Variation of measured drag coefficient with nozzle pressure ratio, $M_\infty = 0.68$.

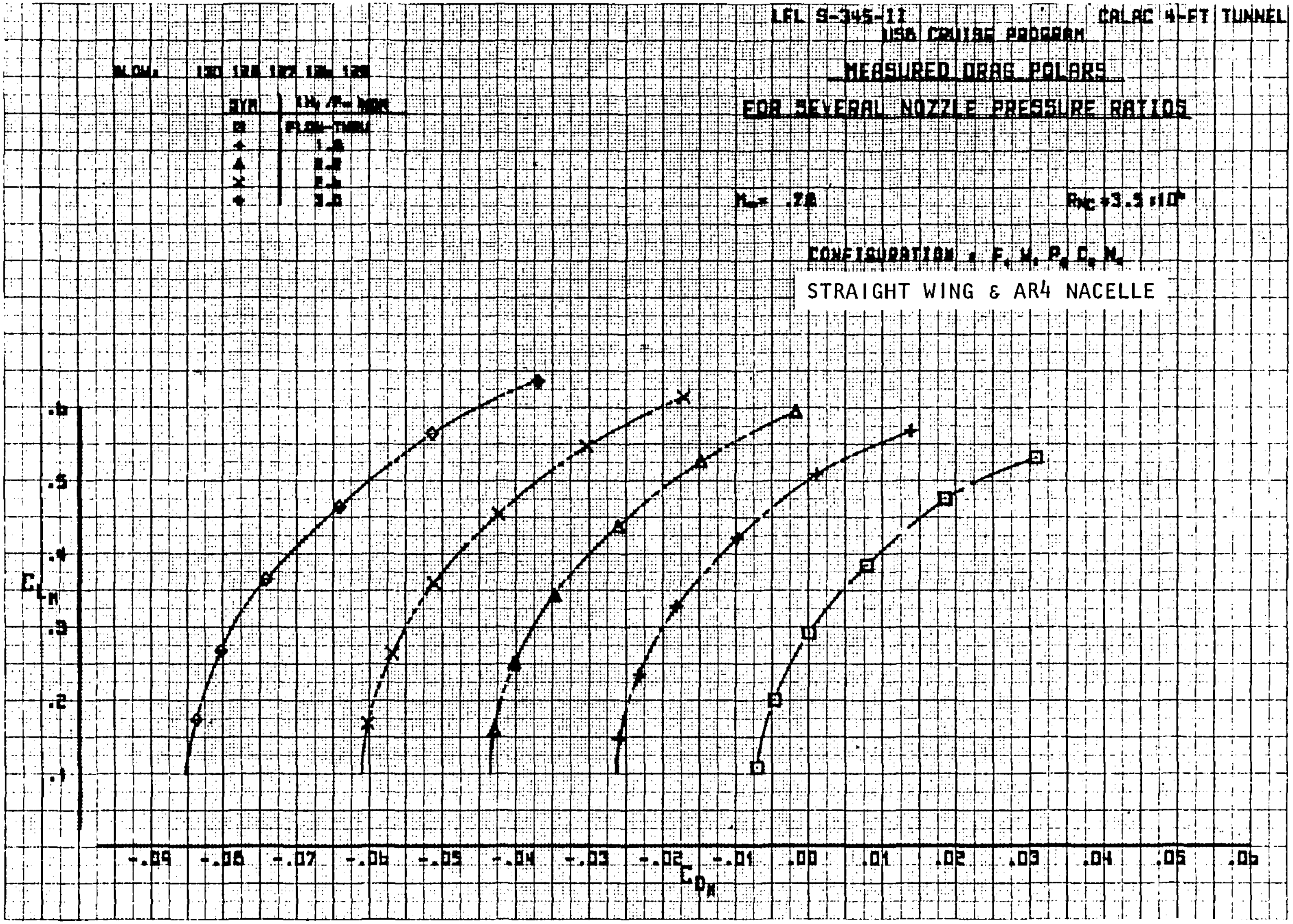

Figure 59. Variation of measured lift coefficient with measured drag coefficient and nozzle pressure ratio, $M_\infty = 0.72$.

USB CRUISE PROGRAM

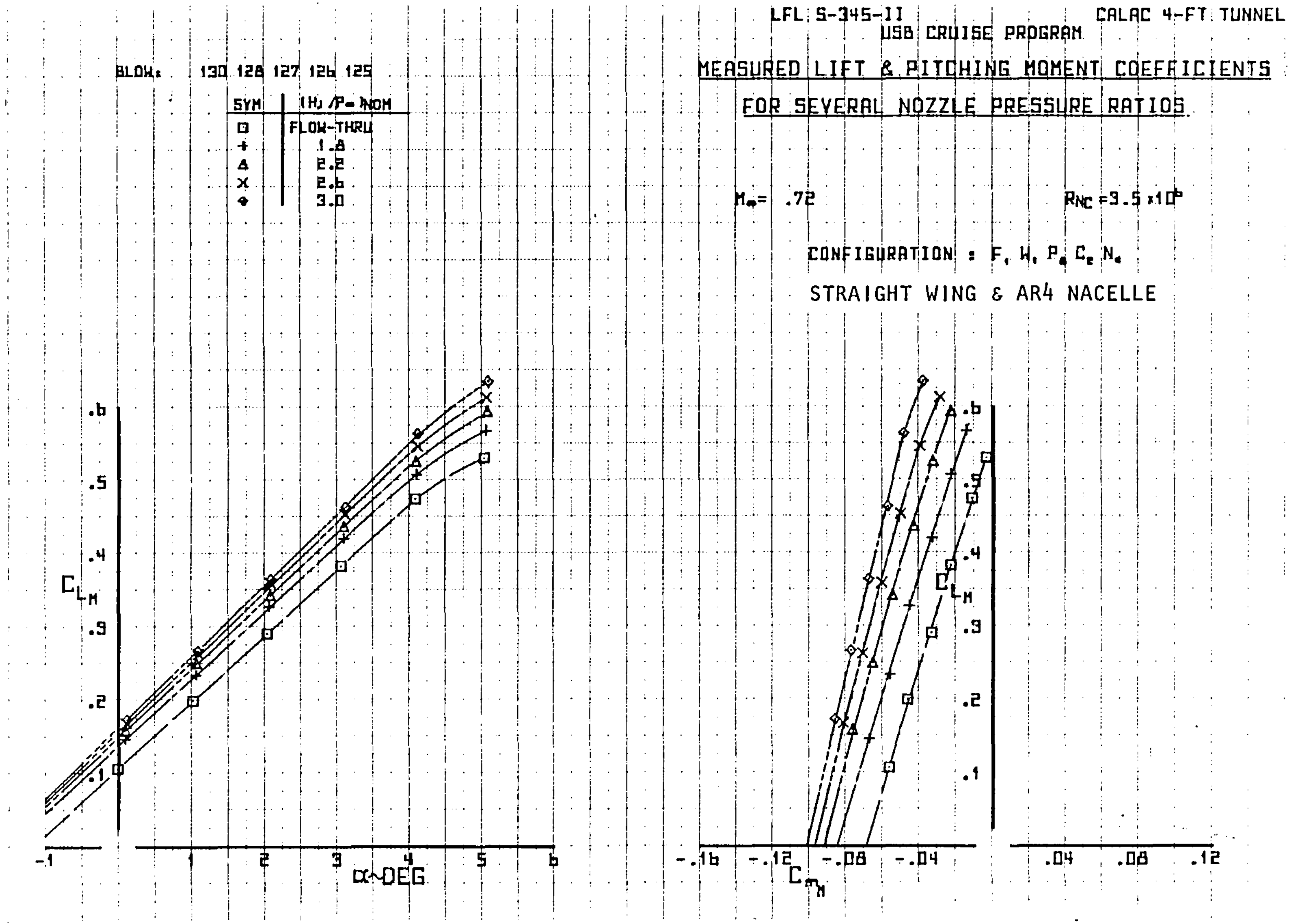

Figure 60. Variation of measured lift coefficient with angle of attack and moment coefficient, $M_\infty = 0.72$.

USB CRUISE PROGRAM

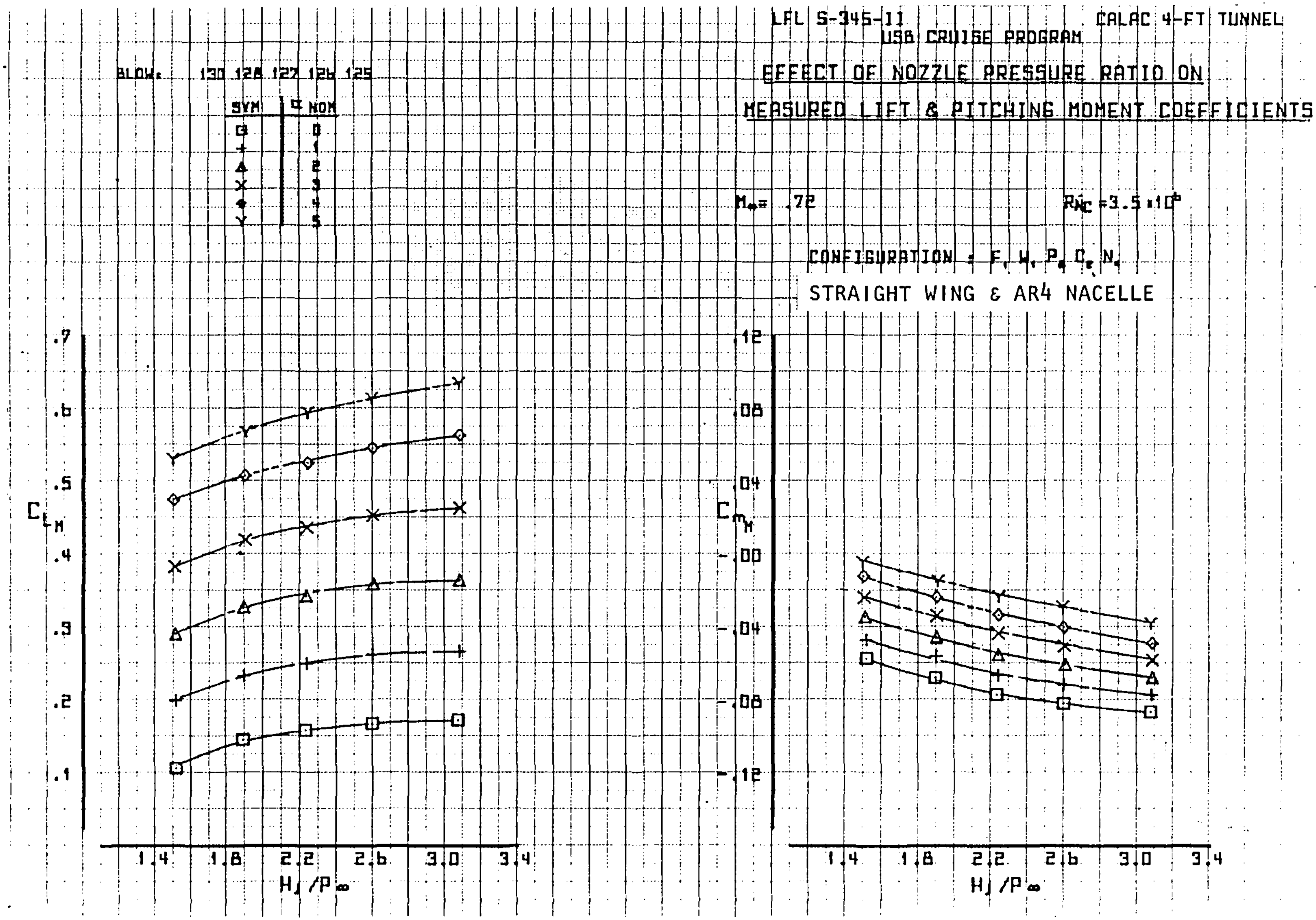

Figure 61. Variation of lift coefficient and moment coefficient with nozzle pressure ratio, $M_\infty = 0.72$.

USB CRUISE PROGRAM

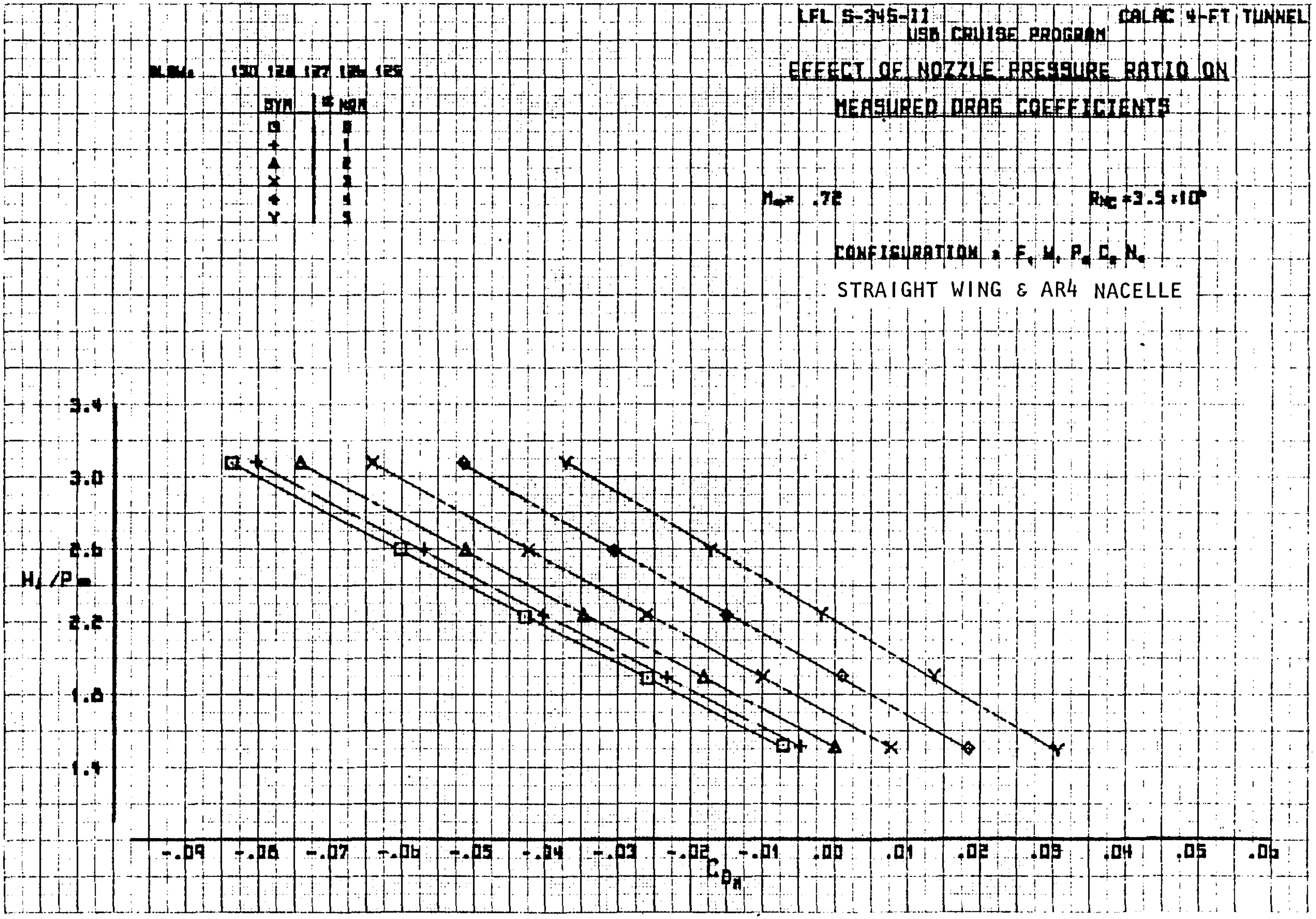

Figure 62. Variation of measured drag coefficient with nozzle pressure ratio, $M_\infty = 0.72$.

USB CRUISE PROGRAM

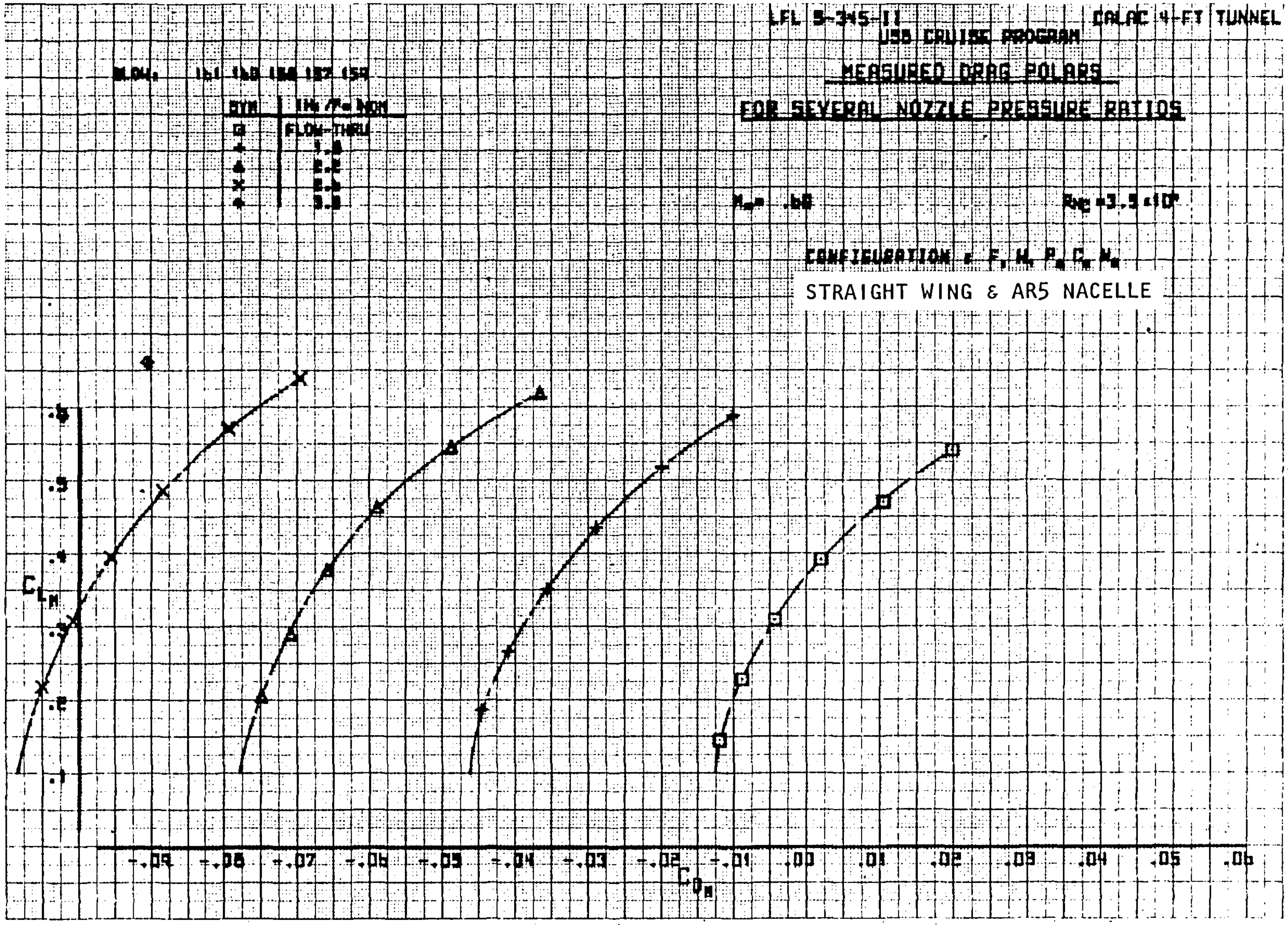

Figure 63. Variation of measured lift coefficient with measured drag coefficient and nozzle pressure ratio, $M_\infty = 0.60$.

USB CRUISE PROGRAM

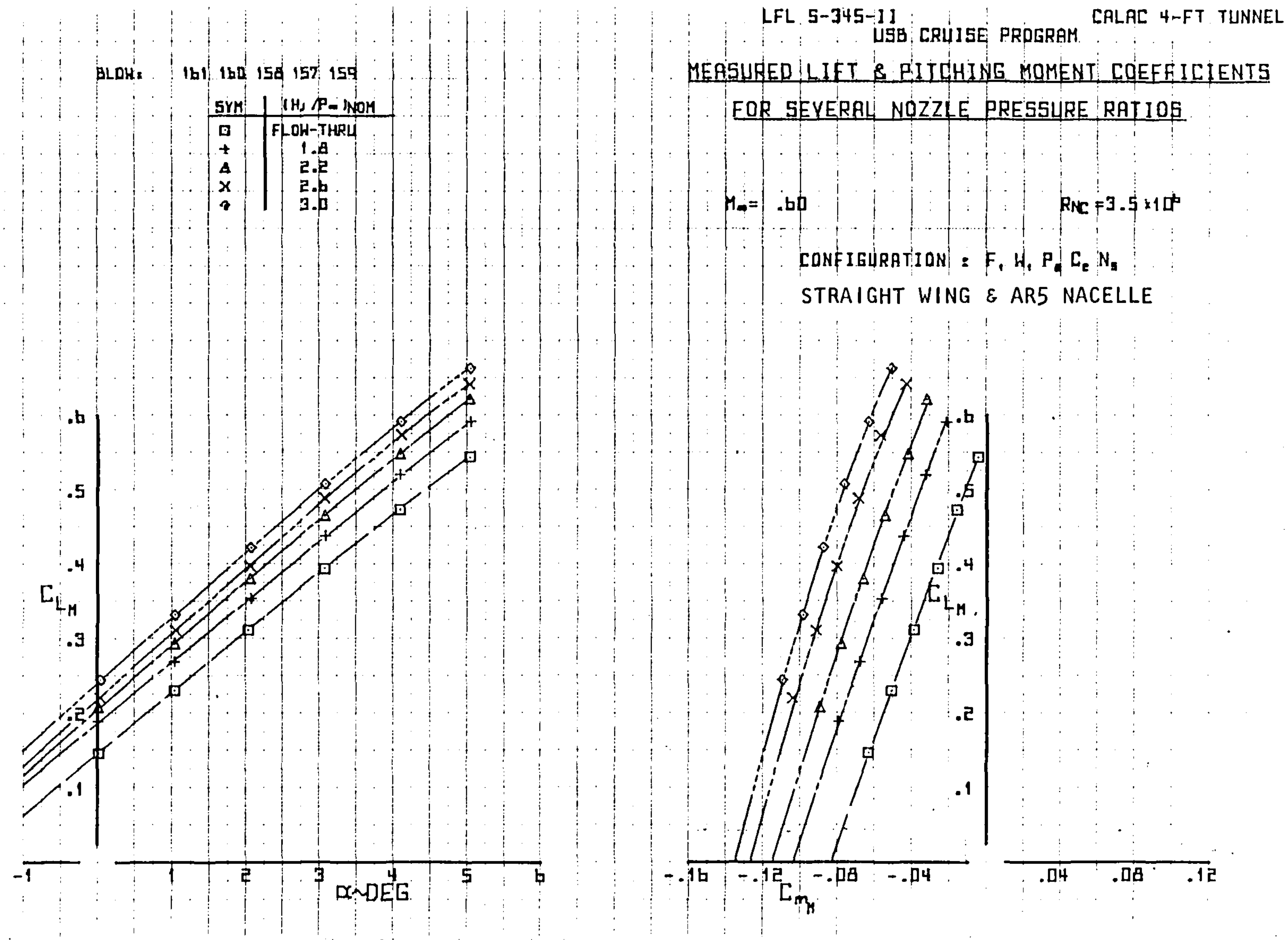

Figure 64. Variation of measured lift coefficient with angle of attack and moment coefficient, $M_\infty = 0.60$.

USB CRUISE PROGRAM

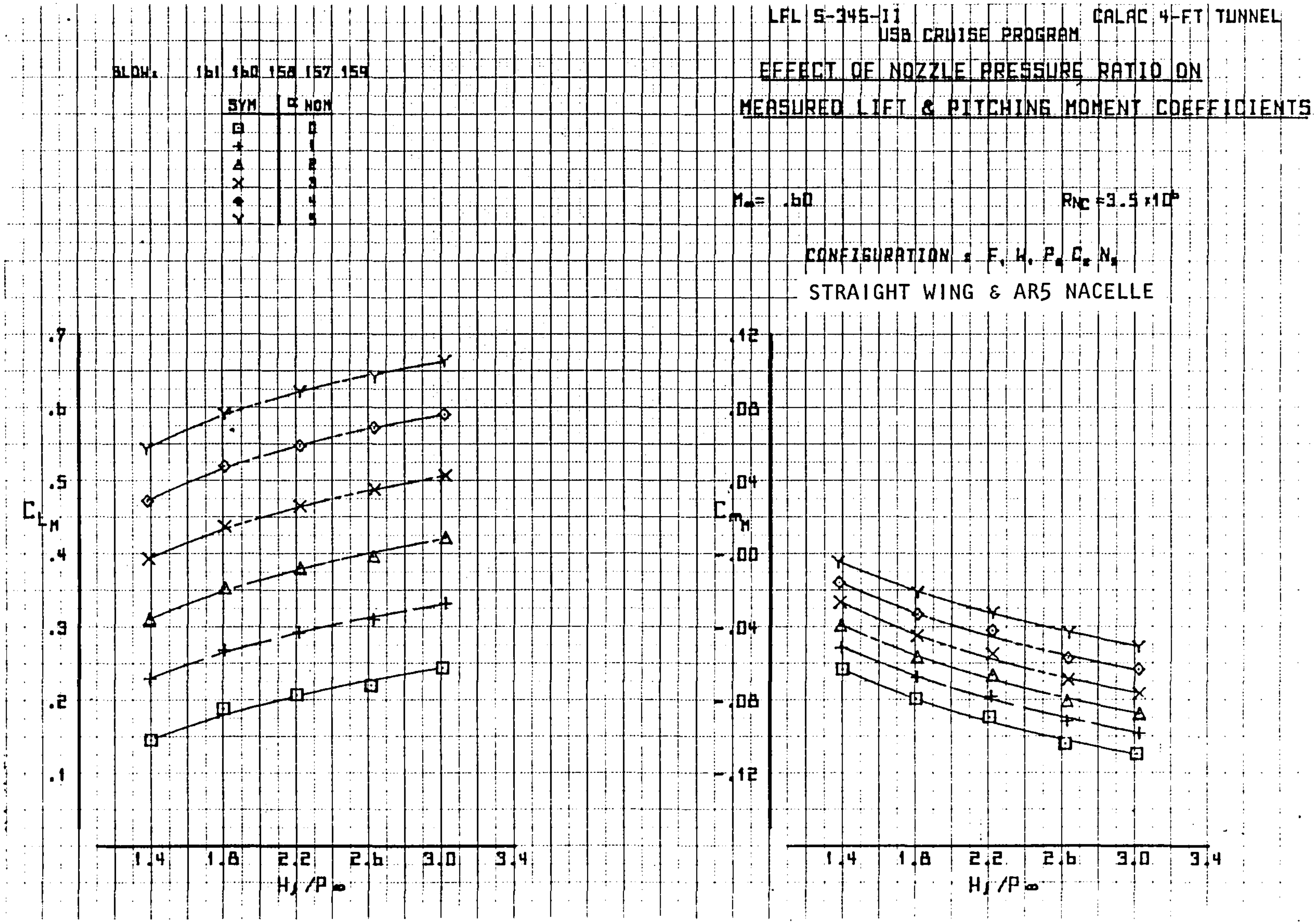

Figure 65. Variation of lift coefficient and moment coefficient with nozzle pressure ratio, $M_\infty = 0.60$.

USB CRUISE PROGRAM

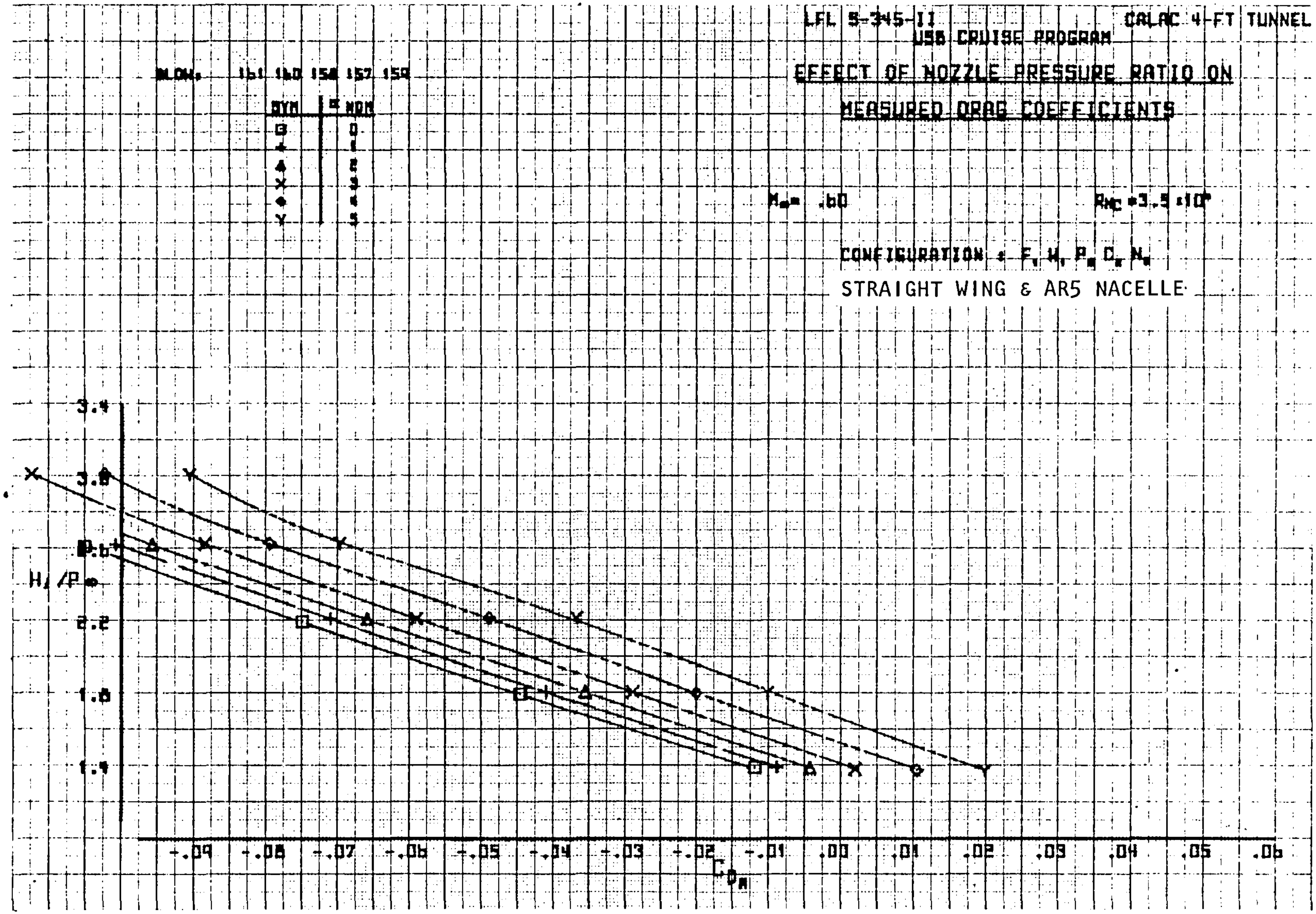

Figure 66. Variation of measured drag coefficient with nozzle pressure ratio, $M_\infty = 0.60$.

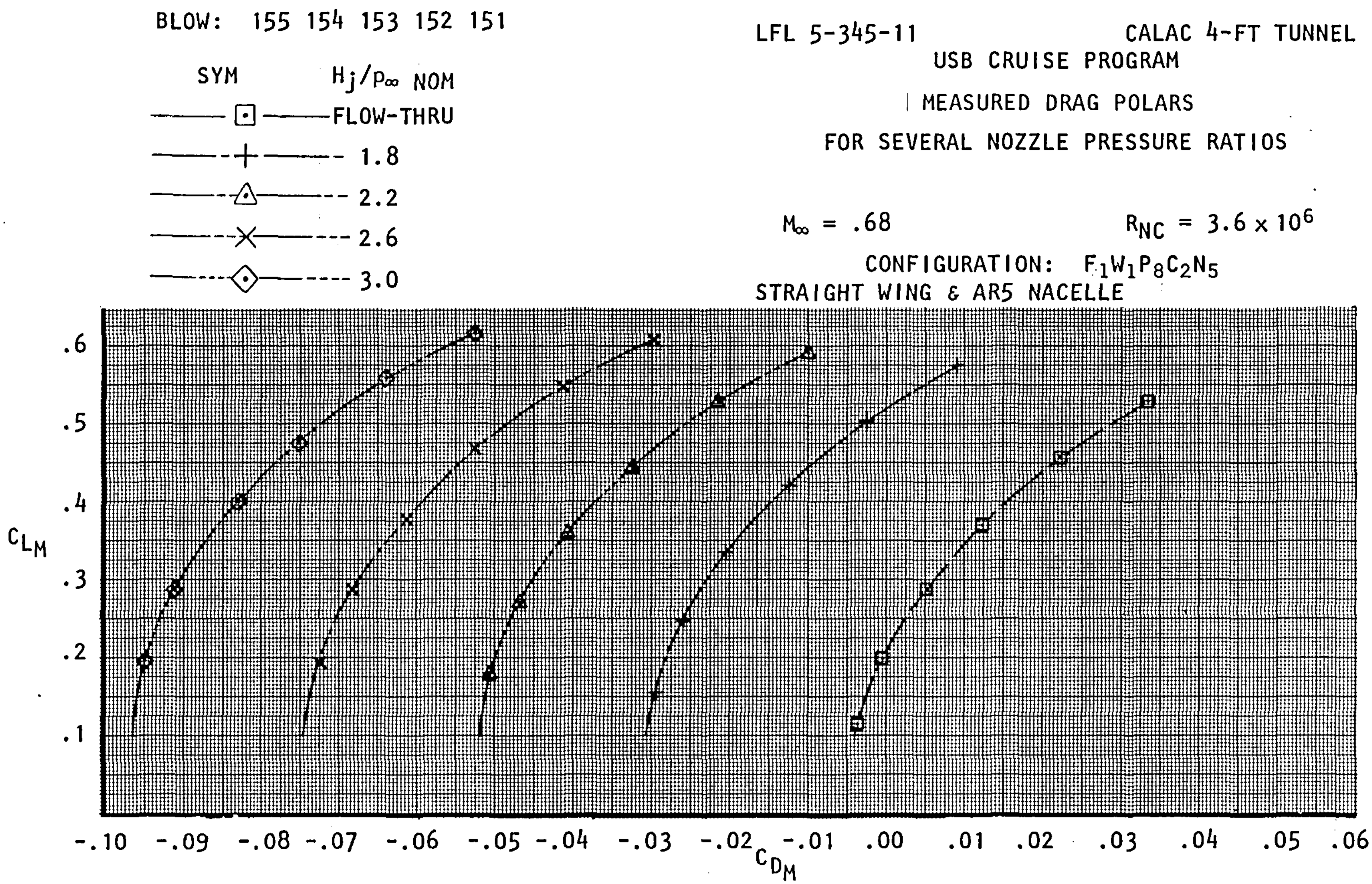

Figure 67. Variation of measured lift coefficient with measured drag coefficient and nozzle pressure ratio, M_∞ = 0.68.

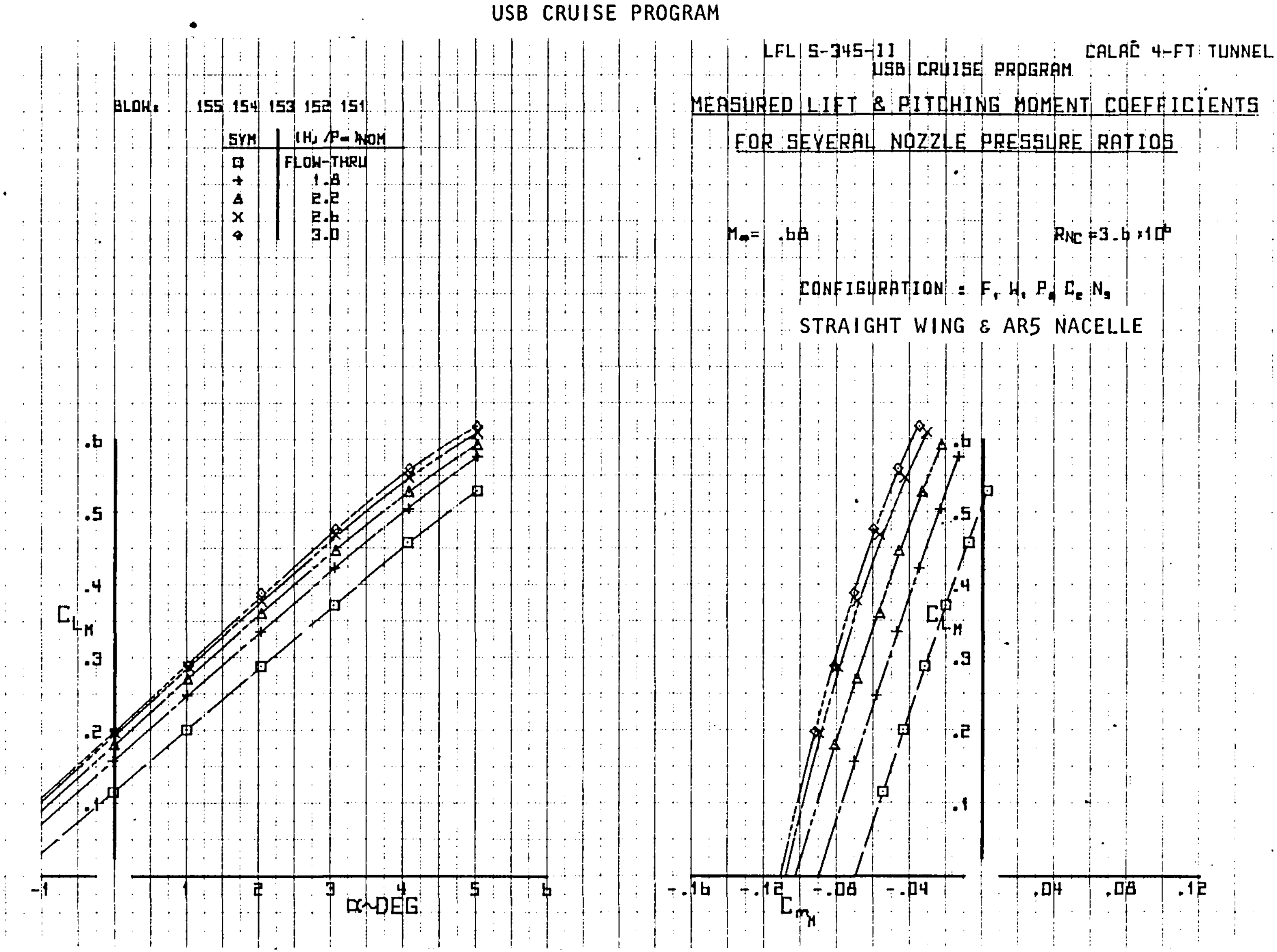

Figure 68. Variation of measured lift coefficient with angle of attack and moment coefficient, $M_\infty = 0.68$.

USB CRUISE PROGRAM

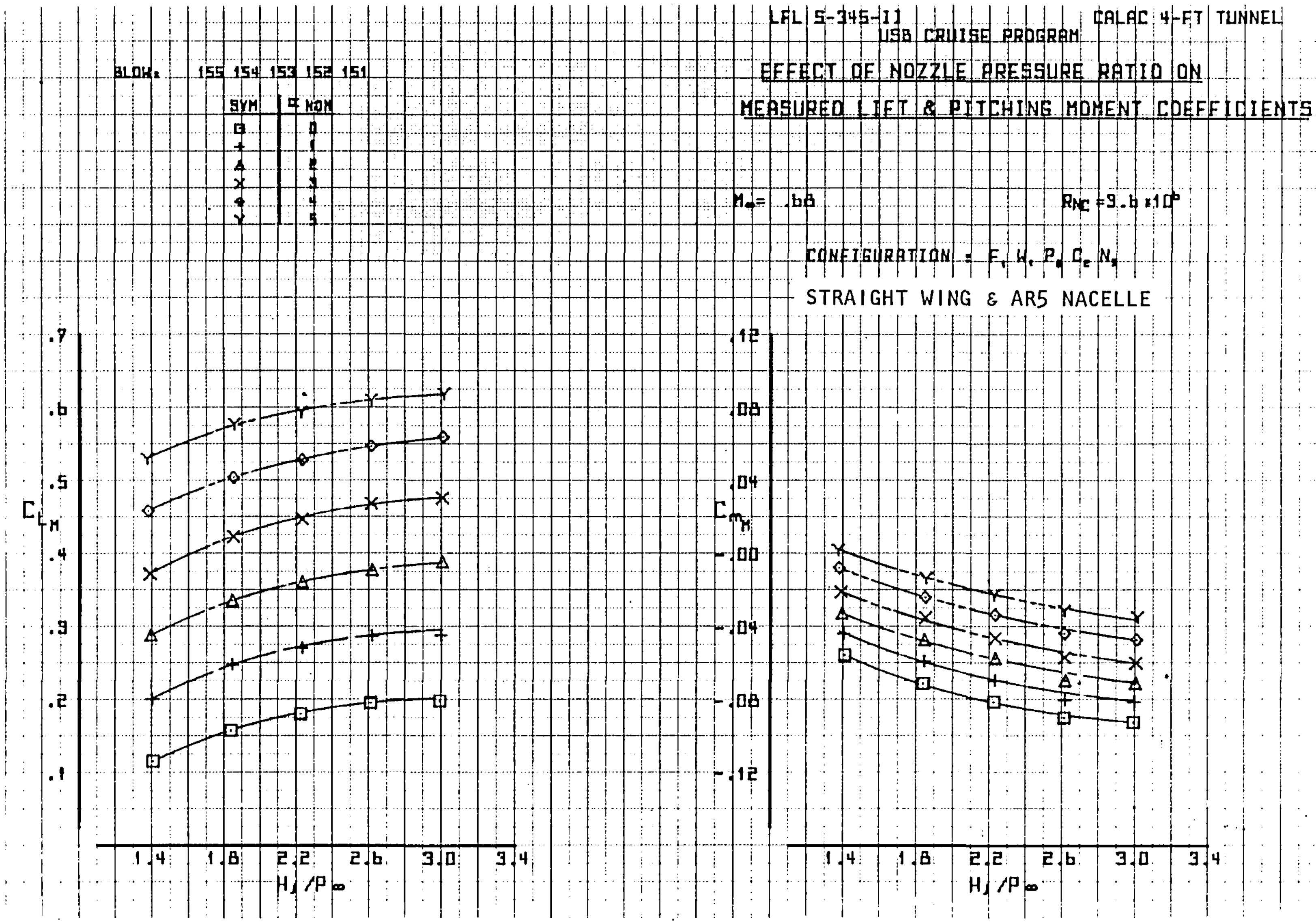

Figure 69. Variation of lift coefficient and moment coefficient with nozzle pressure ratio, $M_\infty = 0.68$.

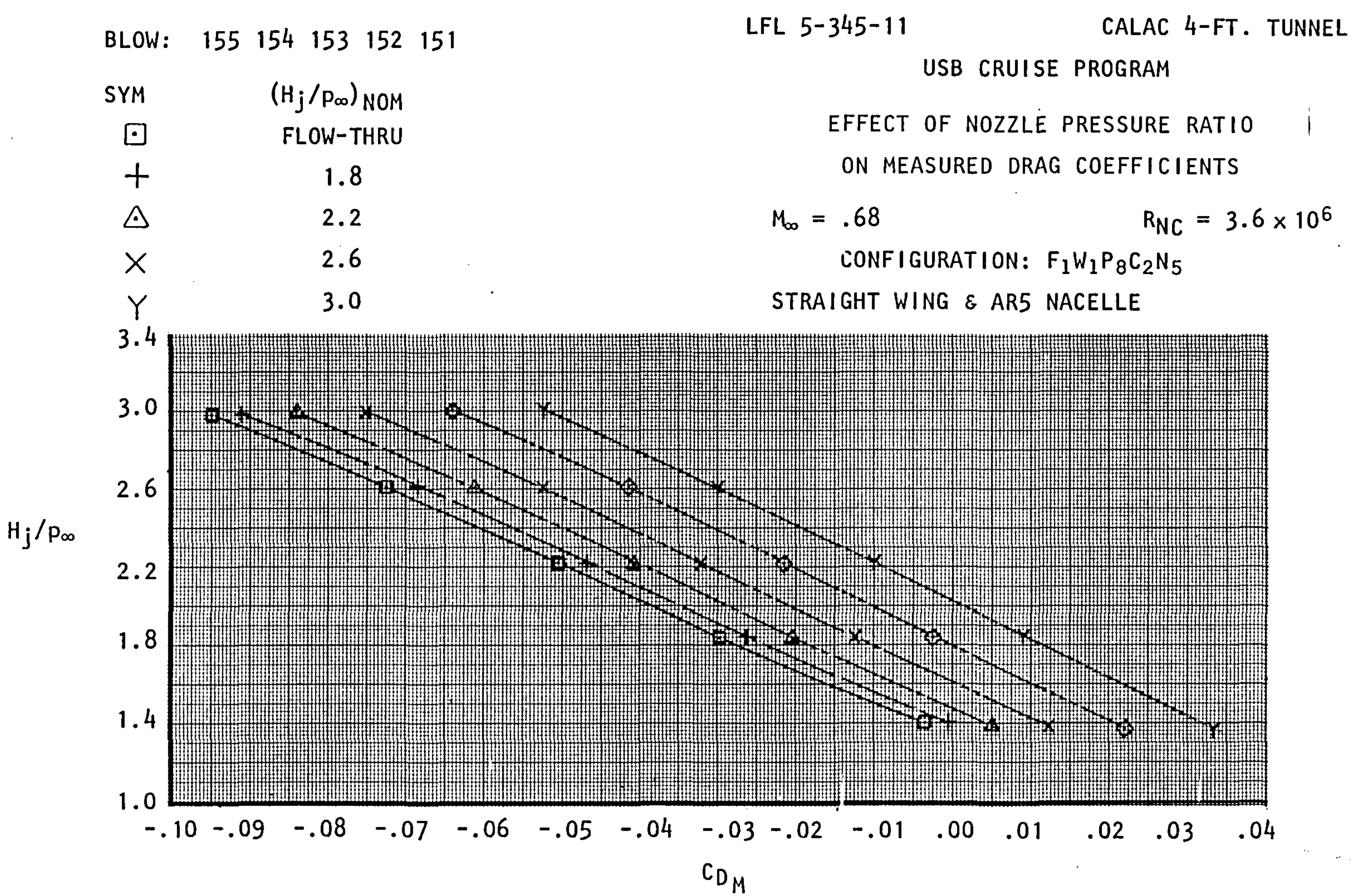

Figure 70. Variation of measured drag coefficient with nozzle pressure ratio, $M_\infty = 0.68$.

USB CRUISE PROGRAM

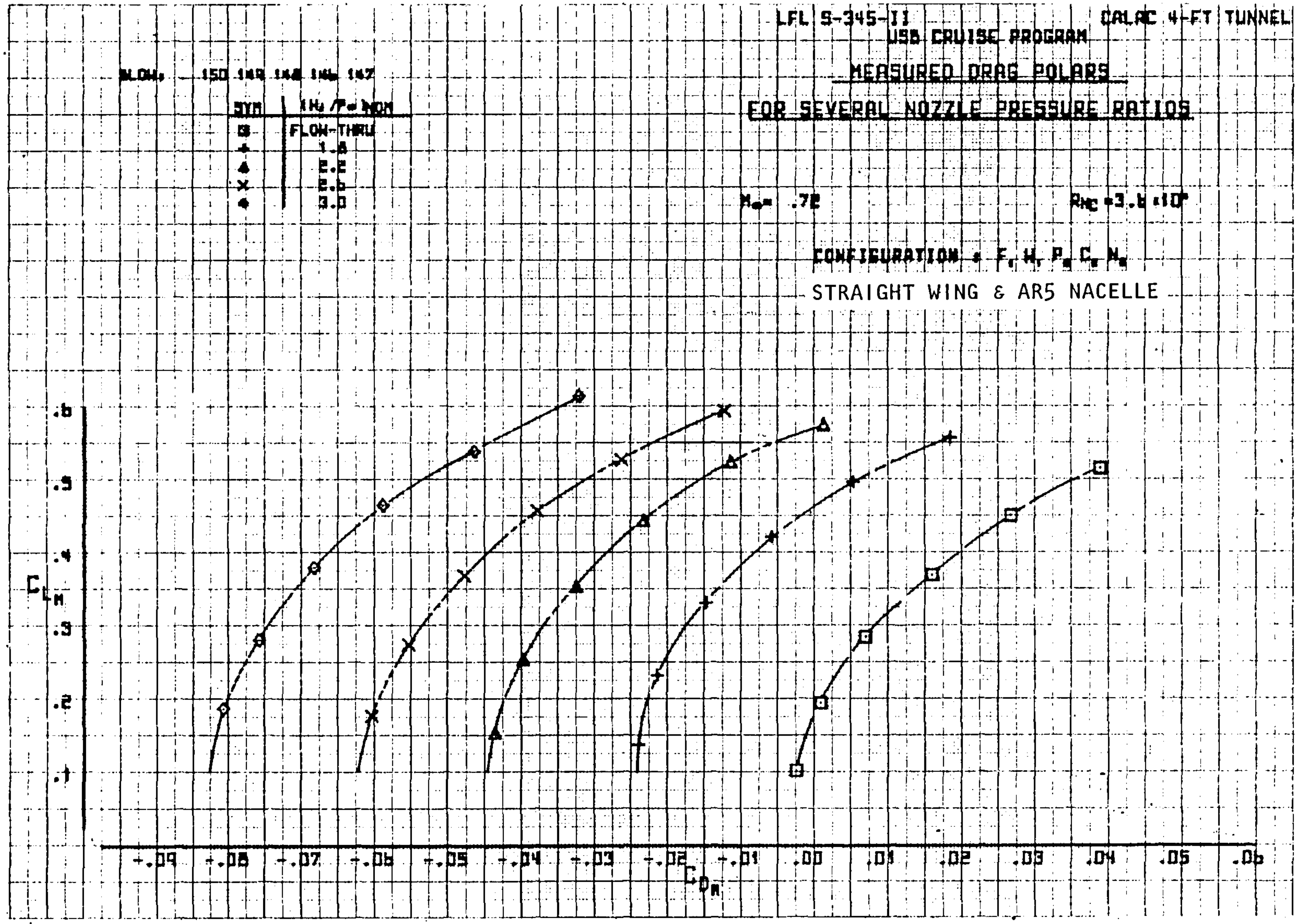

Figure 71. Variation of measured lift coefficient with measured drag coefficient and nozzle pressure ratio, $M_\infty = 0.72$.

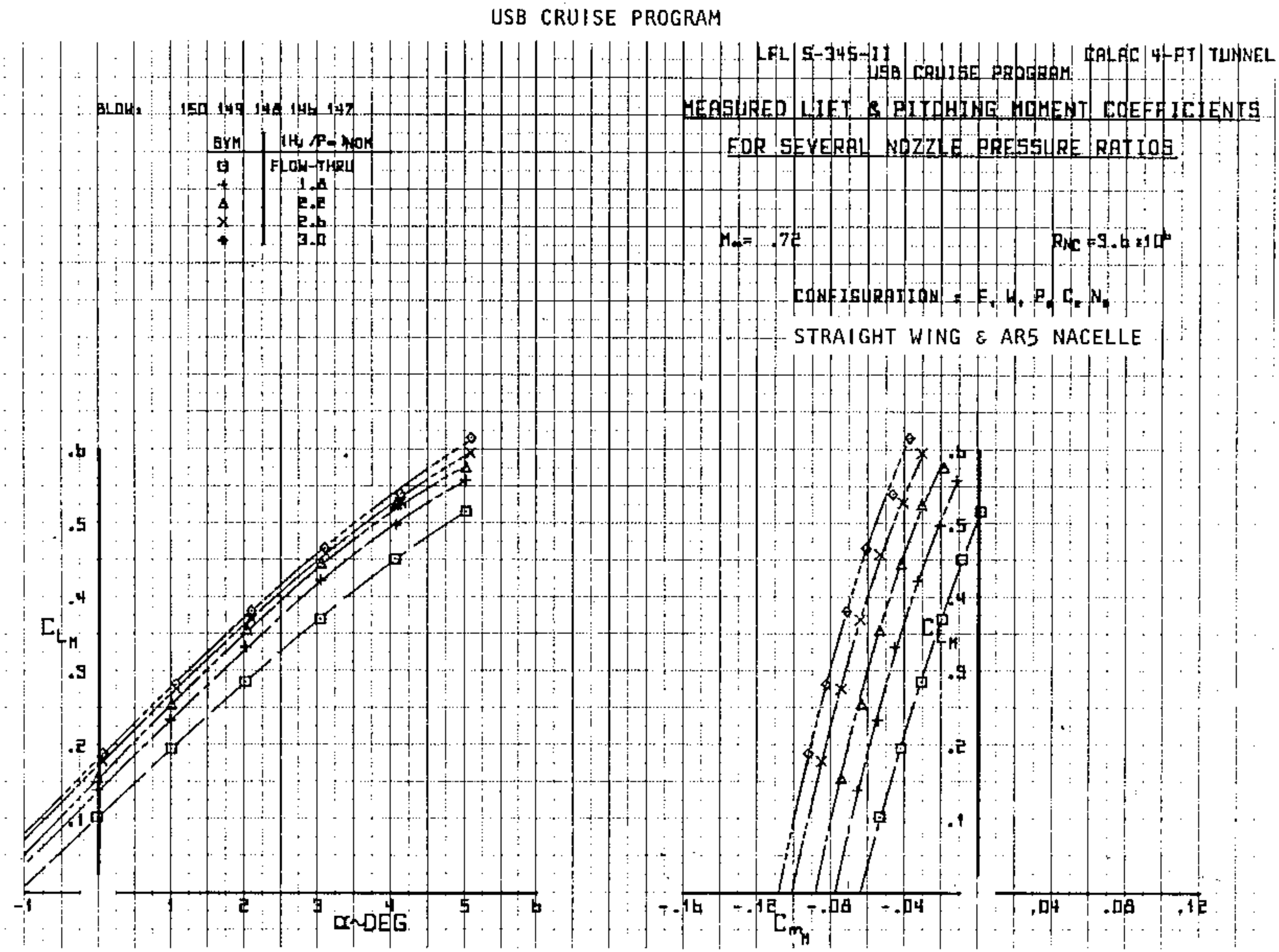

Figure 72. Variation of measured lift coefficient with angle of attack and moment coefficient, $M_\infty = 0.72$.

USB CRUISE PROGRAM

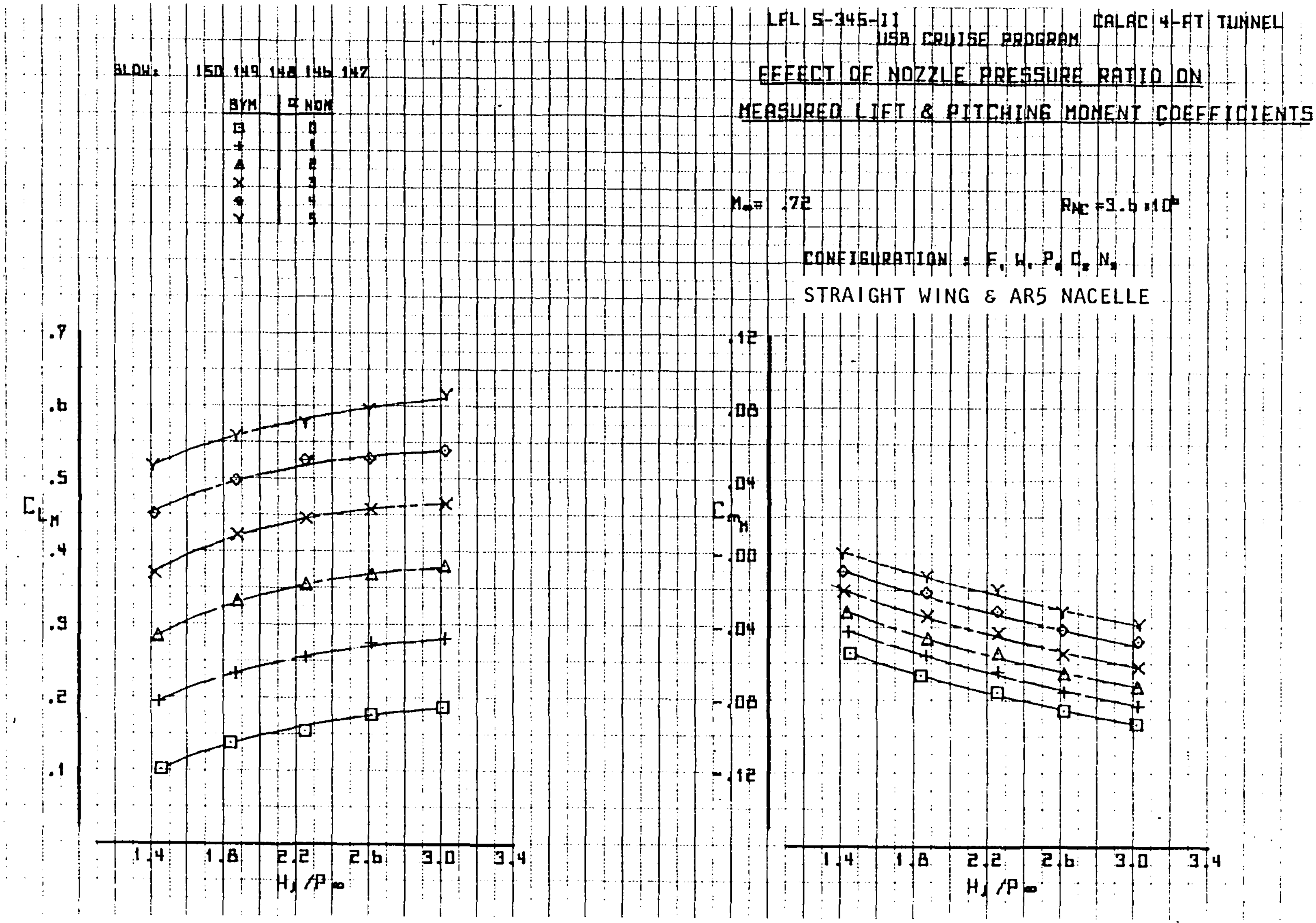

Figure 73. Variation of lift coefficent and moment coefficient with nozzle pressure ratio, $M_\infty = 0.72$.

USB CRUISE PROGRAM

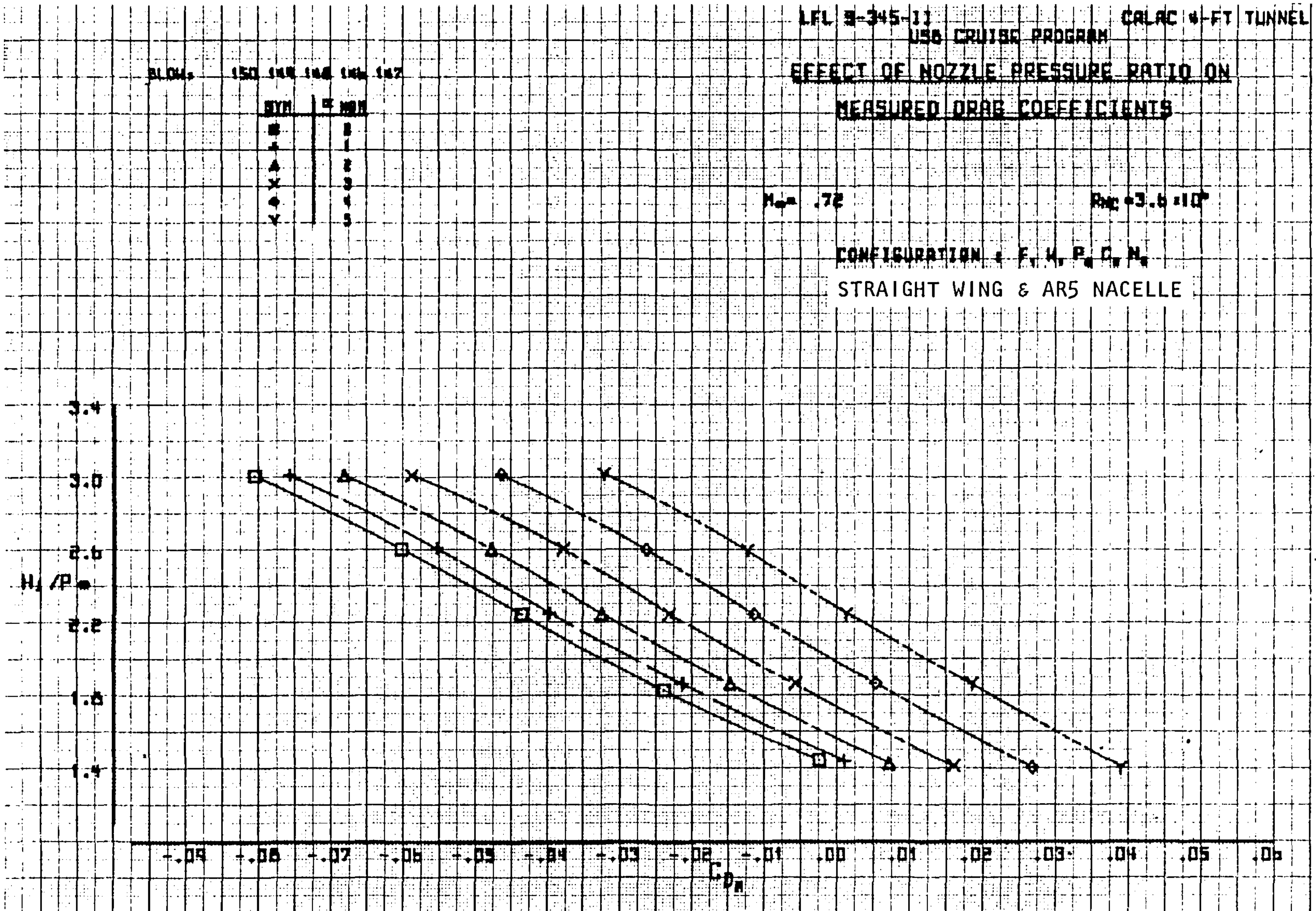

Figure 74. Variation of measured drag coefficient with nozzle pressure ratio, $M_\infty = 0.72$.

USB CRUISE PROGRAM

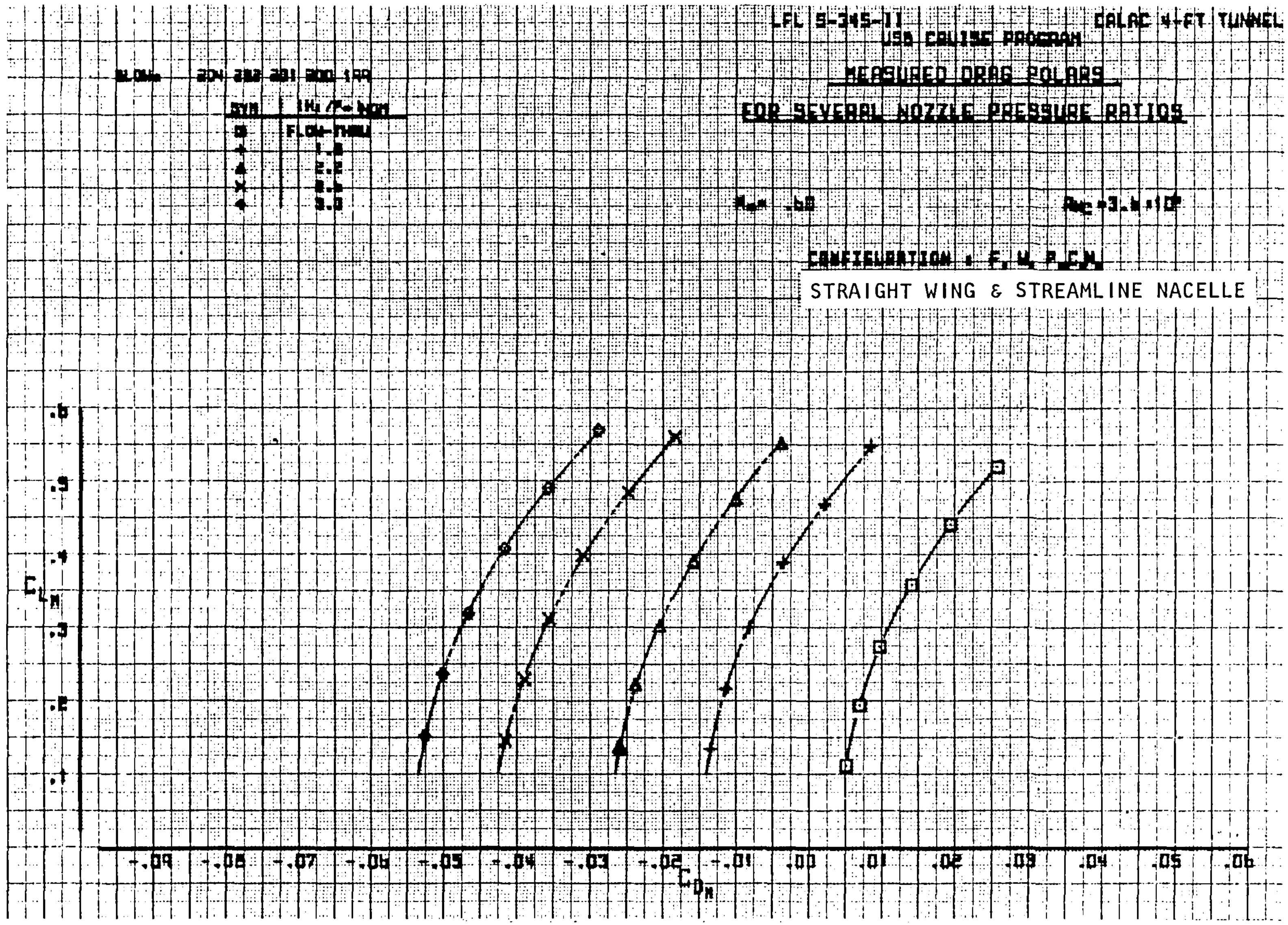

Figure 75. Variation of measured lift coefficient with measured drag coefficient and nozzle pressure ratio, $M_\infty = 0.60$.

USB CRUISE PROGRAM

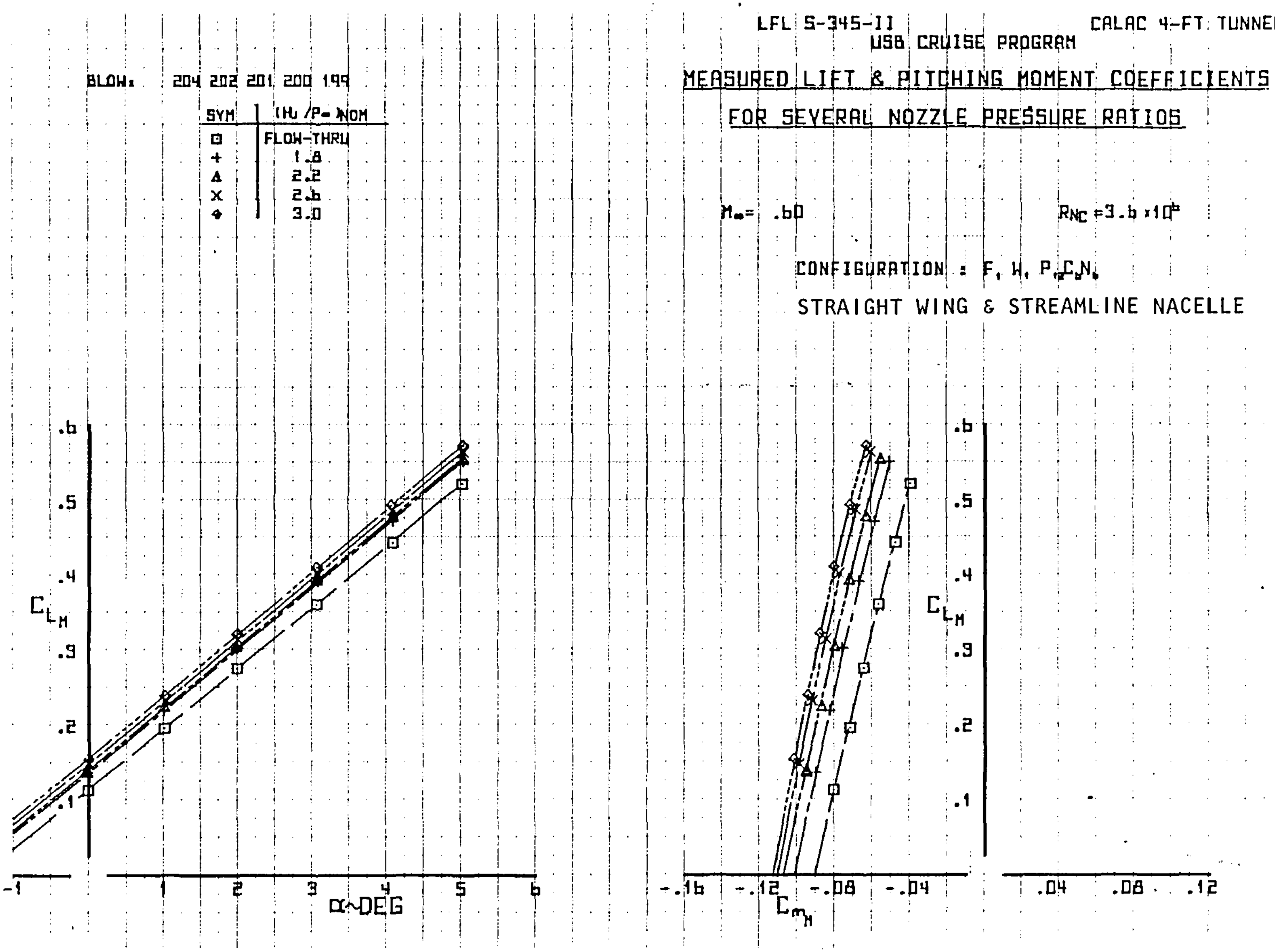

Figure 76. Variation of measured lift coefficient with angle of attack and moment coefficient, $M_\infty = 0.60$.

USB CRUISE PROGRAM

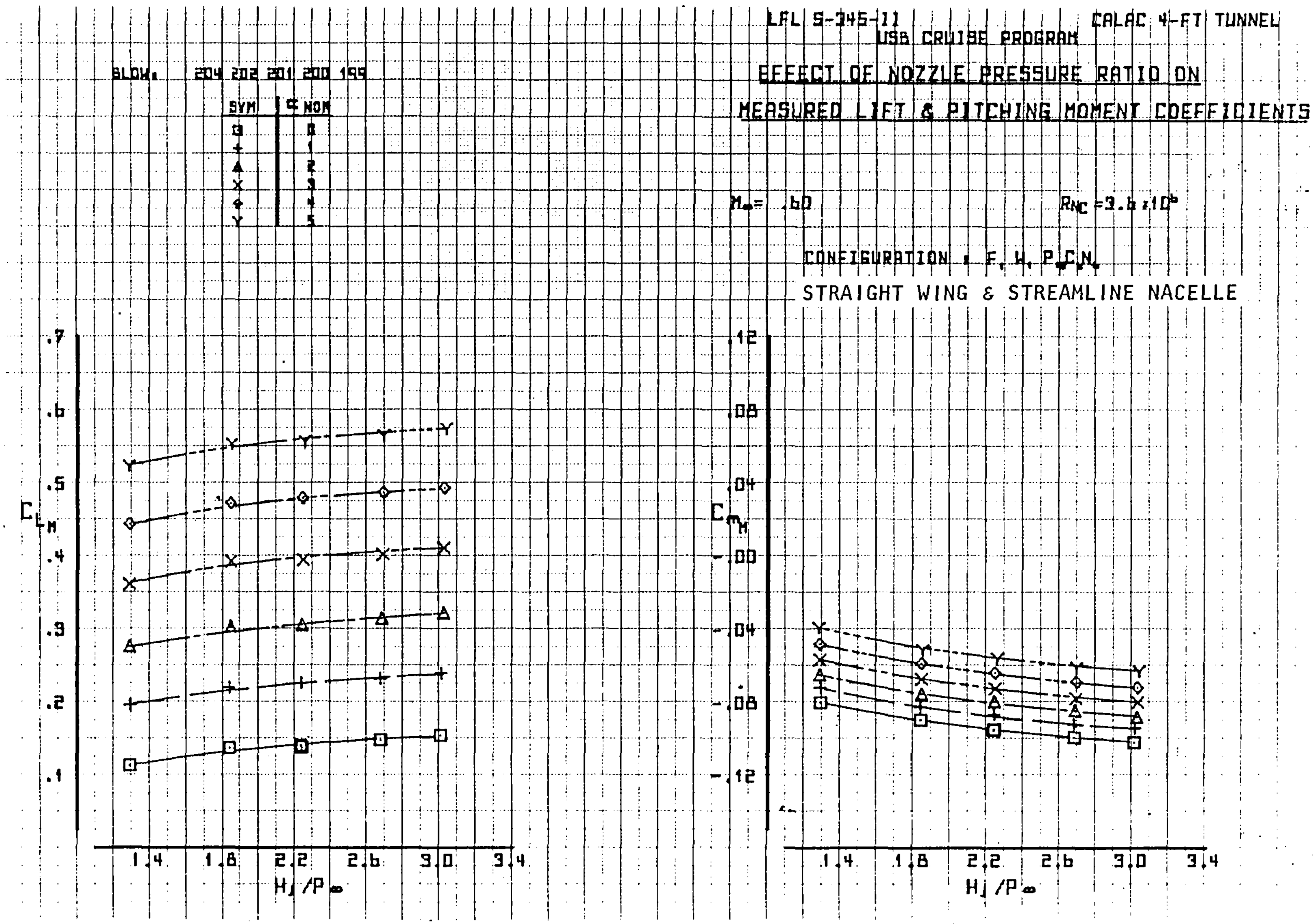

Figure 77. Variation of lift coefficient and moment coefficient with nozzle pressure ratio, $M_\infty = 0.60$.

USB CRUISE PROGRAM

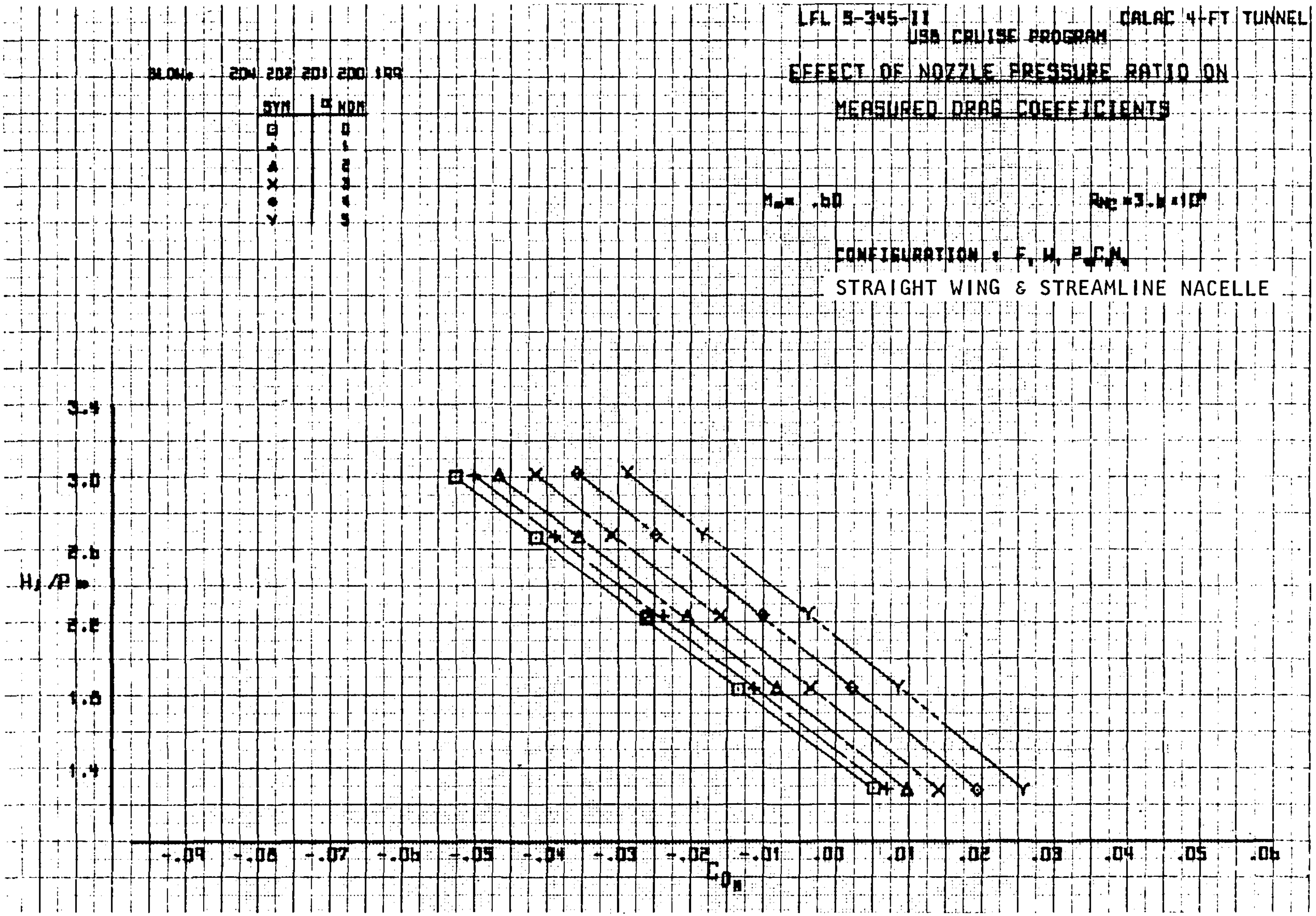

Figure 78. Variation of measured drag coefficient with nozzle pressure ratio, $M_\infty = 0.60$.

USB CRUISE PROGRAM

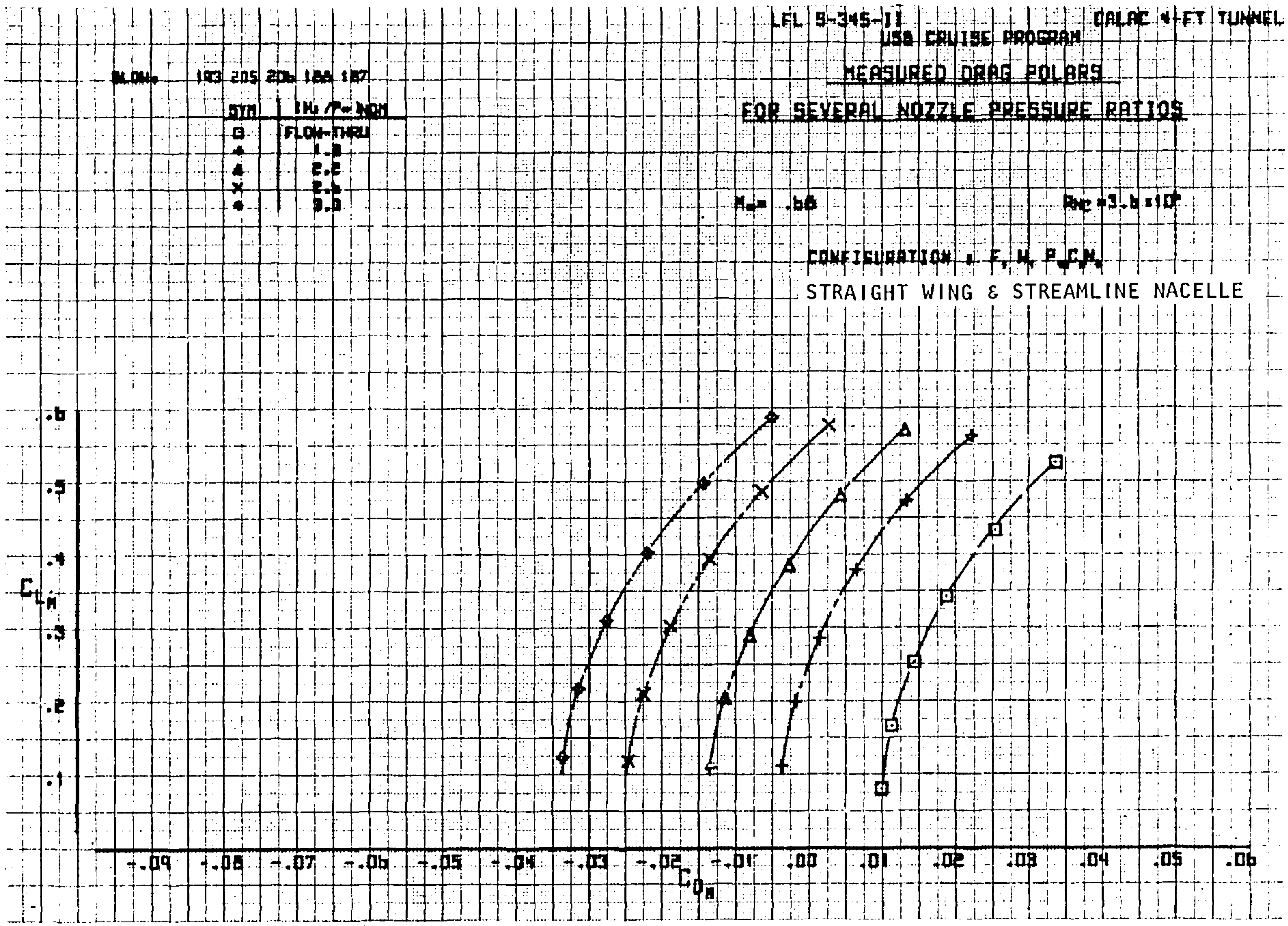

Figure 79. Variation of measured lift coefficient with measured drag coefficient and nozzle pressure ratio, $M_\infty = 0.68$.

USB CRUISE PROGRAM

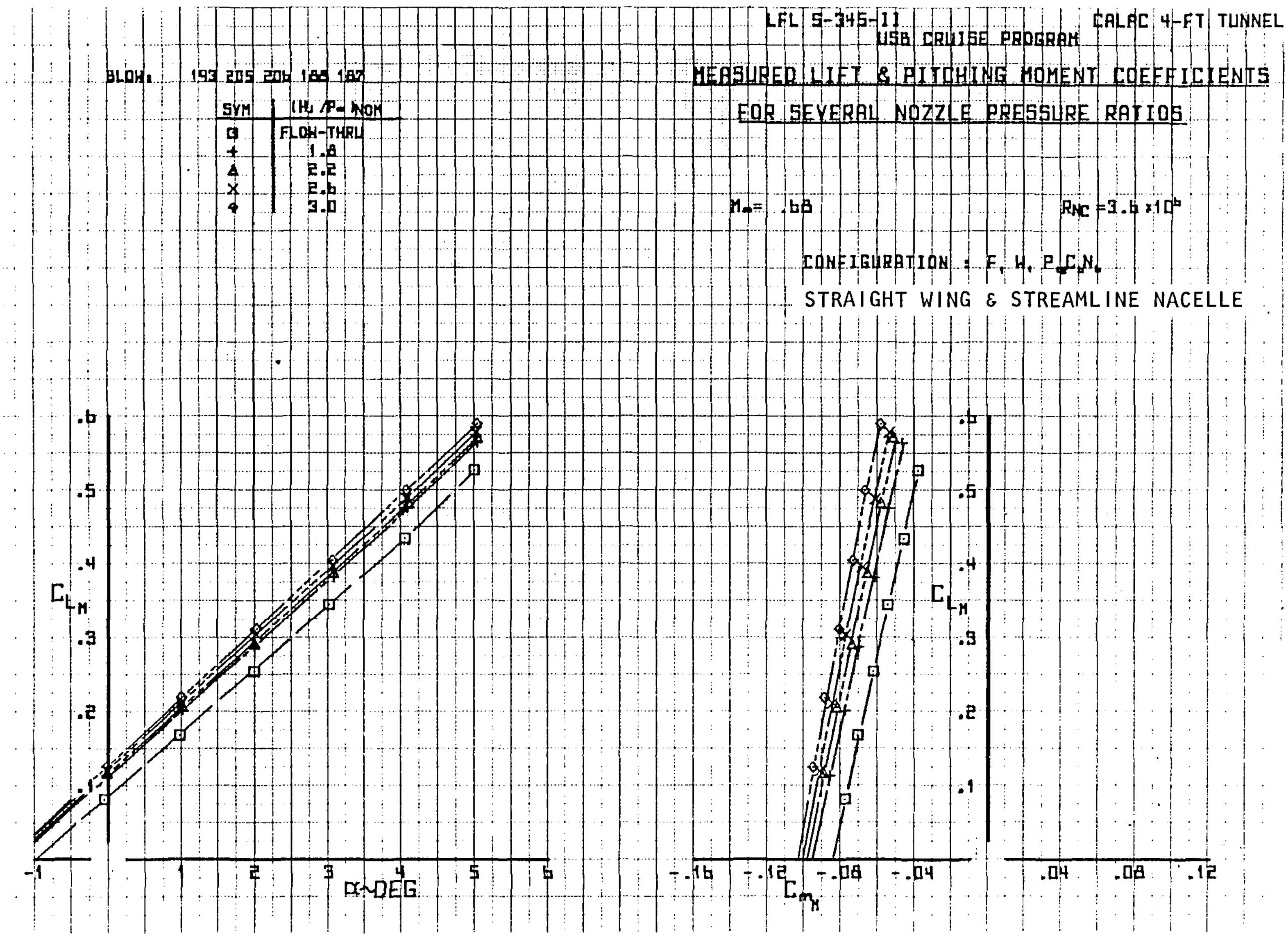

Figure 80. Variation of measured lift coefficient with angle of attack and moment coefficient, $M_\infty = 0.68$.

USB CRUISE PROGRAM

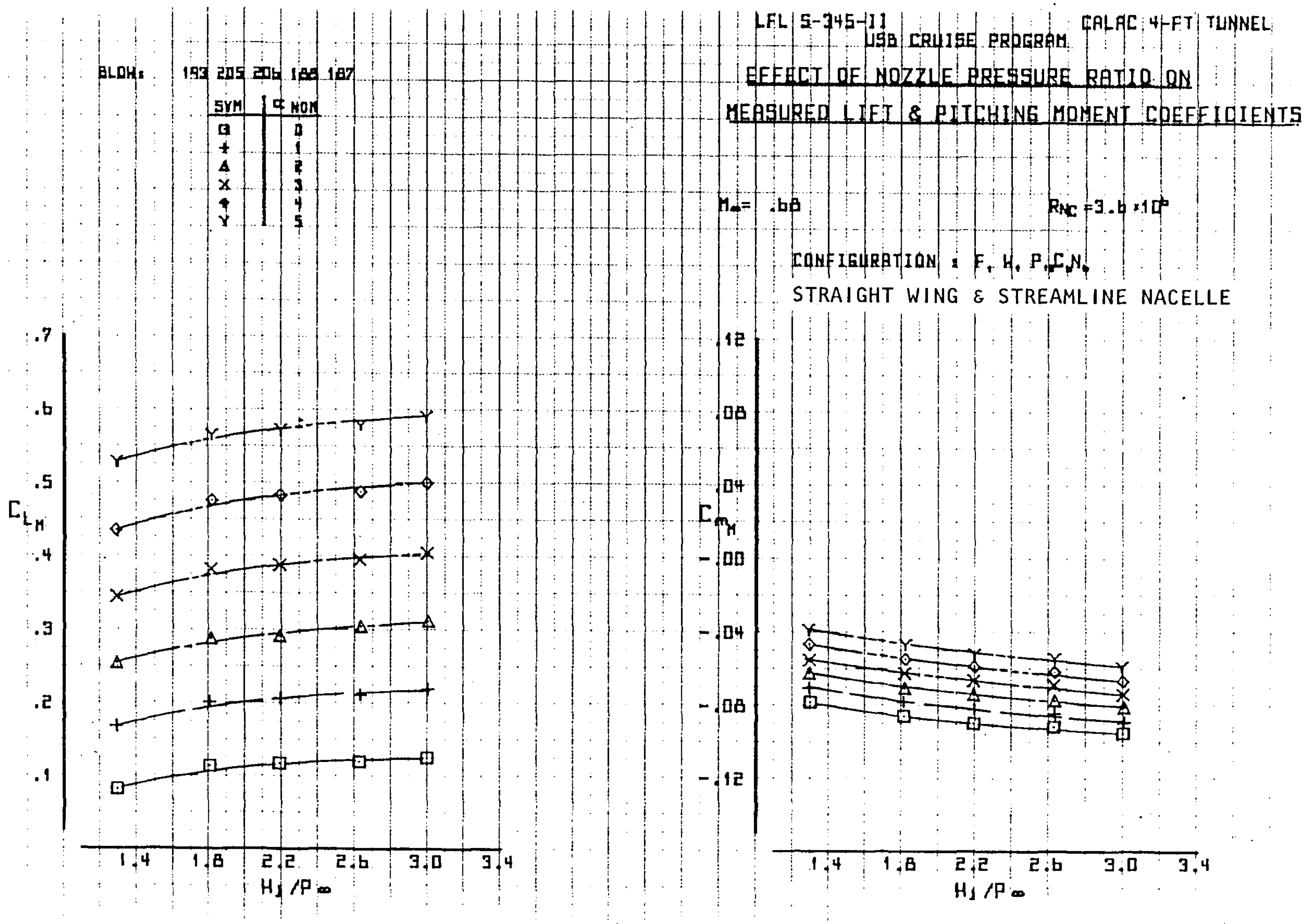

Figure 81. Variation of lift coefficient and moment coefficient with nozzle pressure ratio, $M_\infty = 0.68$.

USB CRUISE PROGRAM

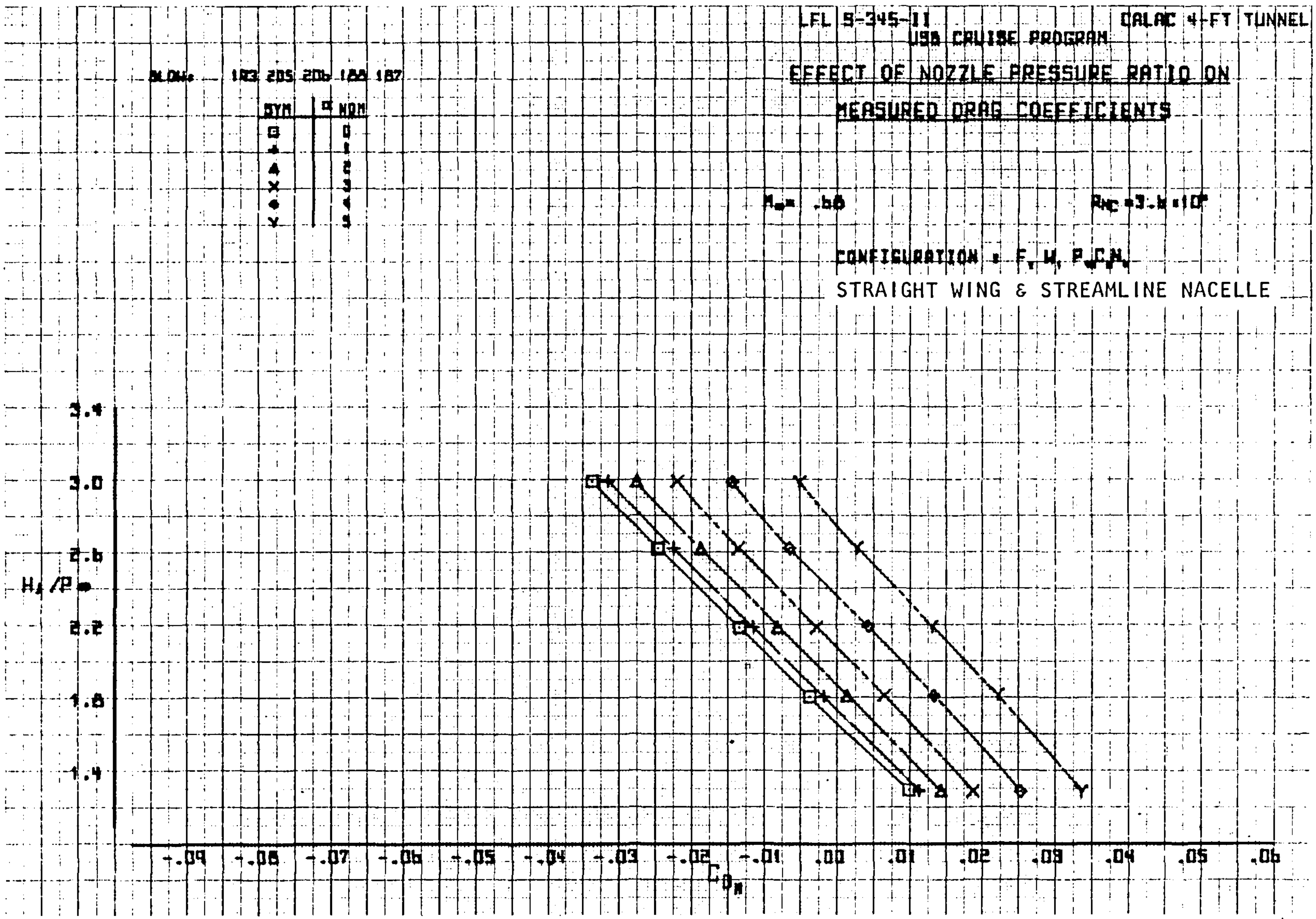

Figure 82. Variation of measured drag coefficient with nozzle pressure ratio, $M_\infty = 0.68$.

USB CRUISE PROGRAM

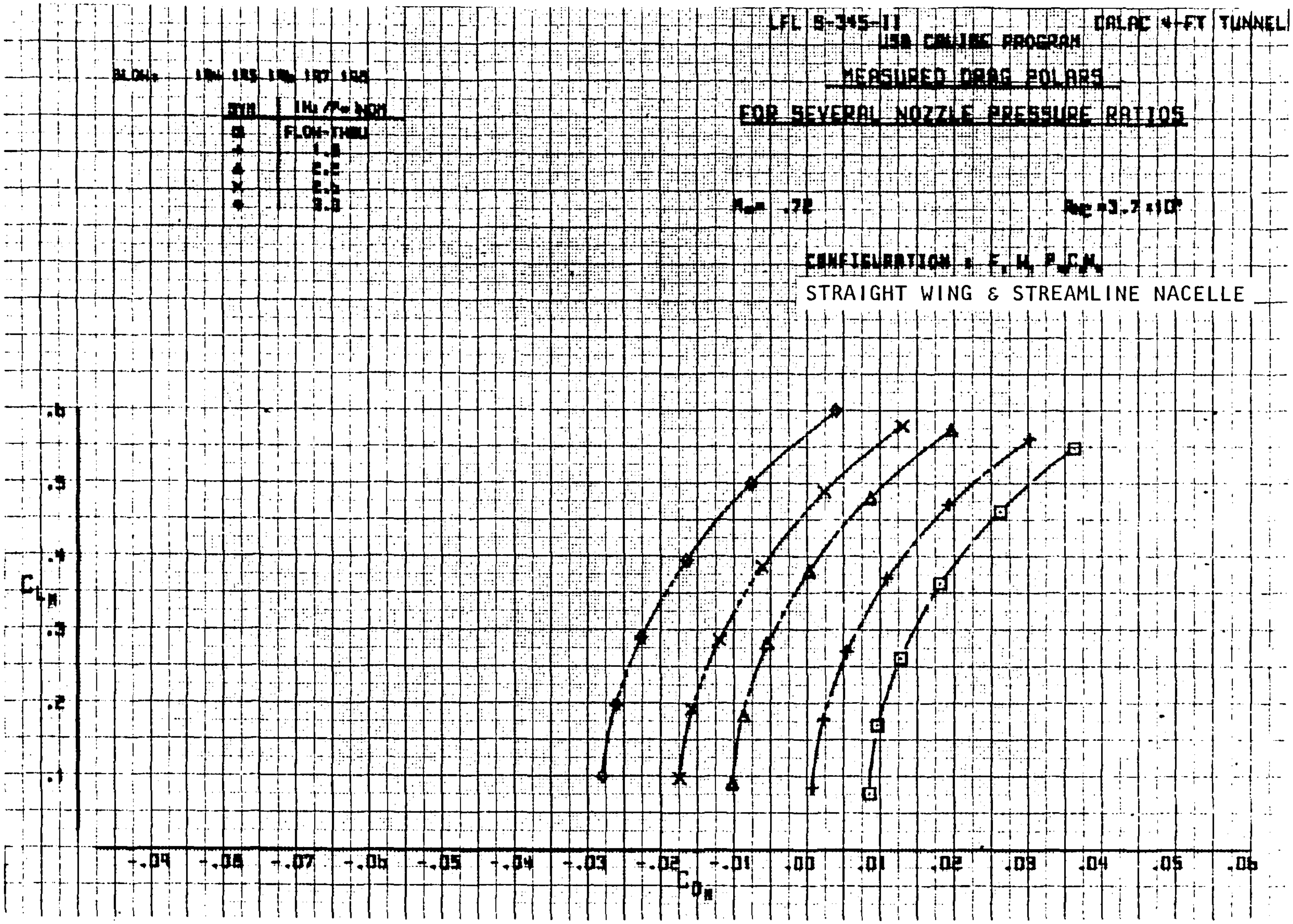

Figure 83. Variation of measured lift coefficient with measured drag coefficient and nozzle pressure ratio, $M_\infty = 0.72$.

USB CRUISE PROGRAM

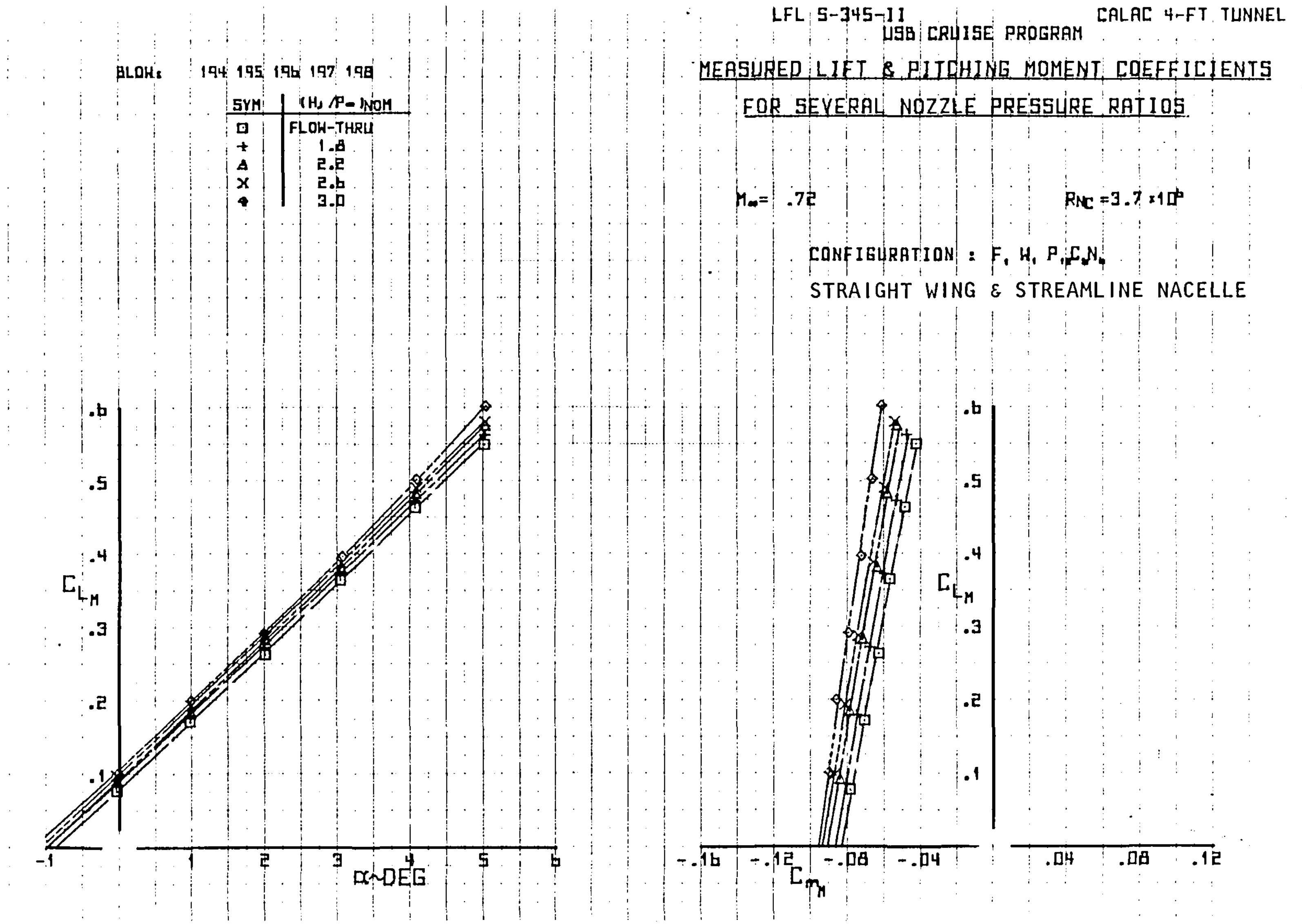

Figure 84. Variation of measured lift coefficient with angle of attack and moment coefficient, $M_\infty = 0.72$.

USB CRUISE PROGRAM

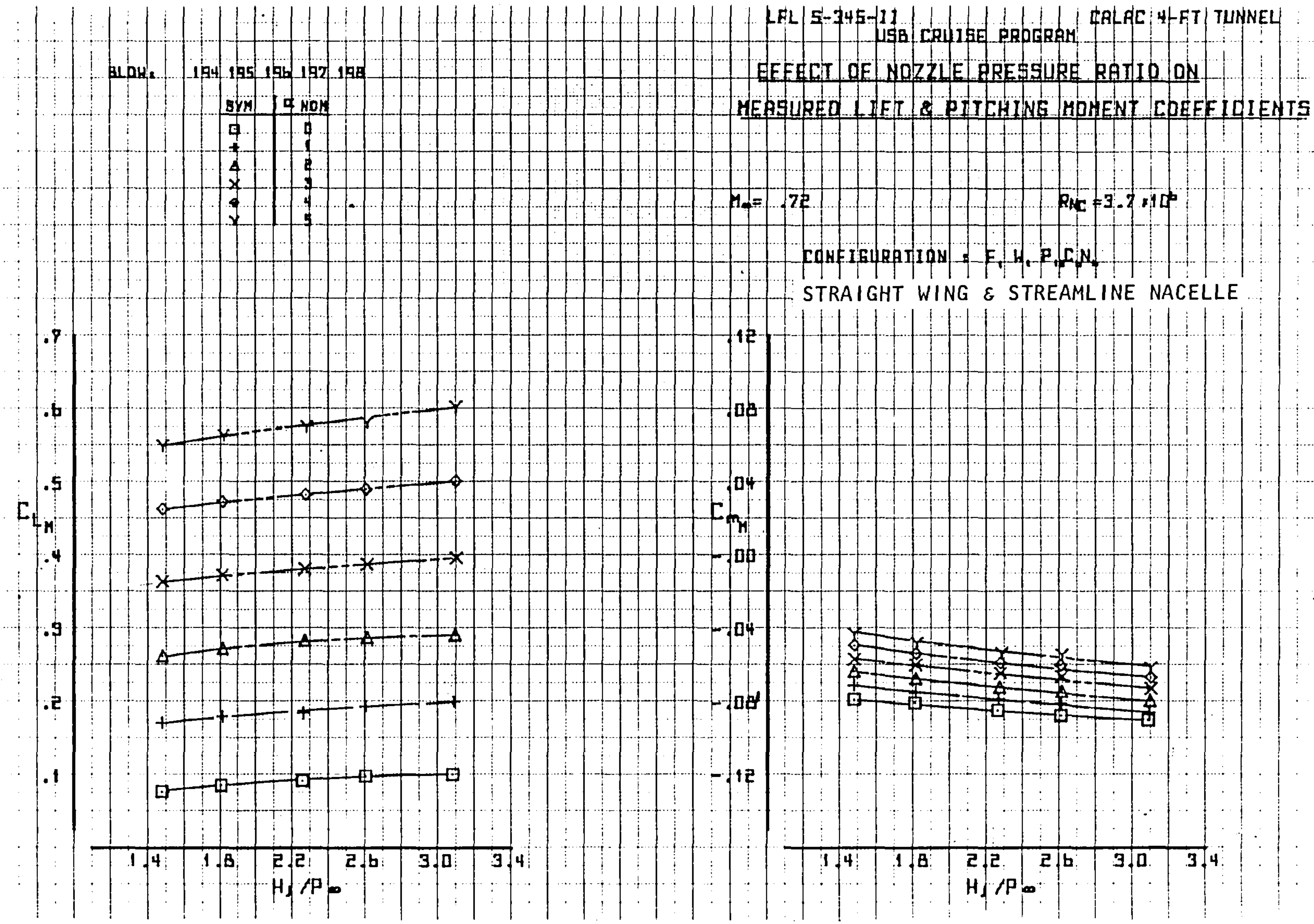

Figure 85. Variation of lift coefficient and moment coefficient with nozzle pressure ratio, $M_\infty = 0.72$.

USB CRUISE PROGRAM

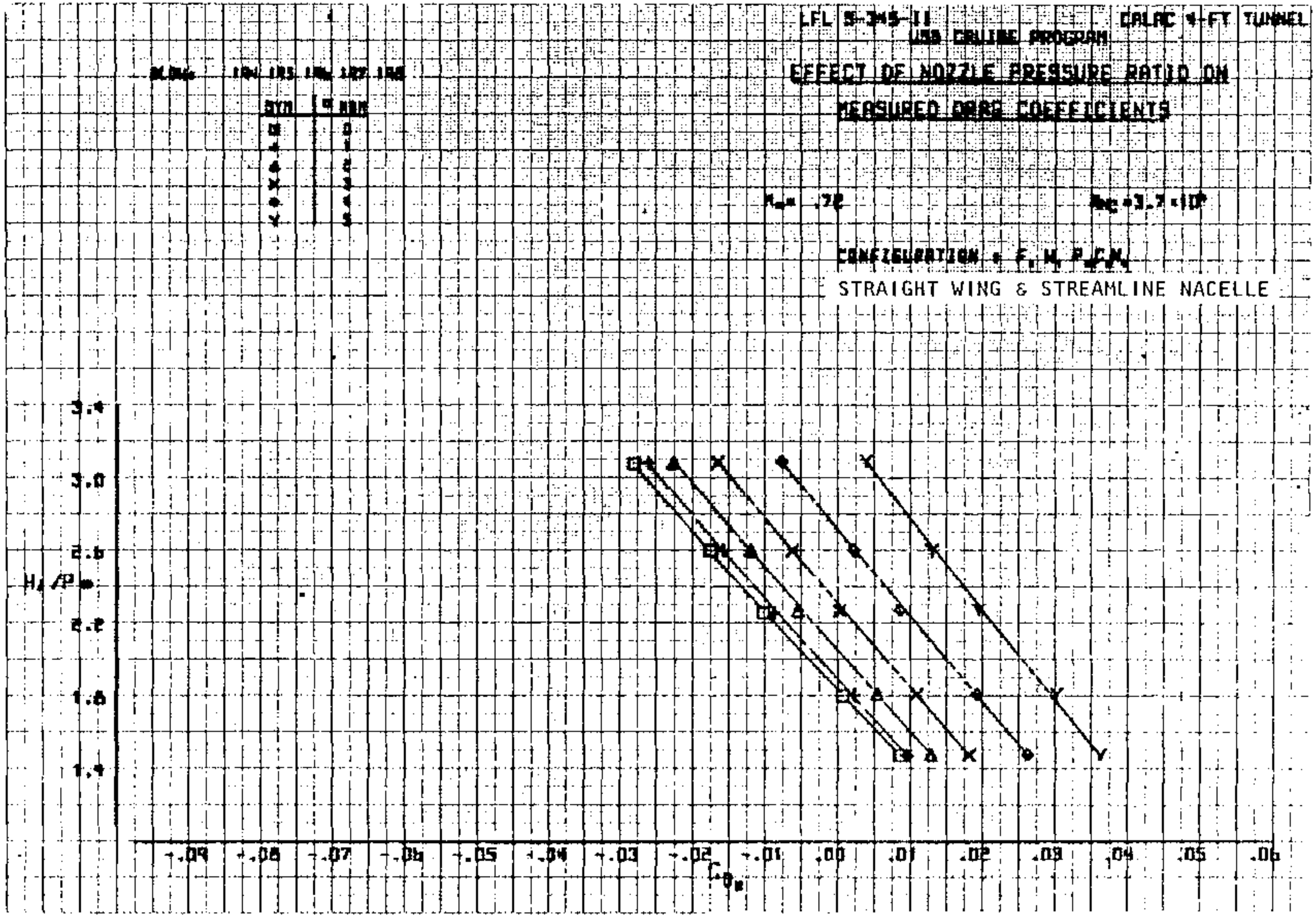

Figure 86. Variation of measured drag coefficient with nozzle pressure ratio, $M_\infty = 0.72$.

USB CRUISE PROGRAM

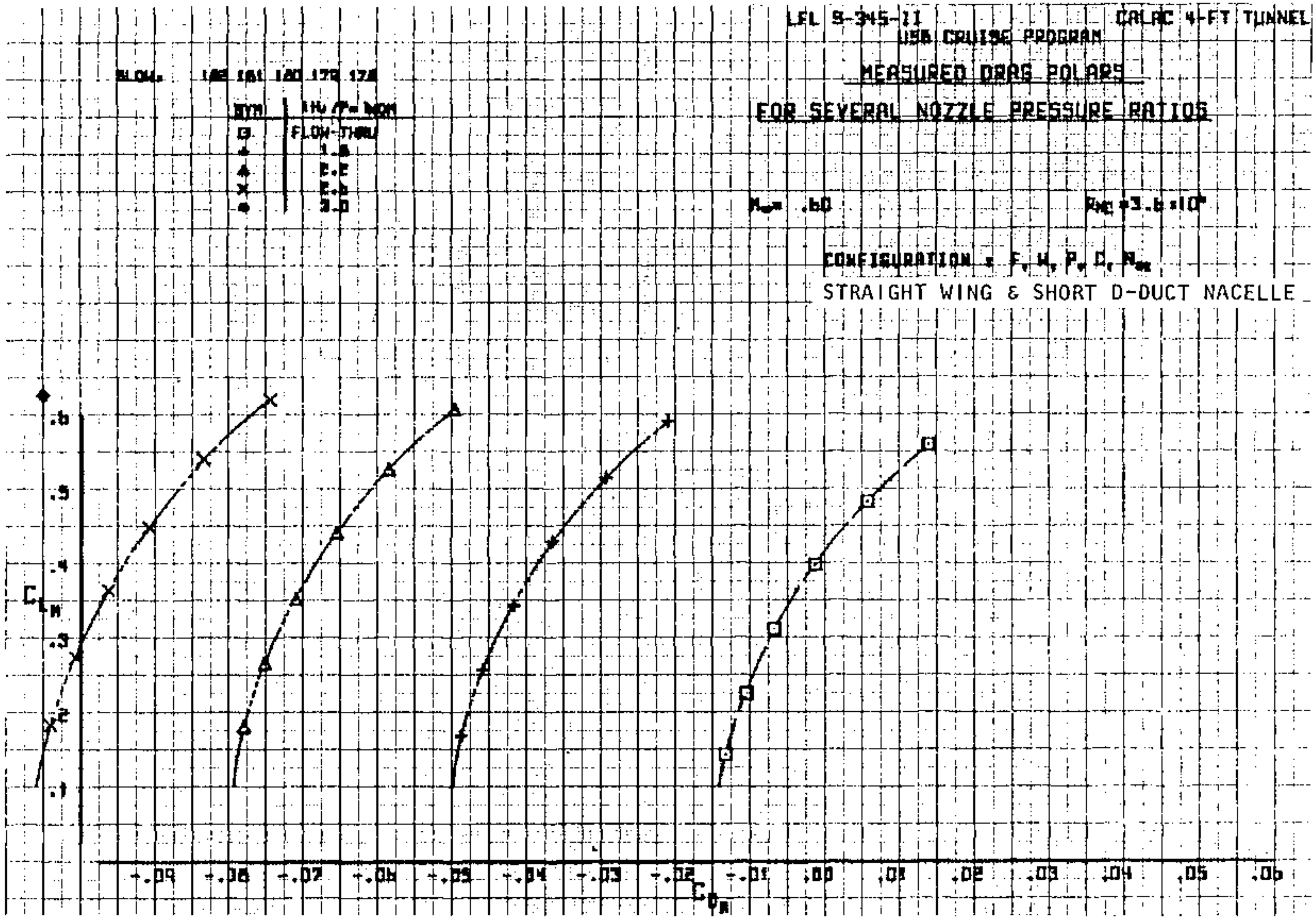

Figure 87. Variation of measured lift coefficient with measured drag coefficient and nozzle pressure ratio, $M_\infty = 0.60$.

USB CRUISE PROGRAM

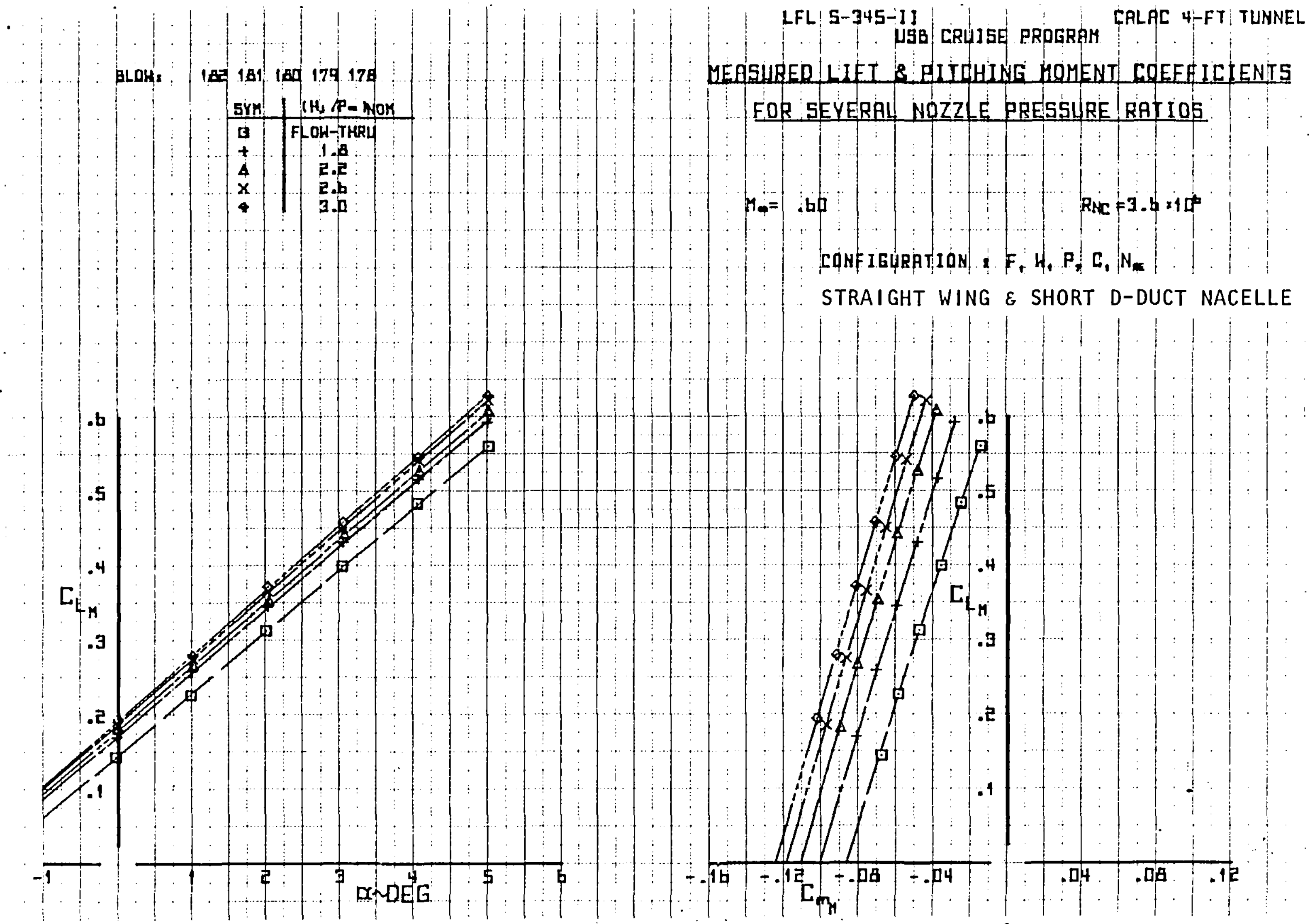

Figure 88. Variation of measured lift coefficient with angle of attack and moment coefficient, $M_\infty = 0.60$.

USB CRUISE PROGRAM

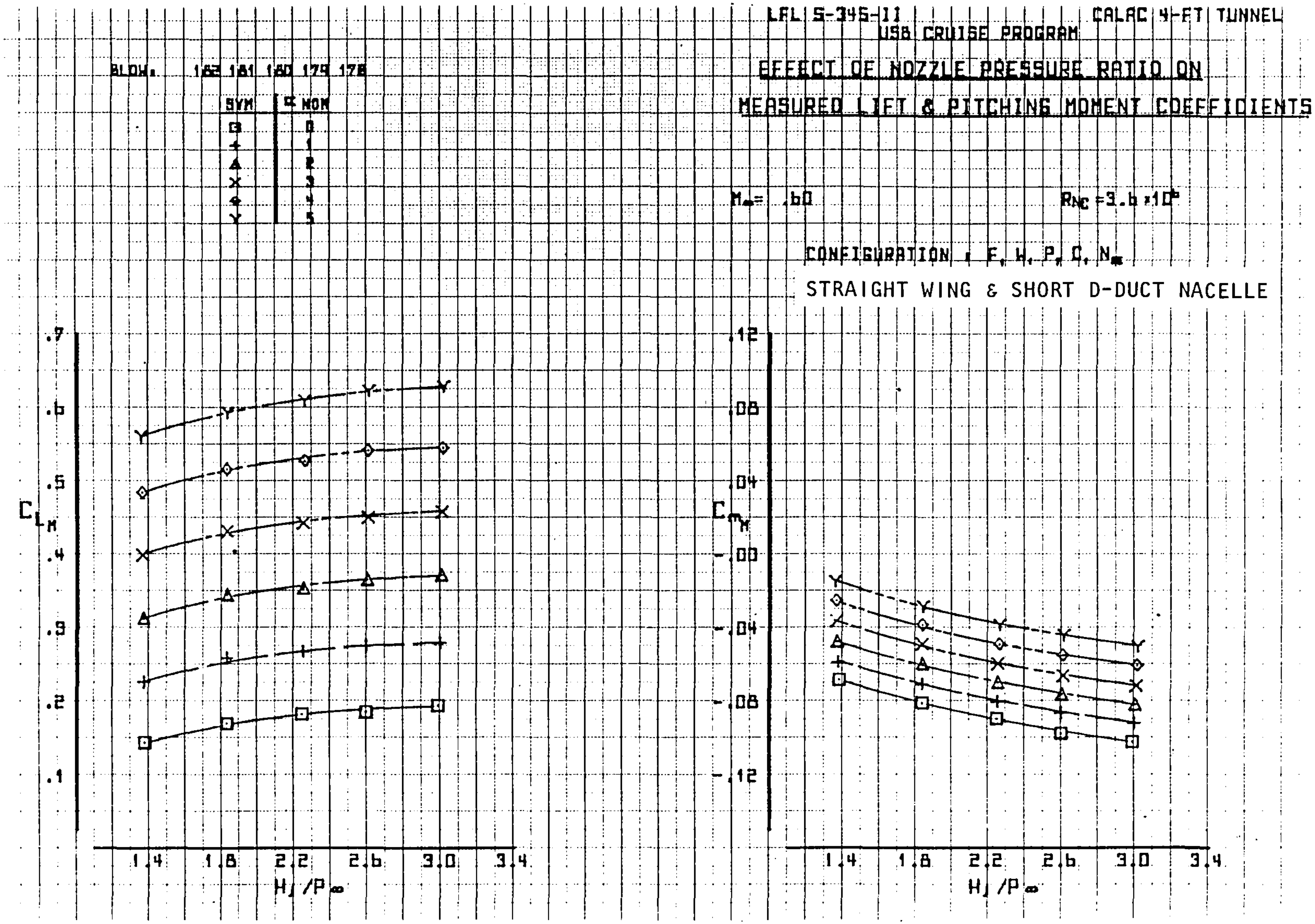

Figure 89. Variation of lift coefficient and moment coefficient with nozzle pressure ratio, M_∞ = 0.60.

USB CRUISE PROGRAM

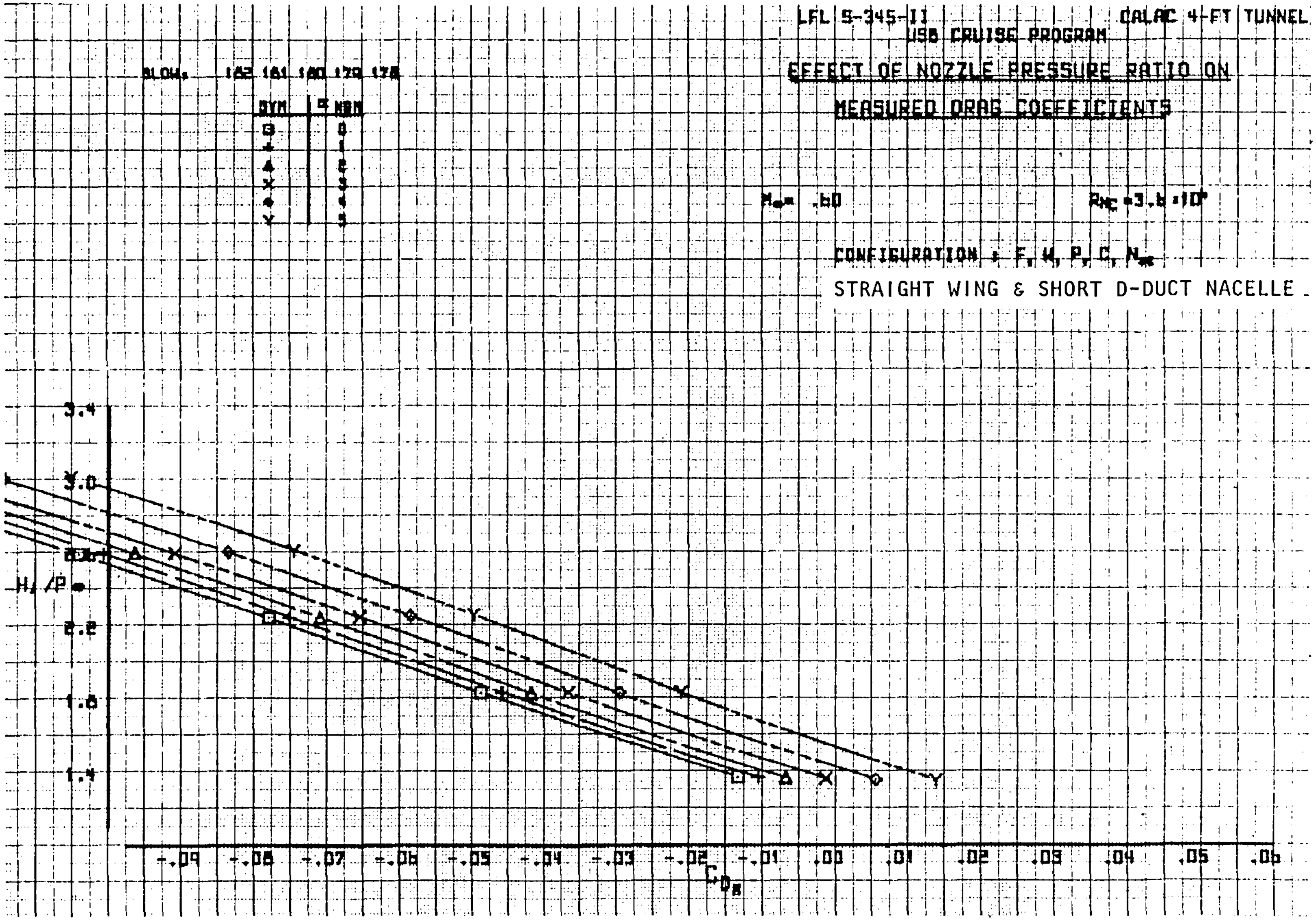

Figure 90. Variation of measured drag coefficient with nozzle pressure ratio, $M_\infty = 0.60$.

USB CRUISE PROGRAM

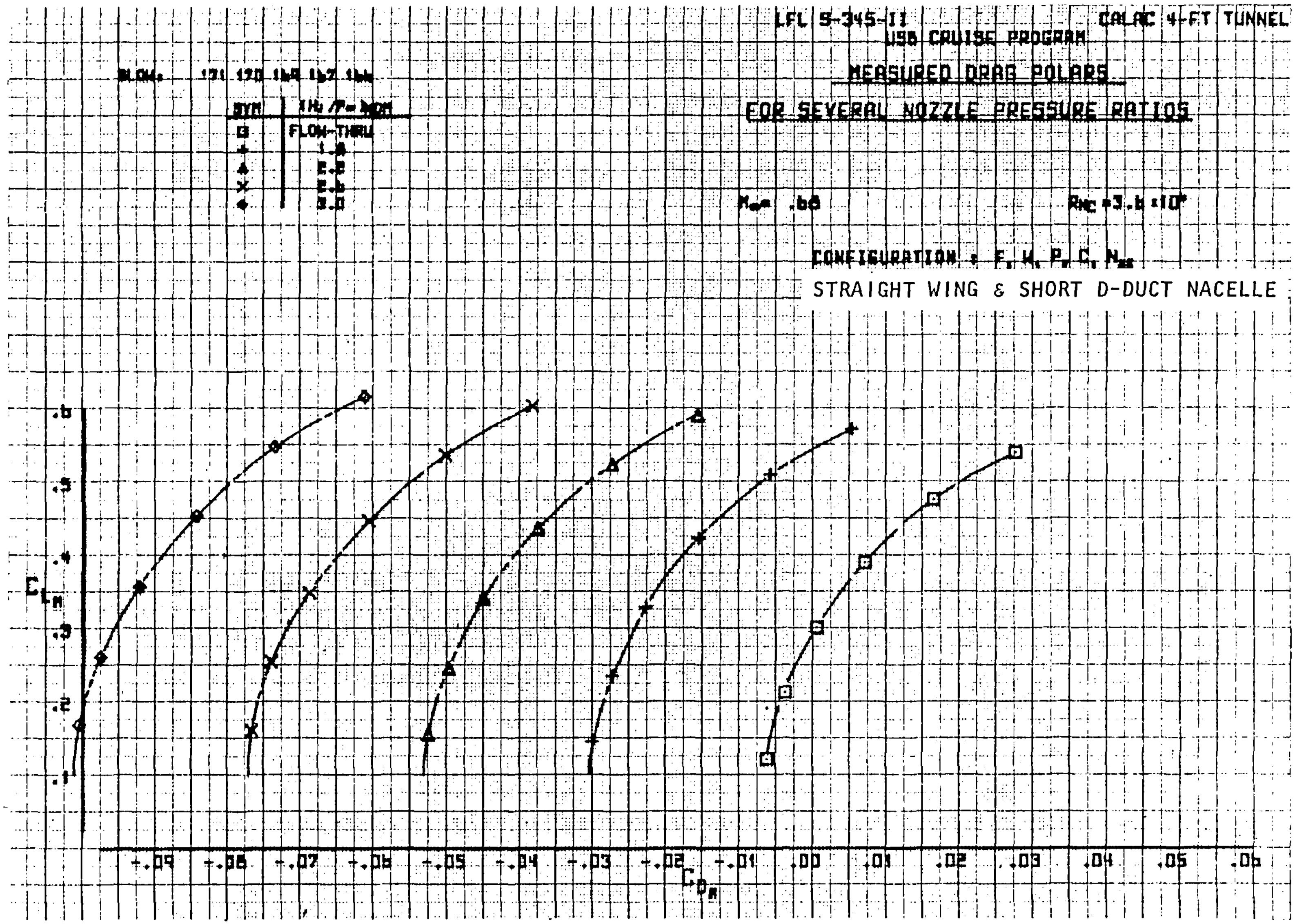

Figure 91. Variation of measured lift coefficient with measured drag coefficient and nozzle pressure ratio, $M_\infty = 0.68$.

USB CRUISE PROGRAM

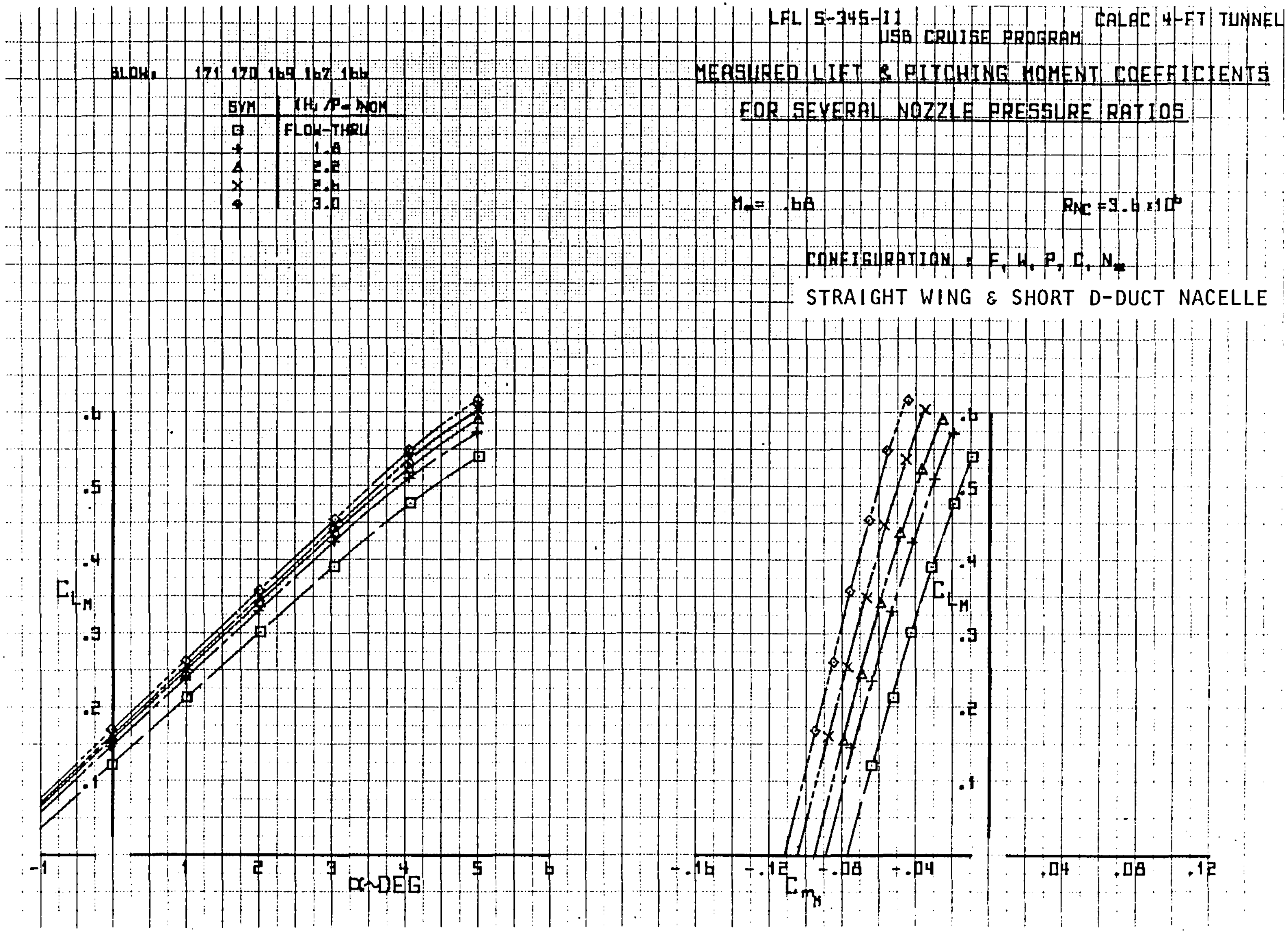

Figure 92. Variation of measured lift coefficient with angle of attack and moment coefficient, $M_\infty = 0.68$.

USB CRUISE PROGRAM

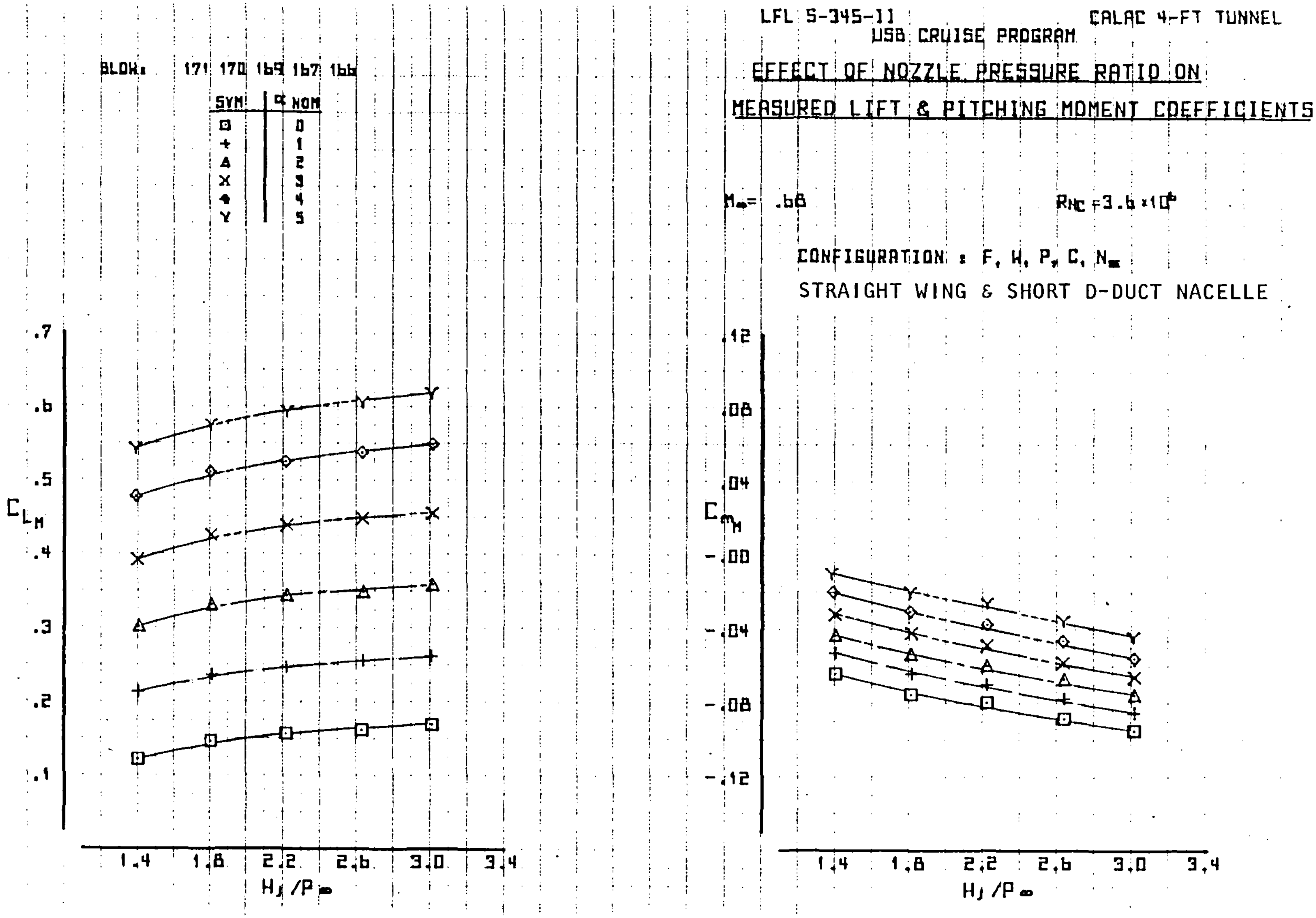

Figure 93. Variation of lift coefficient and moment coefficient with nozzle pressure ratio, M_∞ = 0.68.

USB CRUISE PROGRAM

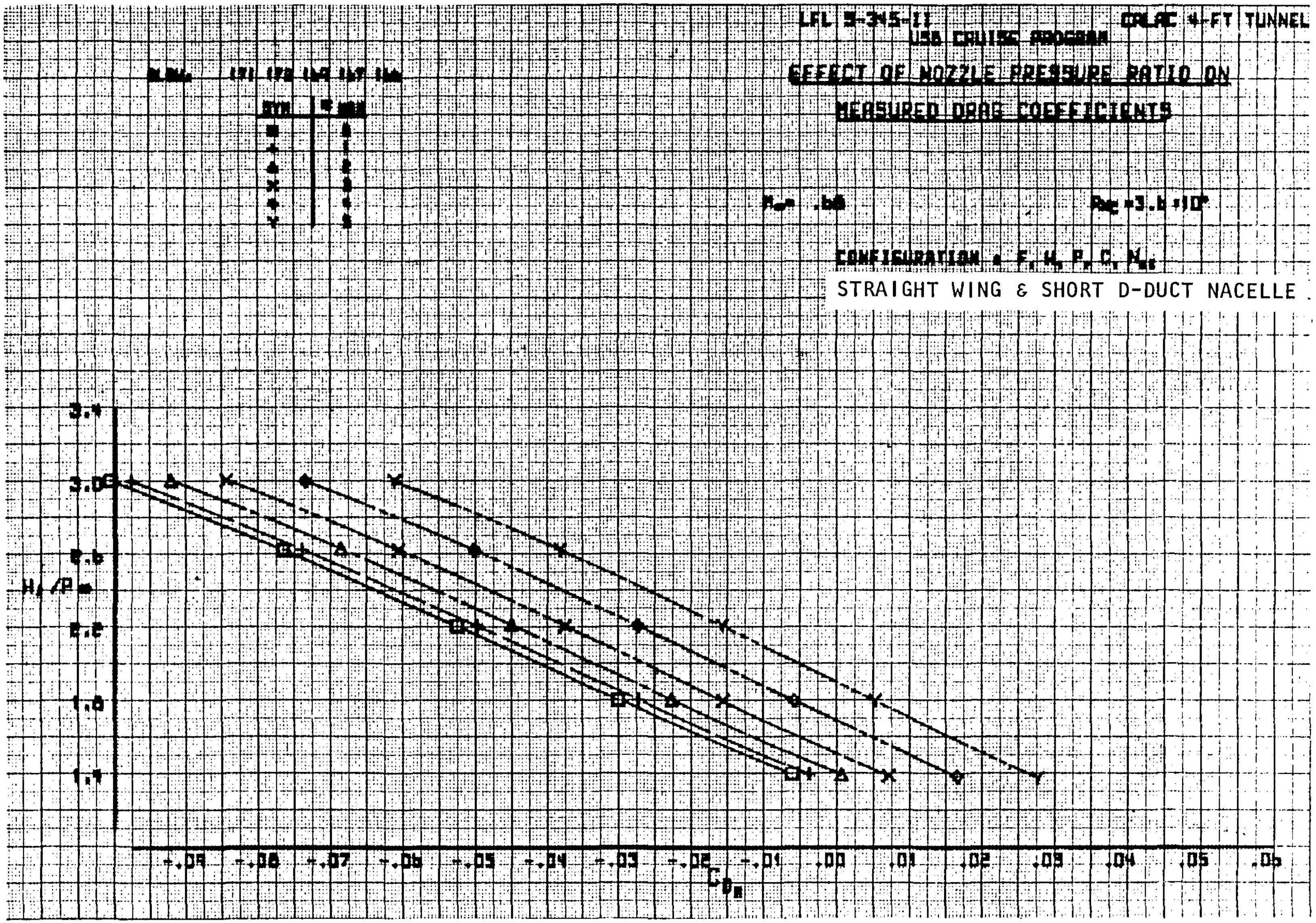

Figure 94. Variation of measured drag coefficient with nozzle pressure ratio, $M_\infty = 0.68$.

USB CRUISE PROGRAM

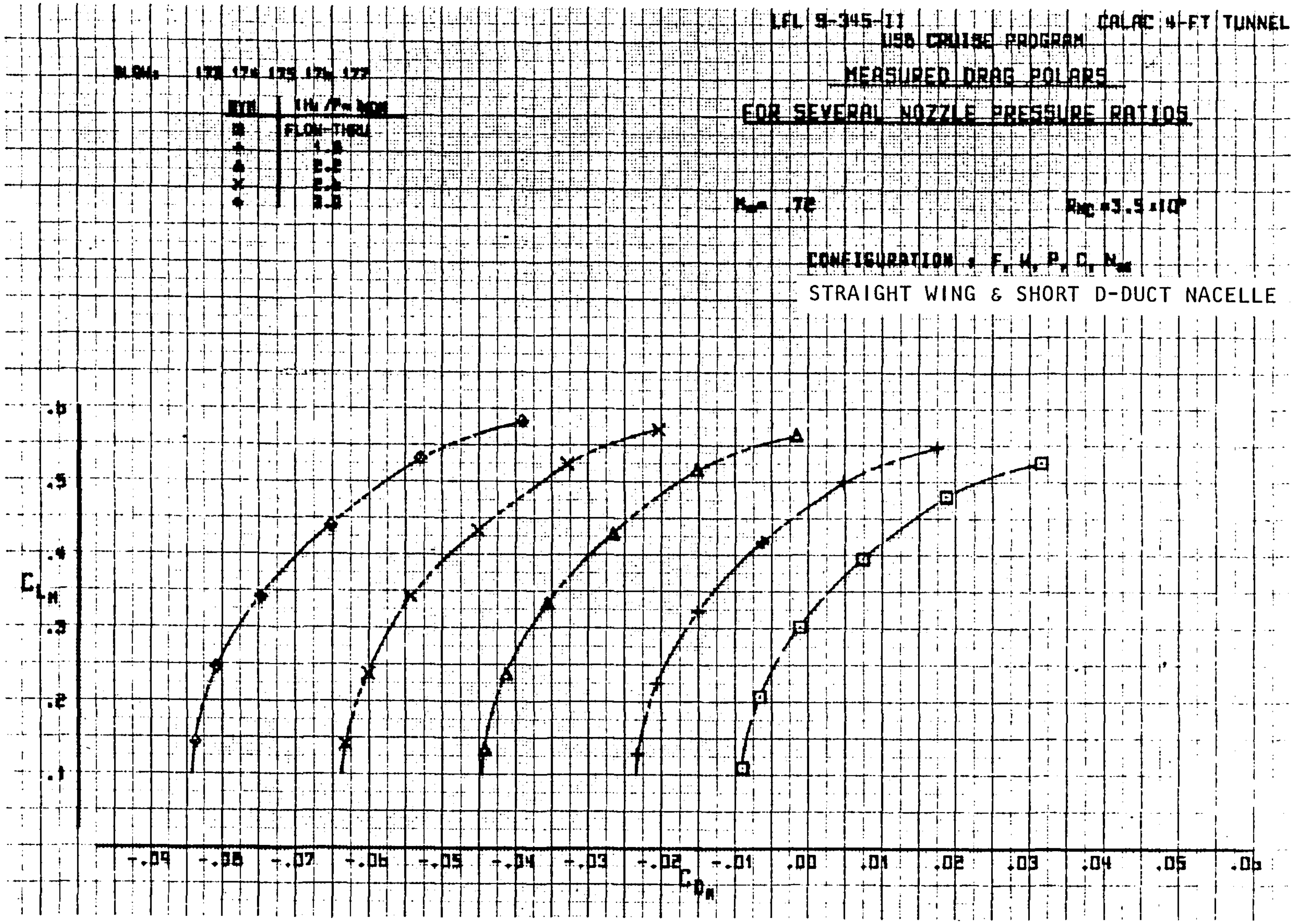

Figure 95. Variation of measured lift coefficient with measured drag coefficient and nozzle pressure ratio, $M_\infty = 0$.

USB CRUISE PROGRAM

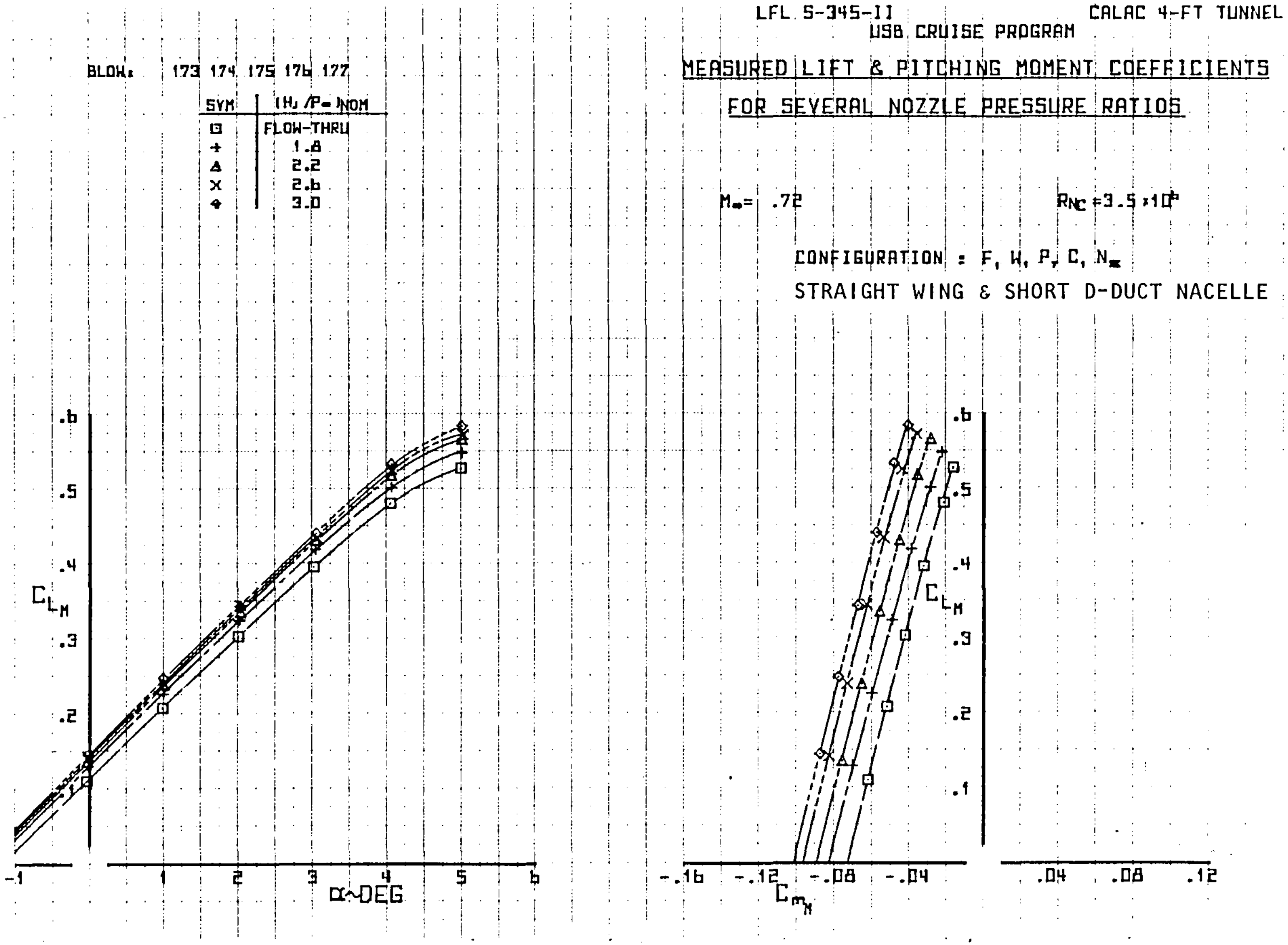

Figure 96. Variation of measured lift coefficient with angle of attack and moment coefficient, $M_\infty = 0.72$.

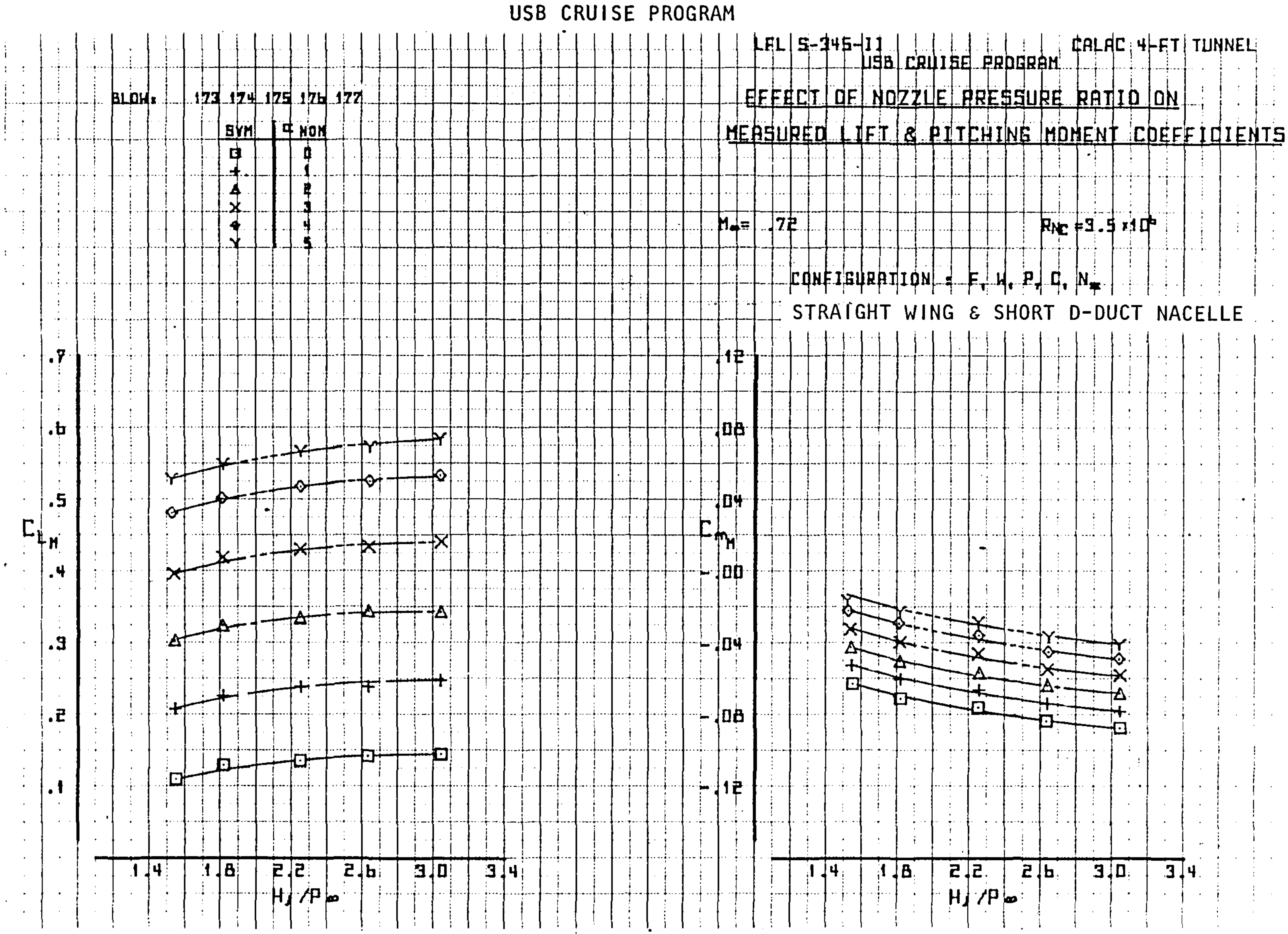

Figure 97. Variation of lift coefficient and moment coefficient with nozzle pressure ratio, $M_\infty = 0.72$.

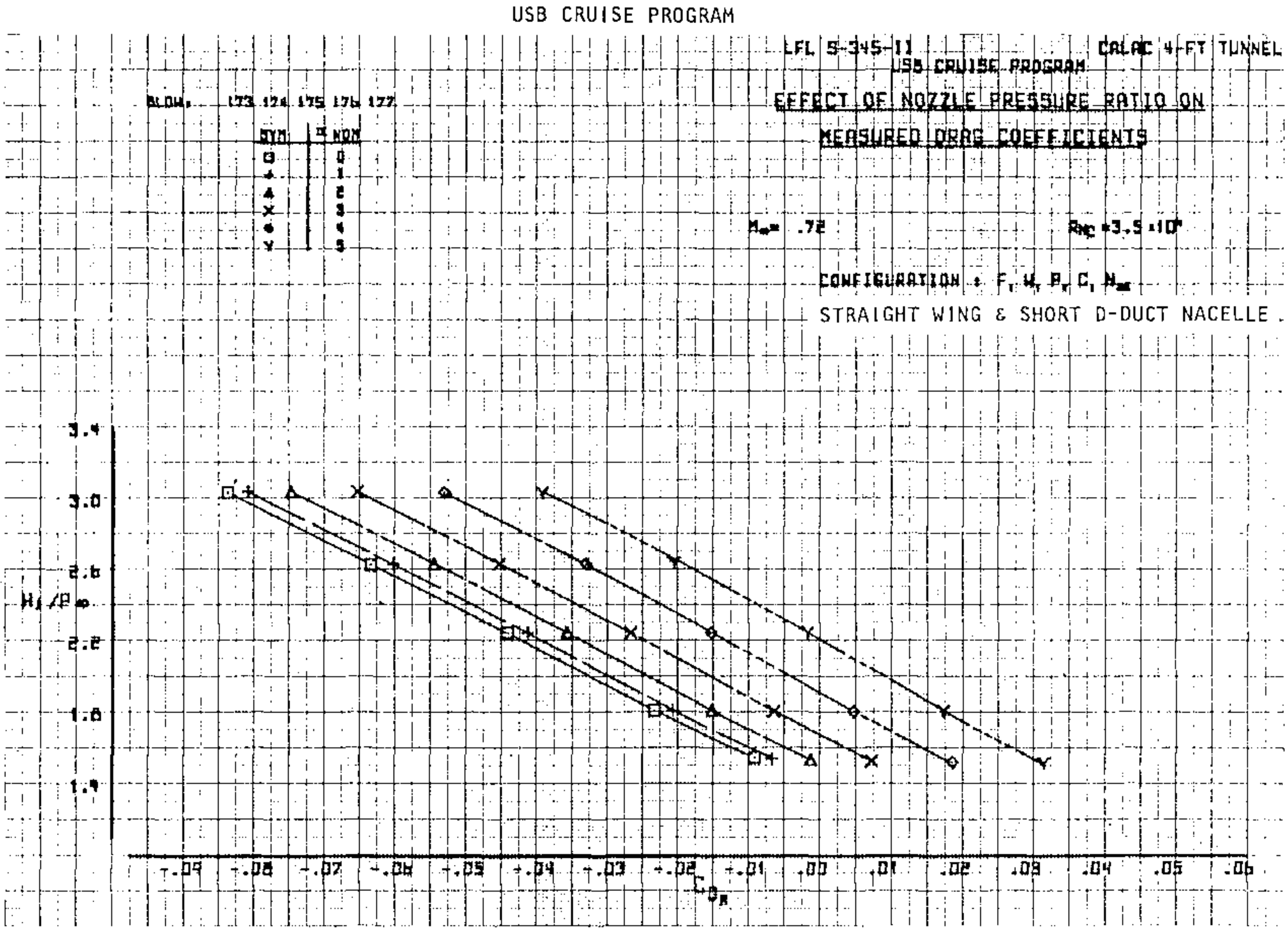

Figure 98. Variation of measured drag coefficient with nozzle pressure ratio, $M_\infty = 0.72$.

USB CRUISE PROGRAM

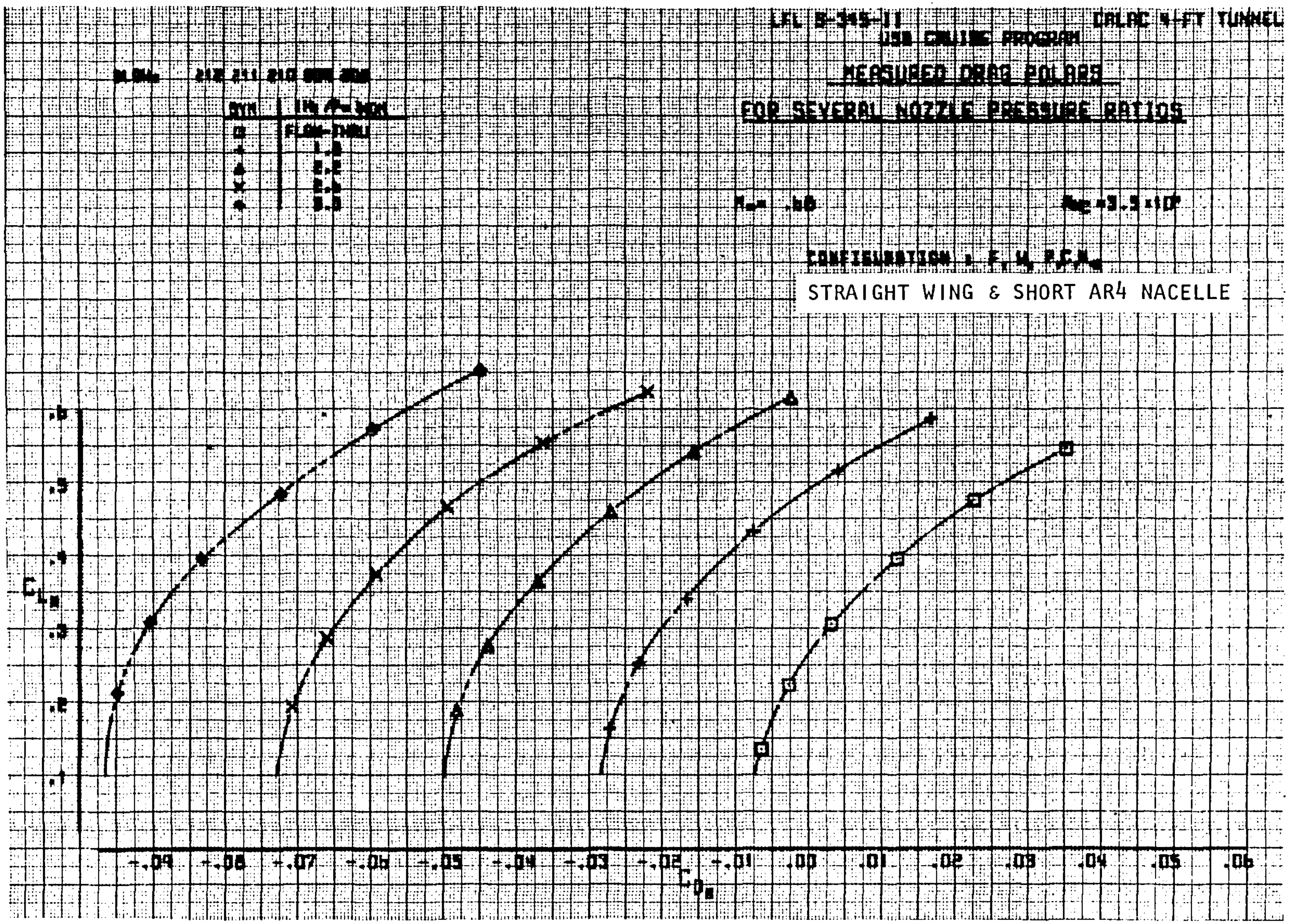

Figure 99. Variation of measured lift coefficient with measured drag coefficient and nozzle pressure ratio, $M_\infty = 0.68$.

USB CRUISE PROGRAM

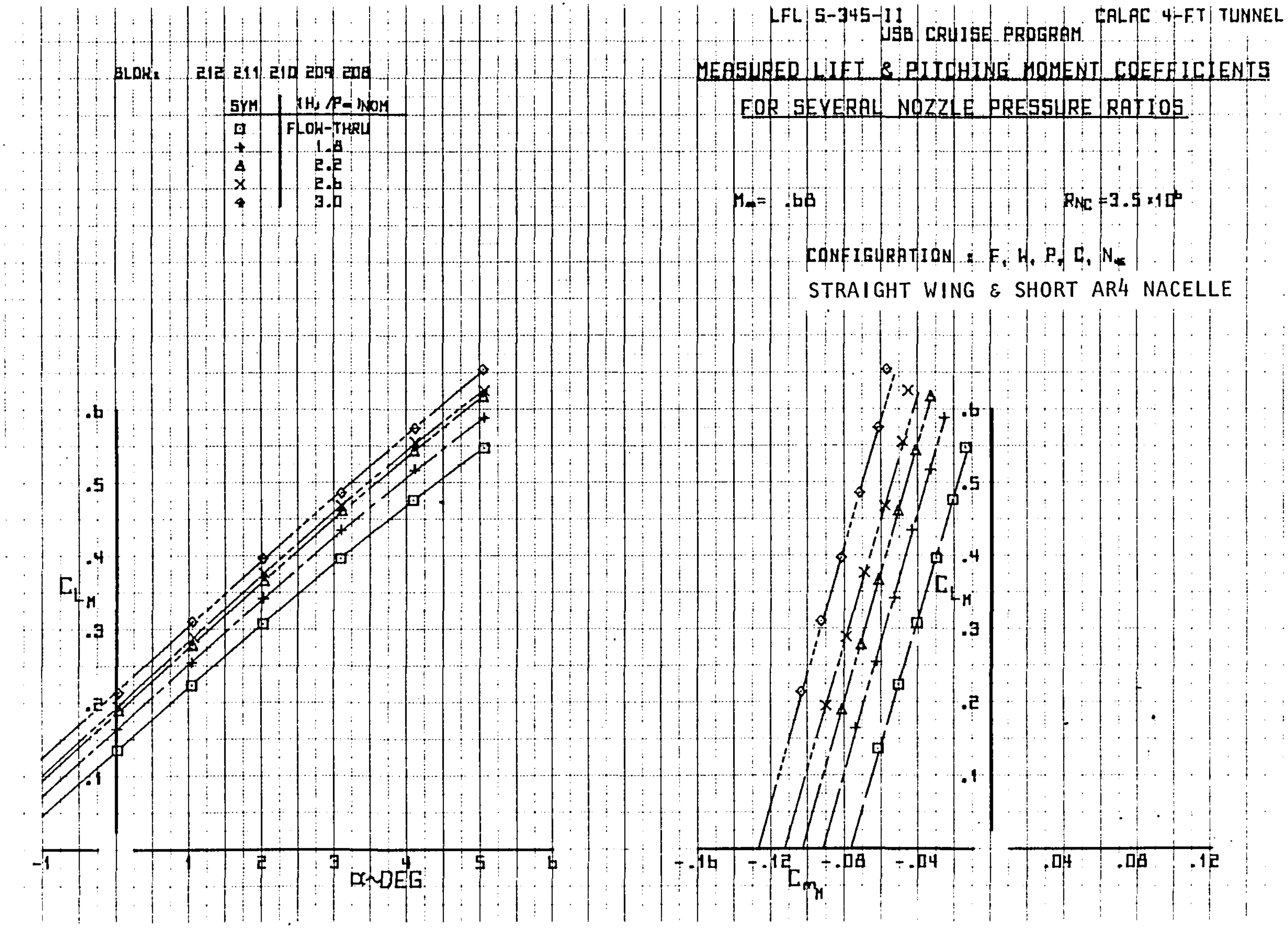

Figure 100. Variation of measured lift coefficient with angle of attack and moment coefficient, $M_\infty = 0.68$.

USB CRUISE PROGRAM

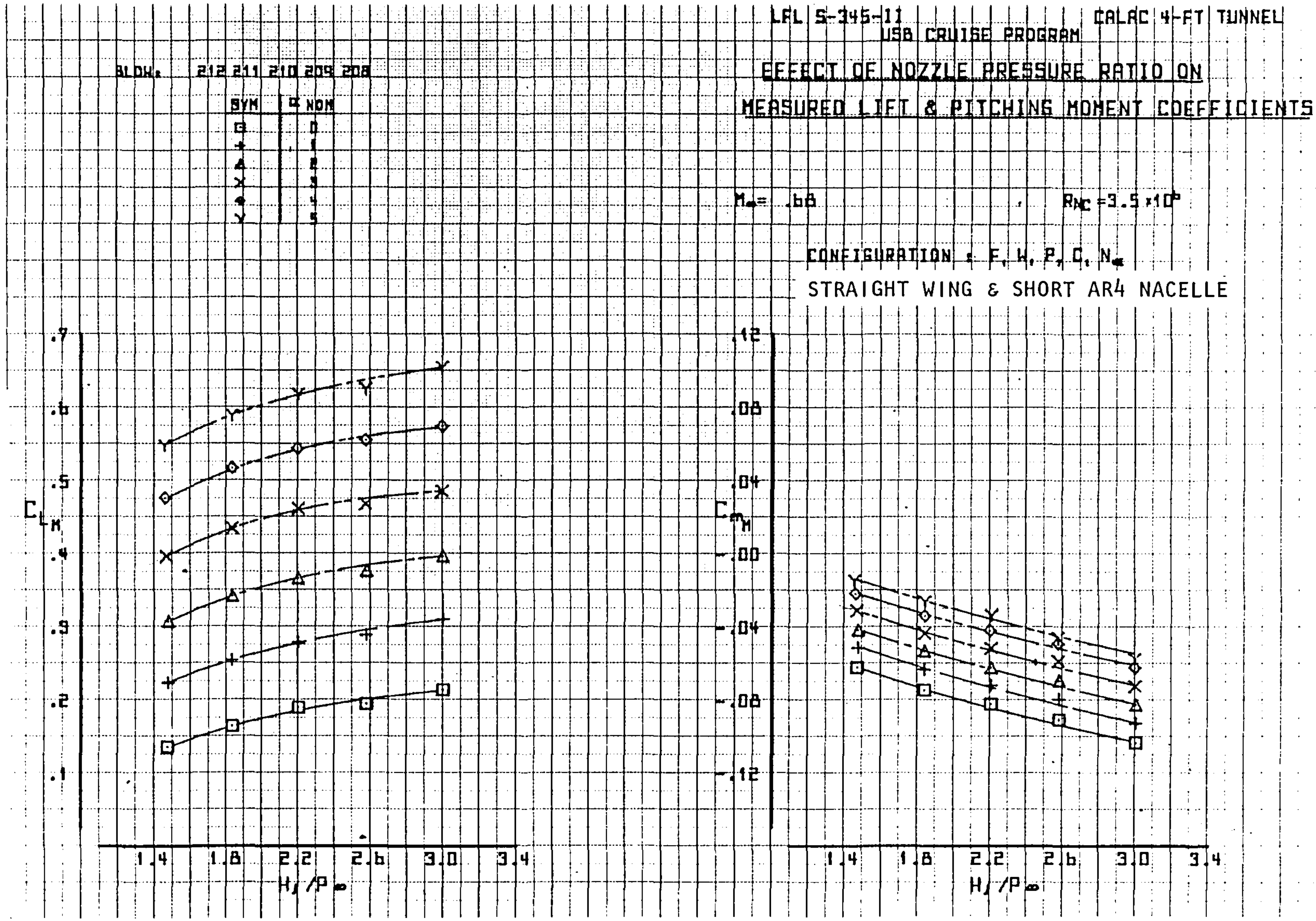

Figure 101. Variation of lift coefficient and moment coefficient with nozzle pressure ratio, M_∞ = 0.68.

USB CRUISE PROGRAM

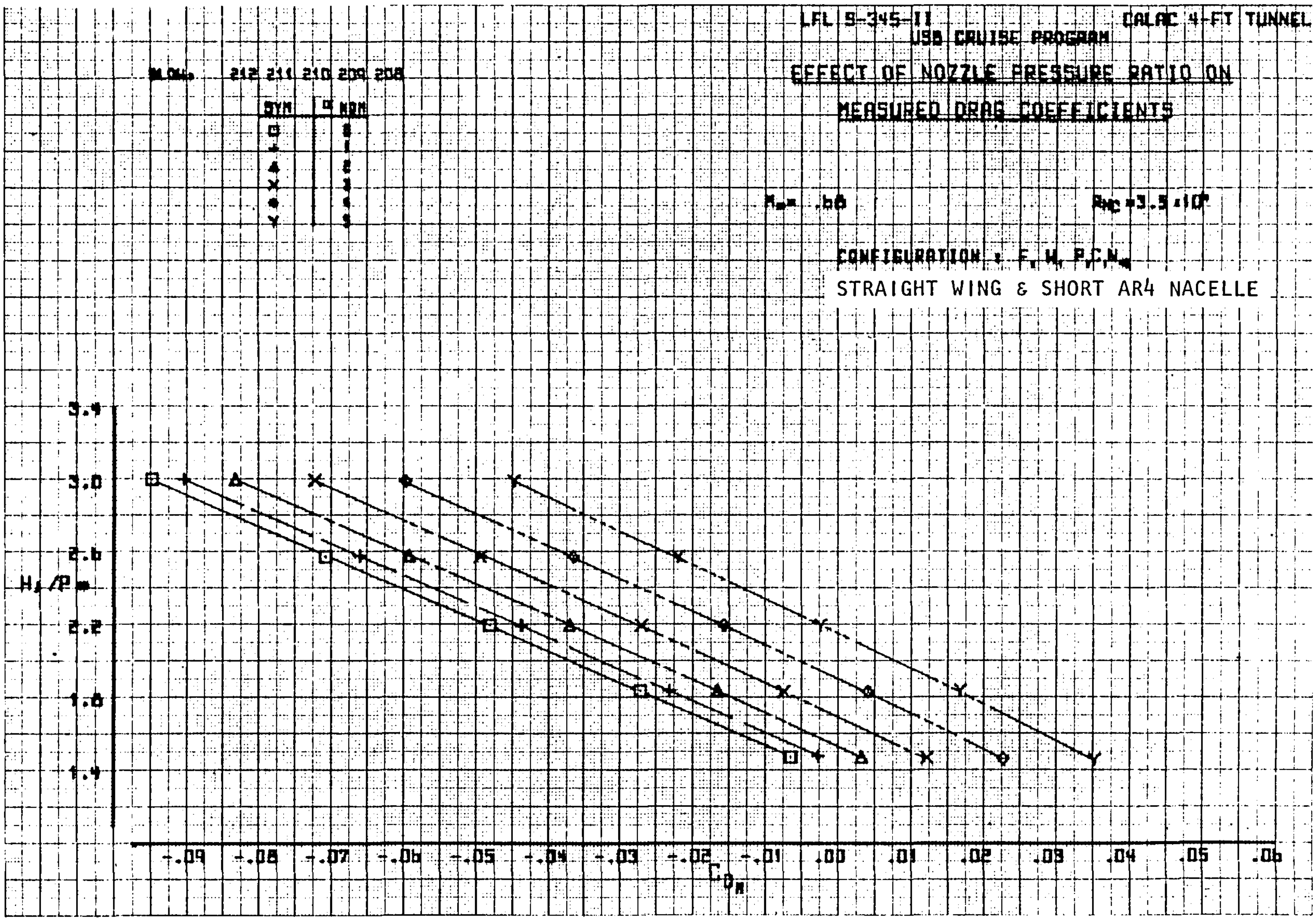

Figure 102. Variation of measured drag coefficient with nozzle pressure ratio, $M_\infty = 0.68$.

6.0 SWEPT WING TEST RESULTS

The presentation of the swept wing force data is divided into 3 parts. The basic clean wing-body is presented first followed by data for the pylon mounted nacelle configuration. Finally, the results of running the standard configurations for the basic parametric analyses are presented.

6.1 Clean Wing-Body

Basic data for the clean wing-body are presented in Figures 103 through 105. These include lift, drag and pitching moment. Curves are presented for 4 different Mach numbers to assure adequate coverage of the full test range.

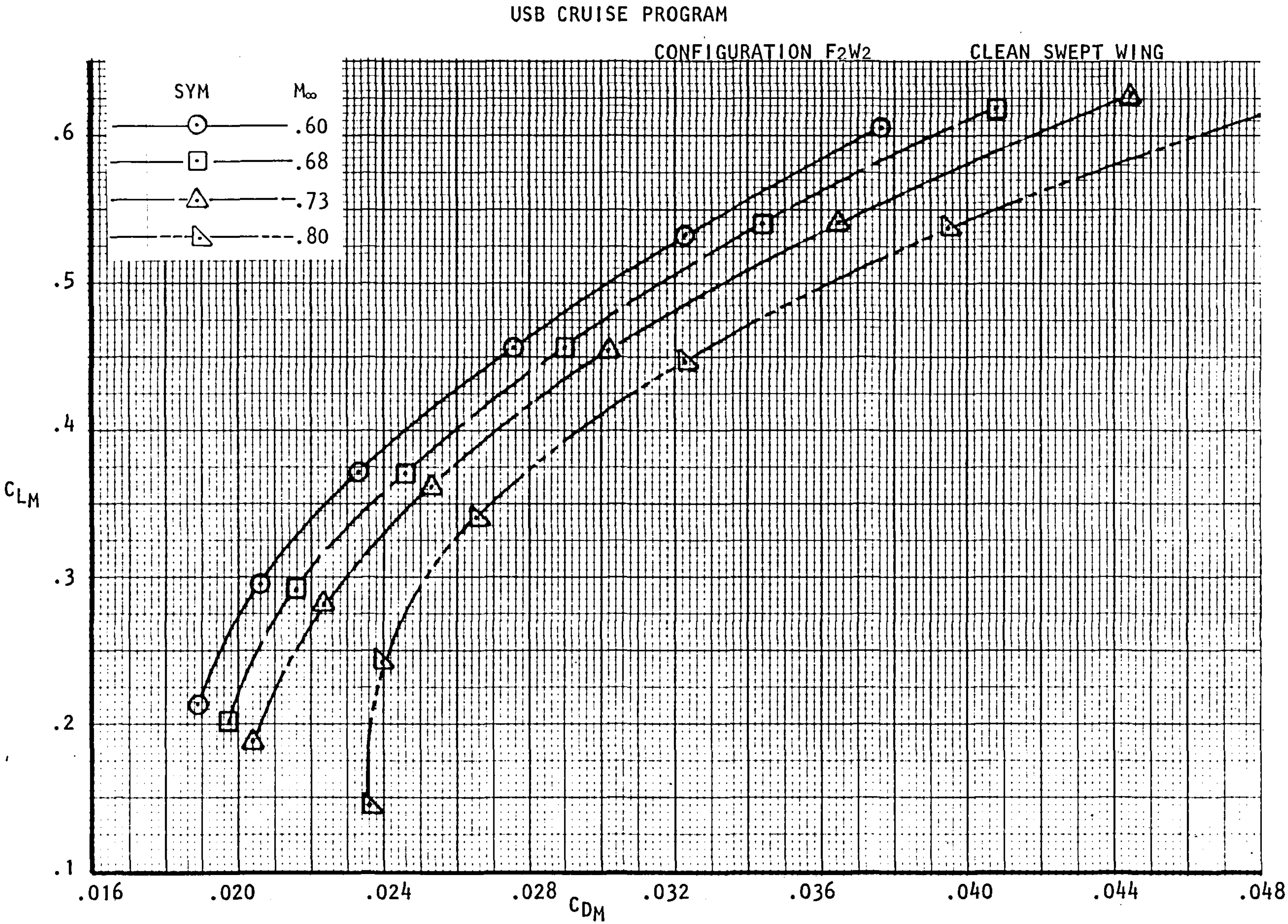

Figure 103. Variation of measured lift coefficient with measured drag coefficient, $R_{NC} = 3.5 \times 10^6$.

USB CRUISE PROGRAM

CONFIGURATION F_2W_2

CLEAN SWEPT WING

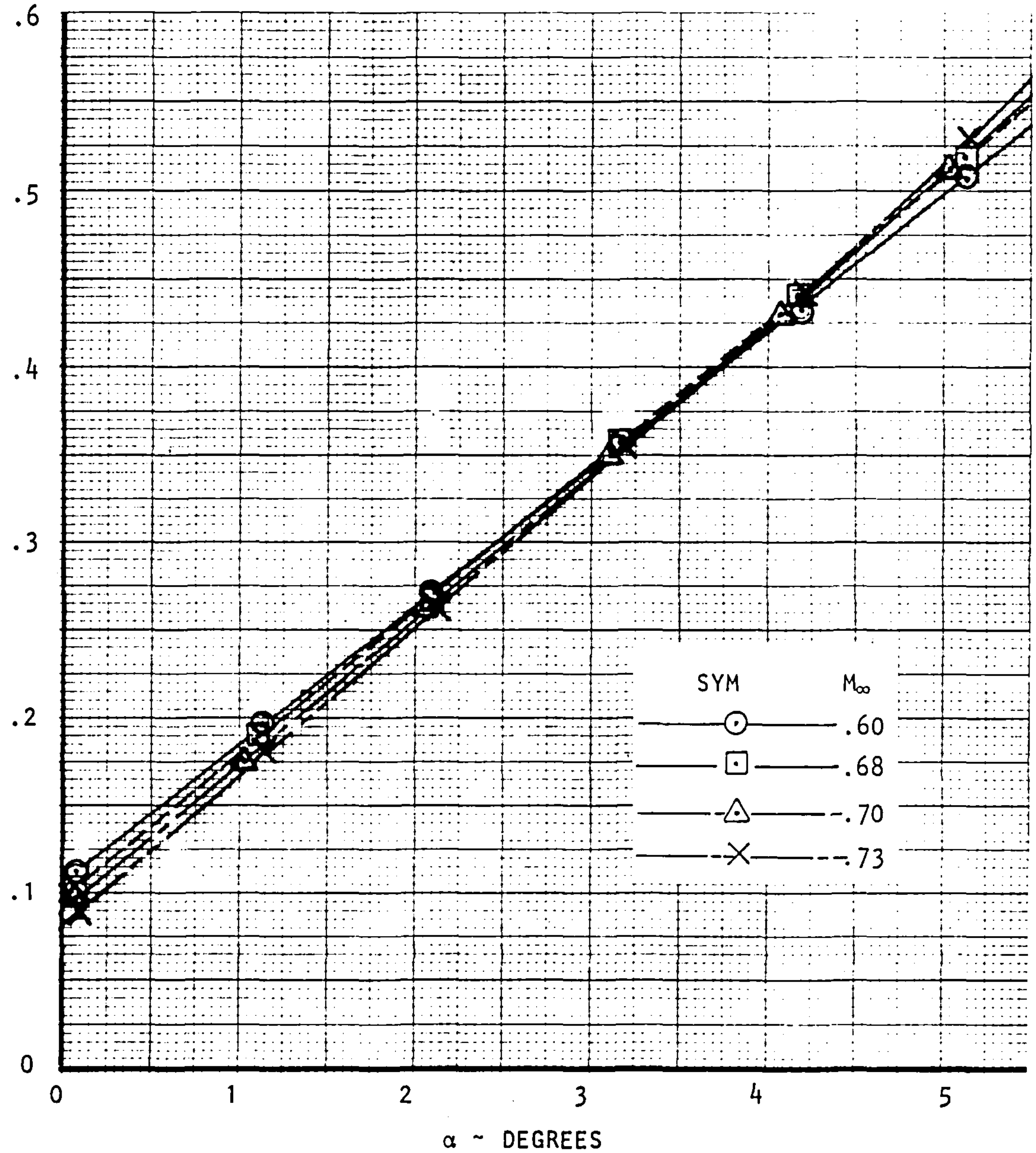

Figure 104. Variation of measured lift coefficient with angle of attack, $R_{NC} = 3.5 \times 10^6$.

USB CRUISE PROGRAM

CONFIGURATION F_2W_2

CLEAN SWEPT WING

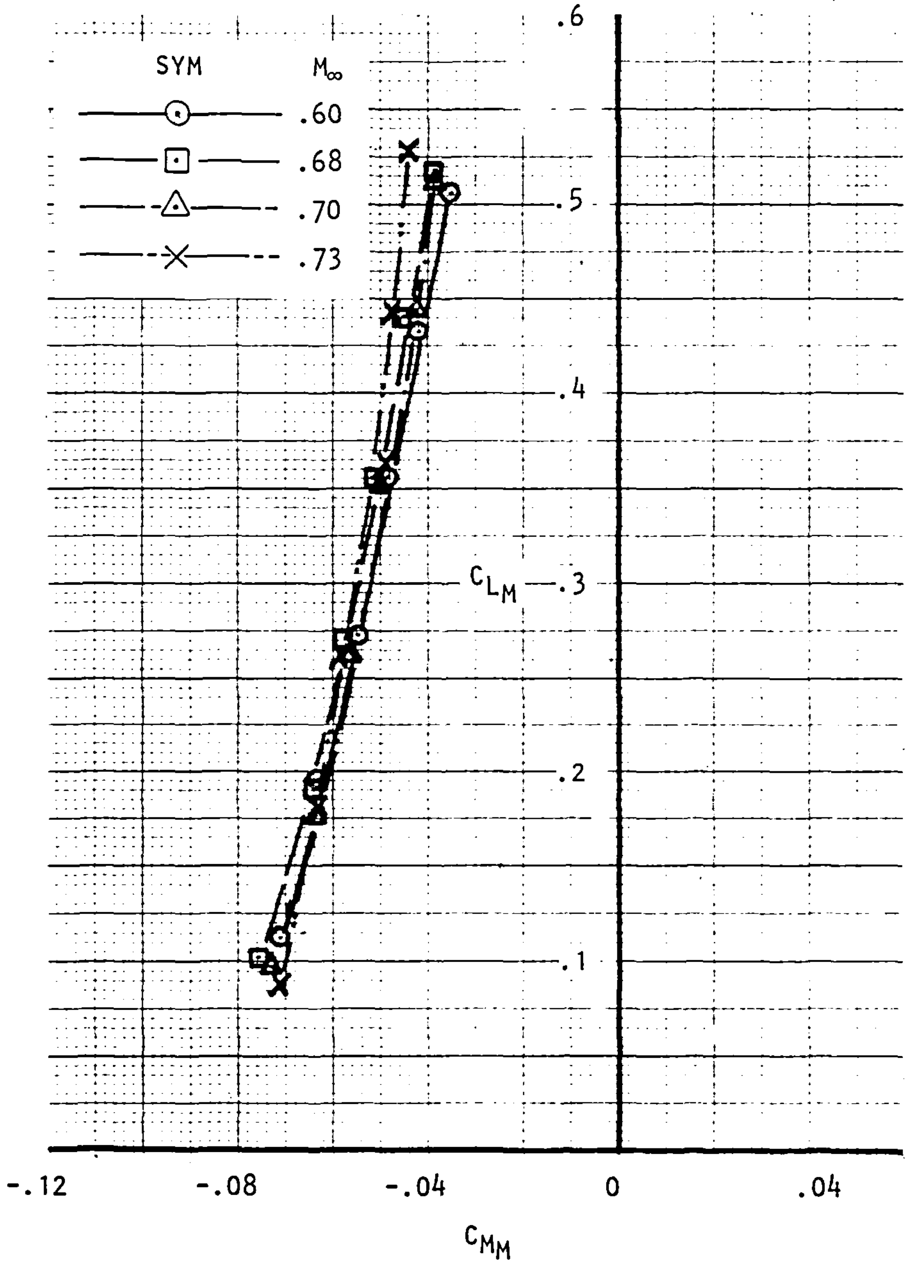

Figure 105. Variation of measured lift coefficient with measured moment coefficient, $R_{NC} = 3.5 \times 10^6$.

6.2 Data For Pylon Mounted Nacelle Configuration

To provide data for performing a comparison between pylon mounted and integrated nacelle configurations, it was necessary to run flow-through versions of these installations. Data for the short pylon mounted circular nacelle on the swept wing are presented in Figures 106 and 107. Test results for the integrated version of the short circular nacelle are contained in the next section.

6.3 Results From CFF Tests, Standard Configurations

Data for the swept wing configurations as tested in the CFF are presented in Figures 108 through 137. The data are presented as measured and contain nozzle thrust forces. Nozzle pressure ratios typically range from 1.4 to 3.0, while Mach numbers extend from 0.60 to 0.73.

USB CRUISE PROGRAM

SHORT PYLON MOUNTED, FLOW-THROUGH NACELLE ON SWEPT WING

CONFIGURATION $F_2W_2B_2P_5C_5N_2$

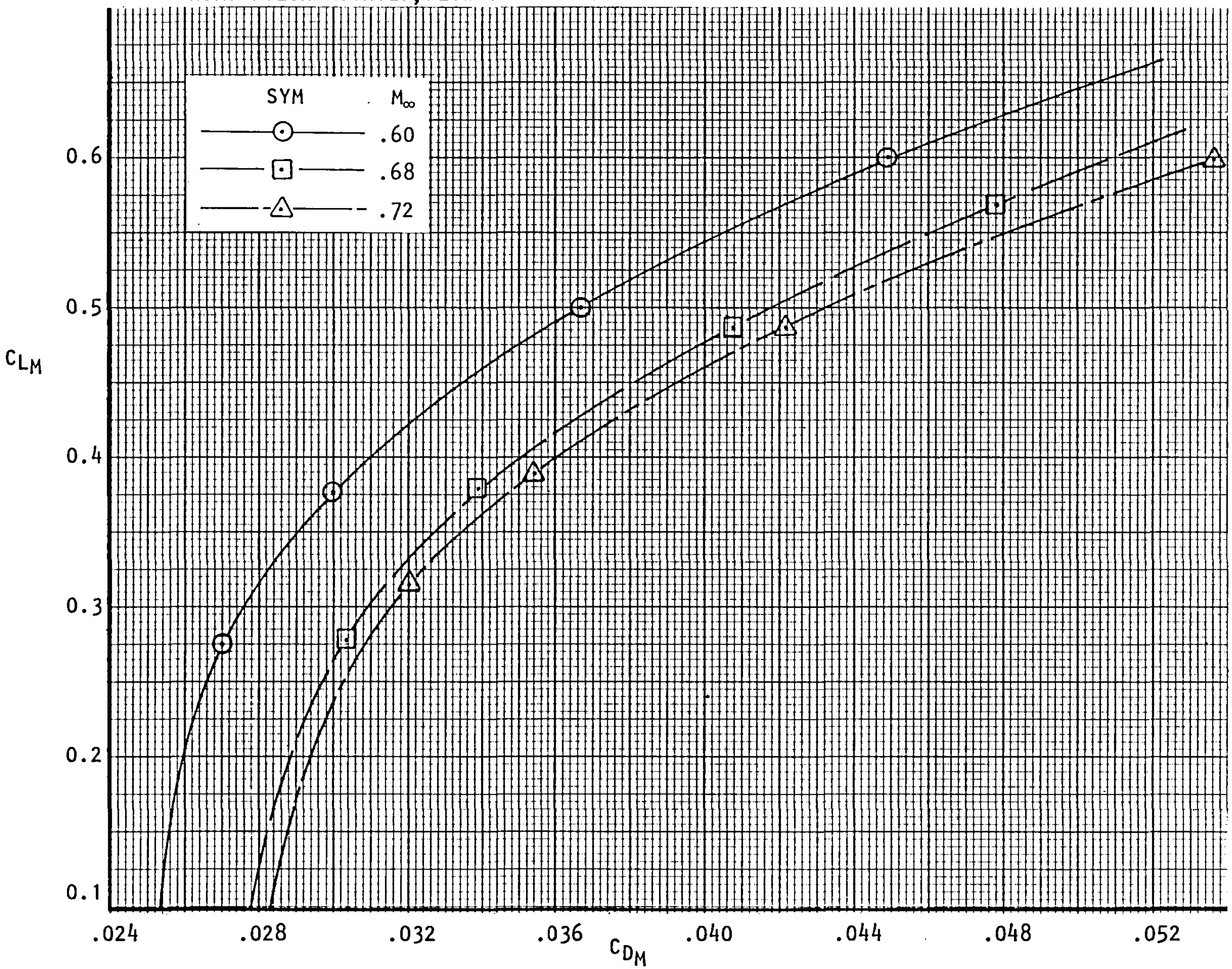

Figure 106. Variation of measured lift coefficient with measured drag coefficient, $R_{NC} = 3.5 \times 10^6$, H_j/p_∞ = RPR.

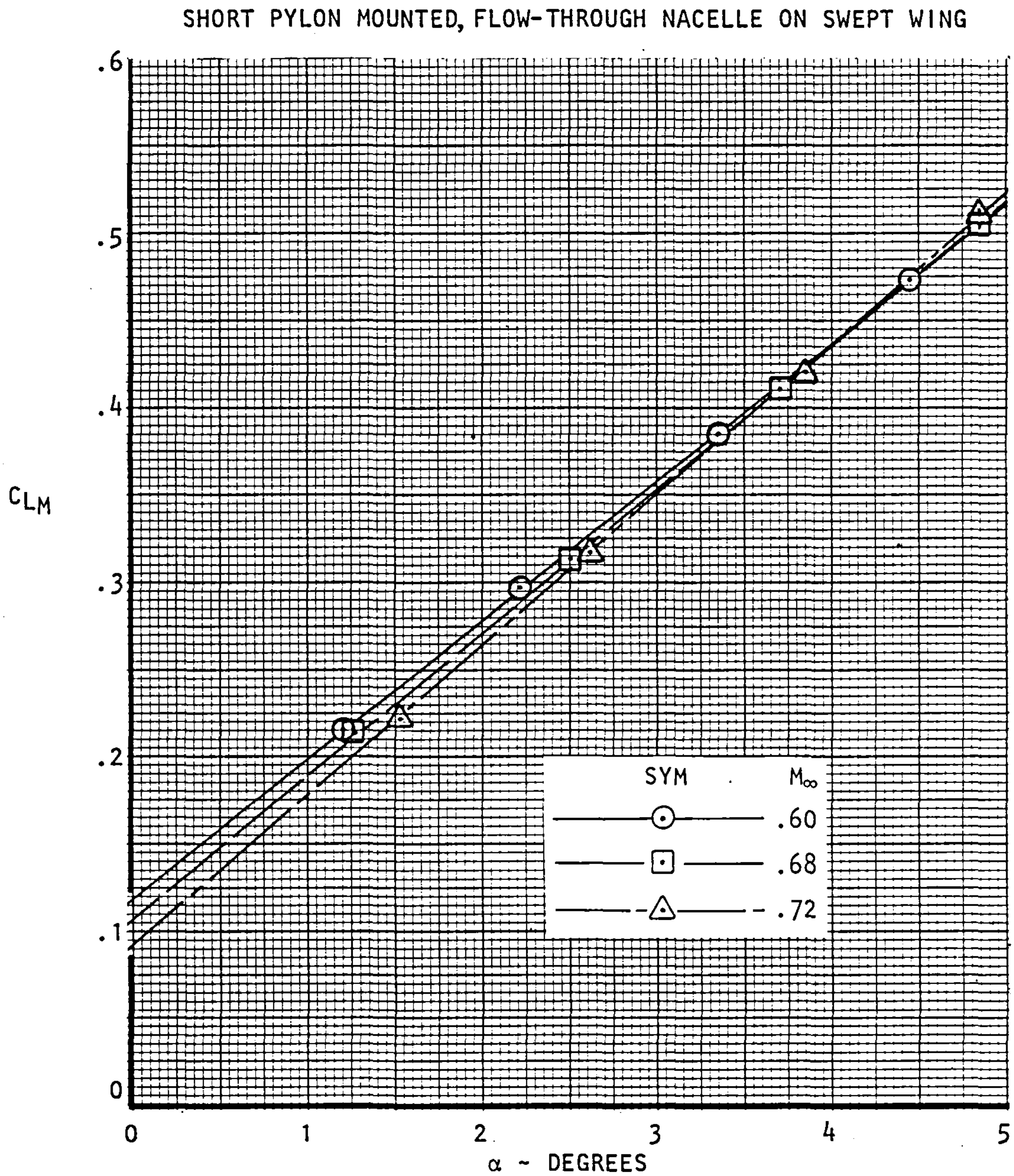

Figure 107. Variation of measured lift coefficient with angle of attack, $R_{NC} = 3.5 \times 10^6$, H_j/p_∞ = RPR.

USB CRUISE PROGRAM

CONFIGURATION $F_2W_2B_{5,6}P_{9,10}C_{3,4}N_8^{\ 1},N_8^{\ 2}$

SWEPT WING & 2 D-DUCT NACELLES

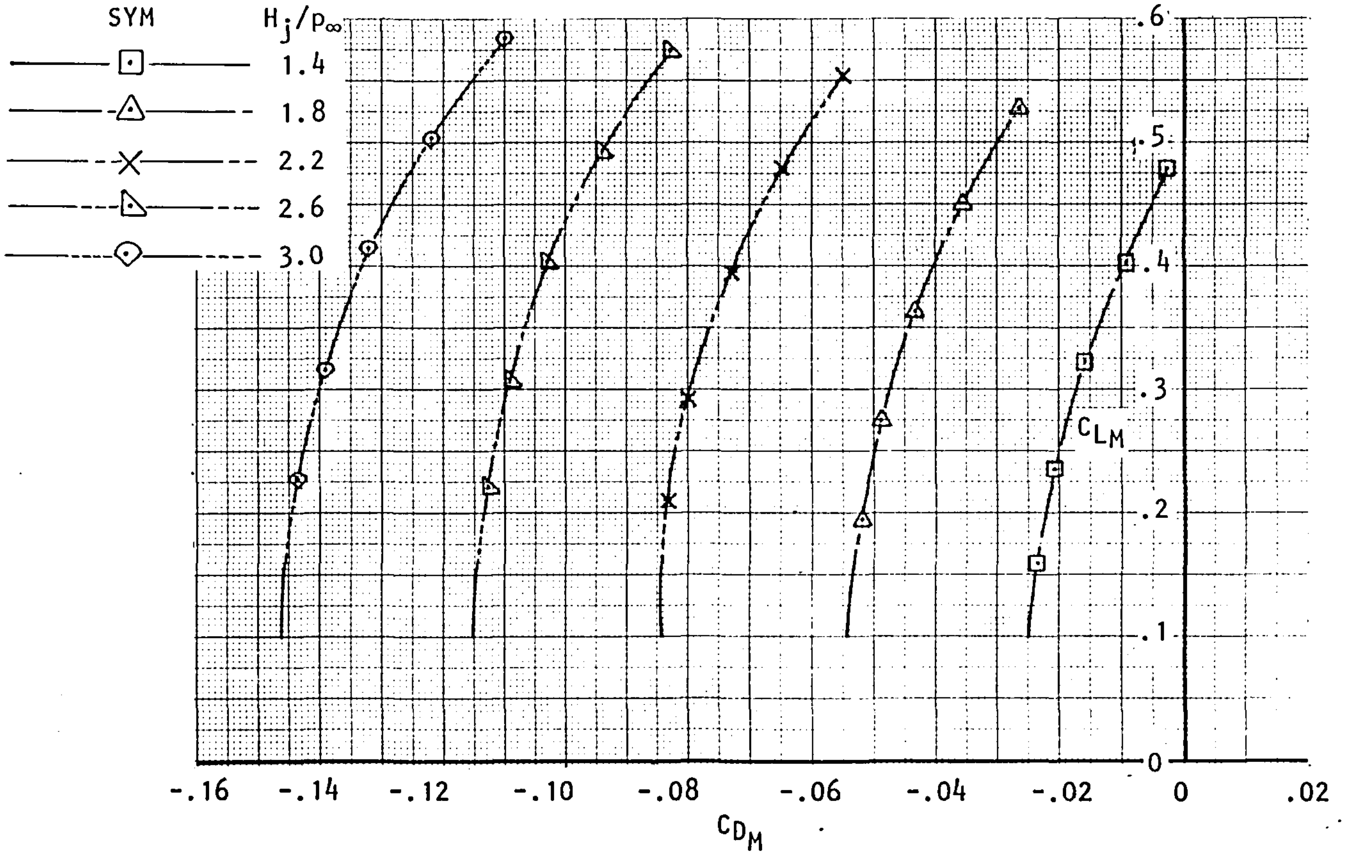

Figure 108. Variation of measured lift coefficient with measured drag coefficient and nozzle pressure ratio, $R_{NC} = 3.5 \times 10^6$, $M_\infty = 0.60$.

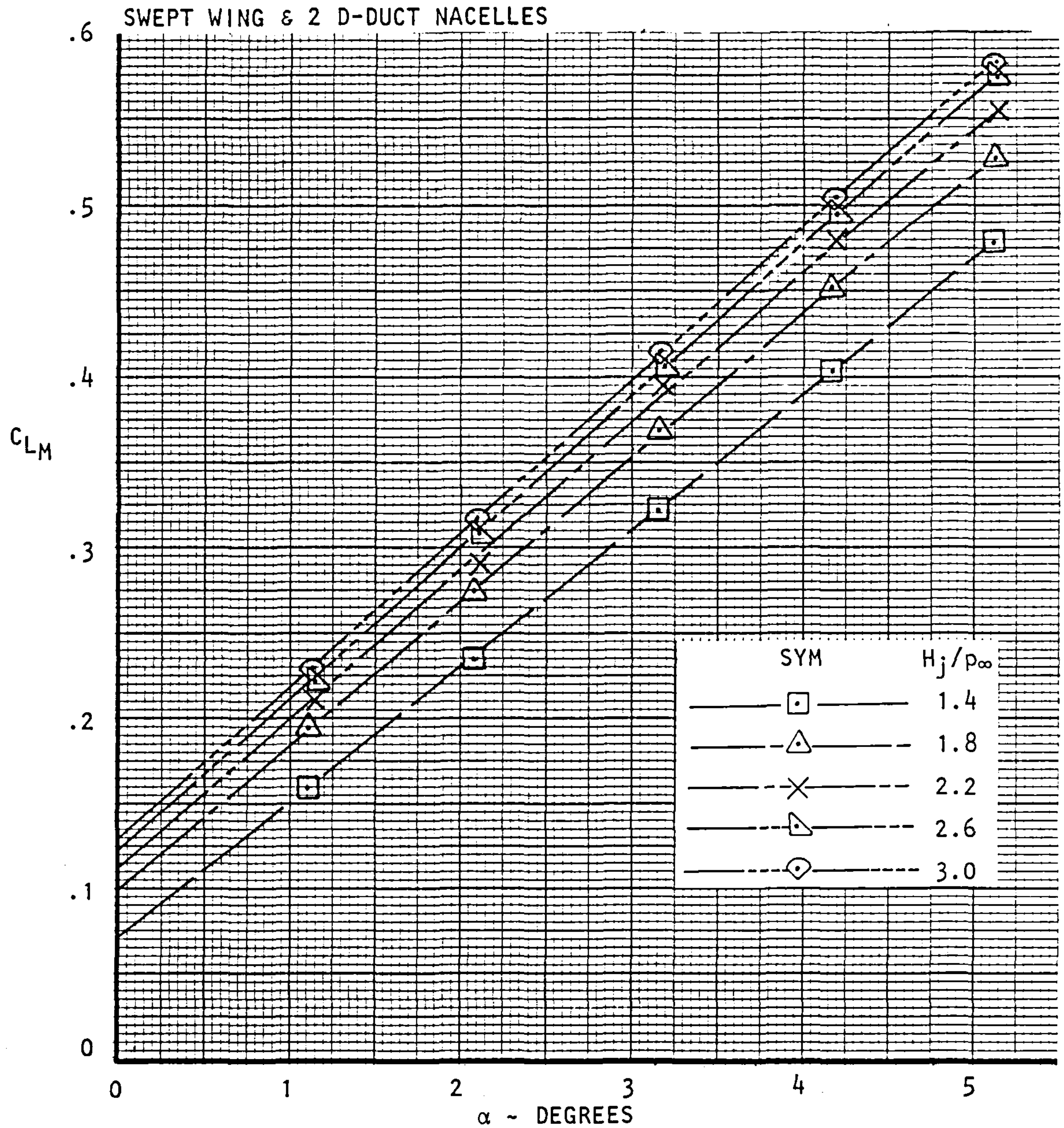

Figure 109. Variation of measured lift coefficient with angle of attack, $R_{NC} = 3.5 \times 10^6$, $M_\infty = 0.60$.

USB CRUISE PROGRAM

CONFIGURATION $F_2W_2B_{5,6}P_{9,10}C_{3,4}N_8^{1}, N_8^{2}$

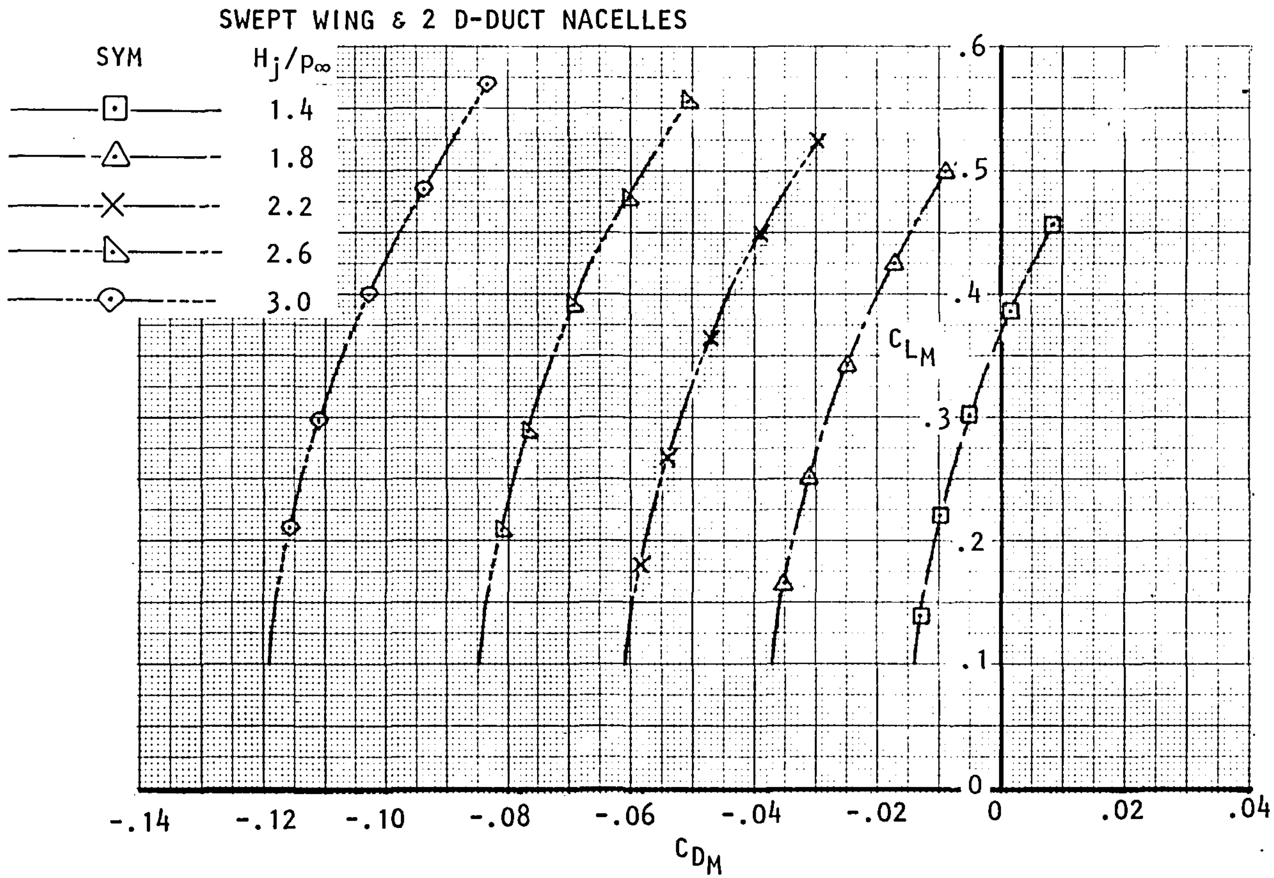

Figure 110. Variation of measured lift coefficient with measured drag coefficient and nozzle pressure ratio, $R_{NC} = 3.5 \times 10^6$, $M_\infty = 0.68$.

CONFIGURATION $F_2W_2B_{5,6}P_{9,10}C_{3,4}N_8^1, N_8^2$

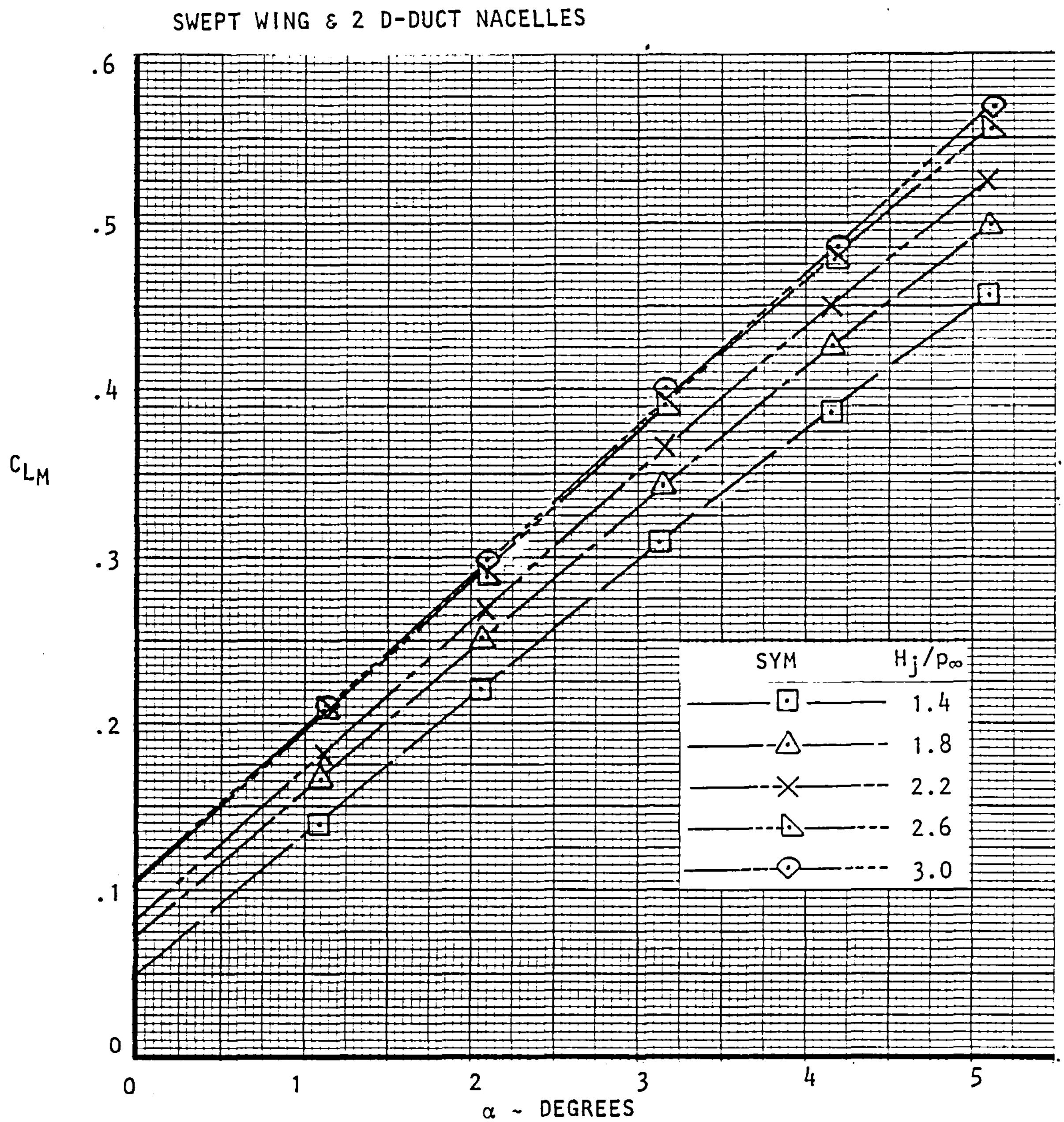

Figure 111. Variation of measured lift coefficient with angle of attack, $R_{NC} = 3.5 \times 10^6$, $M_\infty = 0.68$.

USB CRUISE PROGRAM

CONFIGURATION $F_2W_2B_{5,6}P_{9,10}C_{3,4}N_8^1, N_8^2$

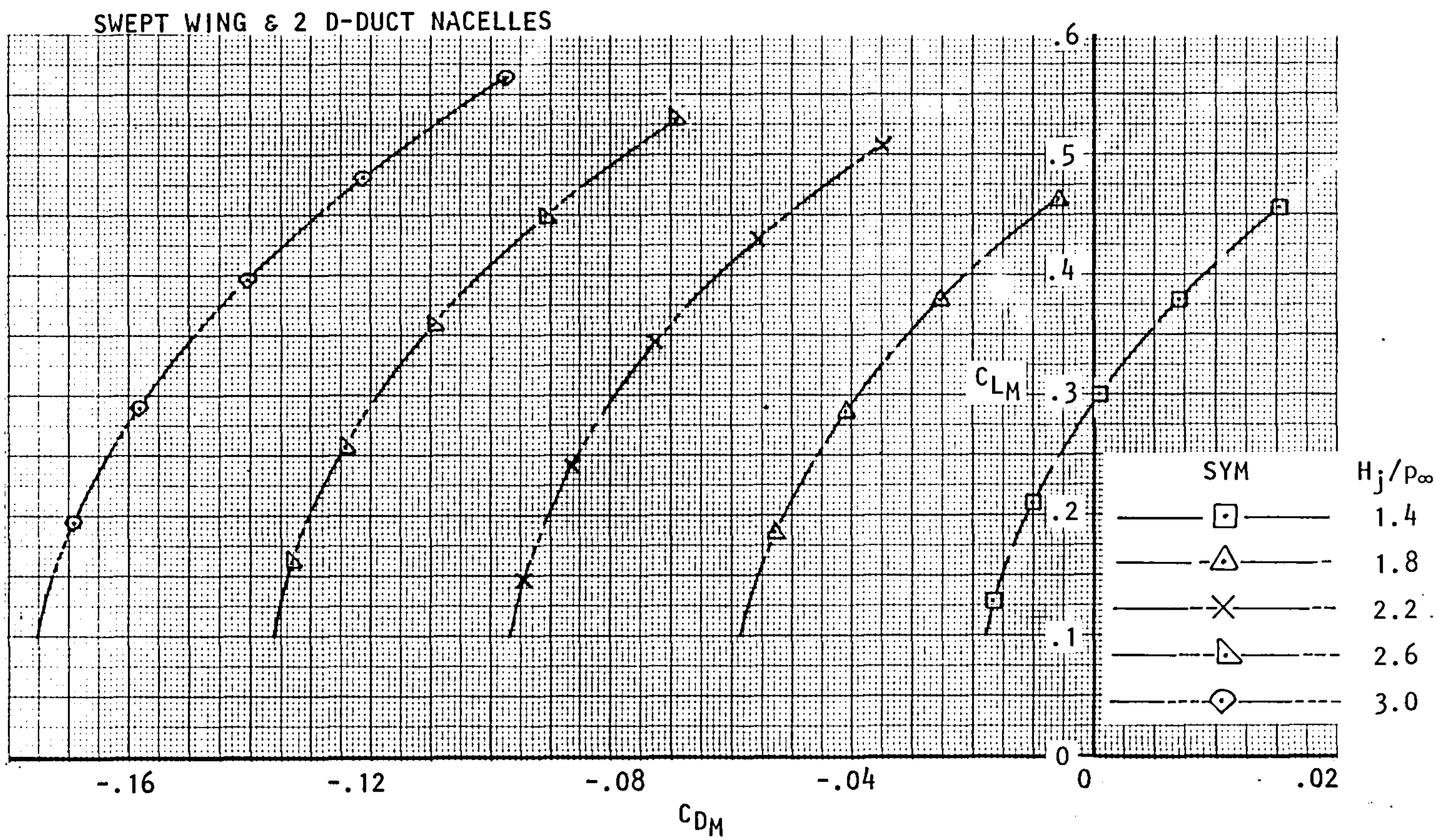

Figure 112. Variation of measured lift coefficient with measured drag coefficient and nozzle pressure ratio, $R_{NC} = 3.5 \times 10^6$, $M_\infty = 0.73$.

USB CRUISE PROGRAM

CONFIGURATION $F_2W_2B_{5,6}P_{9,10}C_{3,4}N_8{}^1,N_8{}^2$

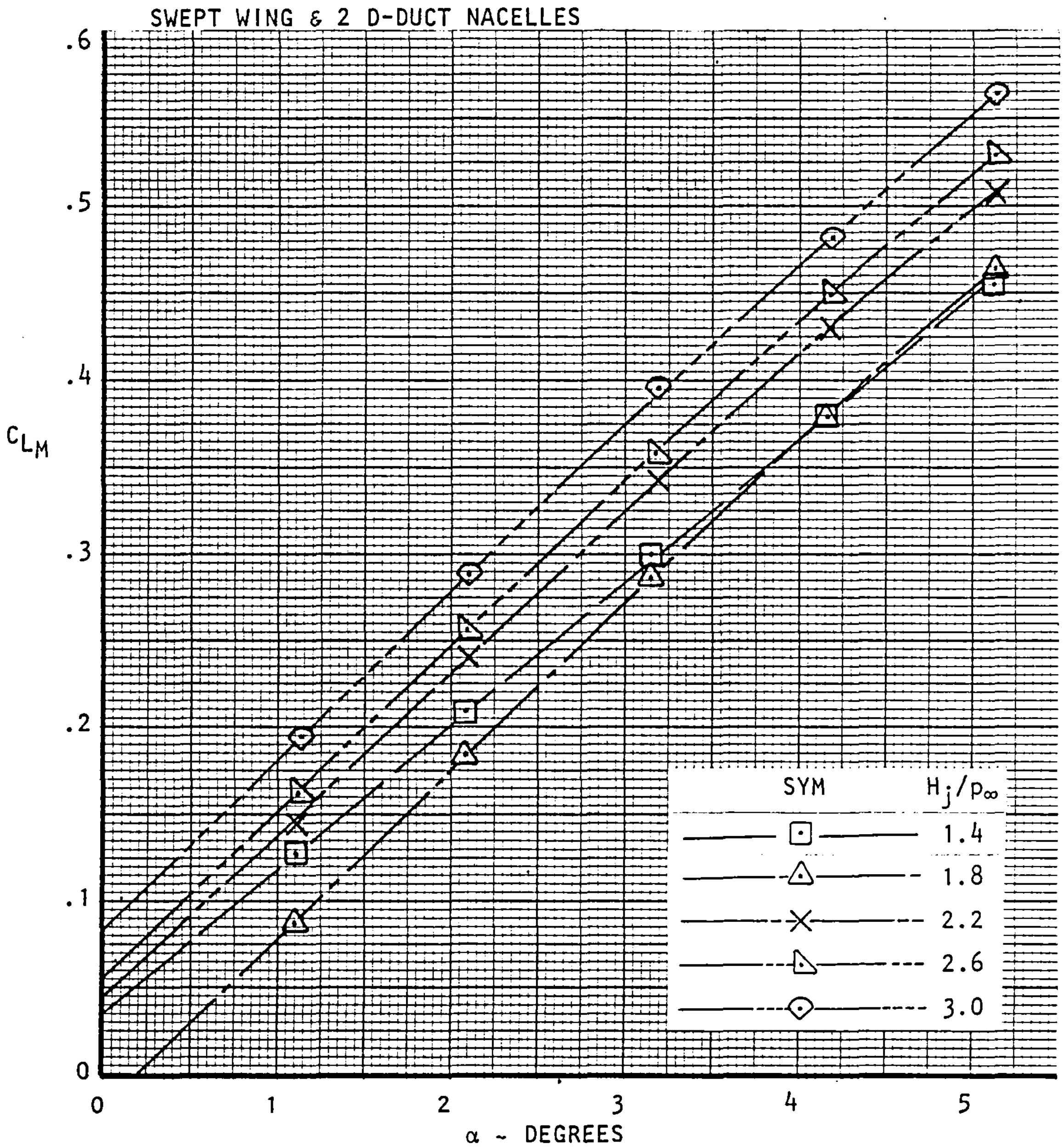

Figure 113. Variation of measured lift coefficient with angle of attack, $R_{NC} = 3.5 \times 10^6$, $M_\infty = 0.73$.

USB CRUISE PROGRAM

CONFIGURATION $F_2W_2B_6P_{10}C_4N_8^2$

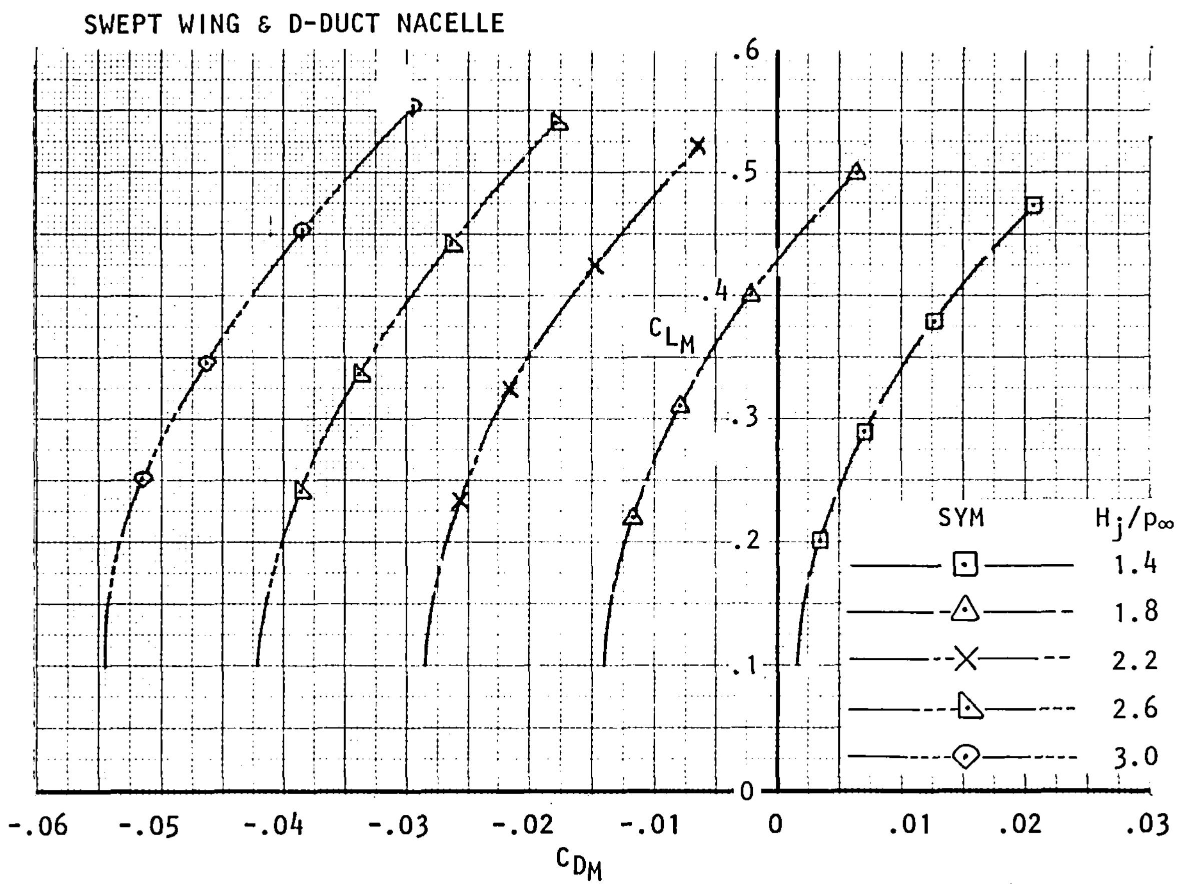

Figure 114. Variation of measured lift coefficient with measured drag coefficient and nozzle pressure ratio, $R_{NC} = 3.5 \times 10^6$, $M_\infty = 0.60$.

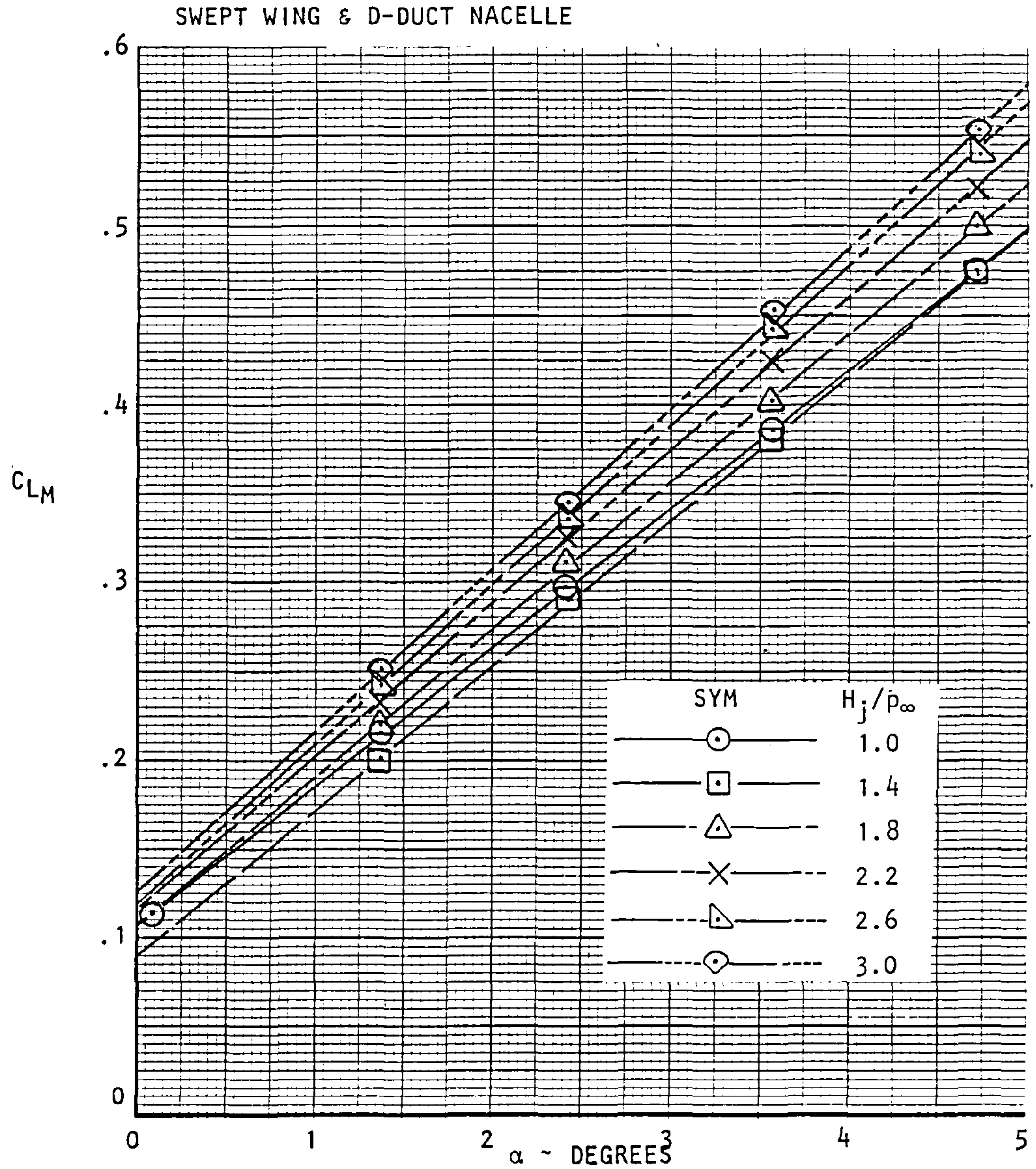

Figure 115. Variation of measured lift coefficient with angle of attack, $R_{NC} = 3.5 \times 10^6$, $M_\infty = 0.60$.

USB CRUISE PROGRAM

CONFIGURATION $F_2W_2B_6P_{10}C_4N_8^2$

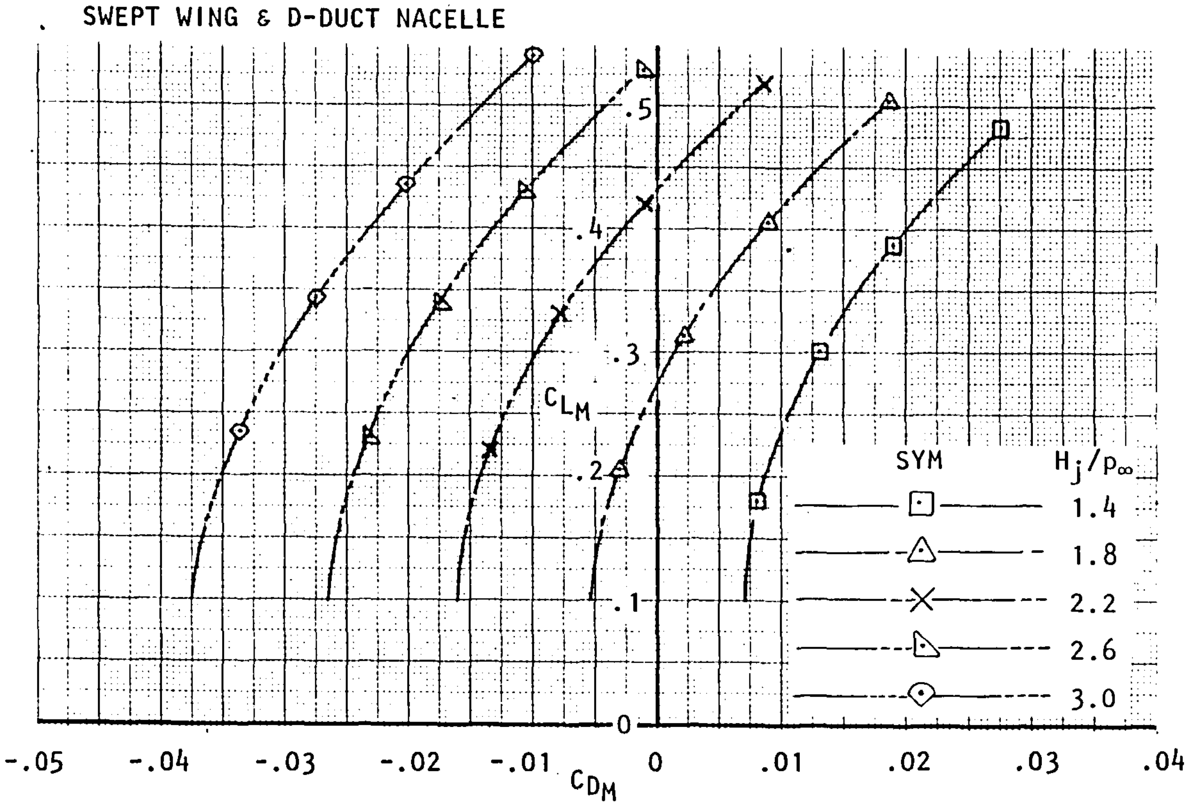

Figure 116. Variation of measured lift coefficient with measured drag coefficient and nozzle pressure ratio, $R_{NC} = 3.5 \times 10^6$, $M_\infty = 0.68$.

USB CRUISE PROGRAM

CONFIGURATION $F_2W_2B_6P_{10}C_4N_8^2$

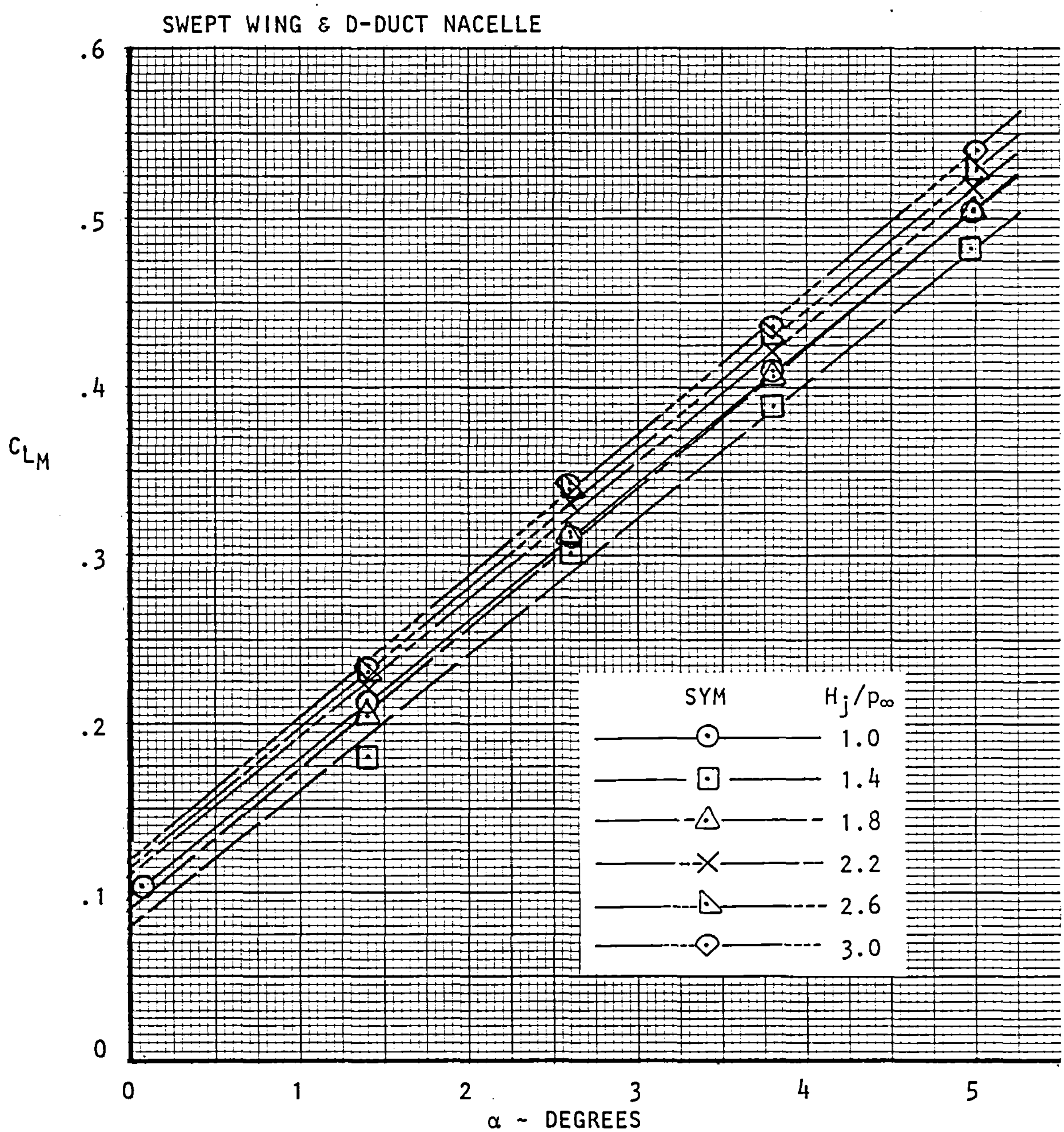

Figure 117. Variation of measured lift coefficient with angle of attack, $R_{NC} = 3.5 \times 10^6$, $M_\infty = 0.68$.

USB CRUISE PROGRAM

CONFIGURATION $F_2W_2B_6P_{10}C_4N_8{}^2$

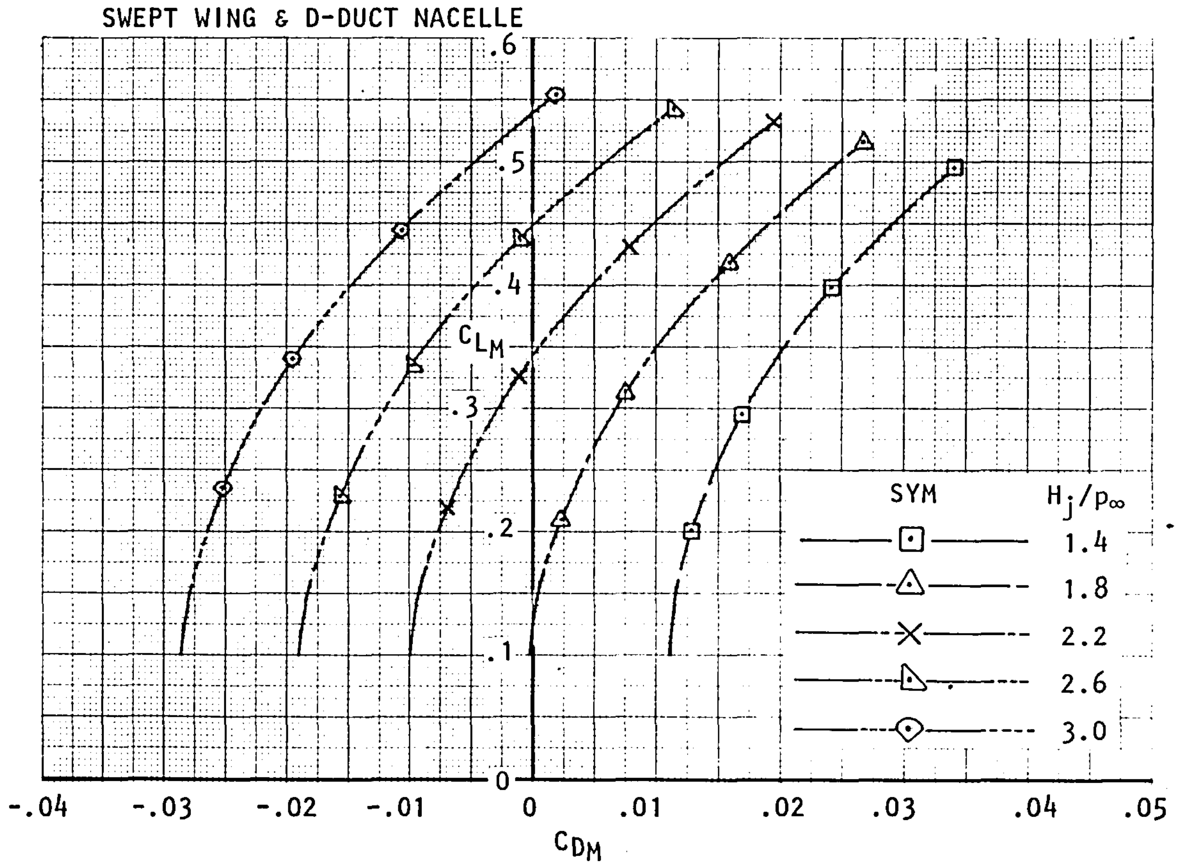

Figure 118. Variation of measured lift coefficient with measured drag coefficient and nozzle pressure ratio, $R_{NC} = 3.5 \times 10^6$, $M_\infty = 0.73$.

USB CRUISE PROGRAM

CONFIGURATION $F_2W_2B_6P_{10}C_4N_8{}^2$

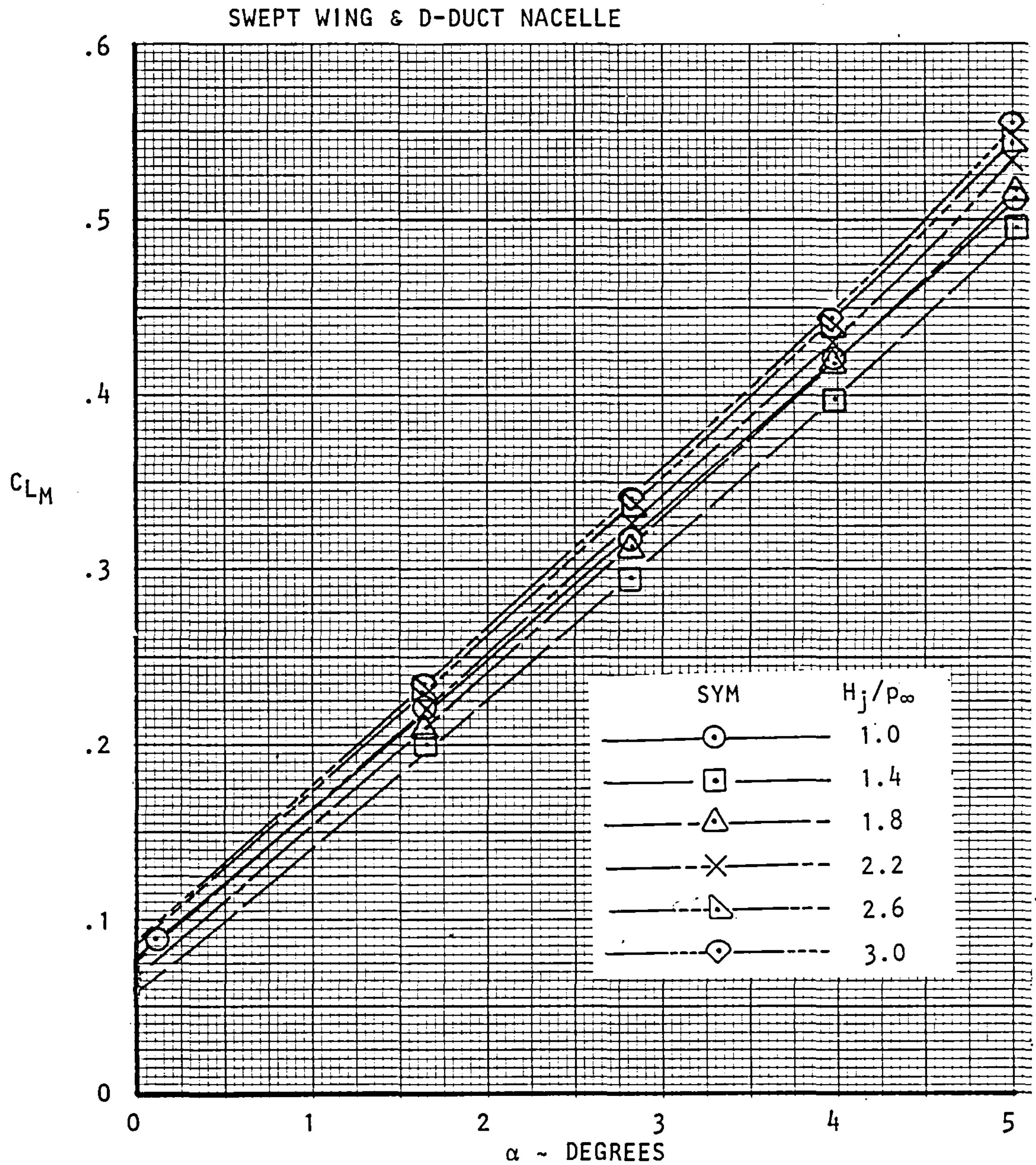

Figure 119. Variation of measured lift coefficient with angle of attack, $R_{NC} = 3.5 \times 10^6$, $M_\infty = 0.73$.

USB CRUISE PROGRAM

CONFIGURATION $F_2W_2B_5P_9C_3N_{11}$

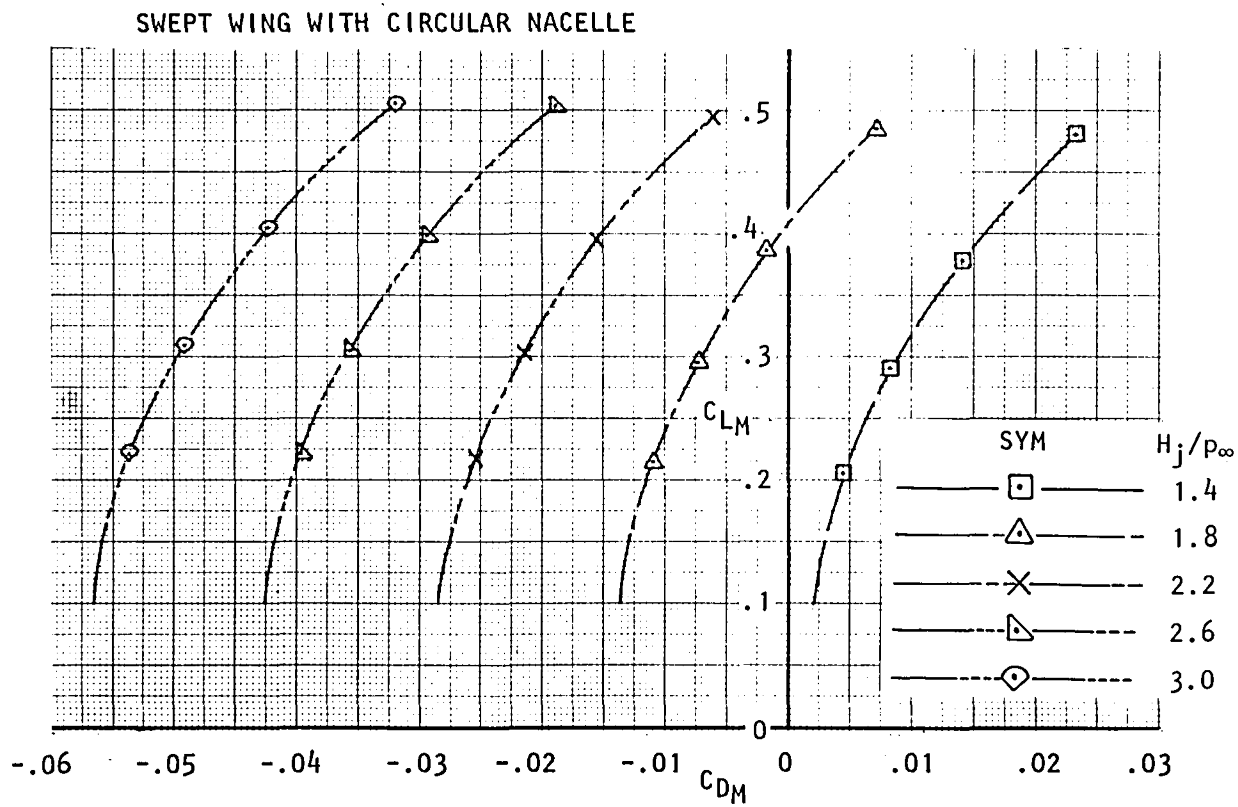

Figure 120. Variation of measured lift coefficient with measured drag coefficient and nozzle pressure ratio, $R_{NC} = 3.5 \times 10^6$, $M_\infty = 0.60$.

USB CRUISE PROGRAM

CONFIGURATION $F_2W_2B_5P_9C_3N_{11}$

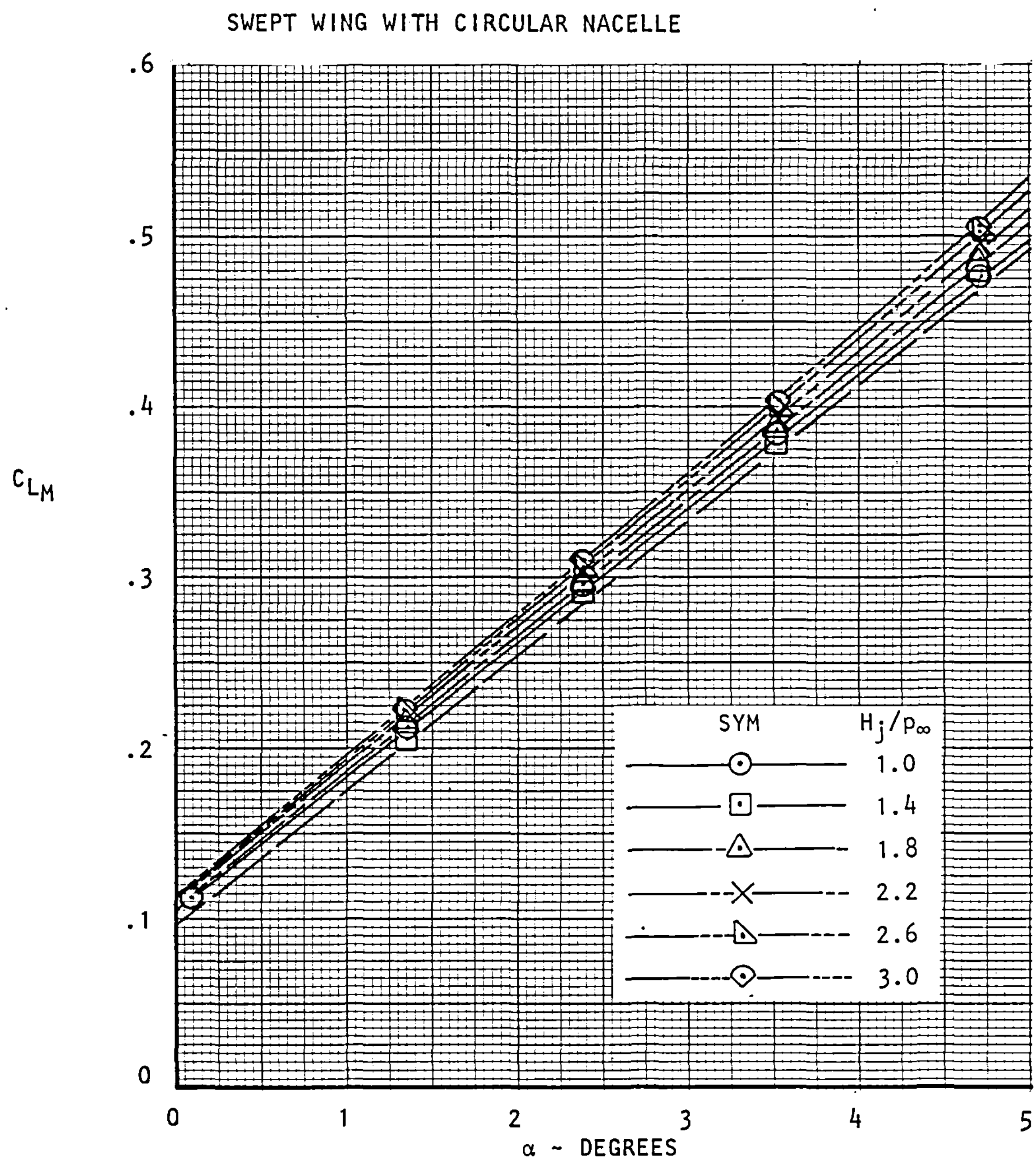

Figure 121. Variation of measured lift coefficient with angle of attack, $R_{NC} = 3.5 \times 10^6$, $M_\infty = 0.60$.

USB CRUISE PROGRAM

CONFIGURATION $F_2W_2B_5P_9C_3N_{11}$

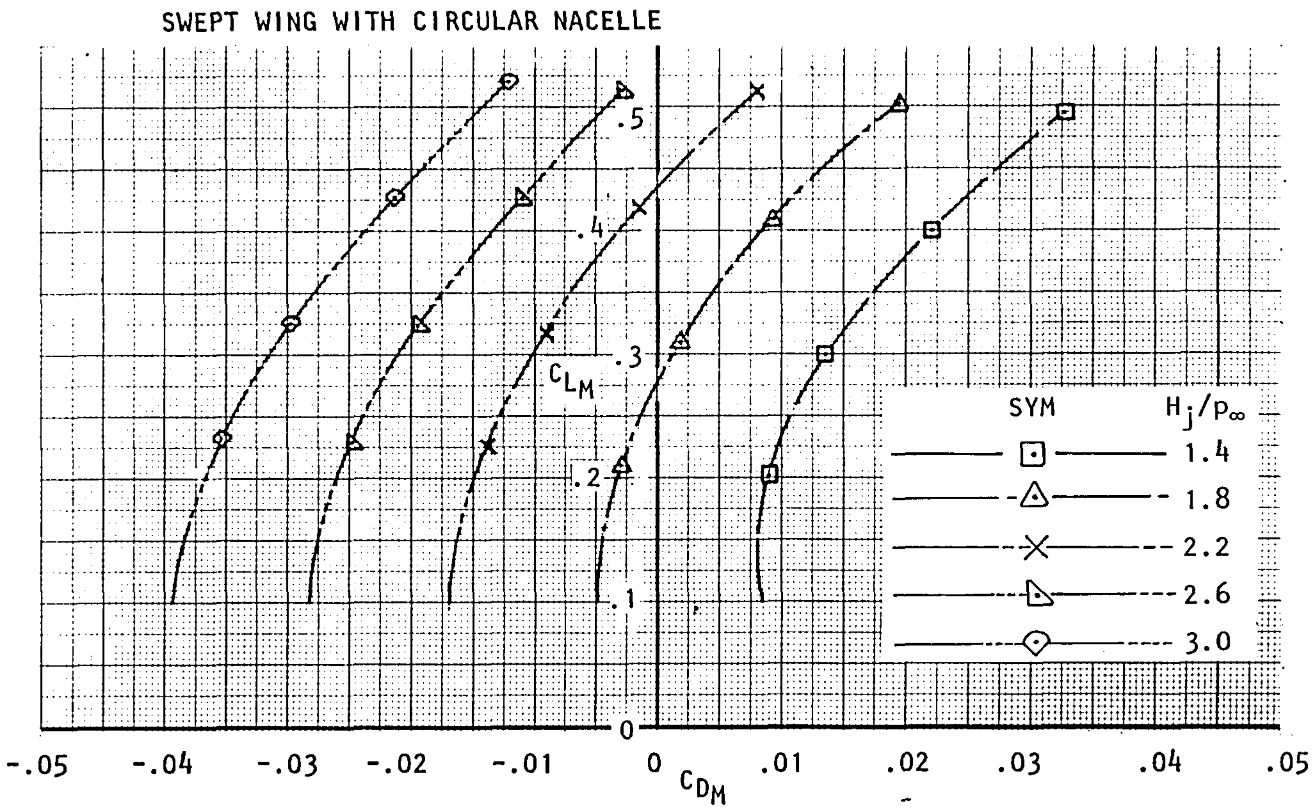

Figure 122. Variation of measured lift coefficient with measured drag coefficient and nozzle pressure ratio, $R_{NC} = 3.5 \times 10^6$, $M_\infty = 0.68$.

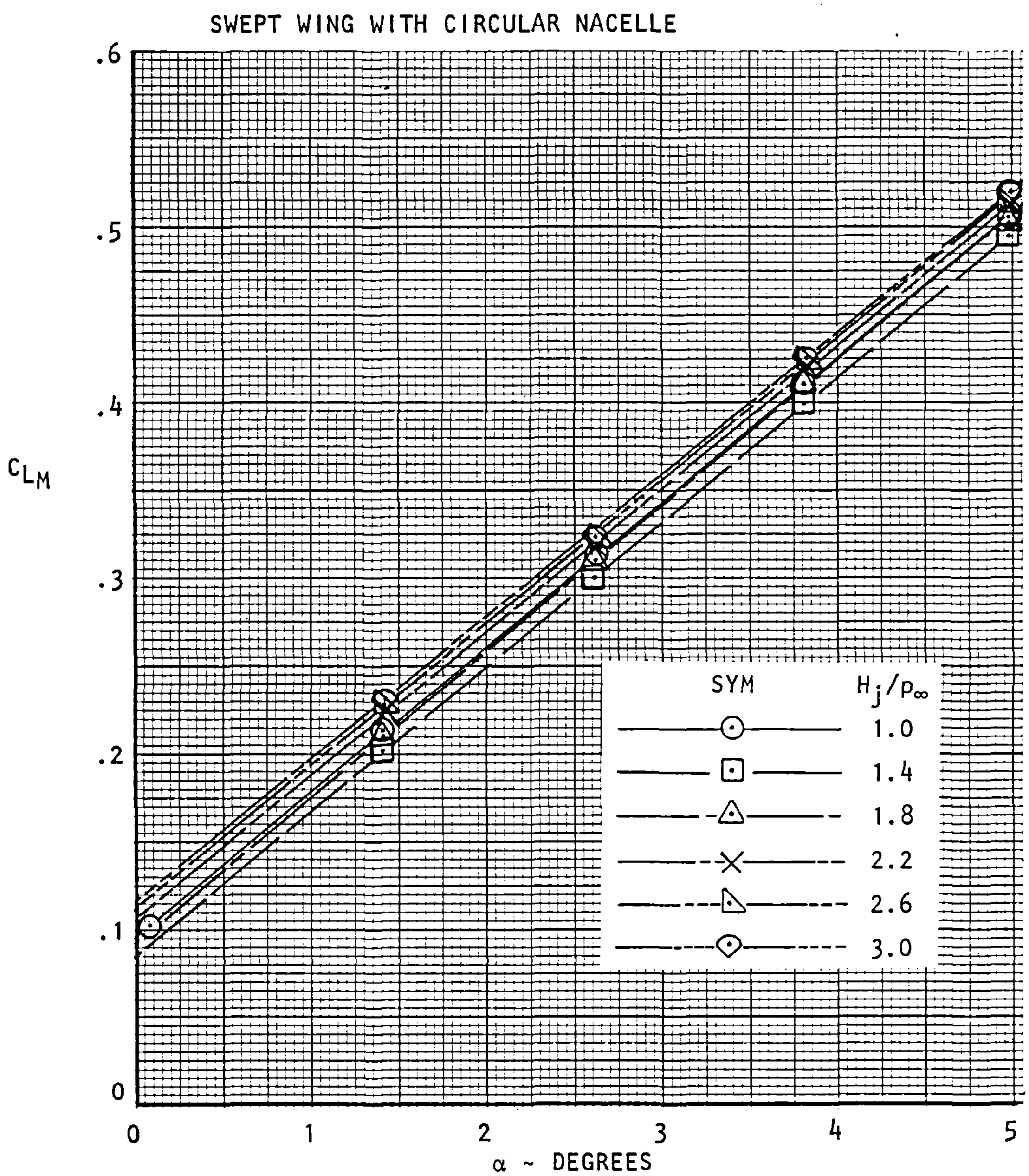

Figure 123. Variation of measured lift coefficient with angle of attack, $R_{NC} = 3.5 \times 10^6$, $M_\infty = 0.68$.

USB CRUISE PROGRAM

CONFIGURATION $F_2W_2B_5P_9C_3N_{11}$

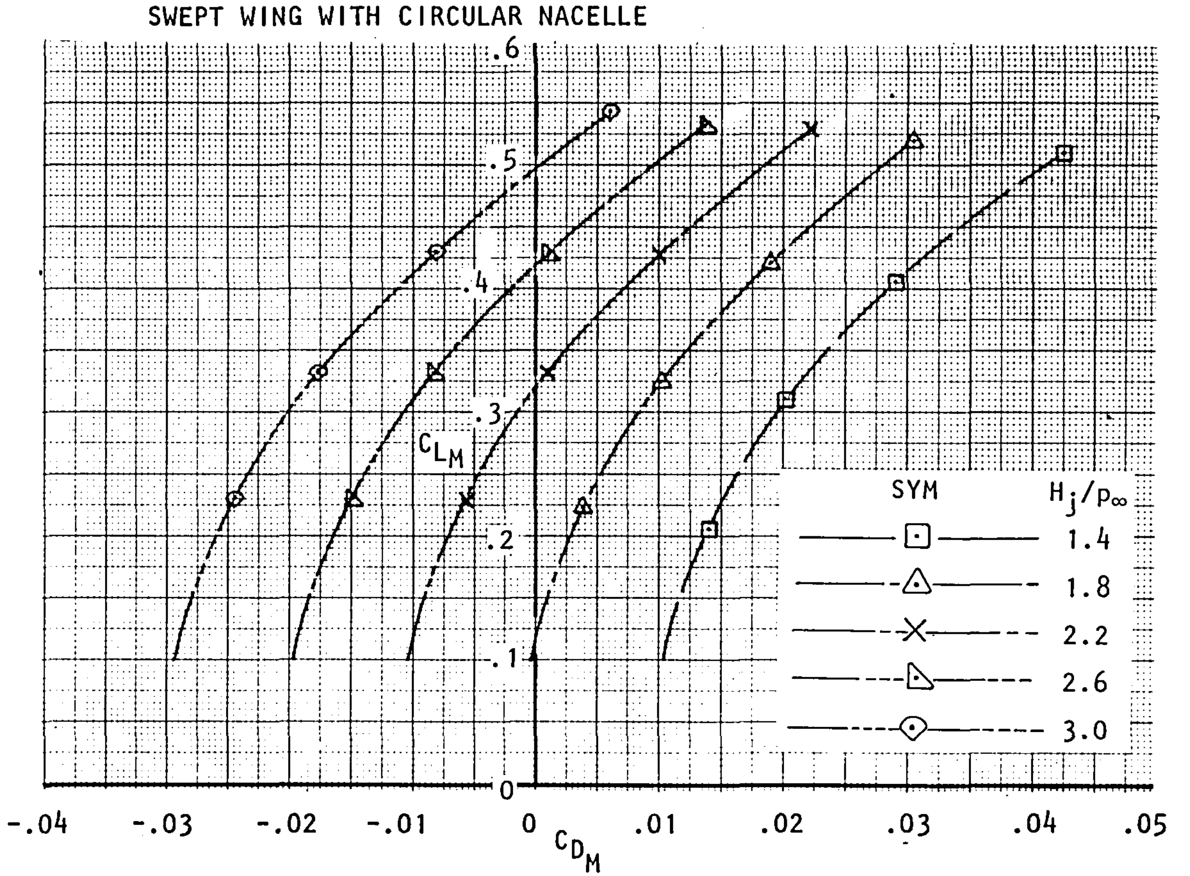

Figure 124. Variation of measured lift coefficient with measured drag coefficient and nozzle pressure ratio, $R_{NC} = 3.5 \times 10^6$, $M_\infty = 0.73$.

USB CRUISE PROGRAM

CONFIGURATION $F_2W_2B_5P_9C_3N_{11}$

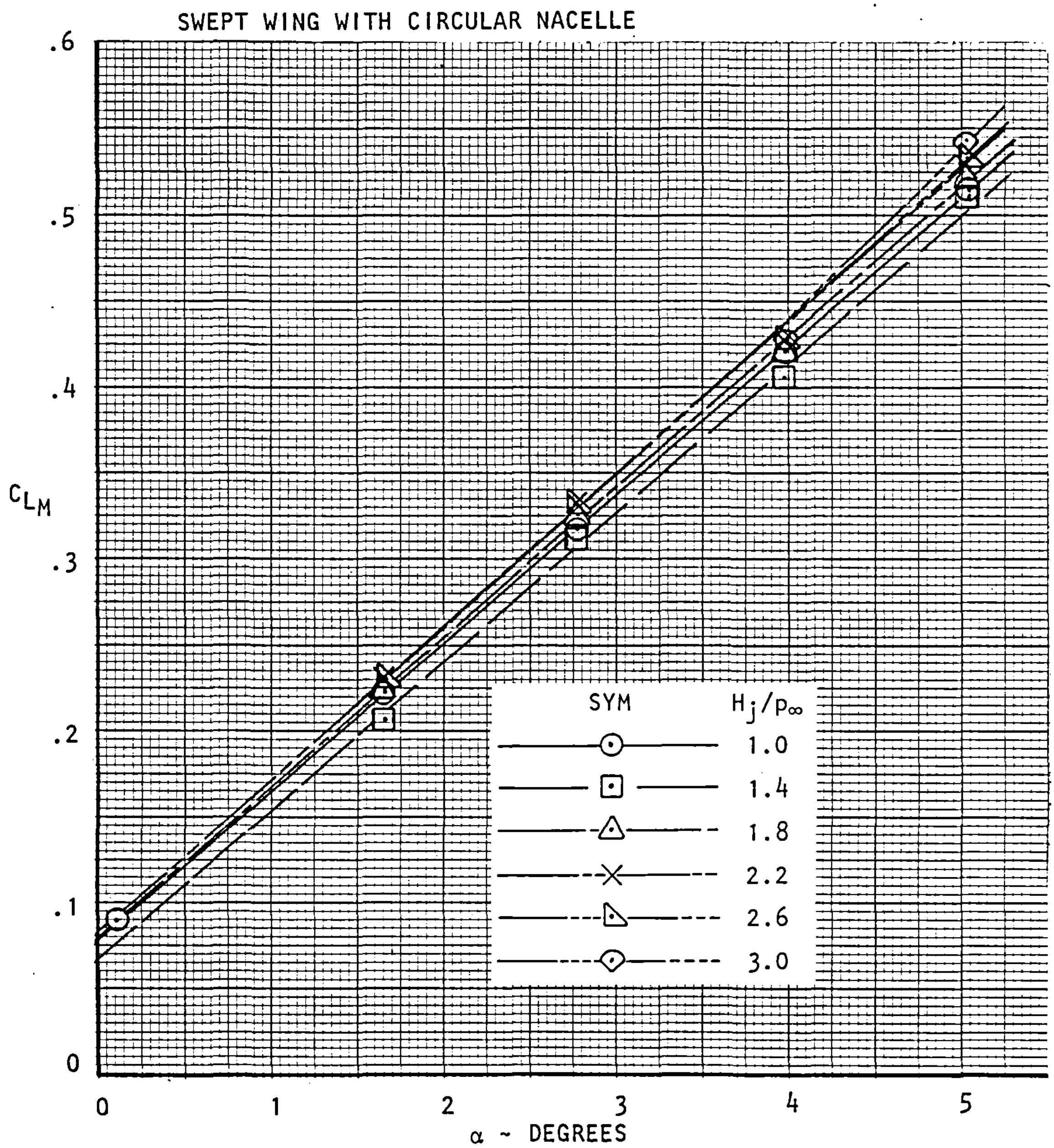

Figure 125. Variation of measured lift coefficient with angle of attack, $R_{NC} = 3.5 \times 10^6$, $M_\infty = 0.73$.

USB CRUISE PROGRAM

CONFIGURATION $F_2W_2B_5P_9C_3N_{12}$

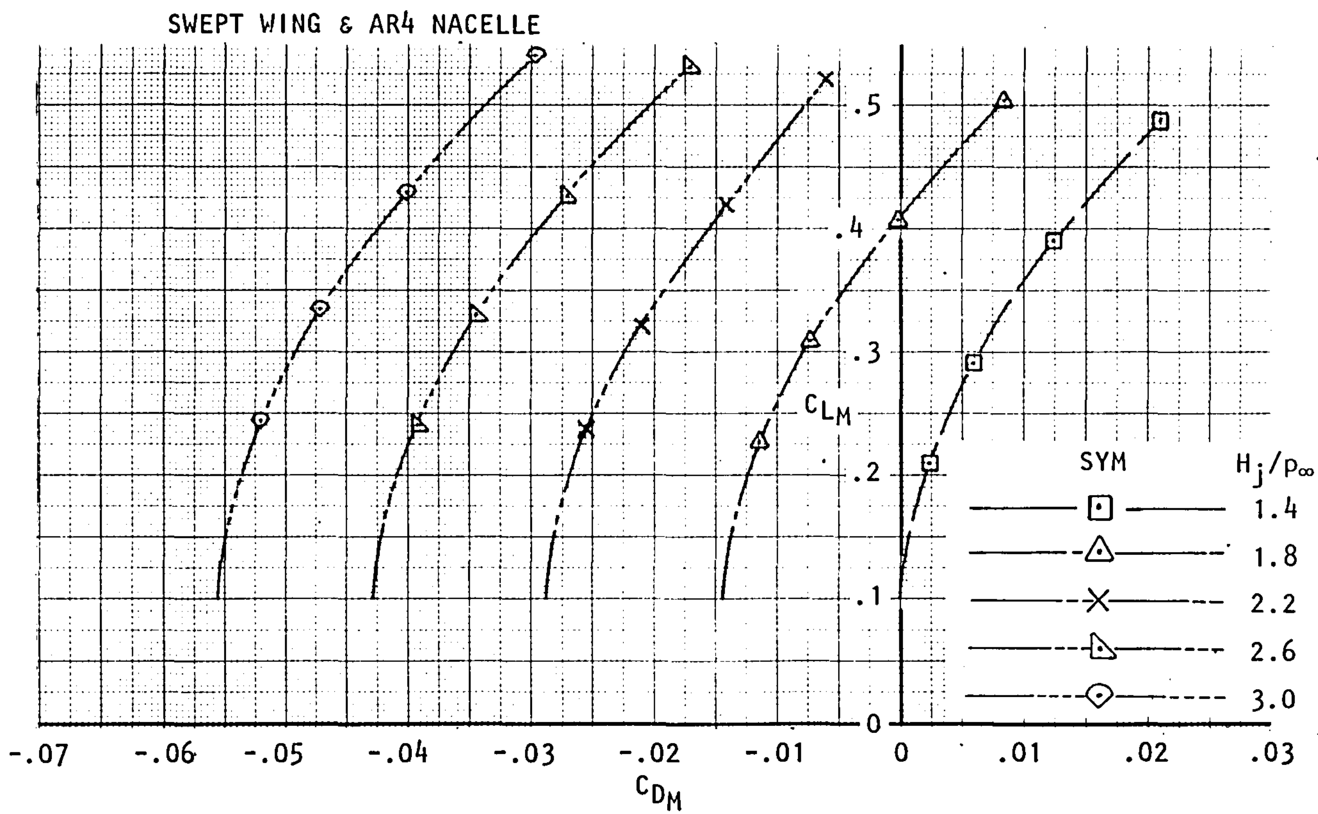

Figure 126. Variation of measured lift coefficient with measured drag coefficient and nozzle pressure ratio, $R_{NC} = 3.5 \times 10^6$, $M_\infty = 0.60$.

USB CRUISE PROGRAM

CONFIGURATION $F_2W_2B_5P_9C_3N_{12}$

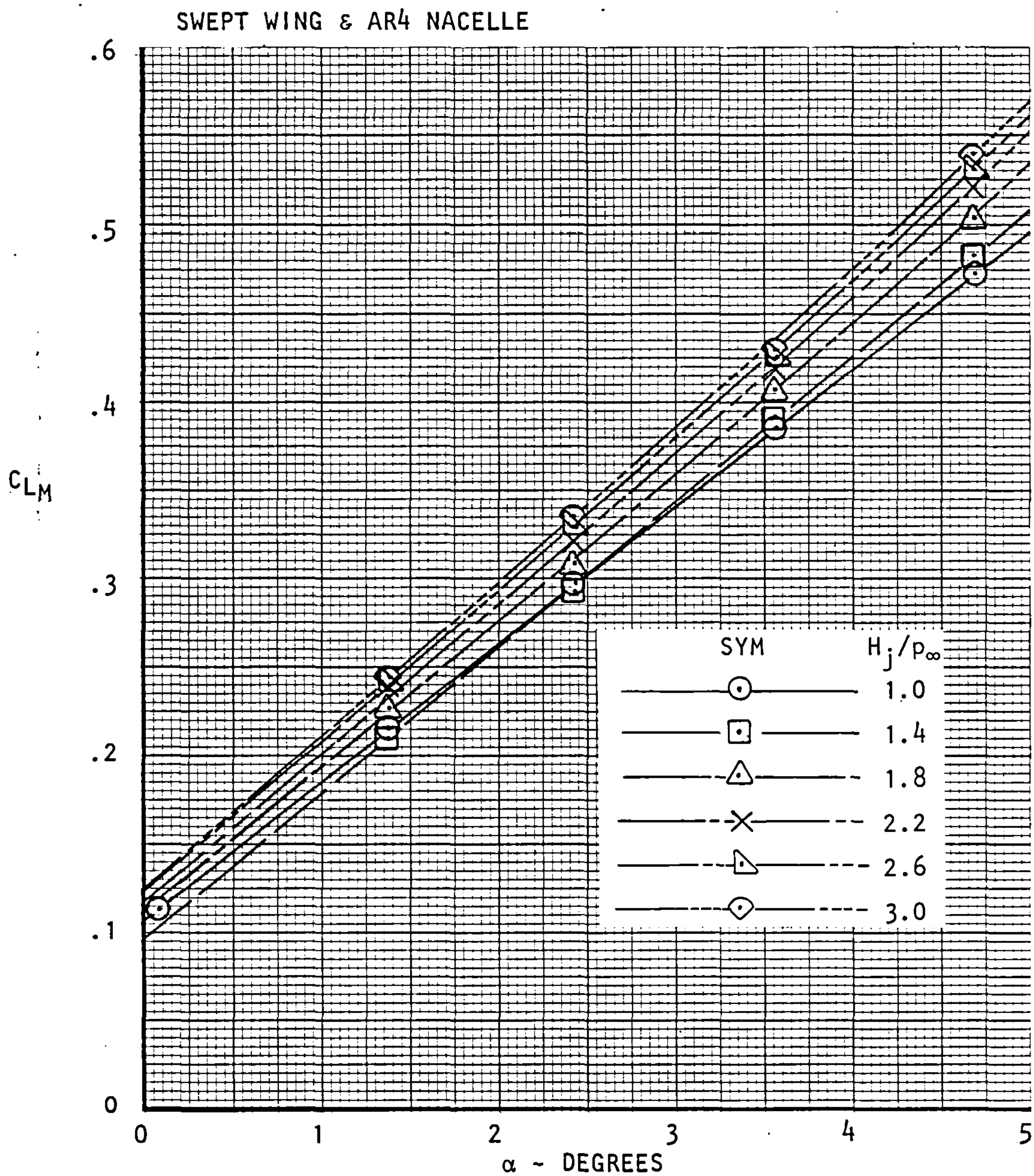

Figure 127. Variation of measured lift coefficient with angle of attack, $R_{NC} = 3.5 \times 10^6$, $M_\infty = 0.60$.

USB CRUISE PROGRAM

CONFIGURATION $F_2W_2B_5P_9C_3N_{12}$

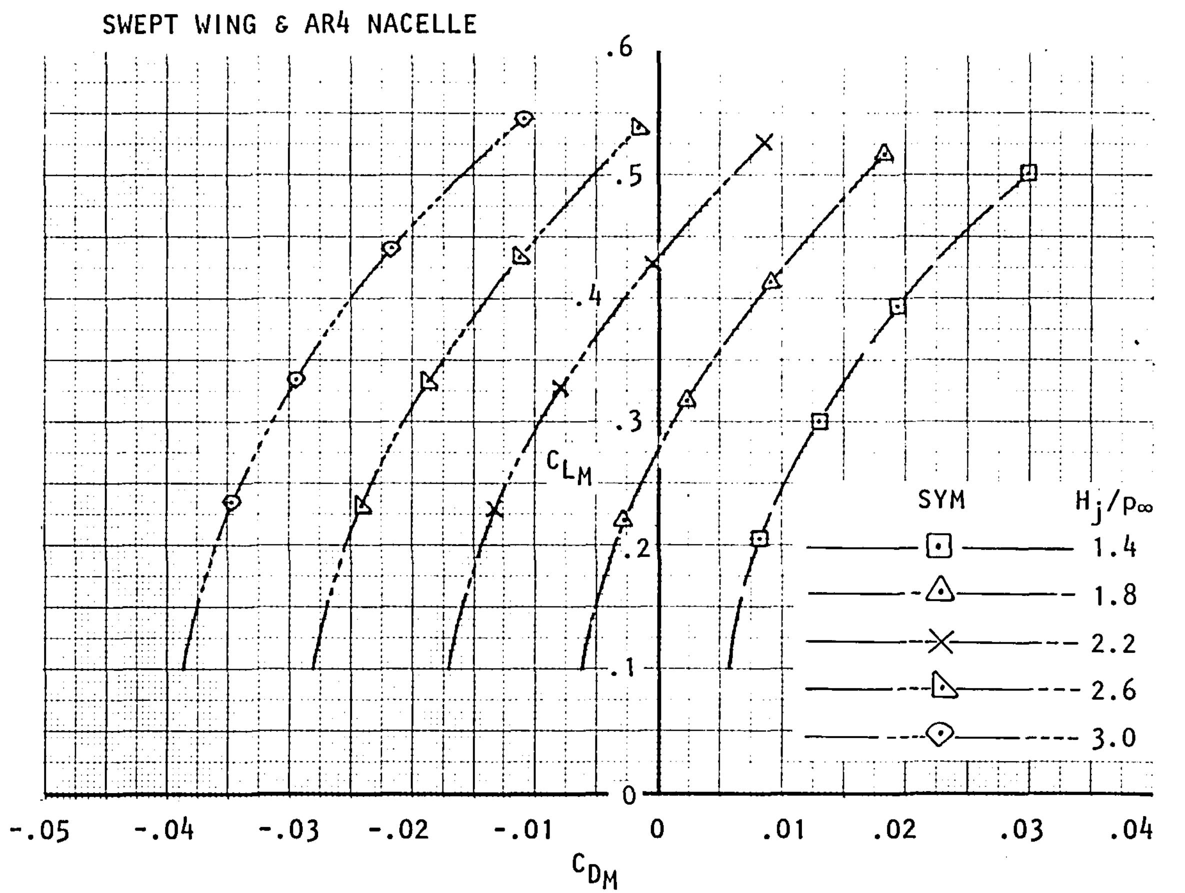

Figure 128. Variation of measured lift coefficient with measured drag coefficient and nozzle pressure ratio, $R_{NC} = 3.5 \times 10^6$, $M_\infty = 0.68$.

USB CRUISE PROGRAM

CONFIGURATION $F_2W_2B_5P_9C_3N_{12}$

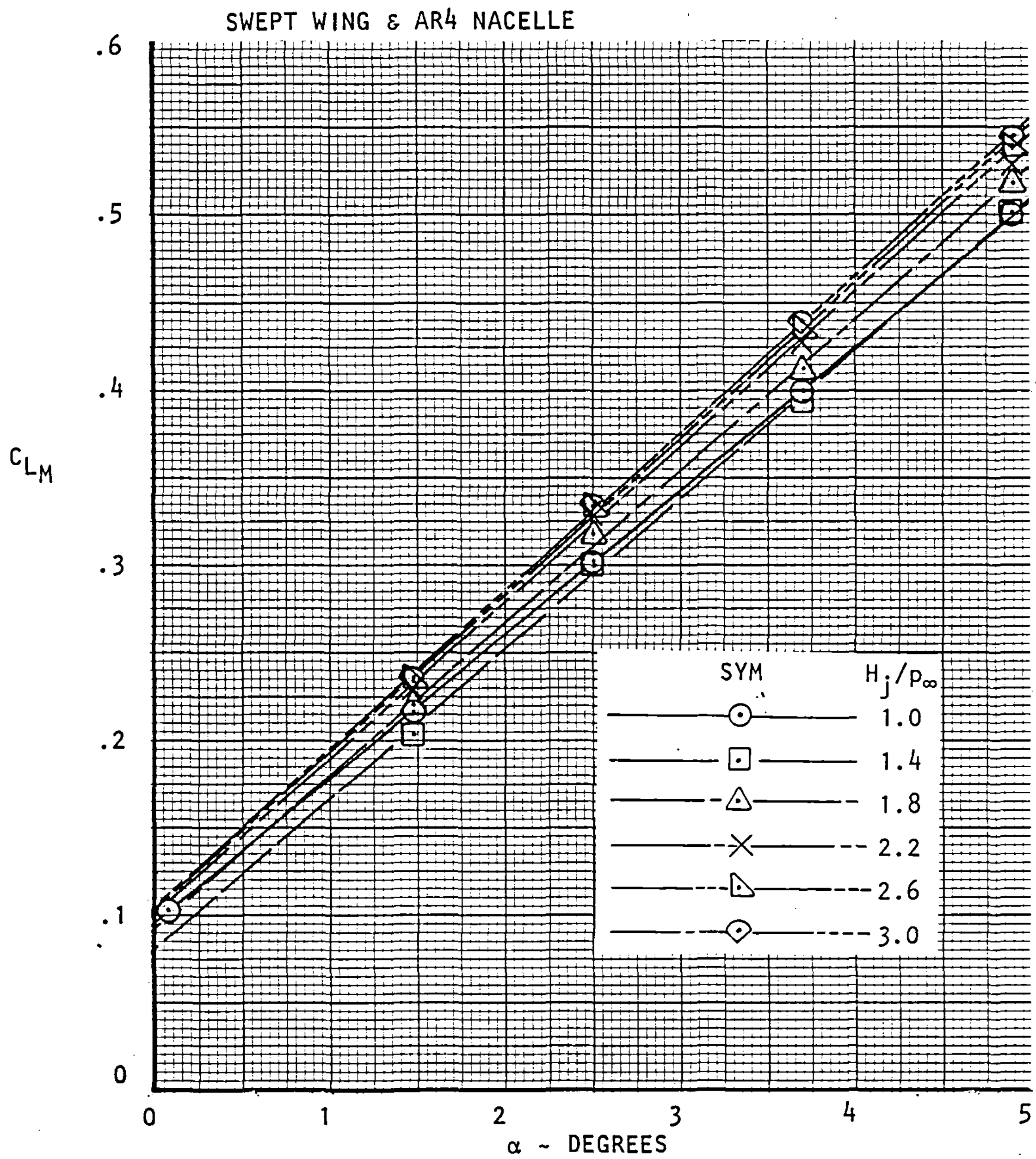

Figure 129. Variation of measured lift coefficient with angle of attack, $R_{NC} = 3.5 \times 10^6$, $M_\infty = 0.68$.

USB CRUISE PROGRAM

CONFIGURATION $F_2W_2B_5P_9C_3N_{12}$

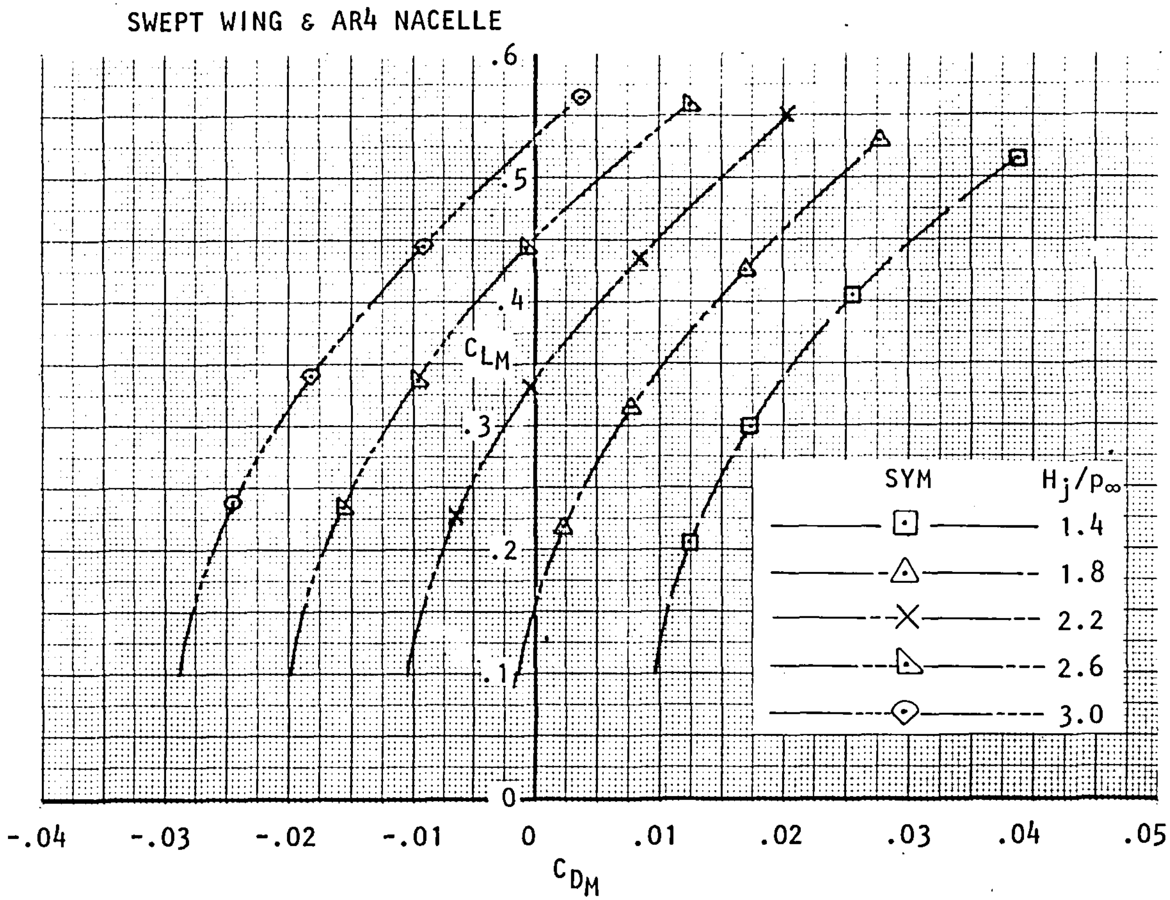

Figure 130. Variation of measured lift coefficient with measured drag coefficient and nozzle pressure ratio, $R_{NC} = 3.5 \times 10^6$, $M_\infty = 0.73$.

USB CRUISE PROGRAM

CONFIGURATION $F_2W_2B_5P_9C_3N_{12}$

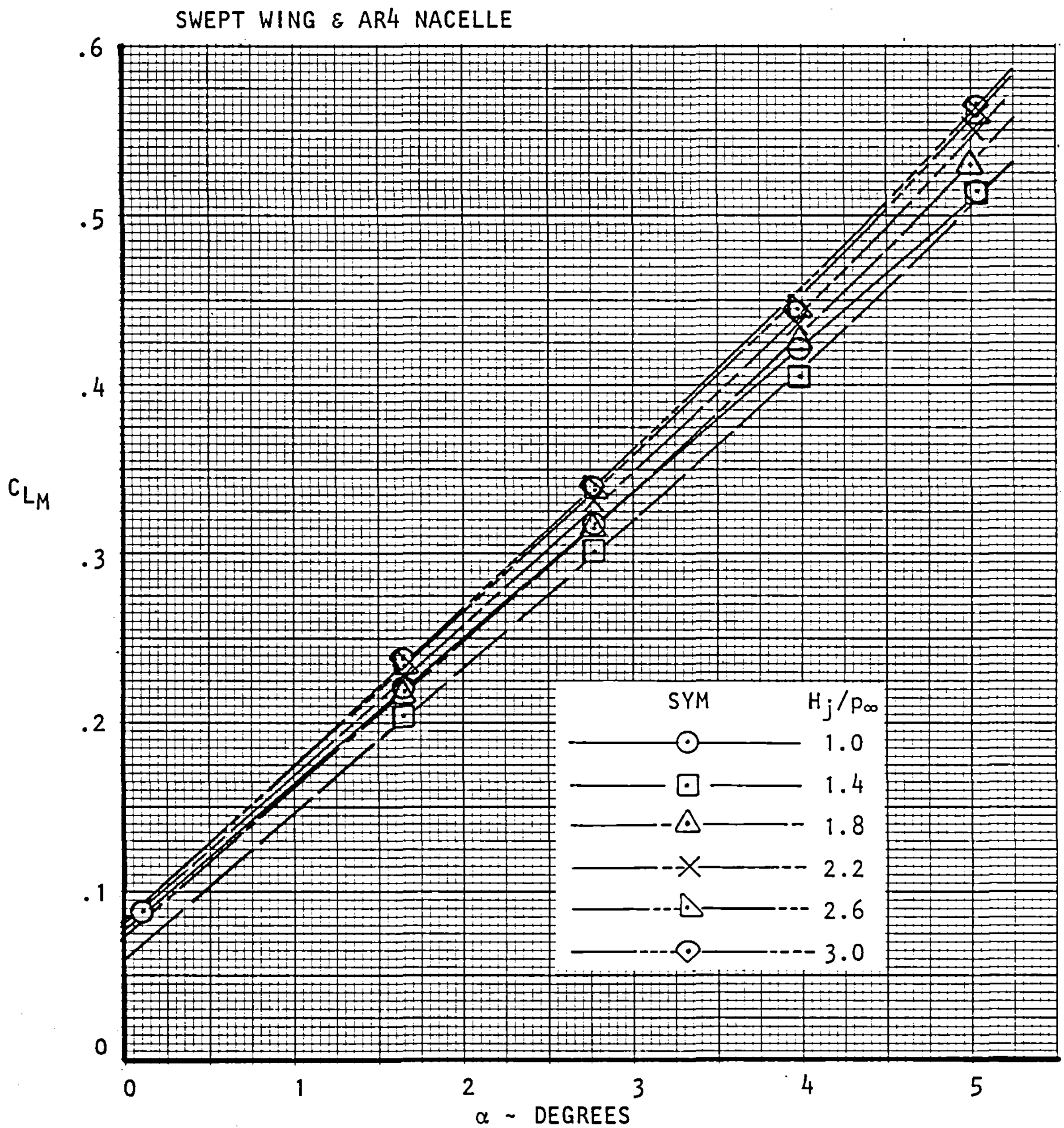

Figure 131. Variation of measured lift coefficient with angle of attack, $R_{NC} = 3.5 \times 10^6$, $M_\infty = 0.73$.

USB CRUISE PROGRAM

CONFIGURATION $F_2W_2B_5P_9C_3N_{13}$

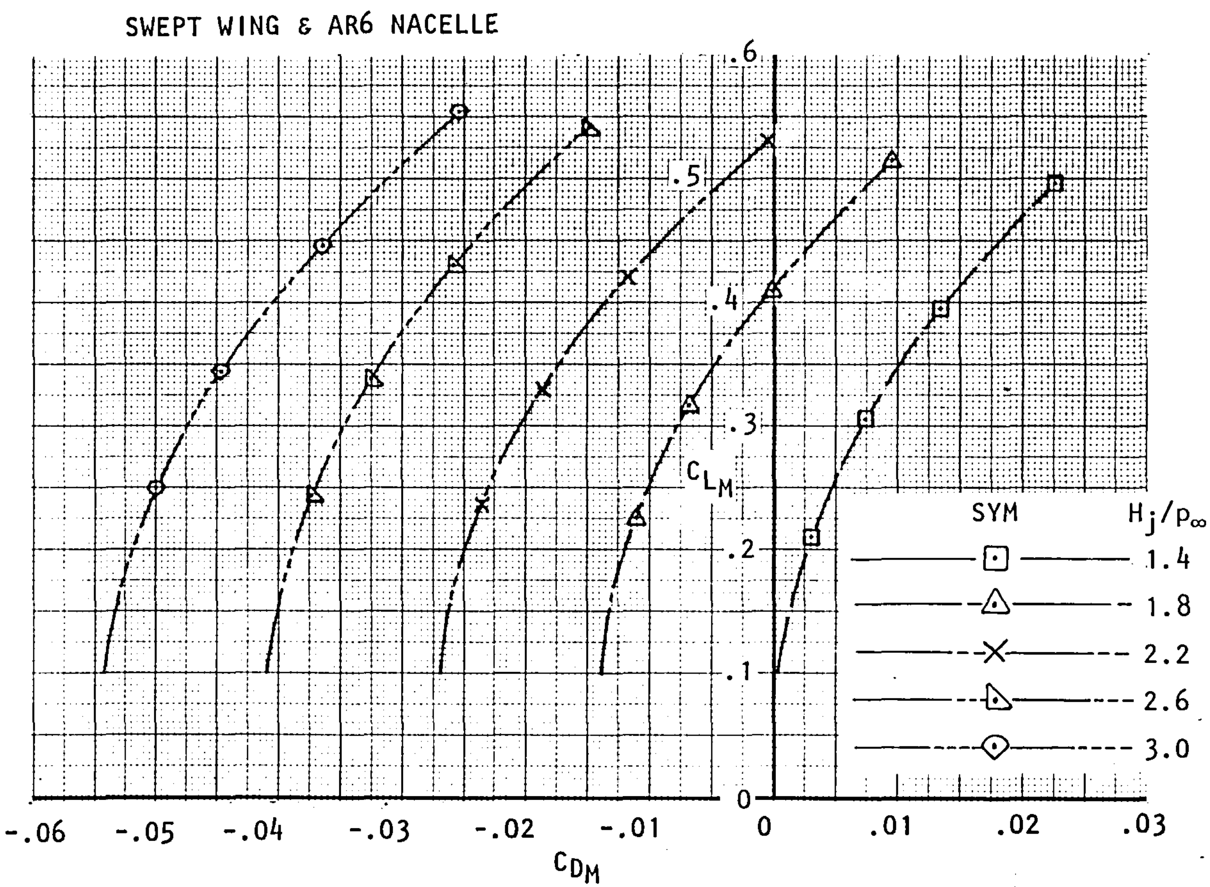

Figure 132. Variation of measured lift coefficient with measured drag coefficient and nozzle pressure ratio, $R_{NC} = 3.5 \times 10^6$, $M_\infty = 0.60$.

USB CRUISE PROGRAM

CONFIGURATION $F_2W_2B_5P_9C_3N_{13}$

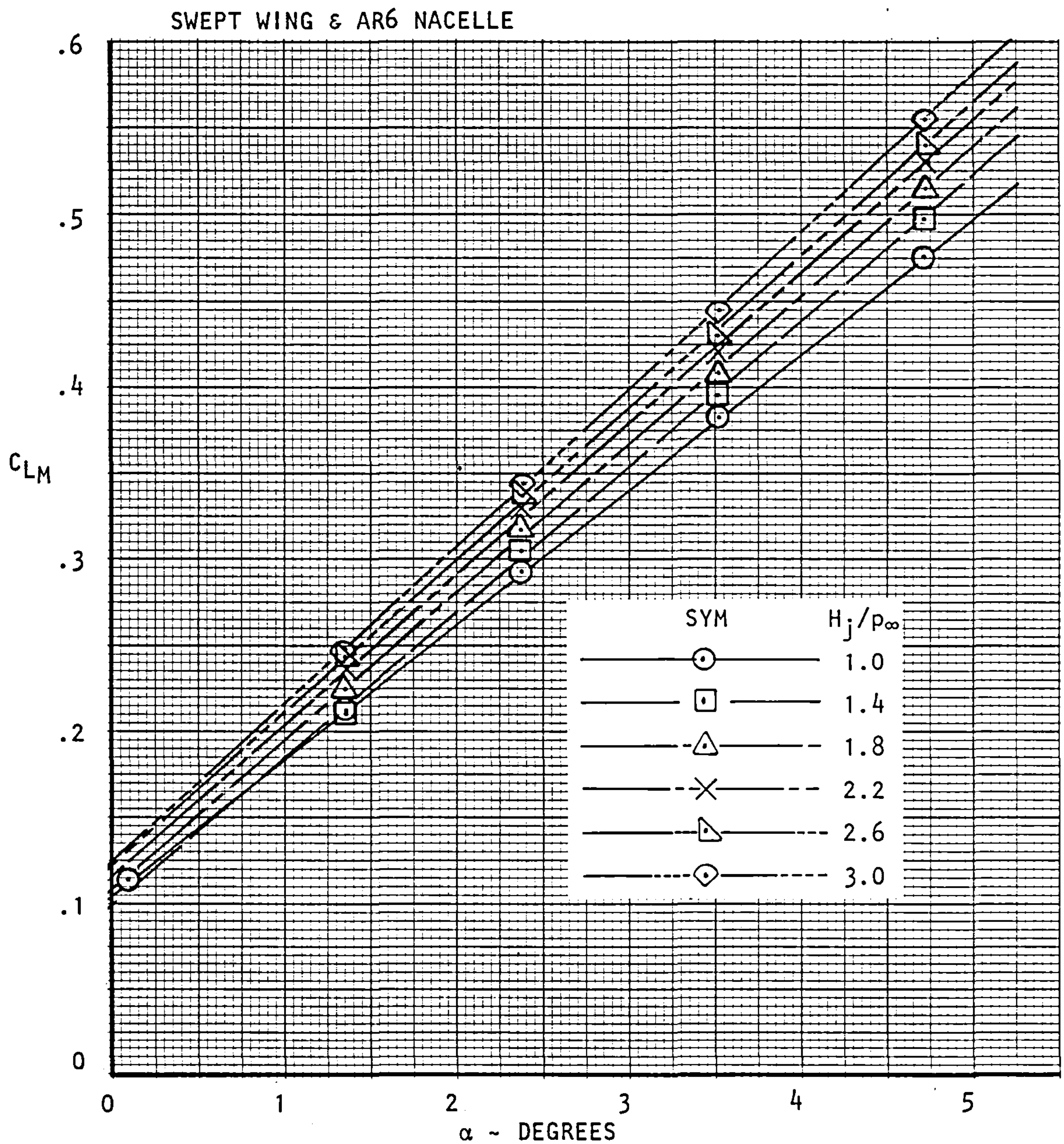

Figure 133. Variation of measured lift coefficient with angle of attack, $R_{NC} = 3.5 \times 10^6$, $M_\infty = 0.60$.

USB CRUISE PROGRAM

CONFIGURATION $F_2W_2B_5P_9C_3N_{13}$

SWEPT WING & AR6 NACELLE

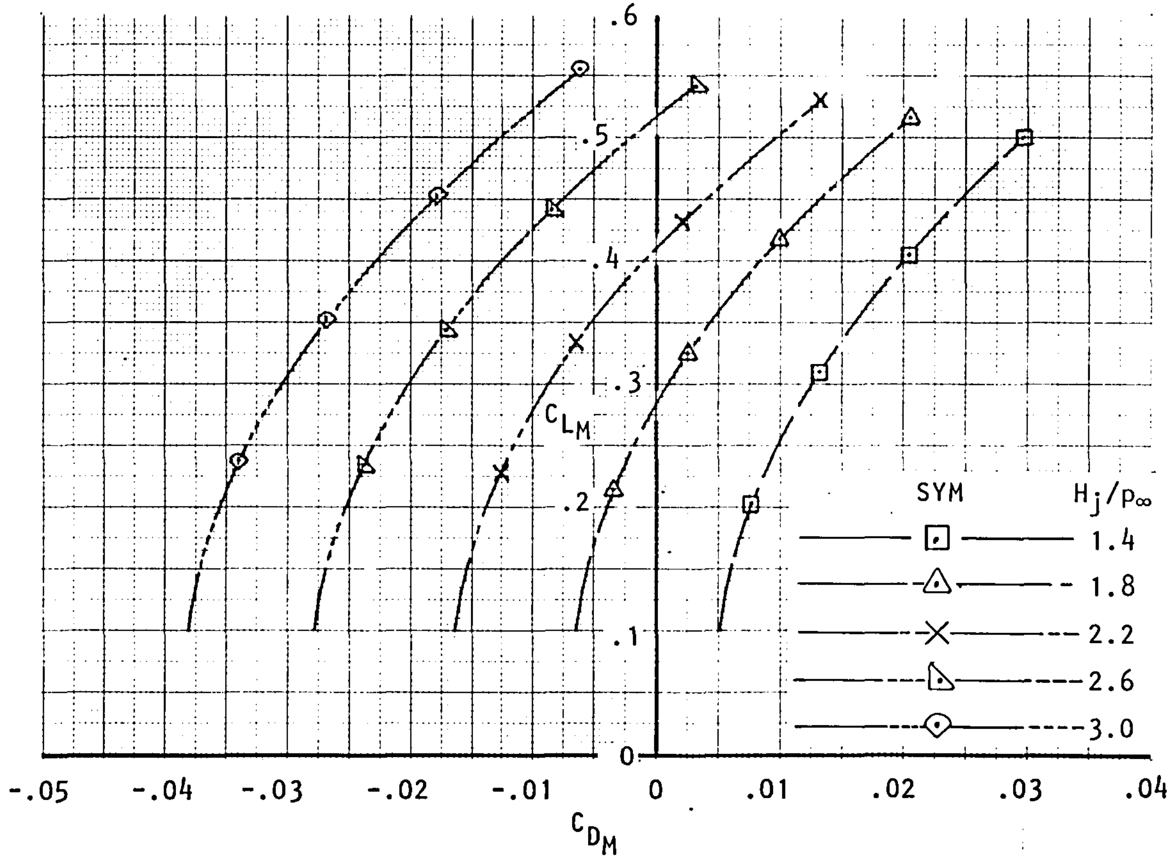

Figure 134. Variation of measured lift coefficient with measured drag coefficient and nozzle pressure ratio, $R_{NC} = 3.5 \times 10^6$, $M_\infty = 0.68$.

USB CRUISE PROGRAM

CONFIGURATION $F_2W_2B_5P_9C_3N_{13}$

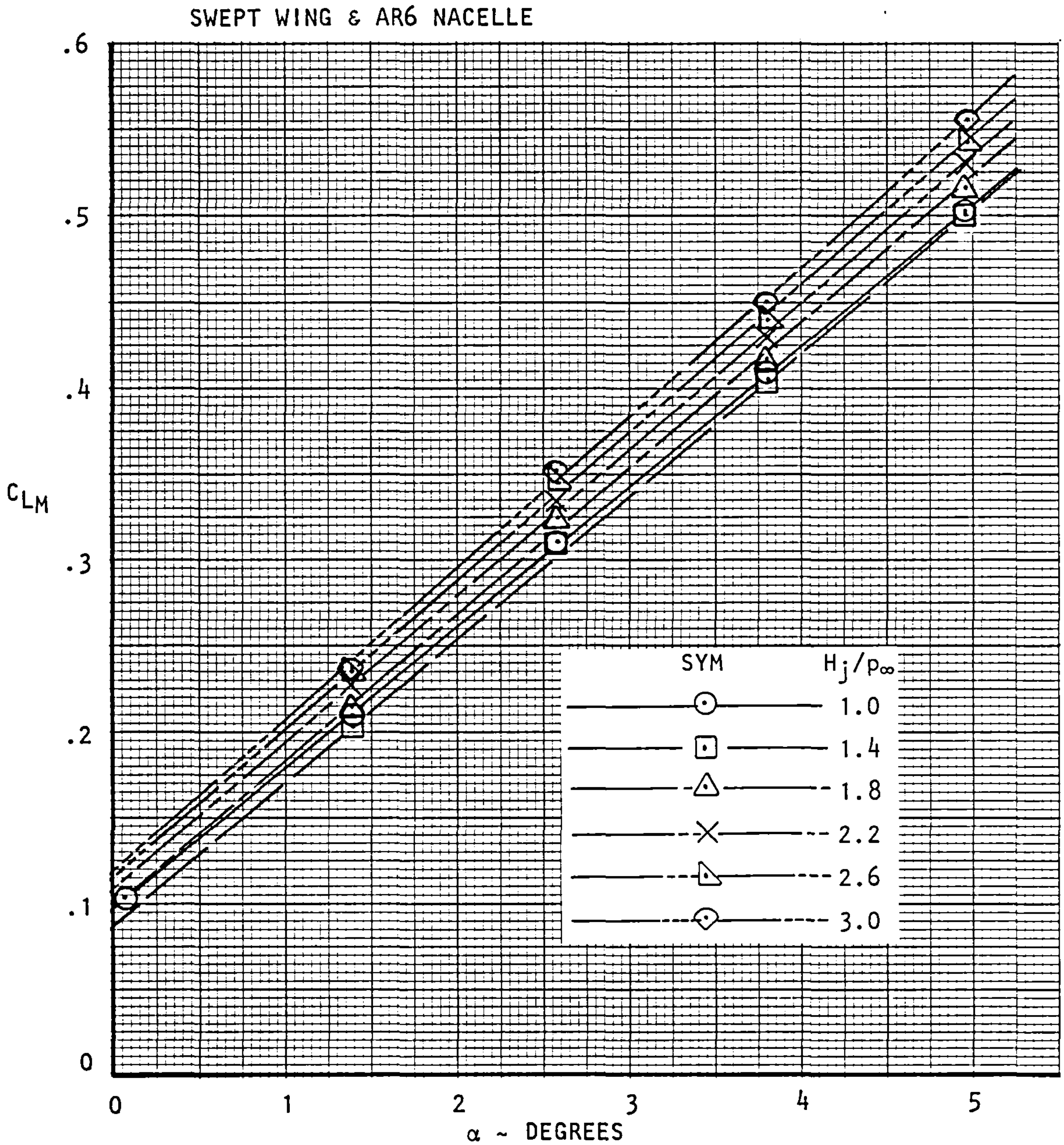

Figure 135. Variation of measured lift coefficient with angle of attack, $R_{NC} = 3.5 \times 10^6$, $M_\infty = 0.68$.

USB CRUISE PROGRAM

CONFIGURATION $F_2W_2B_5P_9C_3N_{13}$

SWEPT WING & AR6 NACELLE

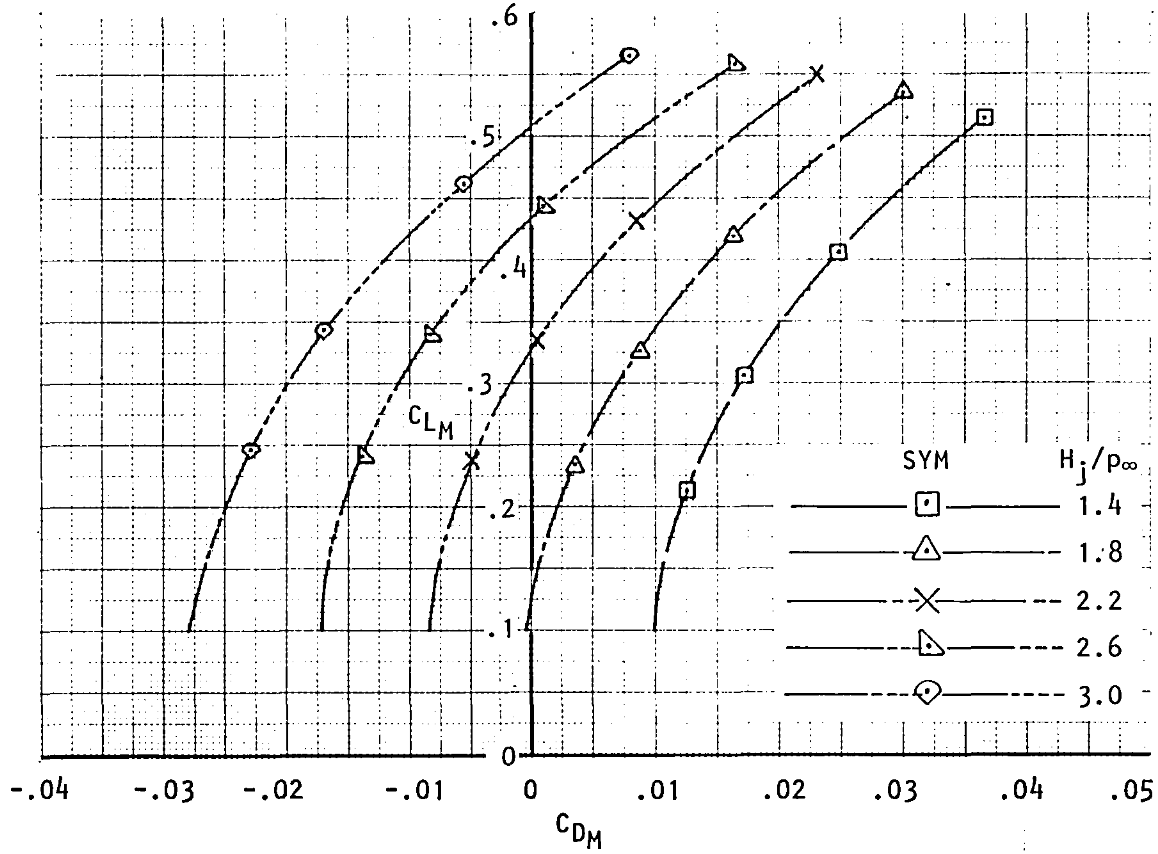

Figure 136. Variation of measured lift coefficient with measured drag coefficient and nozzle pressure ratio, $R_{NC} = 3.5 \times 10^6$, $M_\infty = 0.73$.

USC CRUISE PROGRAM

CONFIGURATION $F_2W_2B_5P_9C_3N_{13}$

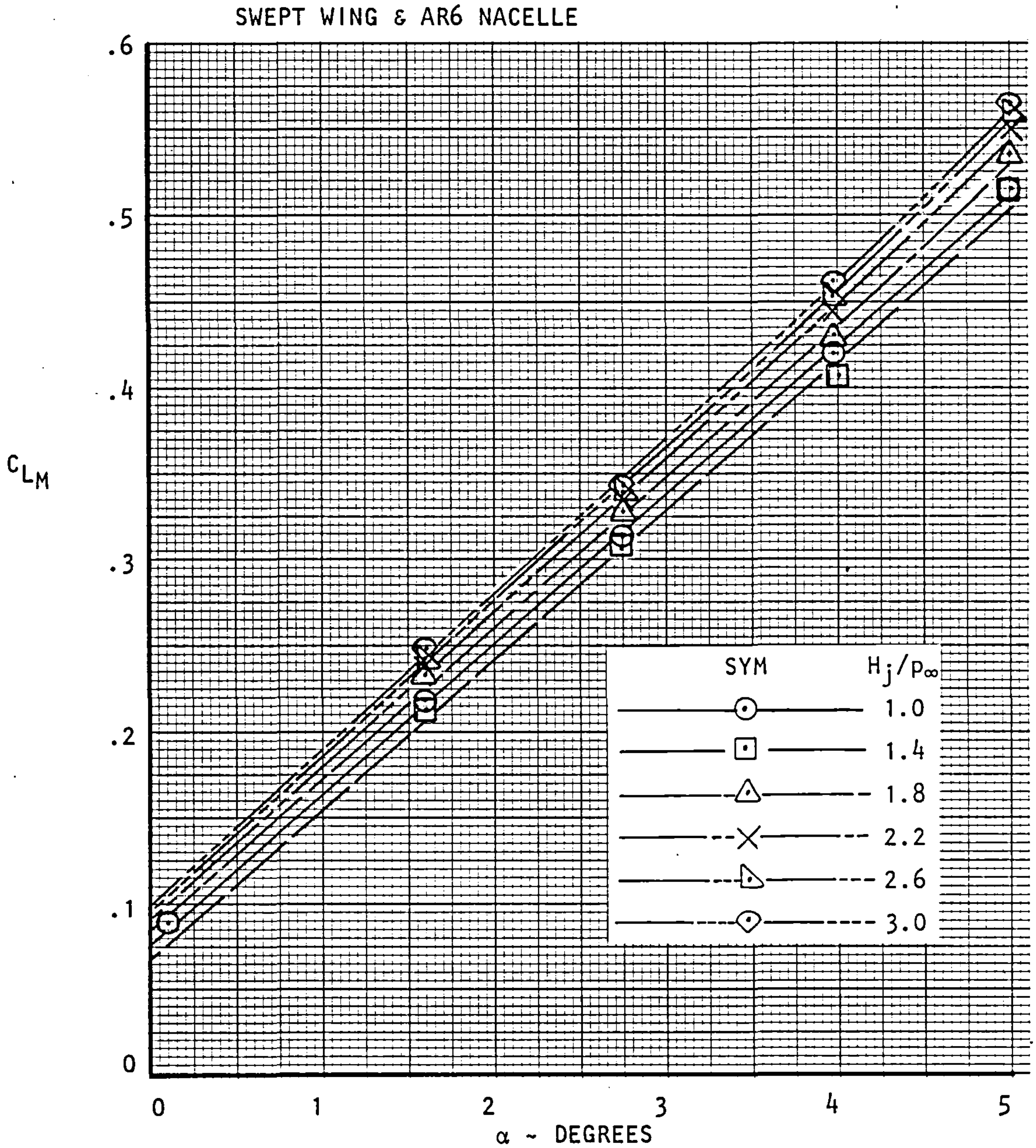

Figure 137. Variation of measured lift coefficient with angle of attack, $R_{NC} = 3.5 \times 10^6$, $M_\infty = 0.73$.

7.0 NOZZLE CALIBRATION

The nozzles designed for the USB Cruise Performance Program covered a wide range of types and shapes. To accurately determine the effects of installing these nozzles on upper surface blowing models, it was considered necessary to first obtain actual nozzle performance on an isolated basis. Static tests were later performed on the fully integrated wing-nozzle combinations.

7.1 Basic Isolated Nozzle Performance

The isolated test nozzles were calibrated using a rig set up in Lockheed-Georgia Low Speed Wind Tunnel. There were three sizes of test nozzles with aspect ratios which ranged from 1.25 to 6. Both forces and pressures were measured in separate sets of runs. Test dates were from 9-8 through 9-19-75. Actual and ideal nozzle pressure ratio as well as thrust parameter were plotted versus reference pressure ratio for each of the test configurations. Discharge coefficients, velocity coefficients and various forms of thrust coefficients were also plotted. These are presented in Figures 138 through 165.

USB CRUISE PROGRAM

SYM	RUN	CONFIGURATION
⊙	9	RAKE ON
×	10	RAKE OFF

USB NOZZLES CALIBRATION
N2E EXISTING INTERMEDIATE CIRCULAR 0.35C

DATE SEPT 1975
LSWT 160
LOCKHEED

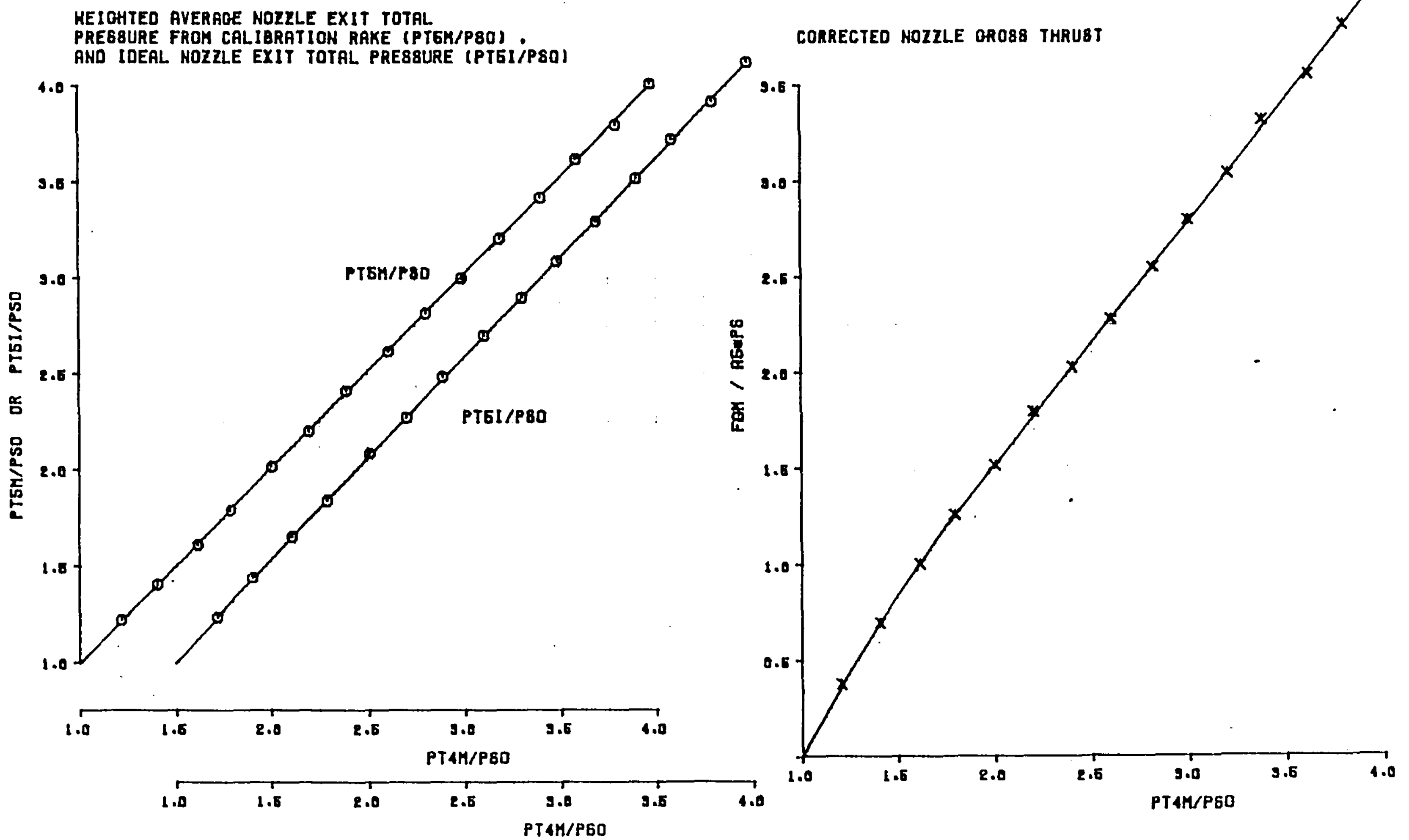

Figure 138. Nozzle exit pressure ratio and thrust parameter versus internal reference pressure ratio, N_{2E}.

USB CRUISE PROGRAM

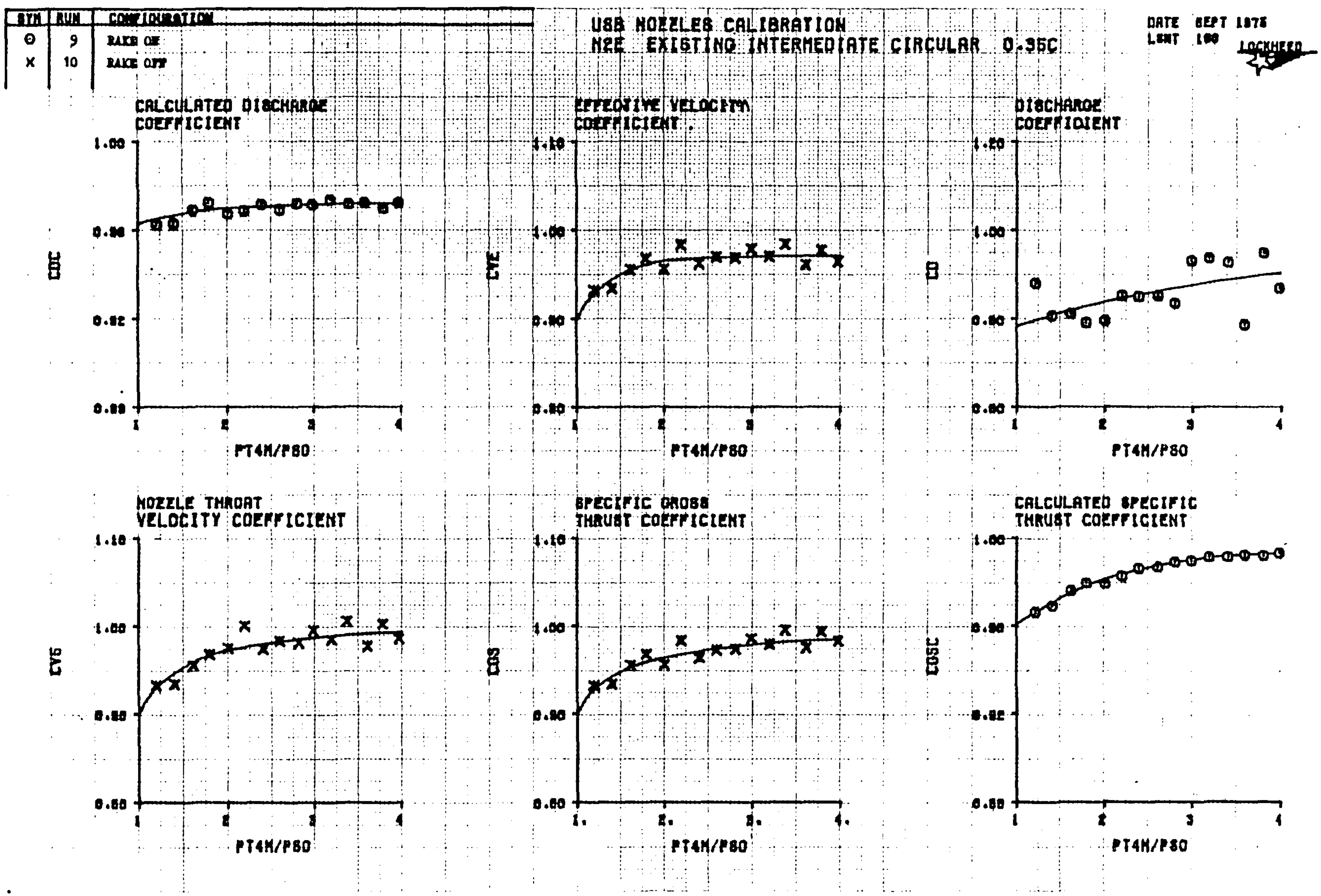

Figure 139. Isolated nozzle performance coefficients from static test rig, N_{2E}.

USB CRUISE PROGRAM

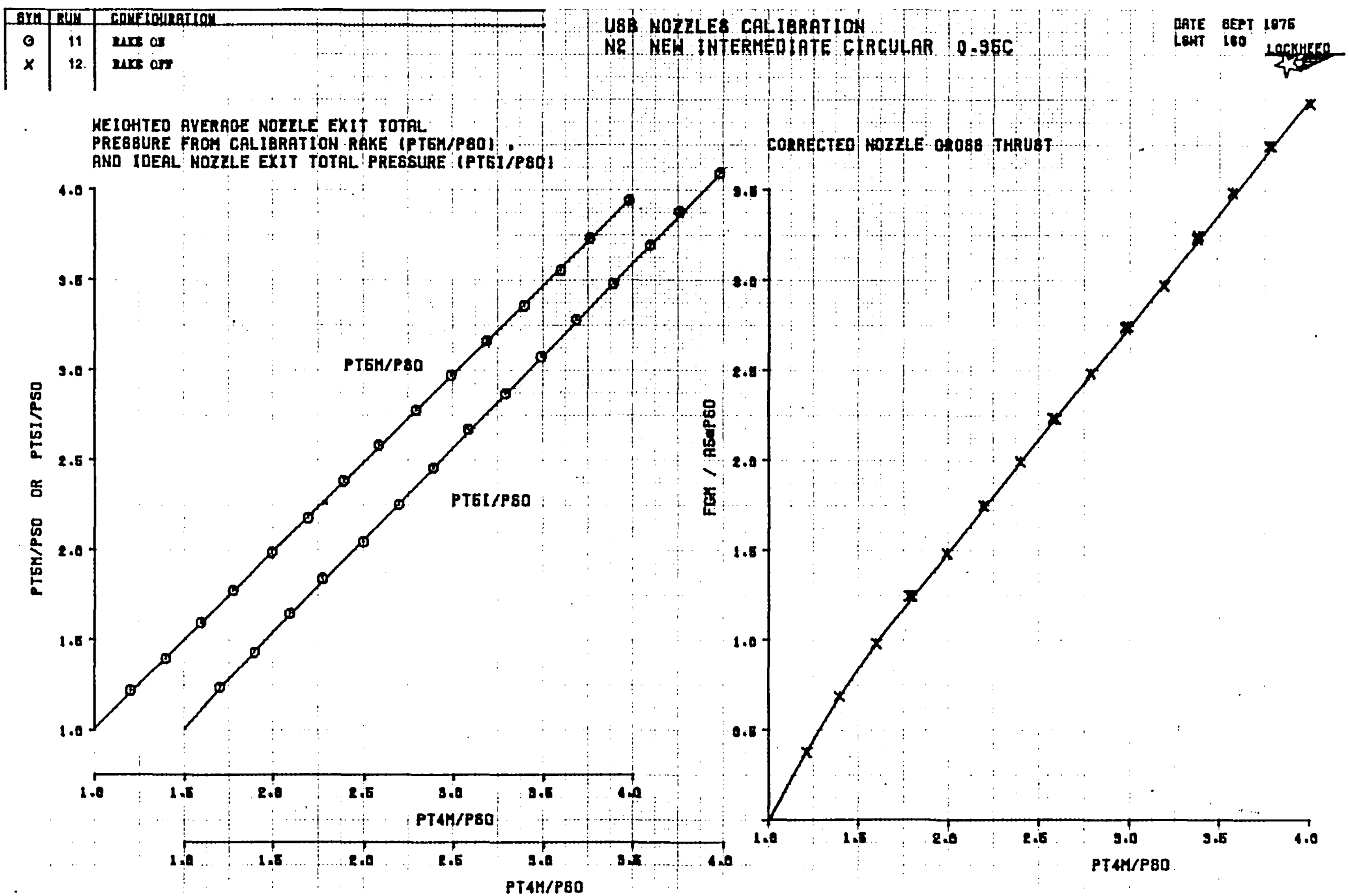

Figure 140. Nozzle exit pressure ratio and thrust parameter versus internal reference pressure ratio, N_2.

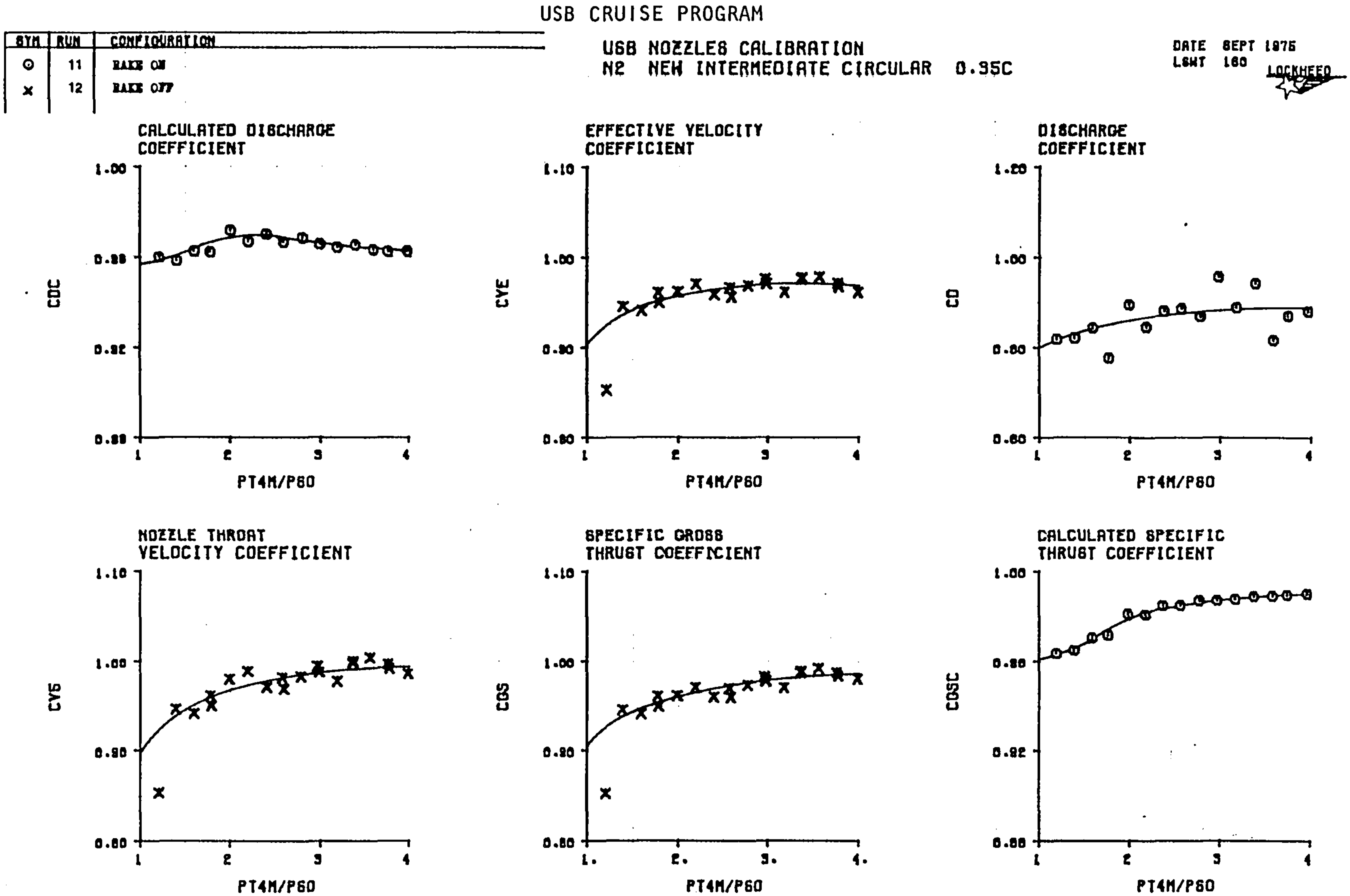

Figure 141. Isolated nozzle performance coefficients from static test rig, N_2.

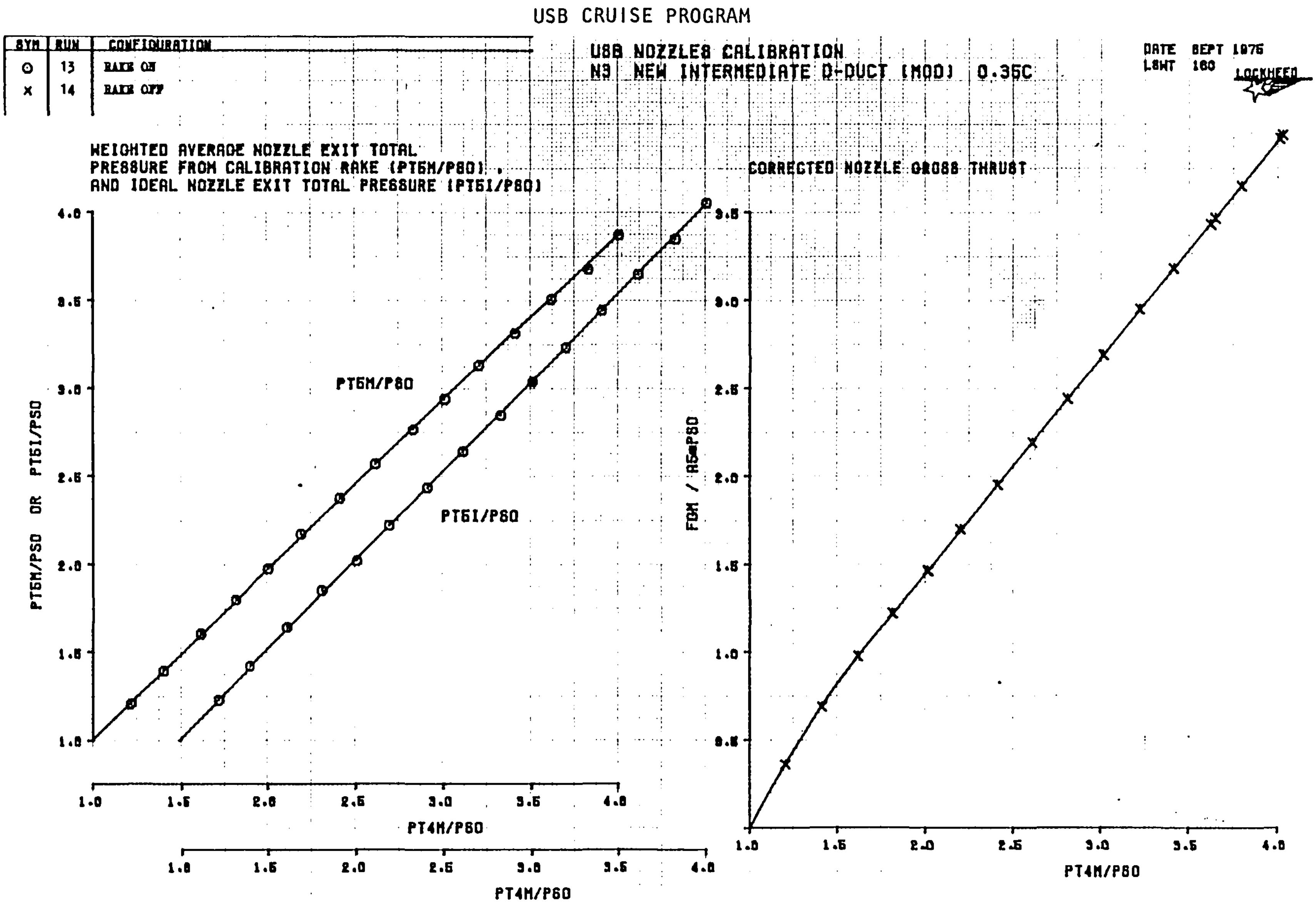

Figure 142 Nozzle exit pressure ratio and thrust parameter versus internal reference pressure ratio, N_3.

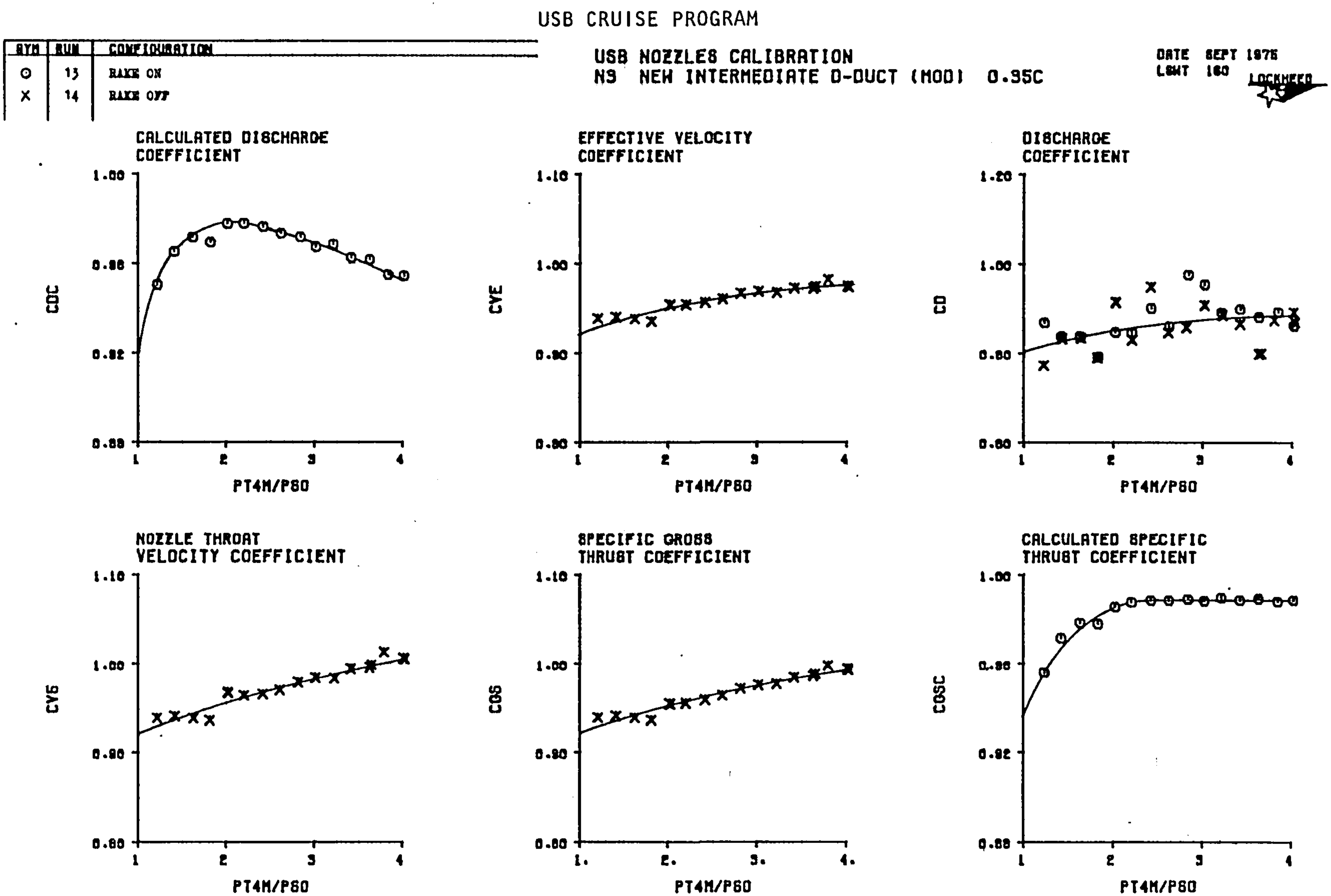

Figure 143. Isolated nozzle performance coefficients from static test rig, N_3.

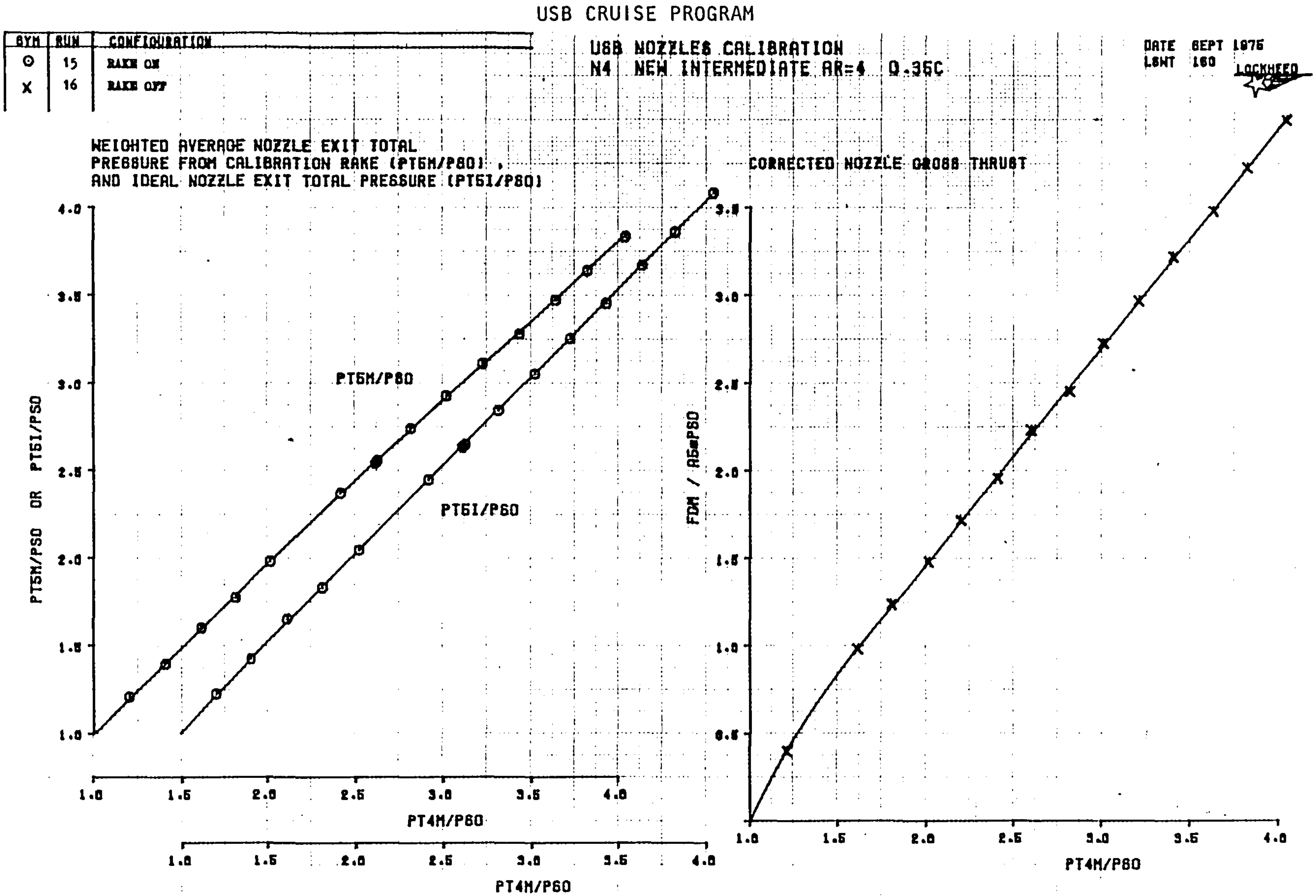

Figure 144. Nozzle exit pressure ratio and thrust parameter versus internal reference pressure ratio, N_4.

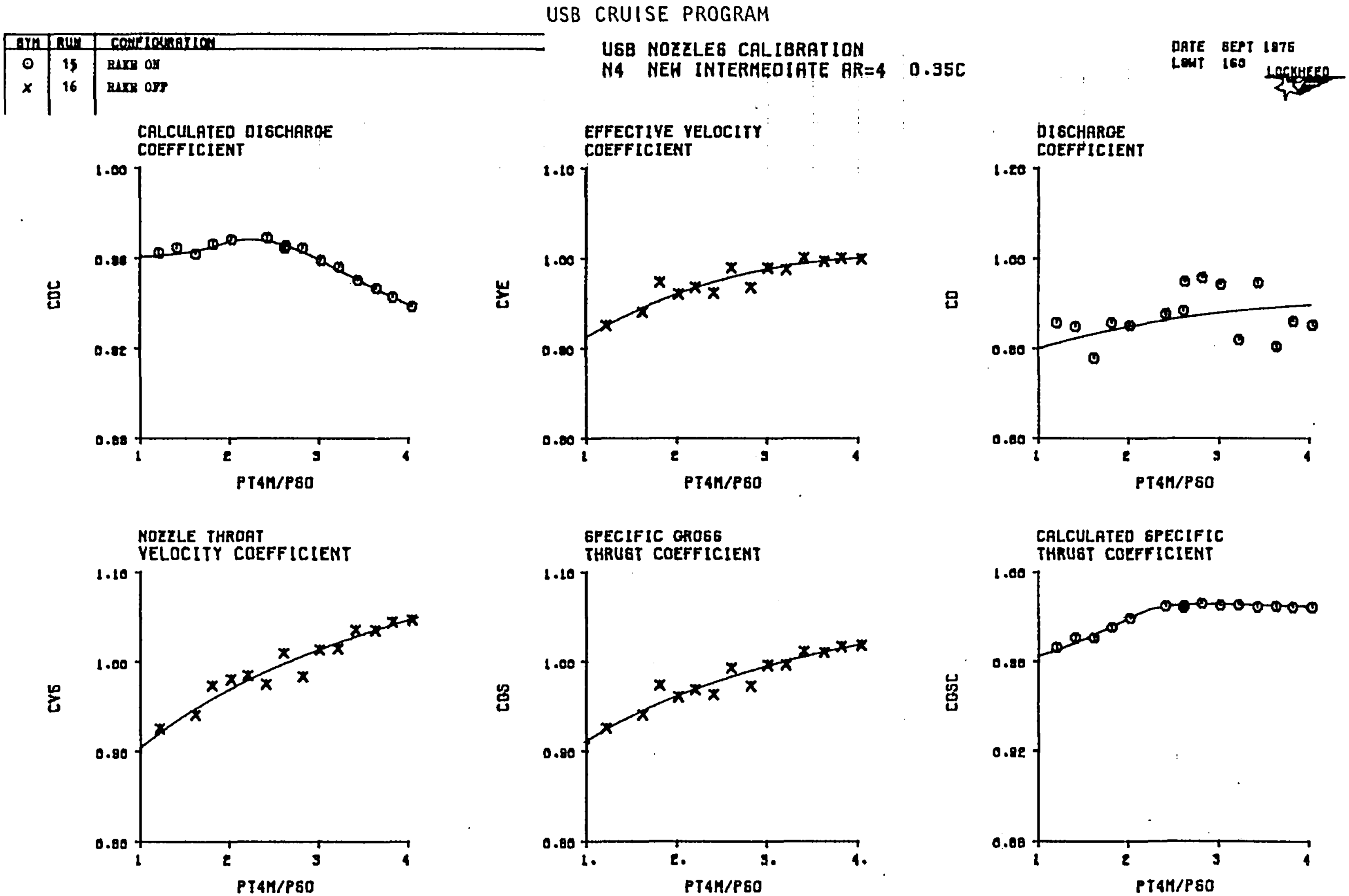

Figure 145. Isolated nozzle performance coefficients from static test rig, N_4.

USB CRUISE PROGRAM

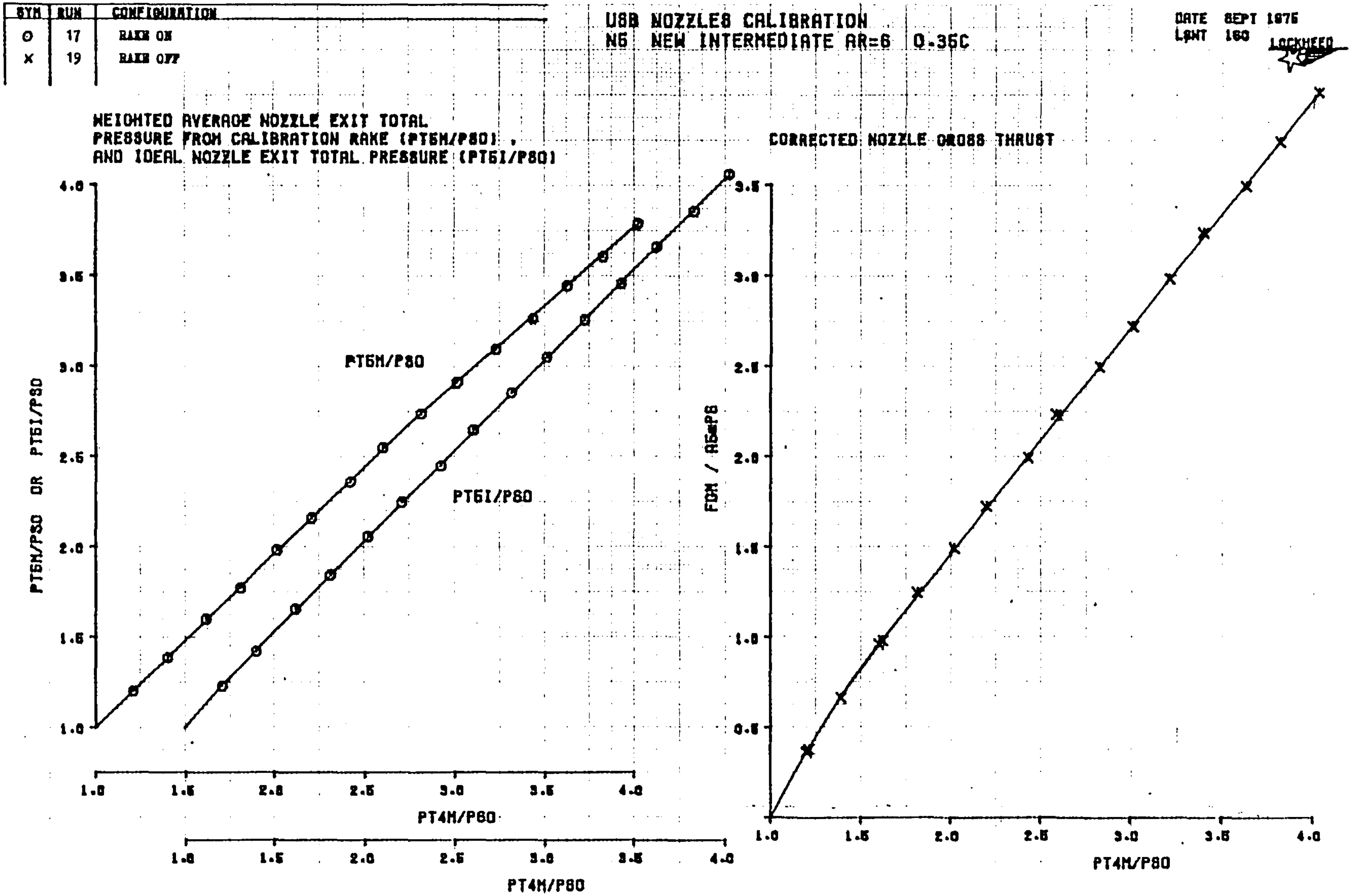

Figure 146. Nozzle exit pressure ratio and thrust parameter versus internal reference pressure ratio, N_5.

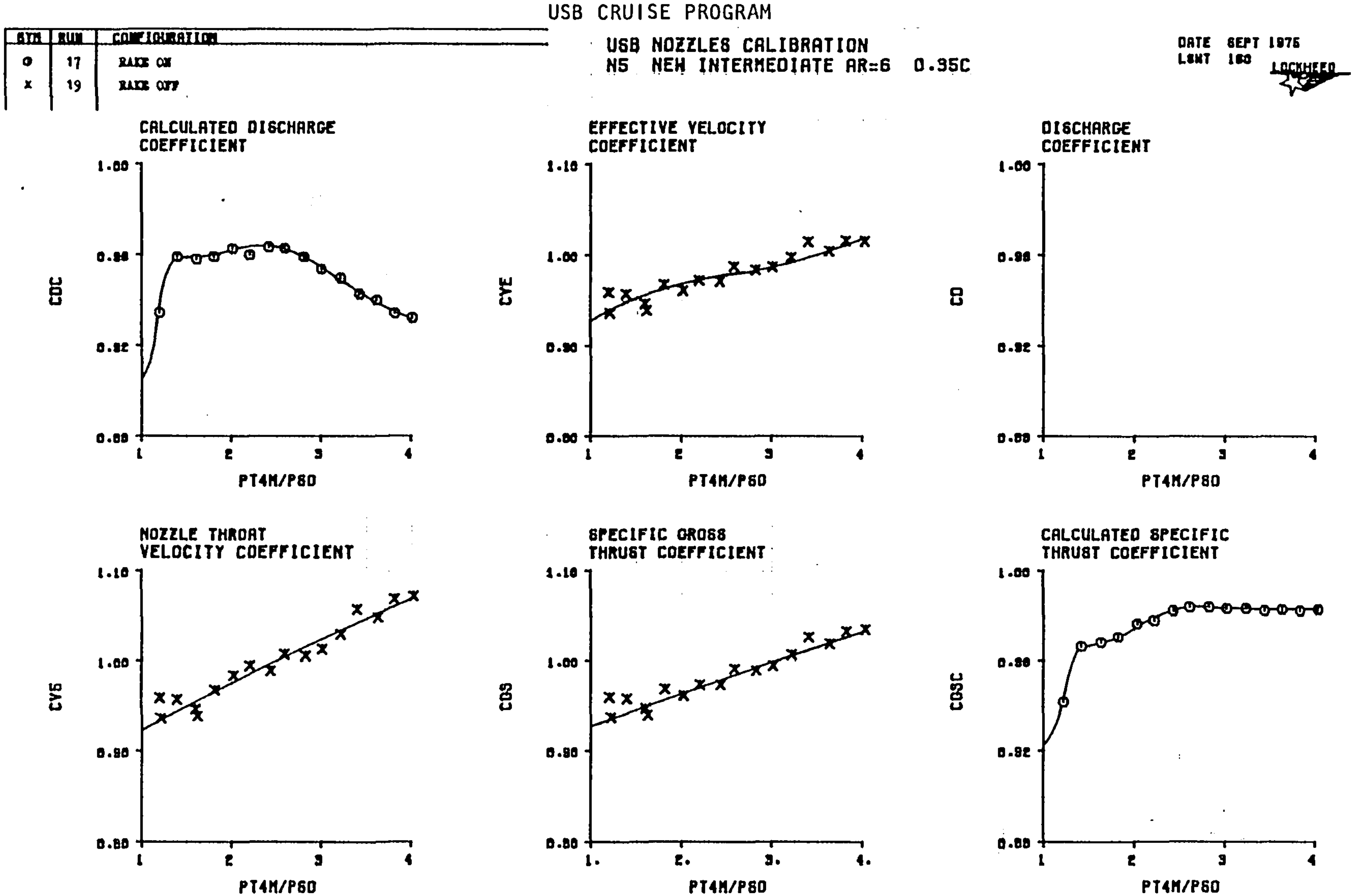

Figure 147. Isolated nozzle performance coefficients from static test rig, N_5.

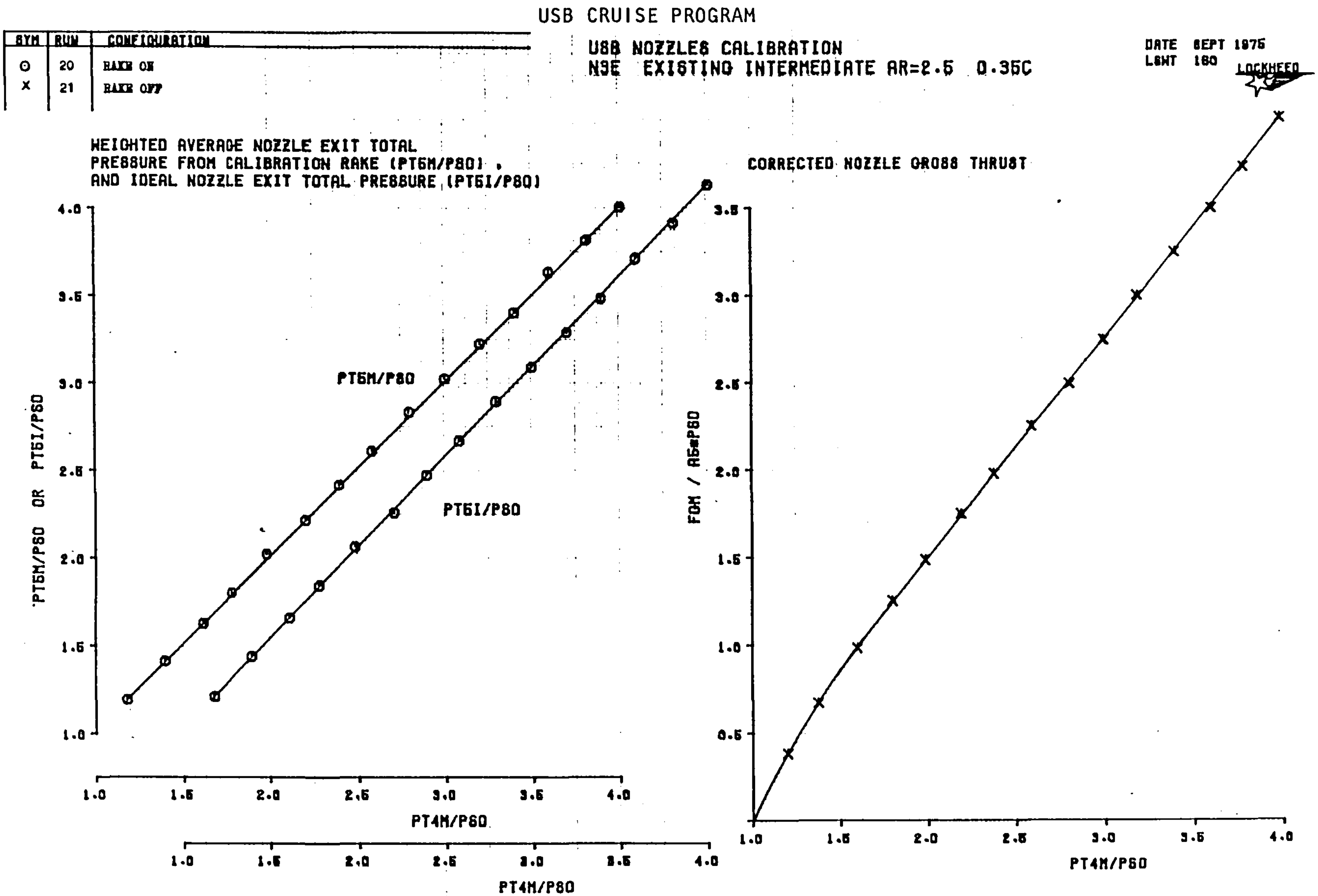

Figure 148. Nozzle exit pressure ratio and thrust parameter versus internal reference pressure ratio, N_{3E}.

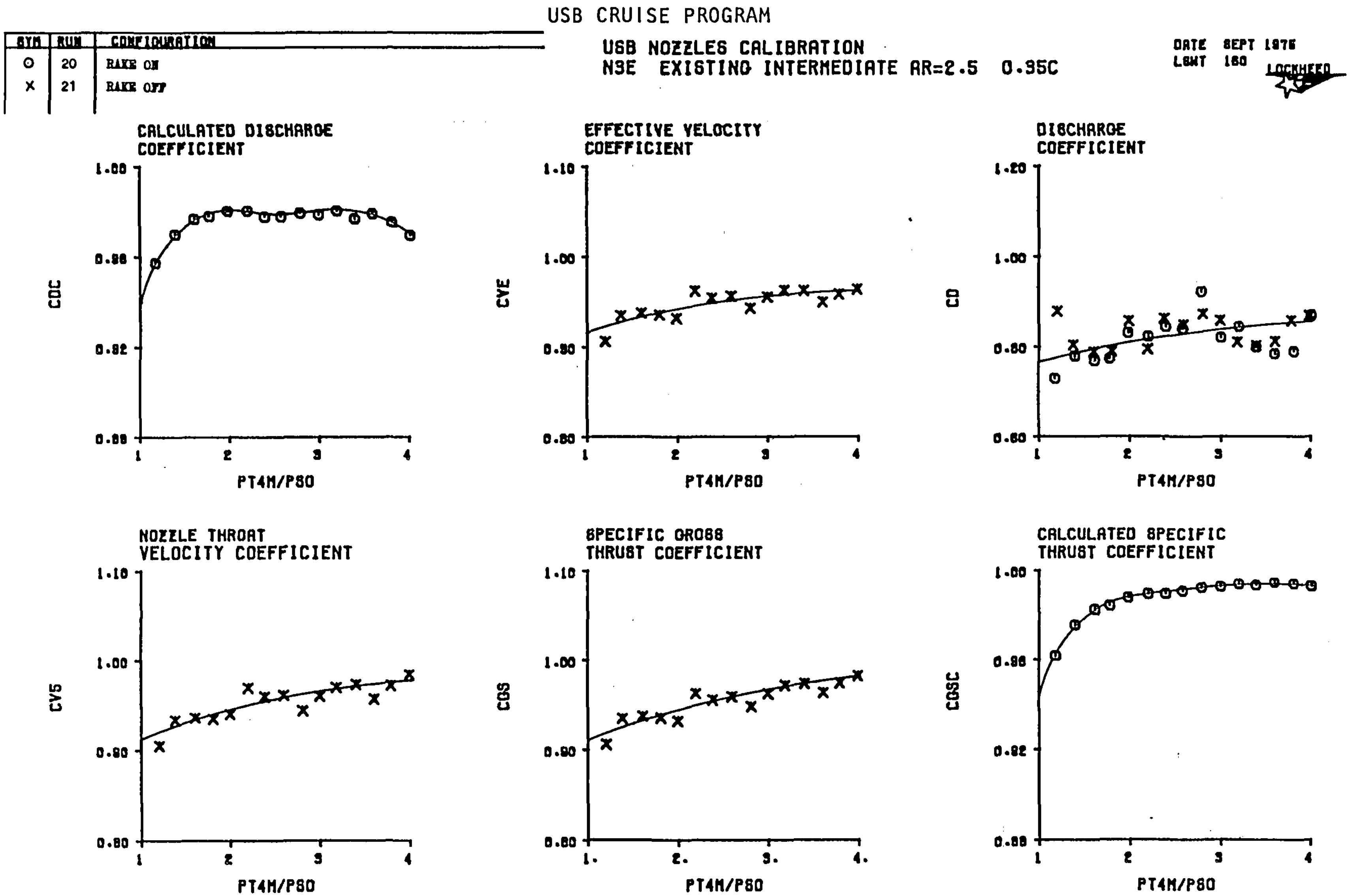

Figure 149. Isolated nozzle performance coefficients from static test rig, N_{3E}.

USB CRUISE PROGRAM

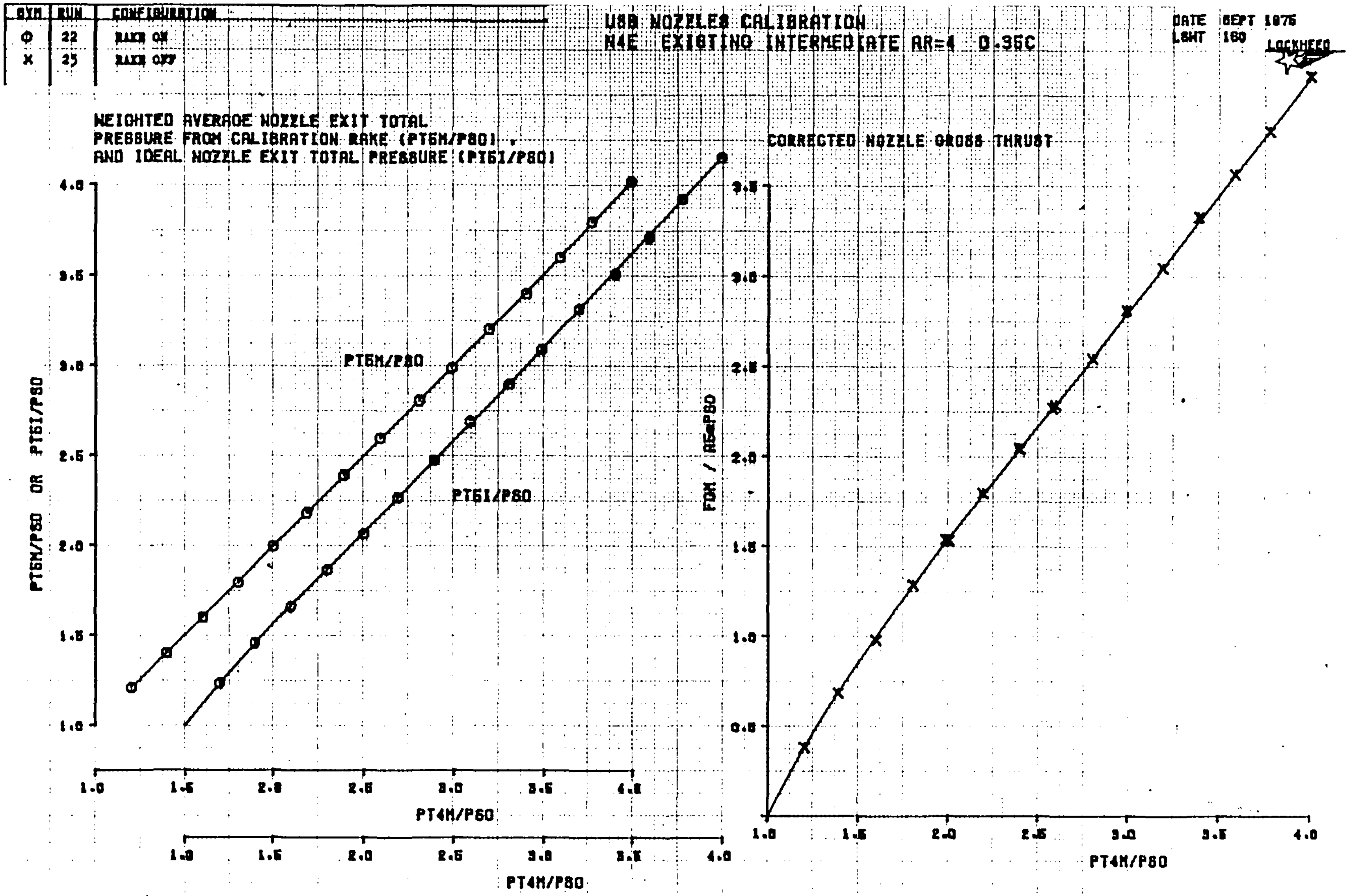

Figure 150. Nozzle exit pressure ratio and thrust parameter versus internal reference pressure ratio, N_{4_E}.

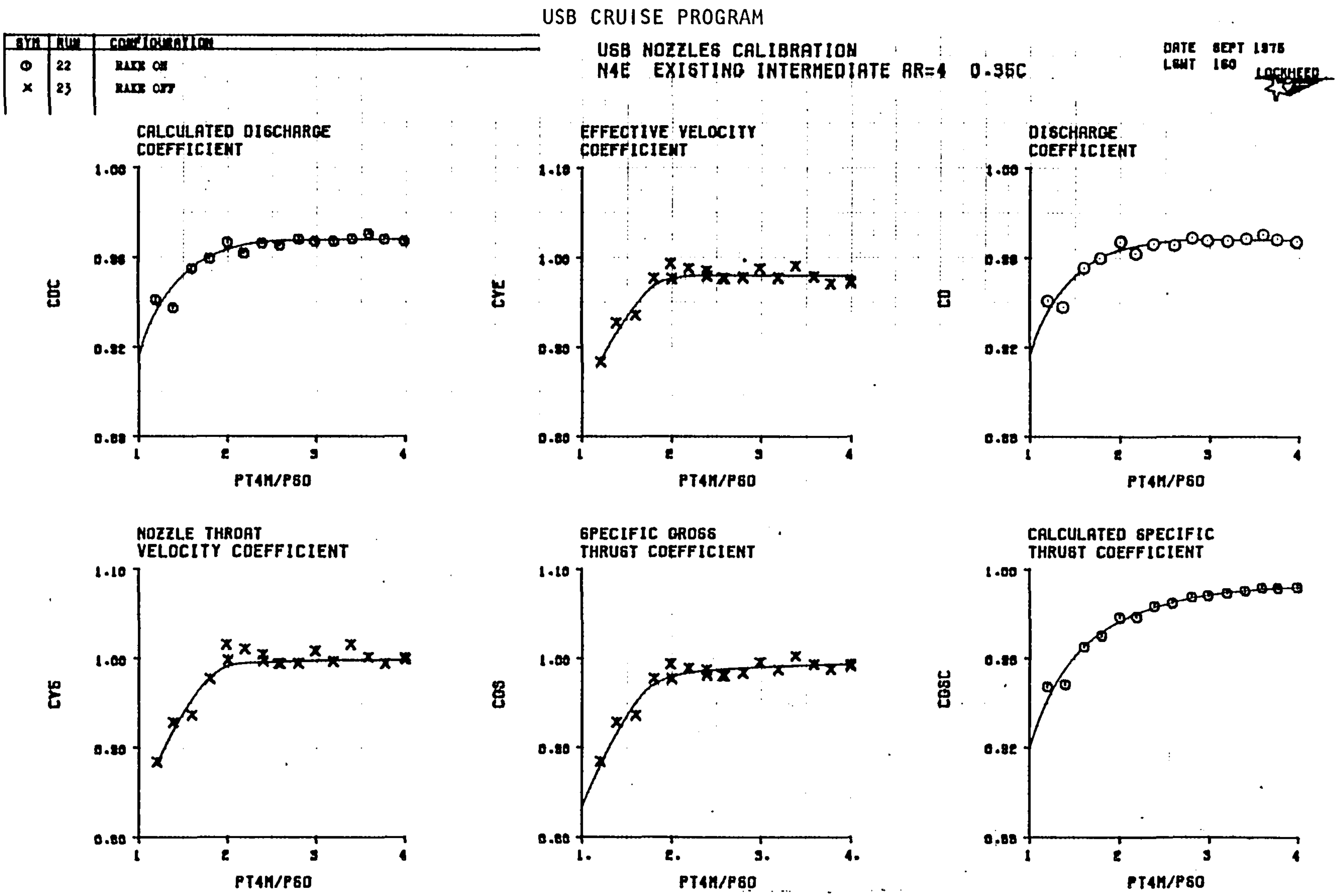

Figure 151. Isolated nozzle performance coefficients from static test rig, N_{4E}.

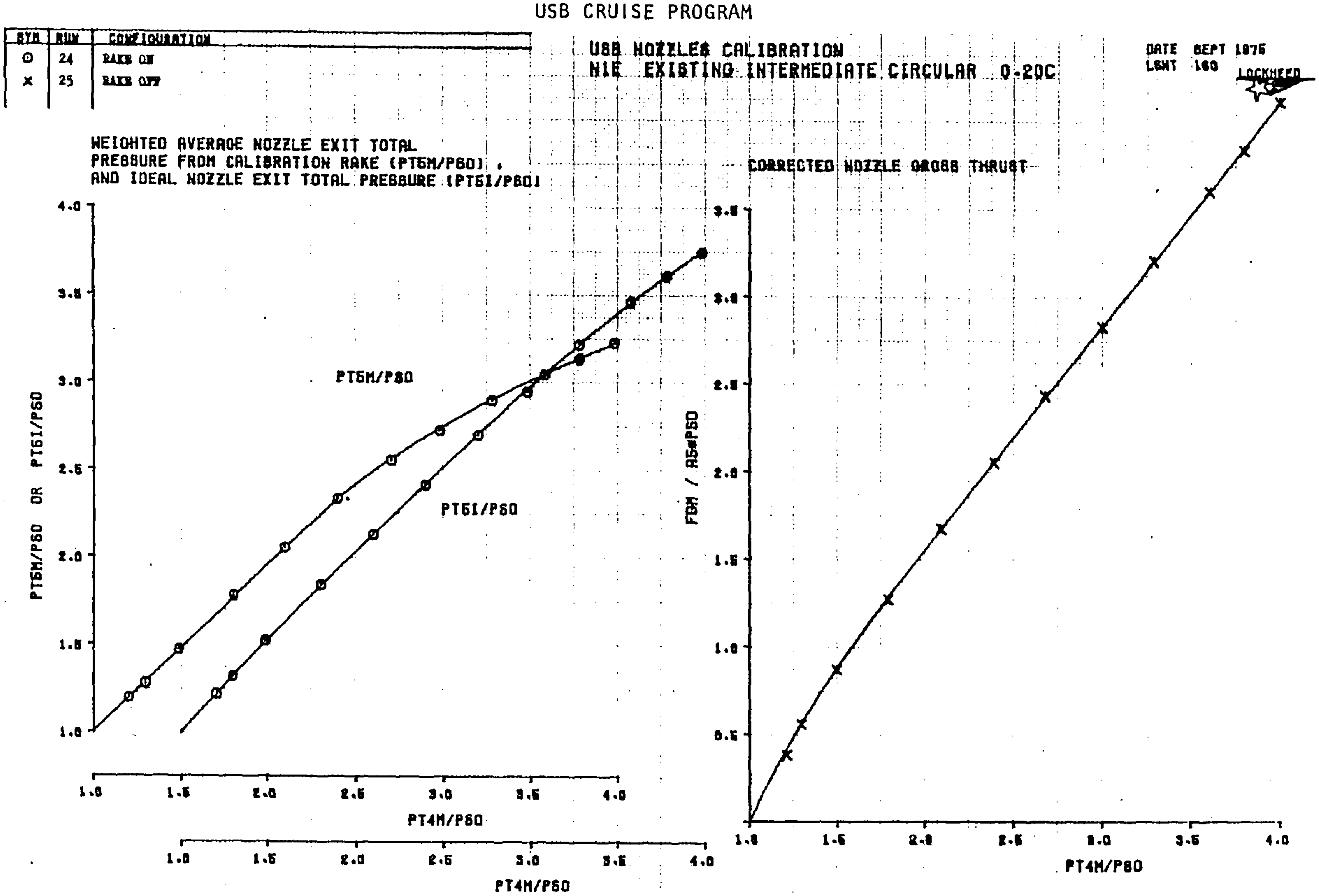

Figure 152. Nozzle exit pressure ratio and thrust parameter versus internal reference pressure ratio, N_{1E}.

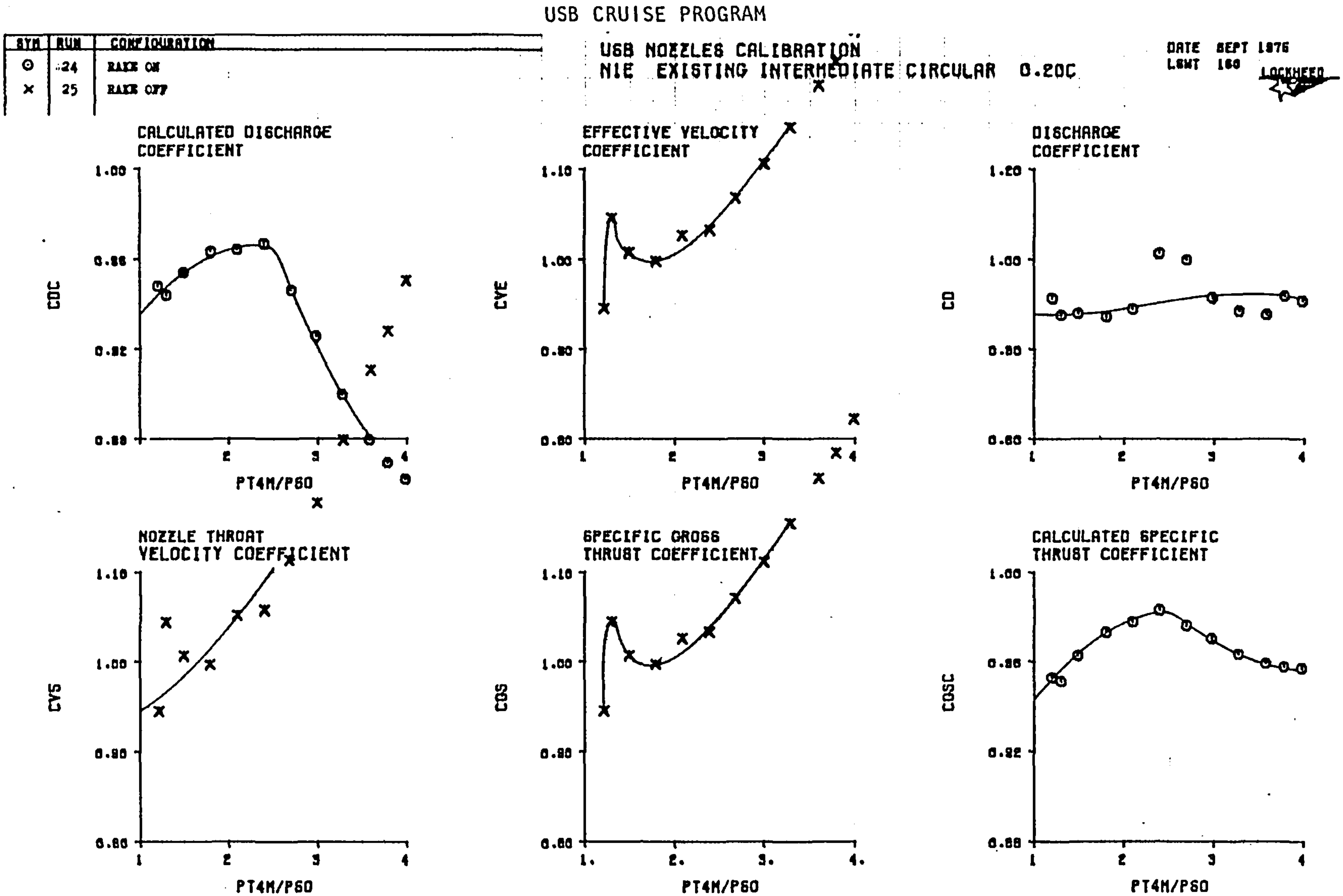

Figure 153. Isolated nozzle performance coefficients from static test rig, N_{1E}.

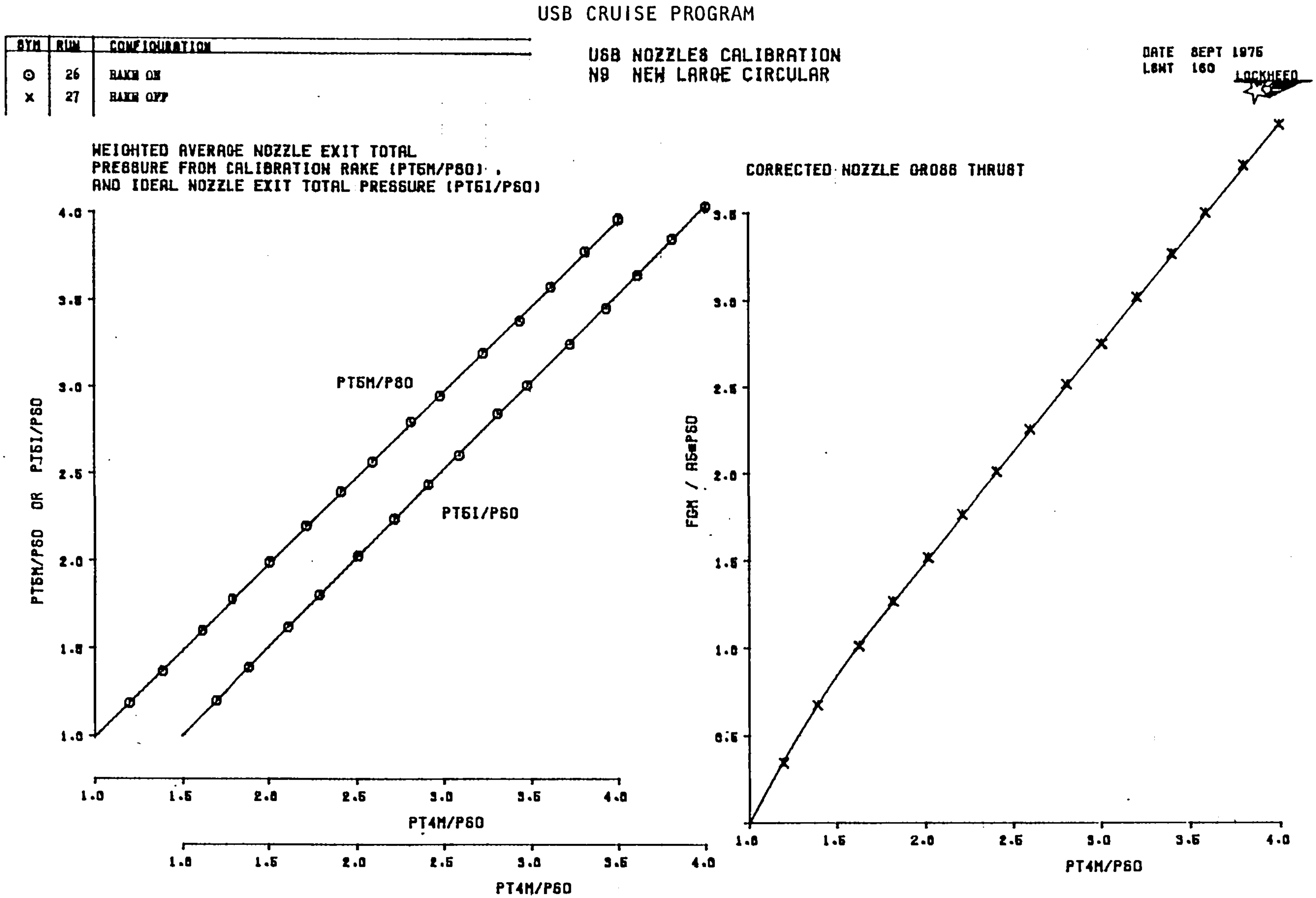

Figure 154. Nozzle exit pressure ratio and thrust parameter versus internal reference pressure ratio, N_9.

USB CRUISE PROGRAM

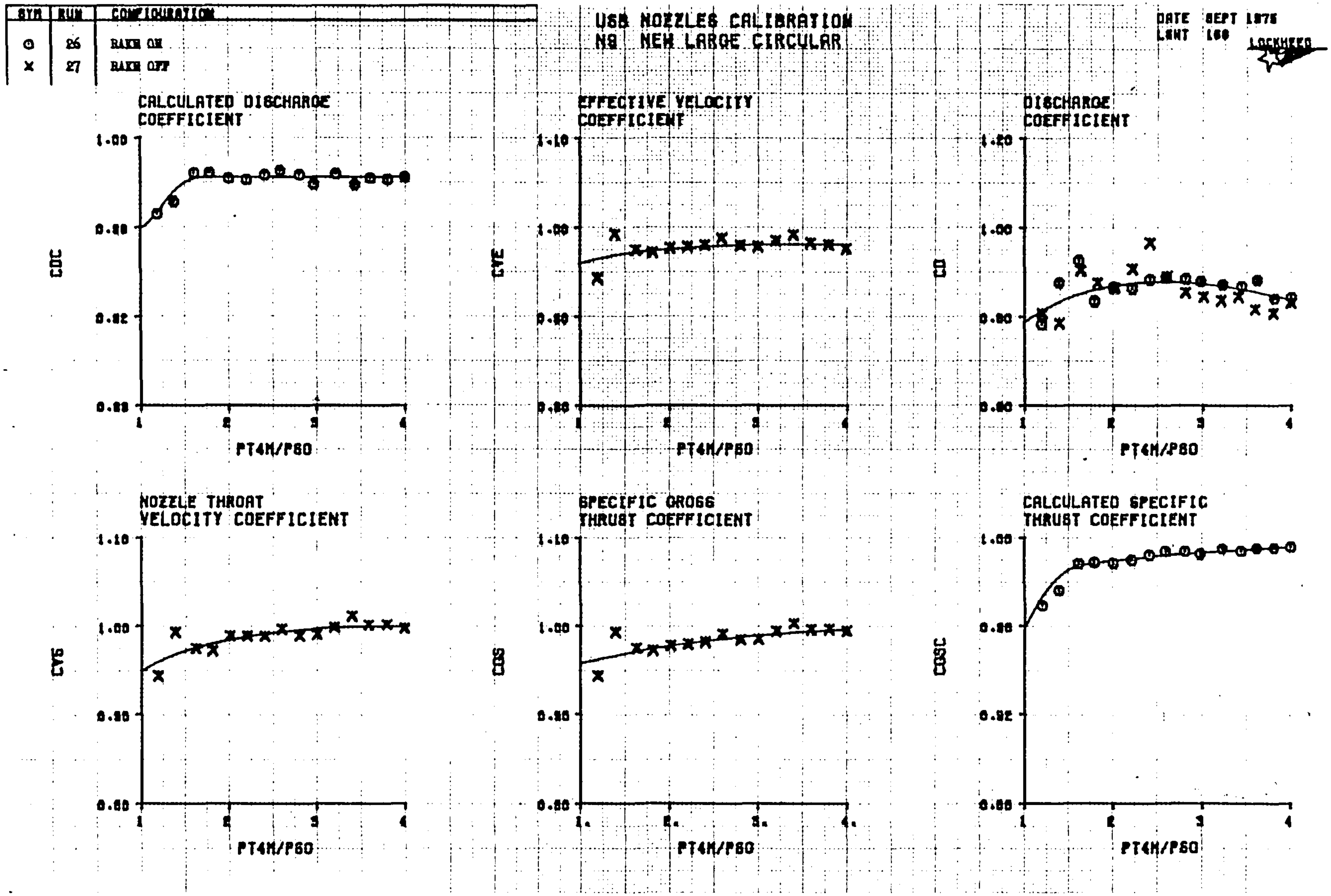

Figure 155. Isolated nozzle performance coefficients from static test rig, N_9.

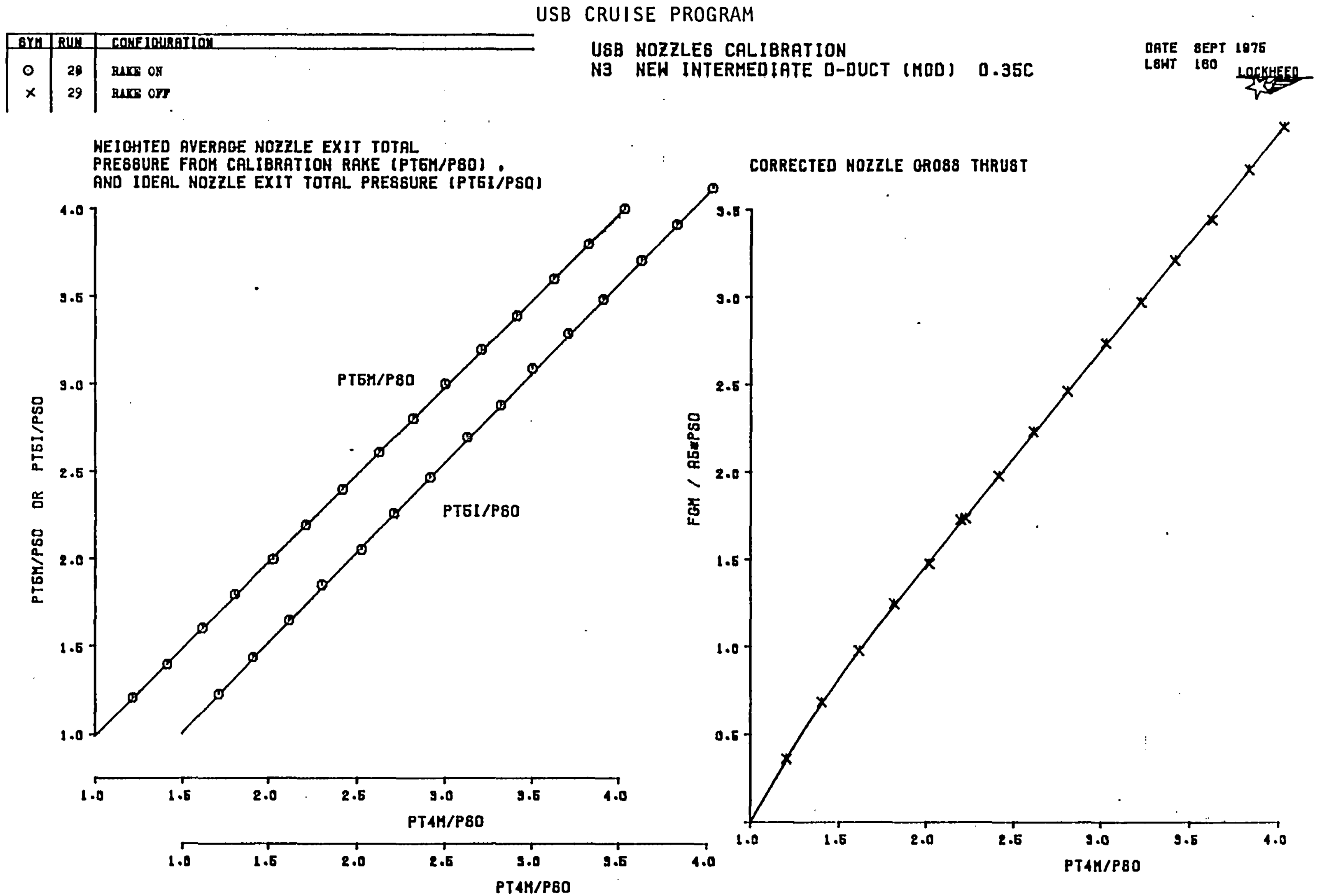

Figure 156. Nozzle exit pressure ratio and thrust parameter versus internal reference pressure ratio, N_3.

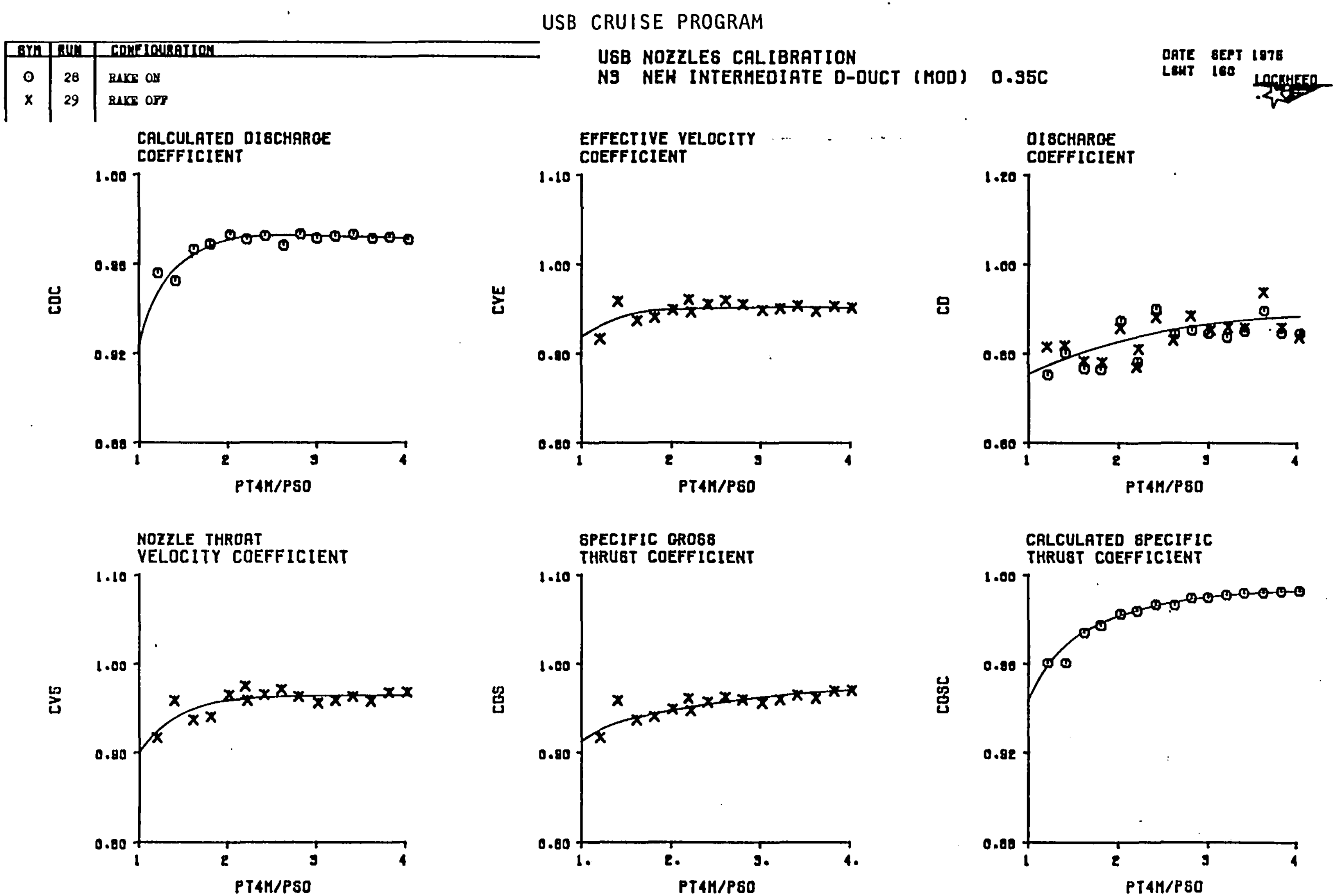

Figure 157. Isolated nozzle performance coefficients from static test rig, N_3.

USB CRUISE PROGRAM

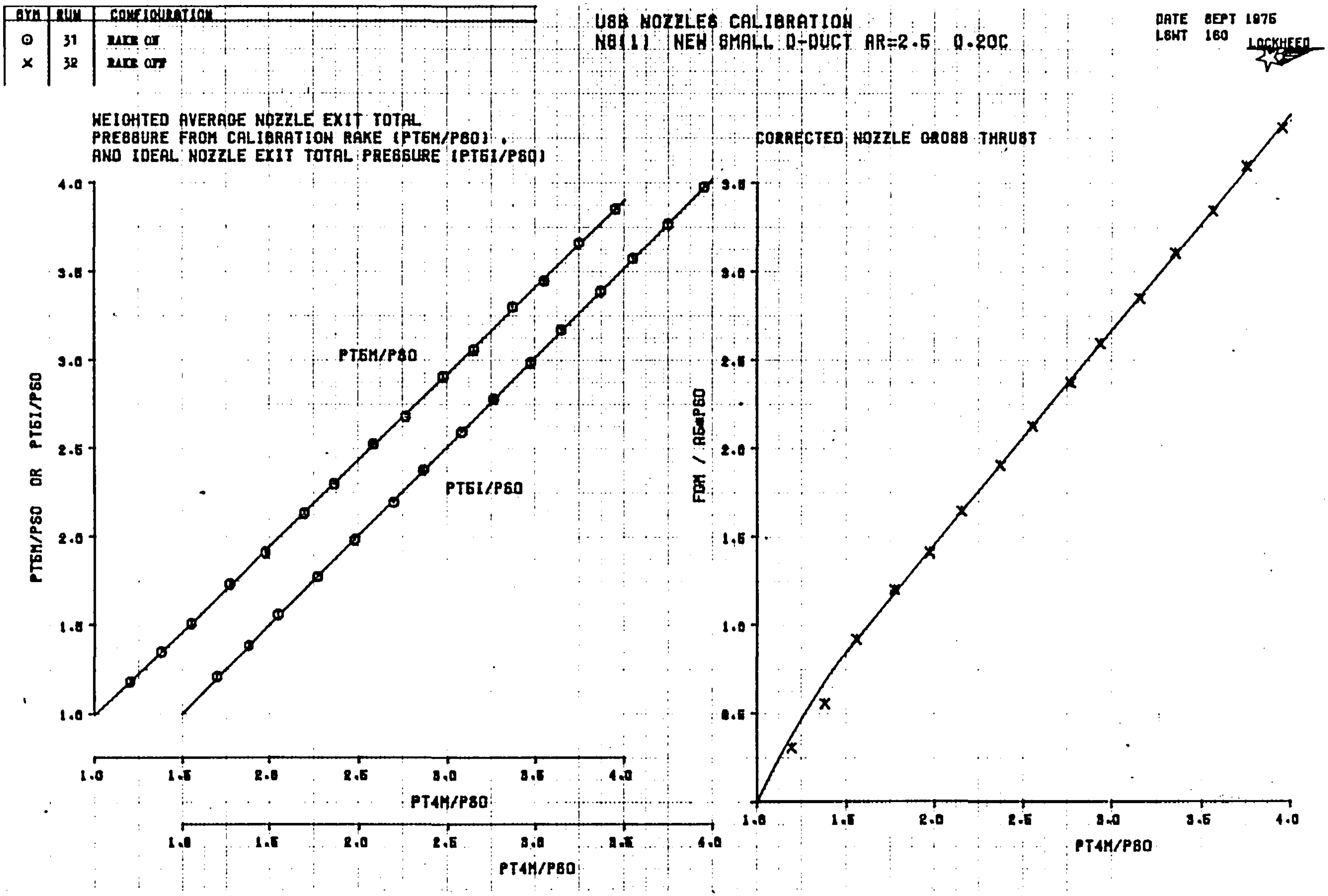

Figure 158. Nozzle exit pressure ratio and thrust parameter versus internal reference pressure ratio, N_8^1.

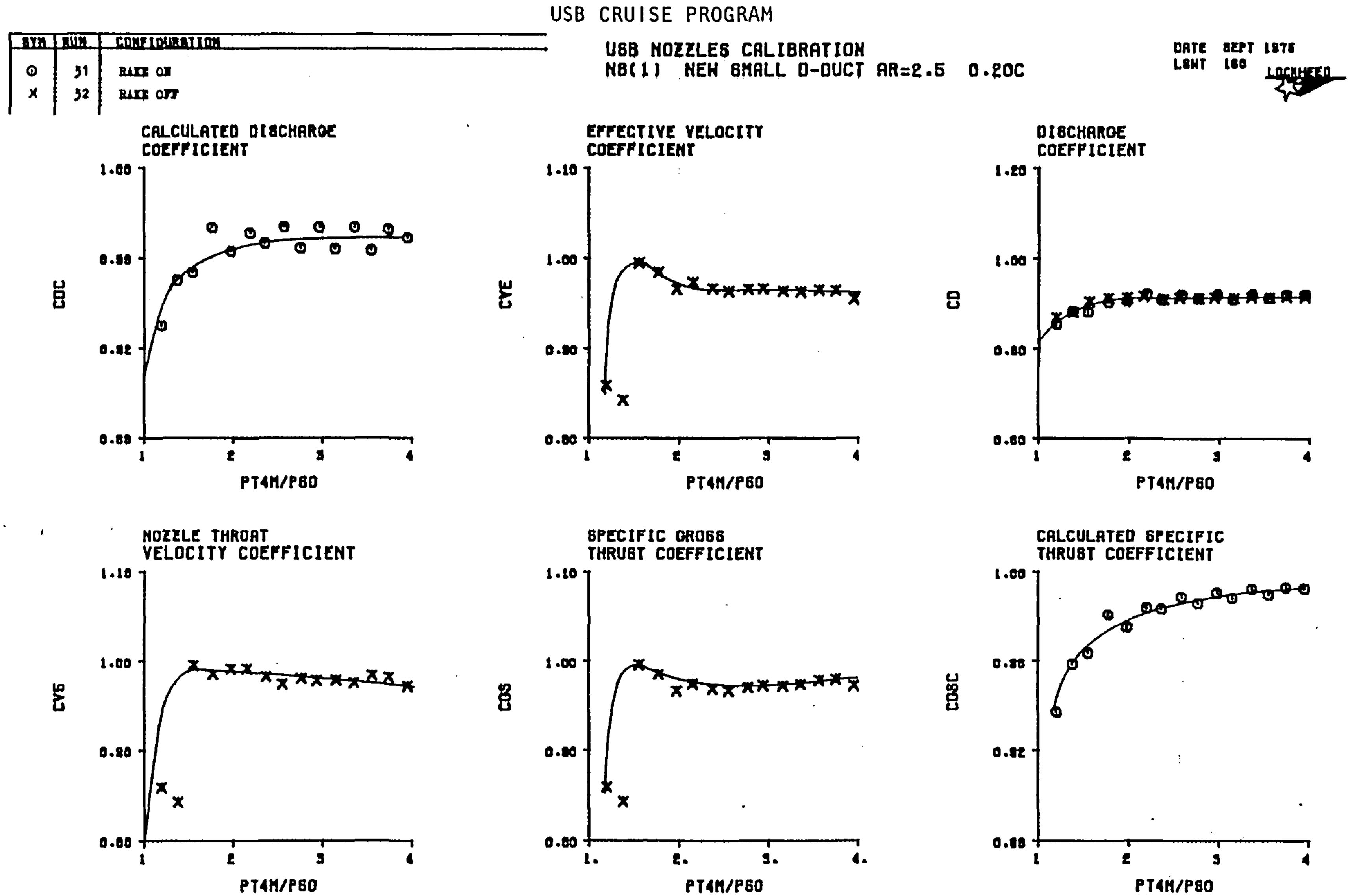

Figure 159. Isolated nozzle performance coefficients from static test rig, N_8^1.

USB CRUISE PROGRAM

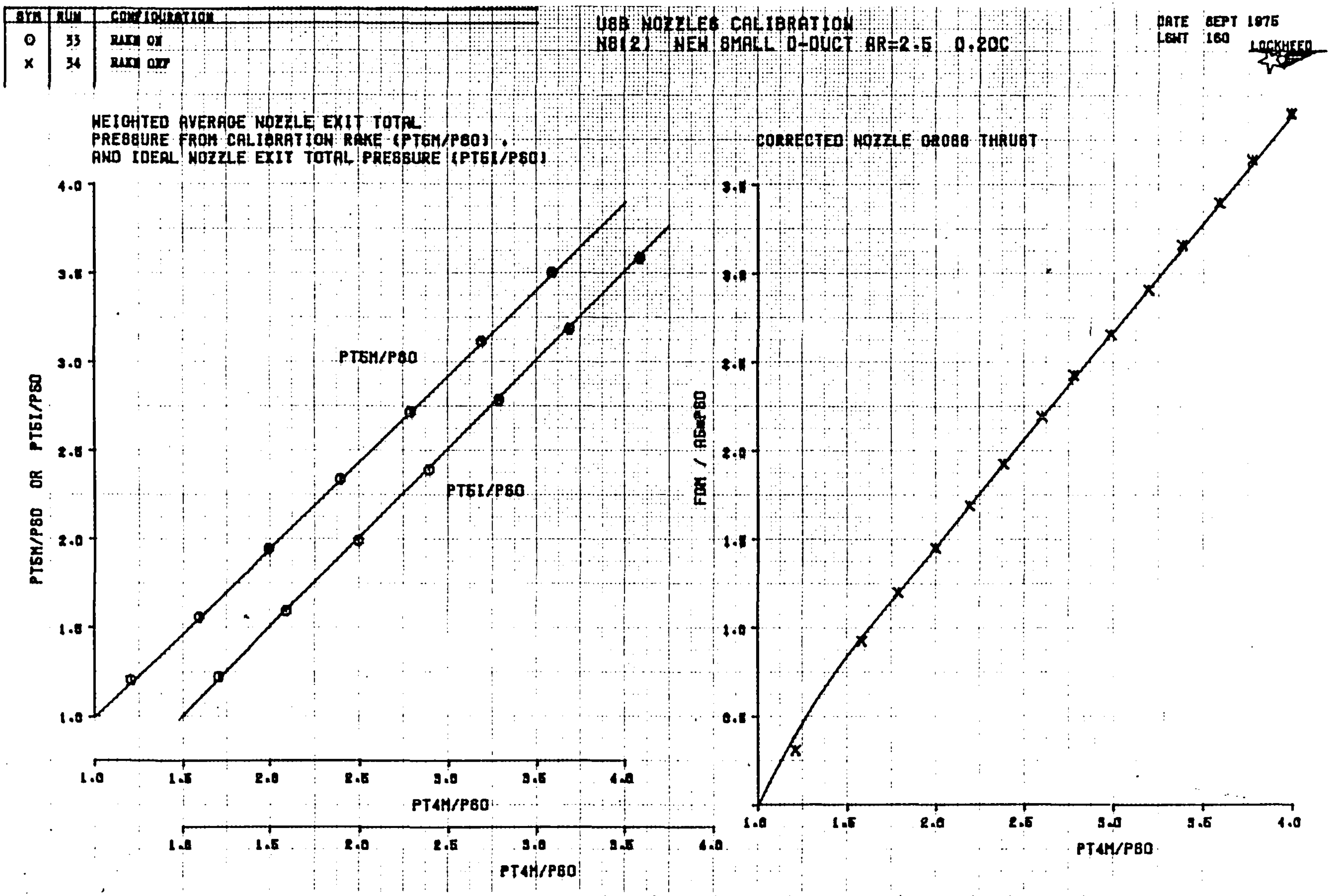

Figure 160. Nozzle exit pressure ratio and thrust parameter versus internal reference pressure ratio, $N_8{}^2$.

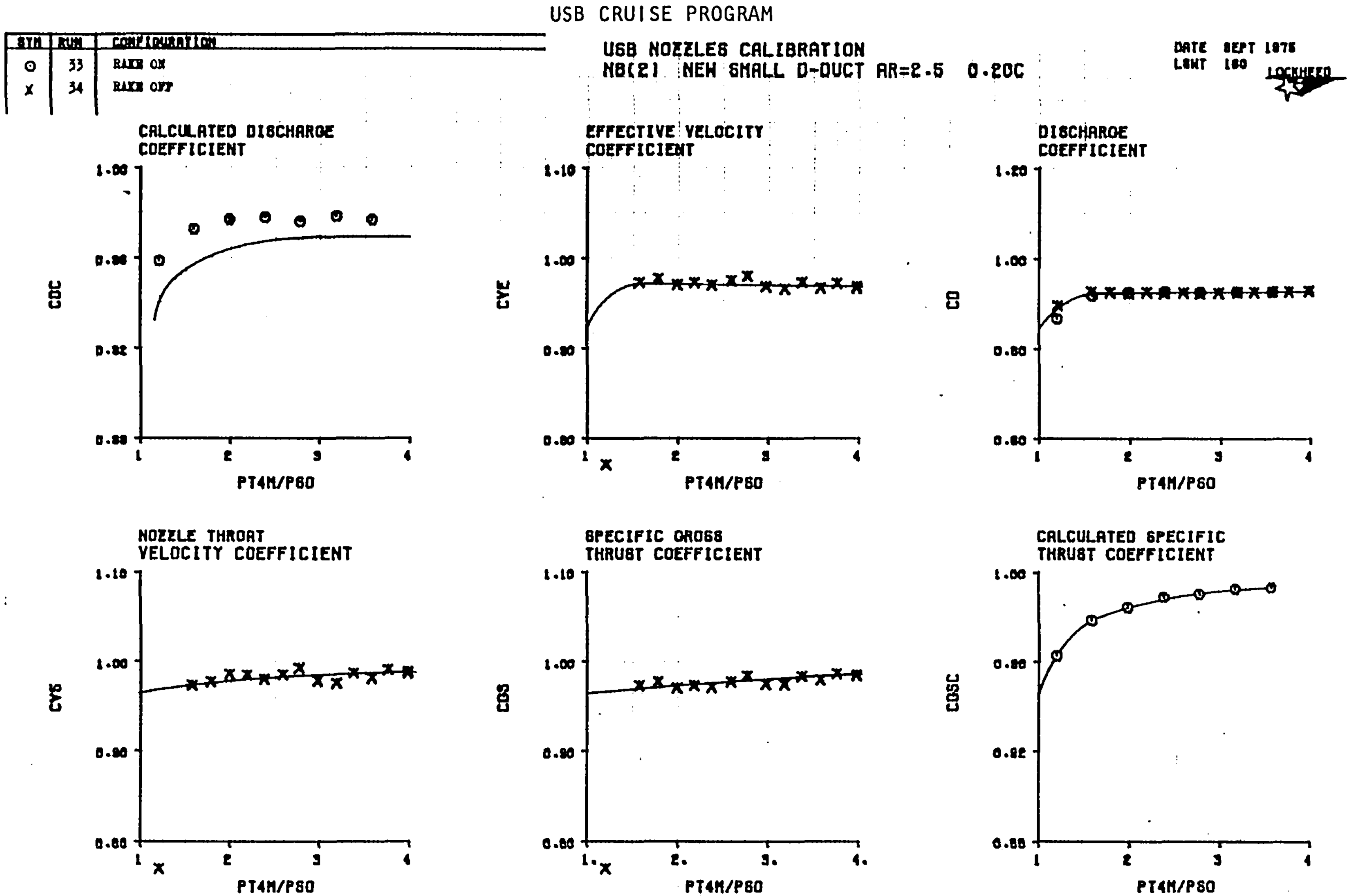

Figure 161. Isolated nozzle performance coefficients from static test rig, N_8^2.

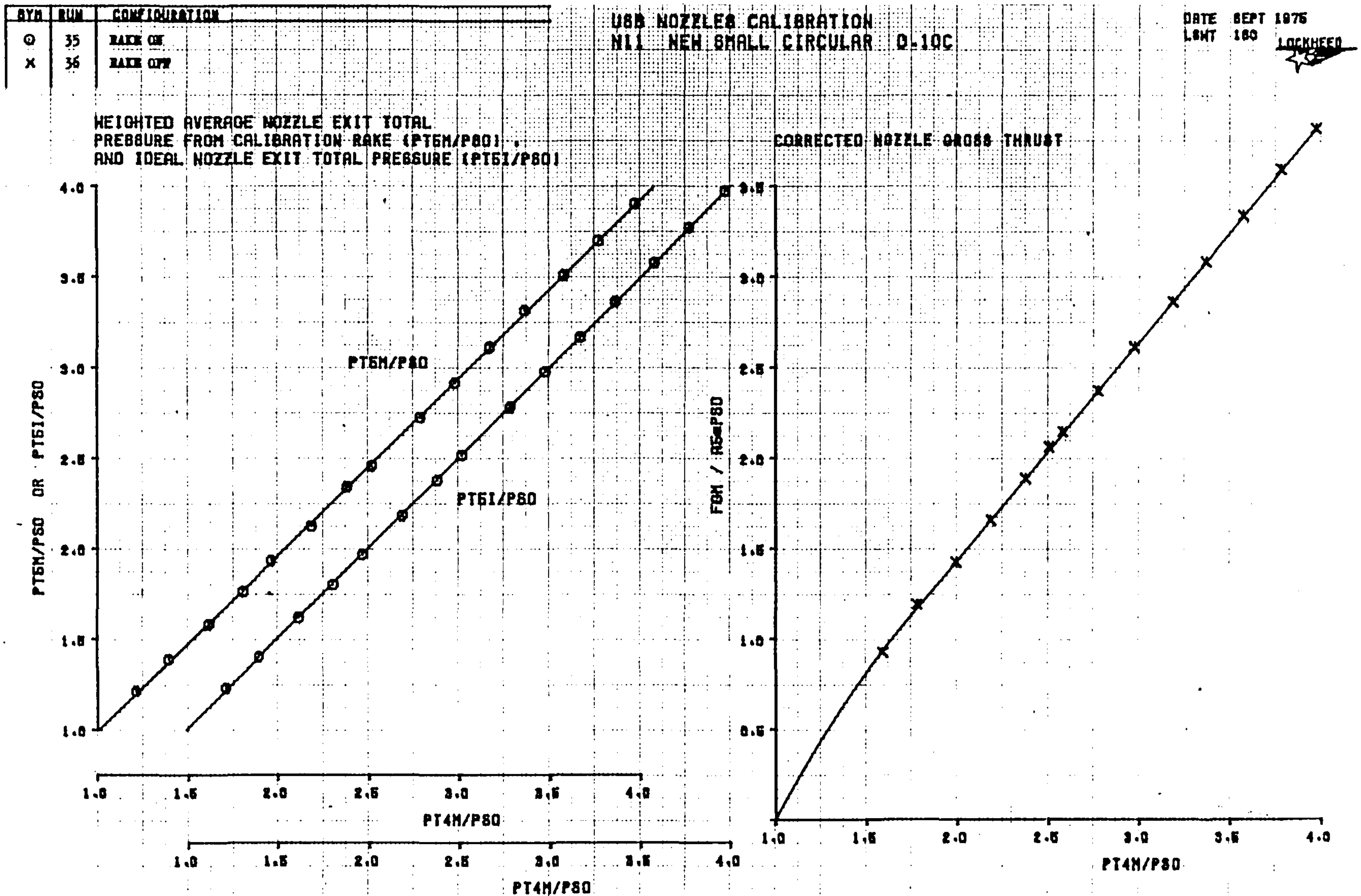

Figure 162. Nozzle exit pressure ratio and thrust parameter versus internal reference pressure ratio, N_{11}.

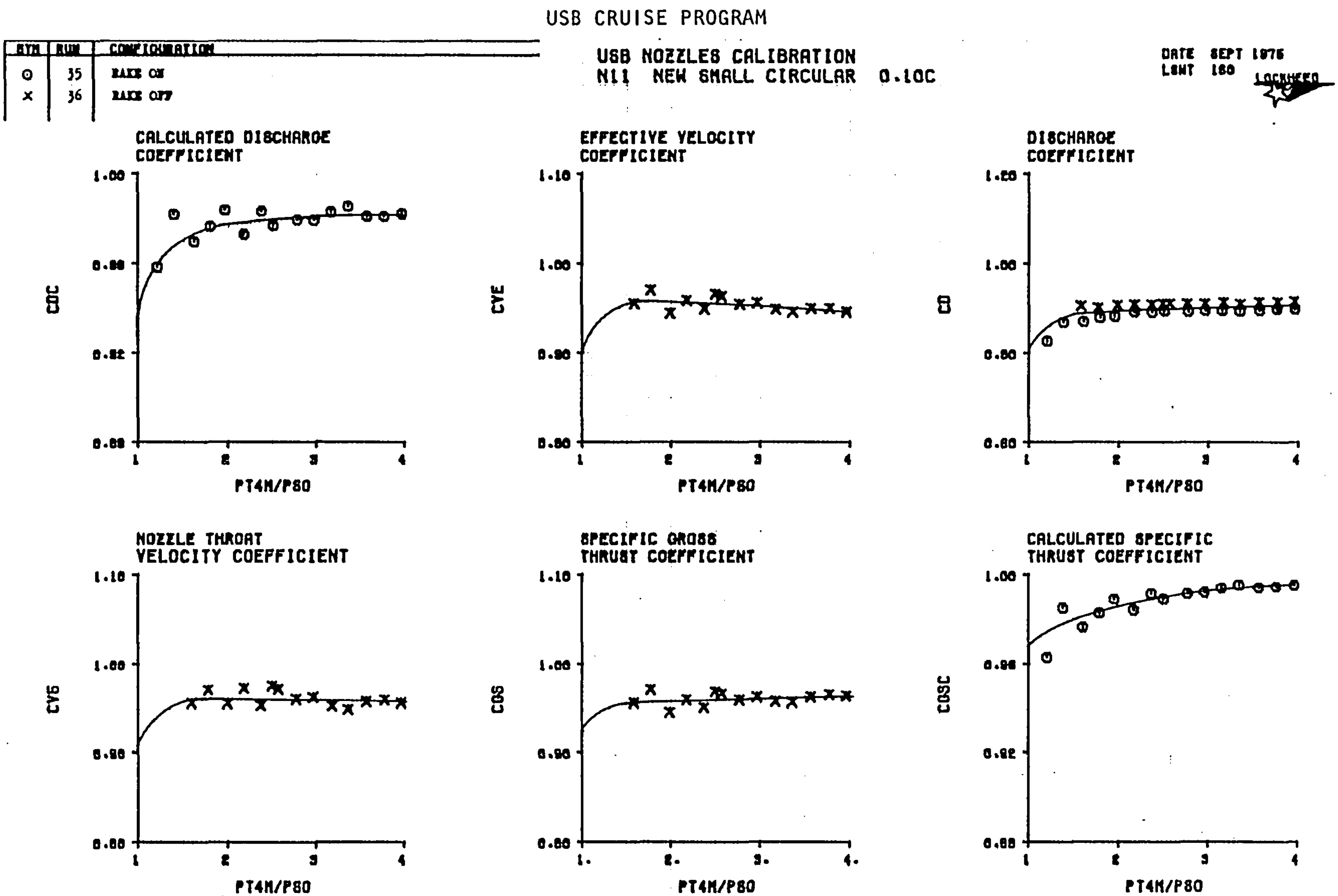

Figure 163. Isolated nozzle performance coefficients from static test rig, N_{11}.

USB CRUISE PROGRAM

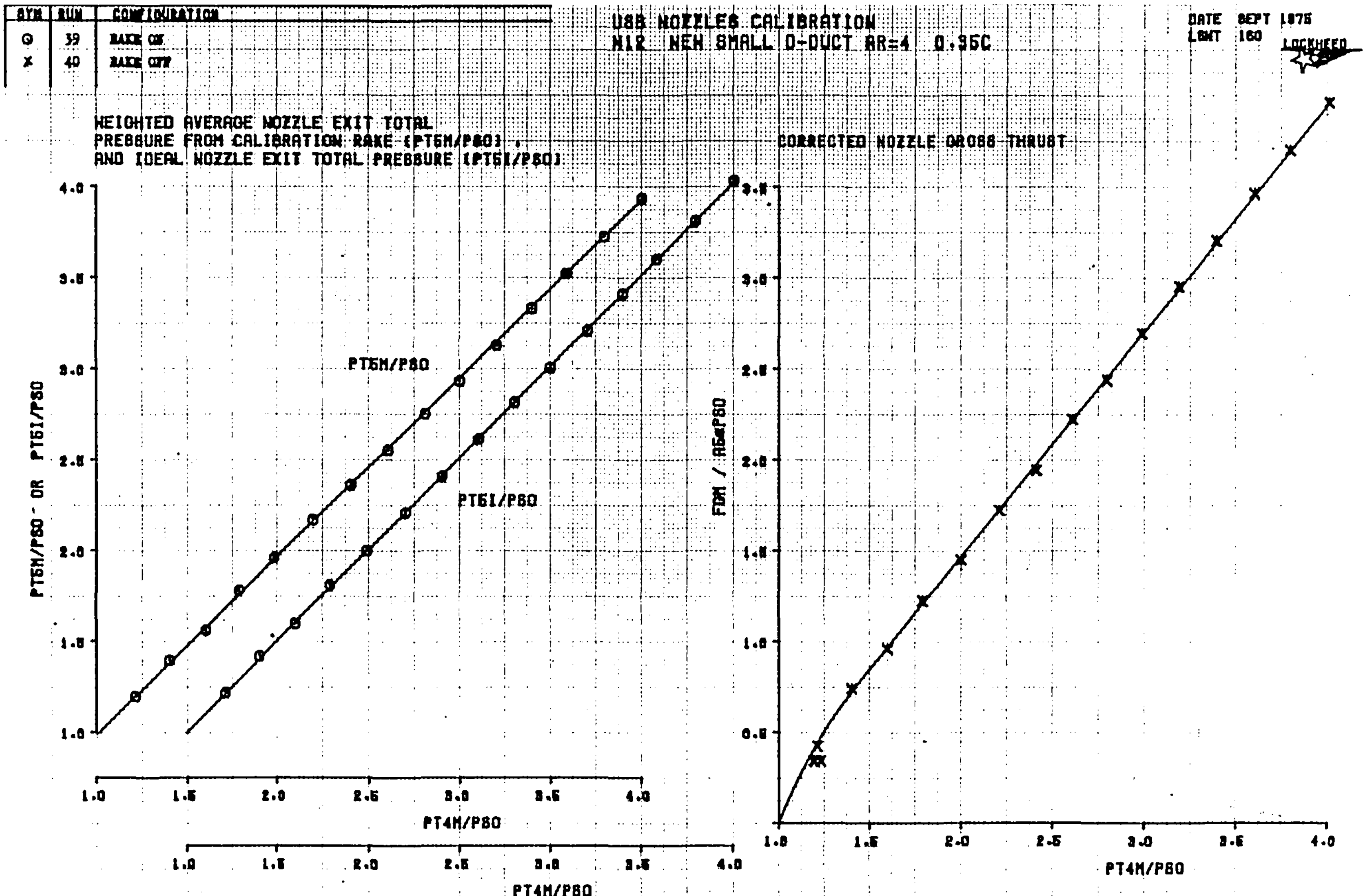

Figure 164. Nozzle exit pressure ratio and thrust parameter versus internal reference pressure ratio, N_{12}.

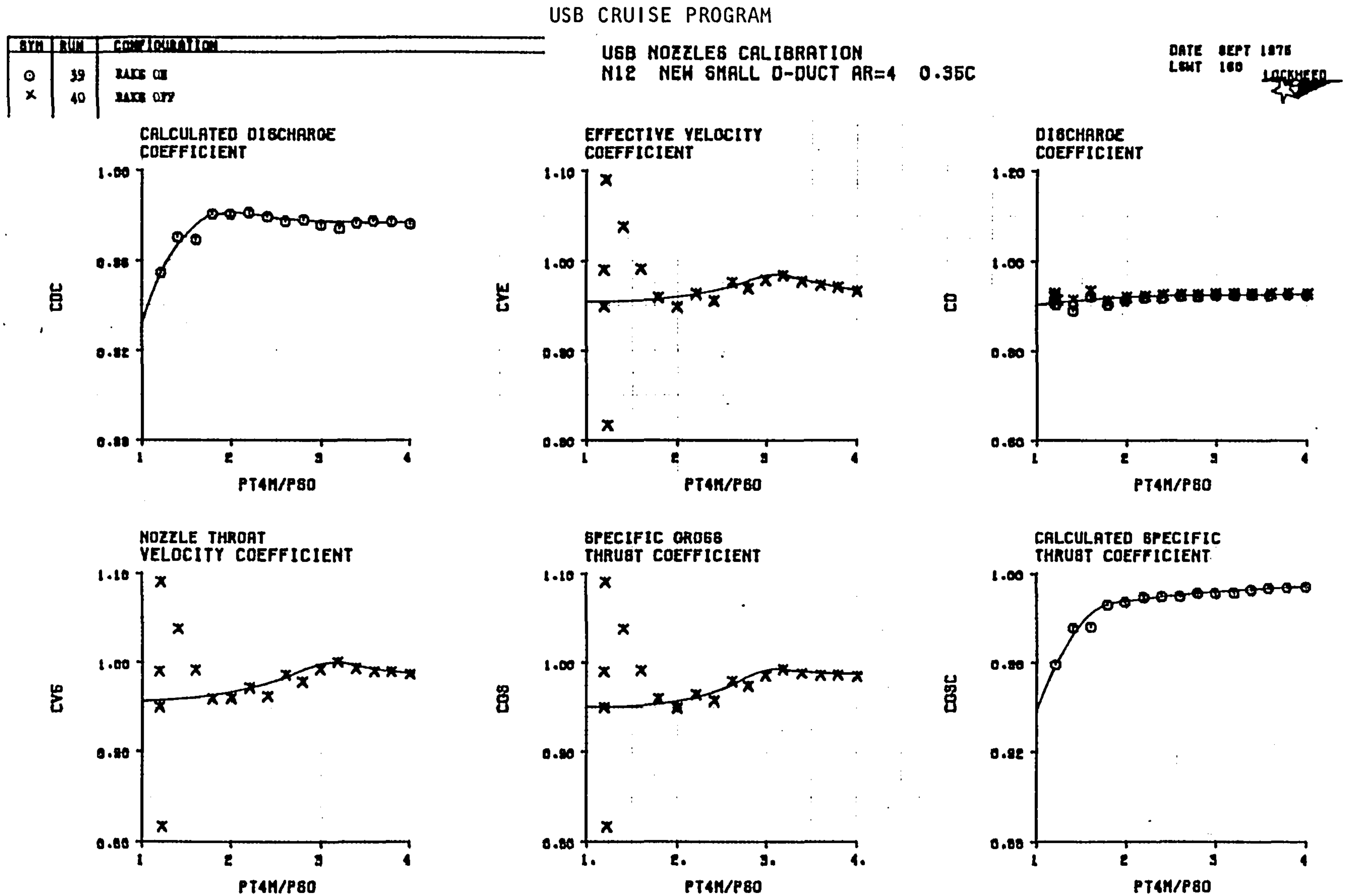

Figure 165. Isolated nozzle performance coefficients from static test rig, N_{12}.

7.2 Summary of Nozzle Performance Coefficients, Isolated and Installed

A tabulated summary of the essential performance coefficients for all the test nozzles is presented in Figure 166, sheets 1 through 5. In addition to the thrust parameter, discharge coefficient and nozzle pressure ratio, the parameters which relate isolated to installed nozzle performance are included. These are turning efficiency, η_t (ETAT), turning angle, δ_j (DJ) and static moment, M_{Y_S} (MYFS). Also included are nozzle areas.

The isolated nozzle coefficients are taken directly from the plots presented earlier. Turning efficiency, turning angle and static moment are data measured in a subsequent static test of the complete wing-nacelle configurations. Both sets of data are provided exactly as utilized in the basic data reduction program.

USB CRUISE PROGRAM

NOZ.	PARAM. / H4M/PO	H5I/PO	FGM/(A5*PO)	CD	H5M/PO	ETAT	DJ	MYFS	A 5 cm²	A 5 in²
N1E	1.0	1.0	0	.963	1.0	1.0	0	0	12.813	1.986
	1.3	1.33	.574	.966	1.31	1.0	-1.3	- .48		
	1.6	1.65	1.018	.968	1.60	.996	-1.1	- .81		
	2.0	2.07	1.556	.970	2.01	.980	-1.0	-1.14		
	2.6	2.70	2.325	.971	2.62	.989	- .9	-1.40		
	3.2	3.31	3.085	.972	3.24	.990	-1.5	-1.48		
	4.0	4.17	4.125	.972	4.04	.990	-1.5	-1.50		
N2E	1.0	1.0	0	.963	1.0	1.0	0	0	12.813	1.986
	1.3	1.33	.530	.966	1.31	1.0	-1.2	- .48		
	1.6	1.65	.980	.968	1.60	.992	-1.2	- .81		
	2.0	2.07	1.520	.970	2.01	.984	-1.0	-1.14		
	2.6	2.70	2.284	.971	2.62	.989	-1.0	-1.40		
	3.2	3.31	3.059	.972	3.24	.989	-1.0	-1.48		
	4.0	4.17	4.081	.972	4.04	.989	-1.0	-1.50		
N3E	1.0	1.0	0	.940	1.0	1.0	0	0	13.464	2.087
	1.3	1.34	.550	.966	1.32	1.0	-5.8	- .50		
	1.6	1.65	.980	.976	1.62	.993	-4.5	- .93		
	2.0	2.07	1.500	.980	2.03	.988	-3.2	-1.30		
	2.6	2.68	2.250	.979	2.63	.978	-3.0	-1.40		
	3.2	3.30	3.000	.980	3.23	.975	-4.0	-1.50		
	4.0	4.13	4.010	.970	4.00	.975	-4.0	-1.63		
N4E	1.0	1.0	0	.916	1.0	1.0	0	0	13.464	2.087
	1.3	1.35	0.550	.943	1.30	.957	-13.0	- .78		
	1.6	1.67	1.000	.956	1.60	.964		-1.22		
	2.0	2.07	1.530	.963	2.00	.975		-1.60		
	2.6	2.68	2.300	.967	2.60	.969		-1.70		
	3.2	3.32	3.070	.968	3.20	.975		-1.70		
	4.0	4.17	4.100	.968	4.03	.975		-1.70		

Figure 166. Summary of nozzle performance coefficients, isolated and installed. (Sheet 1)

USB CRUISE PROGRAM

NOZ.	PARAM. / H4M/PO	H5I/PO	FGM/A5*PO	CD	H5M/PO	ETAT	DJ	MYFS	A 5 cm^2	A 5 in^2
N2	1.0	1.0	0	.957	1.0	1.0	0	0	13.464	2.087
	1.3	1.34	.524	.960	1.31		-1.3	- .50		
	1.6	1.65	.975	.964	1.60		-1.0	- .82		
	2.0	2.06	1.492	.969	1.99		0	-1.17		
	2.6	2.66	2.252	.968	2.59		- .6	-1.40		
	3.2	3.29	3.013	.965	3.19		-1.3	-1.42		
	4.0	4.11	4.007	.963	3.96		-1.3	-1.43		
N3A	1.0	1.0	0	.941	1.0	1.0	0	0	8.894	1.379
	1.3	1.32	.500	.953	1.29	.939	-15.8	- .47		
	1.6	1.63	.920	.962	1.58	.949		- .81		
	2.0	2.04	1.410	.967	1.98	.965		-1.18		
	2.6	2.66	2.120	.969	2.57	.956		-1.42		
	3.2	3.28	2.830	.968	3.16	.965		-1.58		
	4.0	4.10	3.790	.968	3.95	.965		-1.64		
N3B	1.0	1.0	0	.920	1.0	1.0	0	0	12.935	2.005
	1.3	1.32	.526	.954	1.29	1.0	-4.5	- .54		
	1.6	1.63	.950	.964	1.59	1.0	-5.2	- .87		
	2.0	2.04	1.470	.971	1.98	1.0	-5.0	-1.19		
	2.6	2.66	2.220	.973	2.56	.994	-6.0	-1.39		
	3.2	3.27	2.960	.973	3.16	.990	-6.1	-1.40		
	4.0	4.09	3.940	.972	3.95	.990	-6.2	-1.40		
N4	1.0	1.0	0	.961	1.0	1.0	0	0	13.464	2.087
	1.3	1.32	.520	.962	1.29	.925	-8.5	- .70		
	1.6	1.63	.950	.963	1.58	.933	-8.6	-1.12		
	2.0	2.02	1.470	.969	1.96	.966	-9.2	-1.37		
	2.6	2.63	2.205	.966	2.54	.968	-9.8	-1.40		
	3.2	3.23	2.950	.955	3.09	.970	-10.0	-1.44		
	4.0	4.04	3.940	.939	3.80	.970	-10.0	-1.49		

Figure 166. Summary of nozzle performance coefficients, isolated and installed. (Sheet 2)

USB CRUISE PROGRAM

NOZ.	PARAM. / H4M/PO	H5I/PO	FGM/A5*PO	CD	H5M/PO	ETAT	DJ	MYFS		A 5 cm^2	A 5 in^2
N5	1.0	1.0	0	.906	1.0	1.0	0	0		13.464	2.087
	1.3	1.33	.525	.954	1.29	.973	-11.4	- .60			
	1.6	1.63	.950	.959	1.58	.971	-12.0	-1.00			
	2.0	2.03	1.462	.963	1.96	.993	-12.0	-1.35			
	2.6	2.63	2.220	.963	2.53	.977	-12.5	-1.50			
	3.2	3.23	2.975	.950	3.08	.985	-11.0	-1.50			
	4.0	4.04	3.975	.932	3.77	.985	-11.0	-1.50			
N6	1.0	1.0	0	.845	1.0	1.0	0	0		6.732	1.043
	1.3	1.30	.512	.881	1.28	.946	-1.8	- .25			
	1.6	1.60	.908	.891	1.56	.946	-2.0	- .36			
	2.0	2.00	1.356	.898	1.95	.972	-2.0	- .41			
	2.6	2.60	2.030	.901	2.53	.982	-2.8	- .54			
	3.2	3.22	2.710	.902	3.12	.978	-3.3	- .62			
	4.0	4.03	3.613	.902	3.90	.978	-3.3	- .70			
								N81 ONLY	N82 ONLY		
N81	1.0	1.0	0	.907	1.0	1.0	0	0	0	6.732	1.043
OR	1.3	1.30	.550	.946	1.28	.946	-1.8	-.25	-.08		
N82	1.6	1.60	.975	.957	1.56	.946	-2.0	-.36	-.16		
	2.0	2.00	1.456	.964	1.95	.972	-2.0	-.41	-.23		
	2.6	2.60	2.180	.968	2.53	.982	-2.8	-.54	-.30		
	3.2	3.22	2.910	.969	3.12	.978	-3.3	-.62	-.37		
	4.0	4.03	3.880	.969	3.90	.978	-3.3	-.70	-.46		
*N81	1.0	1.0	0	.907	1.0	1.0	0	0		6.732	1.043
AND	1.3	1.30	.550	.946	1.28	.941	-1.3	- .70			
N82	1.6	1.60	.975	.957	1.56	.941	-1.5	-1.19			
	2.0	2.00	1.456	.964	1.95	.967	-1.5	-1.57			
	2.6	2.60	2.180	.968	2.53	.977	-2.1	-1.80			
	3.2	3.22	2.910	.969	3.12	.973	-2.4	-1.84			
	4.0	4.03	3.880	.969	3.90	.973	-2.4	-1.85			

* *Dual Eng. Installation*

Figure 166. Summary of nozzle performance coefficients, isolated and installed. (Sheet 3)

USB CRUISE PROGRAM

NOZ.	PARAM. H4M/PO	H5I/PO	FGM/A5*PO	CD	H5M/PO	ETAT	DJ	MYFS	A 5	
									cm^2	in^2
N11	1.0	1.0	0	.918	1.0	1.0	0	0	6.732	1.043
	1.3	1.31	.522	.964	1.28		+1.6	- .25		
	1.6	1.61	.950	.973	1.57		+2.3	- .40		
	2.0	2.01	1.430	.978	1.96		+2.8	- .49		
	2.6	2.60	2.160	.980	2.55		+2.5	- .66		
	3.2	3.20	2.875	.982	3.13		+2.0	- .82		
	4.0	4.00	3.850	.982	3.92		+2.0	- .99		
N12	1.0	1.0	0	.932	1.0	1.0	0	0	6.732	1.043
	1.3	1.30	.580	.961	1.27	1.0	- .2	- .28		
	1.6	1.60	.975	.976	1.58	.966	- .5	- .44		
	2.0	2.01	1.470	.981	1.97	.968	-2.5	- .56		
	2.6	2.62	2.220	.978	2.55	.972	-4.7	- .66		
	3.2	3.22	2.950	.977	3.15	.964	-4.8	- .76		
	4.0	4.02	3.950	.977	3.93	.964	-4.8	- .88		
N13	1.0	1.0	0	.879	1.0	1.0	0	0	6.732	1.043
	1.3	1.30	.560	.954	1.26	.963	-5.5	- .35		
	1.6	1.60	.950	.972	1.57	1.0	-7.0	- .56		
	2.0	2.01	1.430	.975	1.96	.962	-7.5	- .71		
	2.6	2.62	2.180	.975	2.54	.963	-7.3	- .83		
	3.2	3.22	2.920	.972	3.13	.966	-7.0	- .96		
	4.0	4.02	3.920	.970	3.90	.966	-7.0	-1.11		
N13A (F+5°)	1.0	1.0	0	.879	1.0	1.0	0	0	6.732	1.043
	1.3	1.30	.560	.954	1.26	.960	-7.1	- .50		
	1.6	1.60	.950	.972	1.57	1.0	-8.2	- .60		
	2.0	2.01	1.430	.975	1.96	.962	-9.0	- .70		
	2.6	2.62	2.180	.975	2.54	.945	-9.2	- .79		
	3.2	2.62	2.920	.975	2.54	.960	-8.2	- .80		
	4.0	4.02	3.920	.970	3.90	.960	-8.2	- .81		

Figure 166. Summary of nozzle performance coefficients, isolated and installed. (Sheet 4)

USB CRUISE PROGRAM

NOZ.	PARAM. H4M/PO	H5I/PO	FGM/A5*PO	CD	H5M/PO	ETAT	DJ	MYFS	A 5	
									cm^2	in^2
N13B (F-5°) UP	1.0	1.0	0	.879	1.0	1.0	0	0	6.732	1.043
	1.3	1.30	.560	.954	1.26	.968	-3.1	- .25		
	1.6	1.60	.950	.972	1.57	1.0	-3.2	- .39		
	2.0	2.01	1.430	.975	1.96	.980	-4.2	- .46		
	2.6	2.62	2.180	.975	2.54	.982	-4.5	- .58		
	3.2	3.22	2.920	.972	3.13	.974	-4.4	- .60		
	4.0	4.02	3.920	.970	3.90	.974	-4.4	- .62		

Figure 166. Summary of nozzle performance coefficients, isolated and installed. (Sheet 5)

7.3 Nozzle Thrust Coefficients For Wind-On Data Reduction

For many types of performance calculations it is more convenience to use thrust coefficient, C_T, rather than thrust parameter as presented in Figure 166. Accordingly, thrust coefficients were calculated and plotted for each of the more common test pressure ratios and Mach numbers. These are presented in Figures 167 through 178.

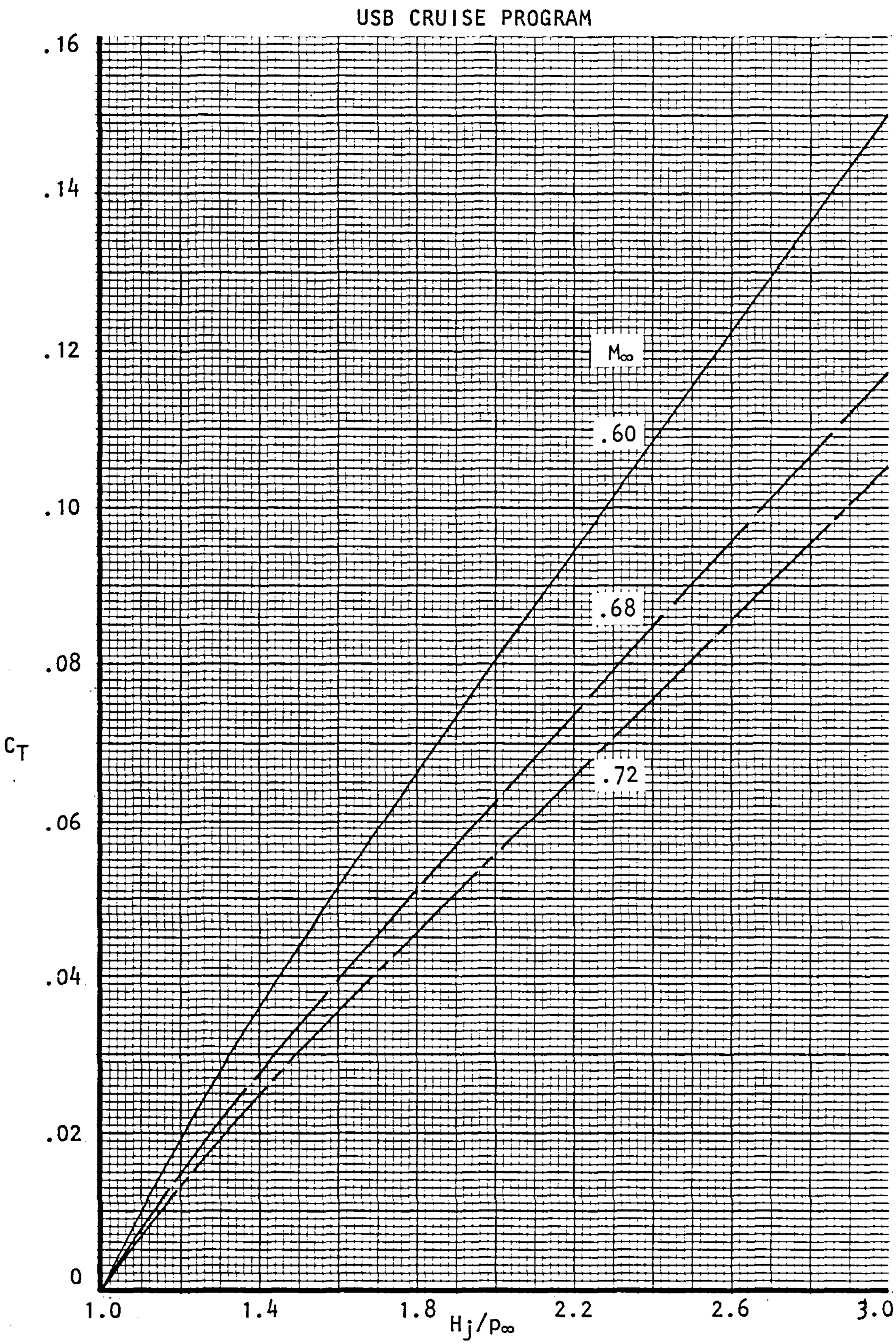

Figure 167 . Variation of nozzle gross thrust with Mach No., and pressure ratio, nozzle N_{2E}.

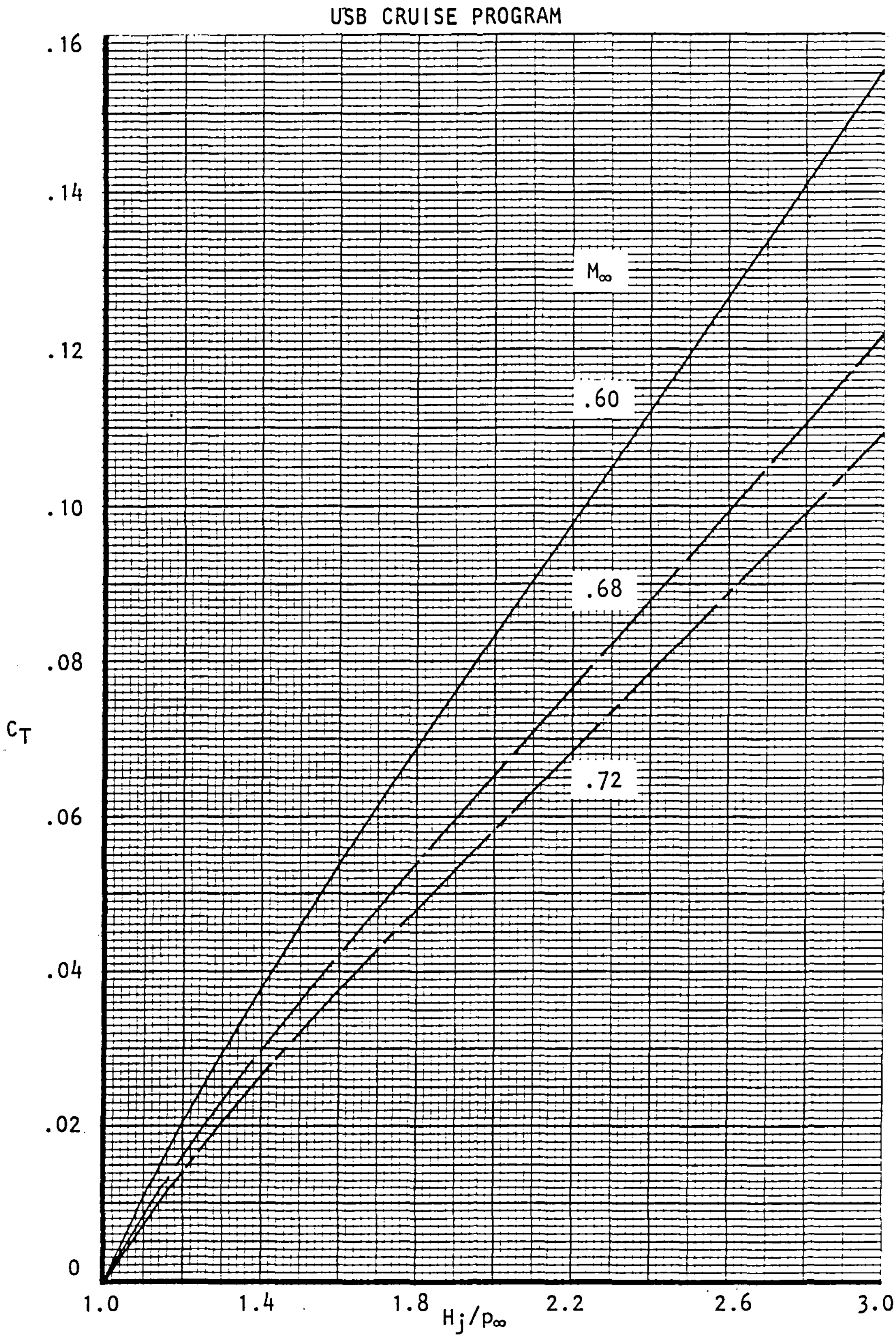

Figure 168 . Variation of nozzle gross thrust with Mach No. and pressure ratio, nozzle N_{3E}.

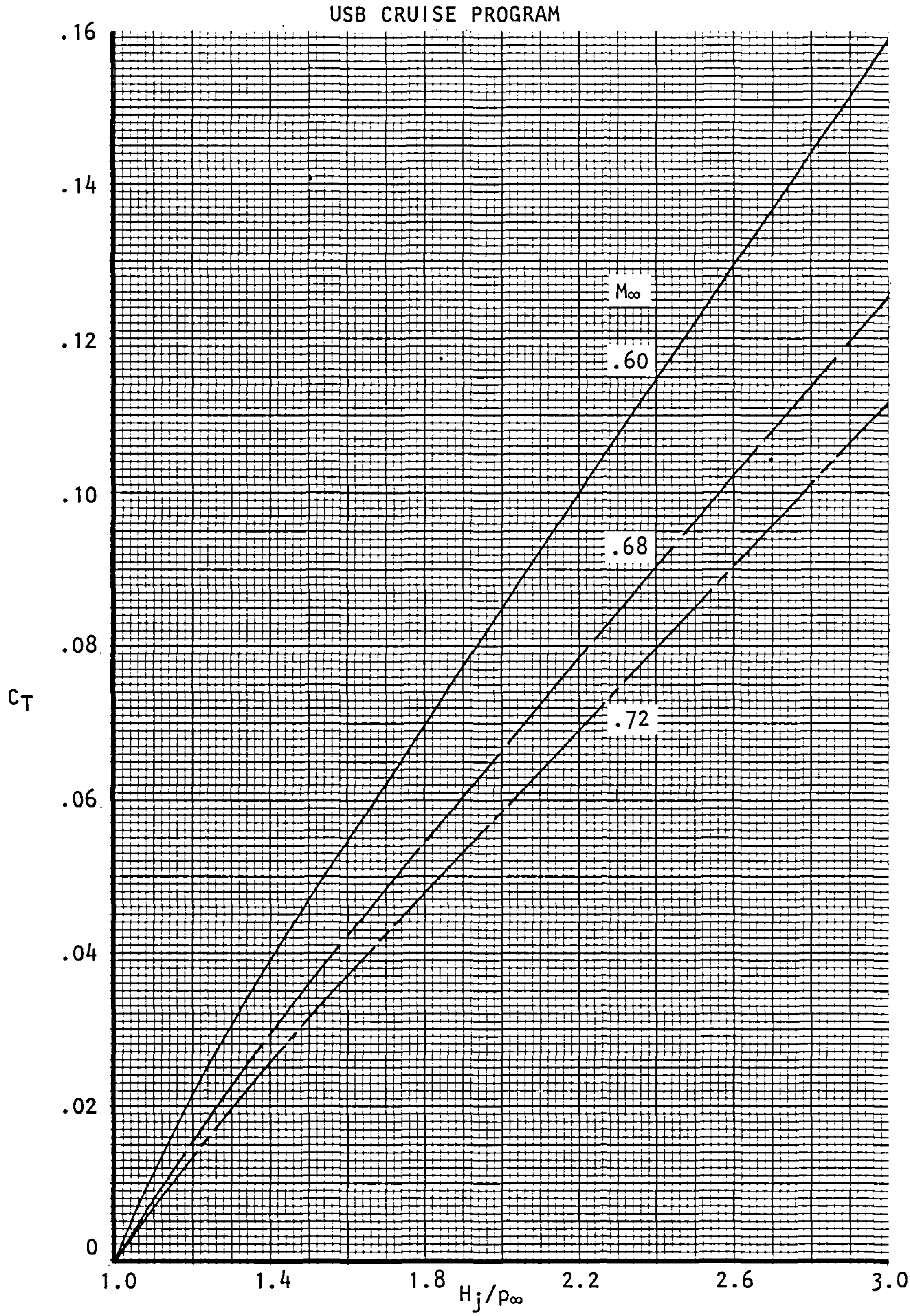

Figure 169 . Variation of nozzle gross thrust with Mach No. and pressure ratio, nozzle N_{4E}.

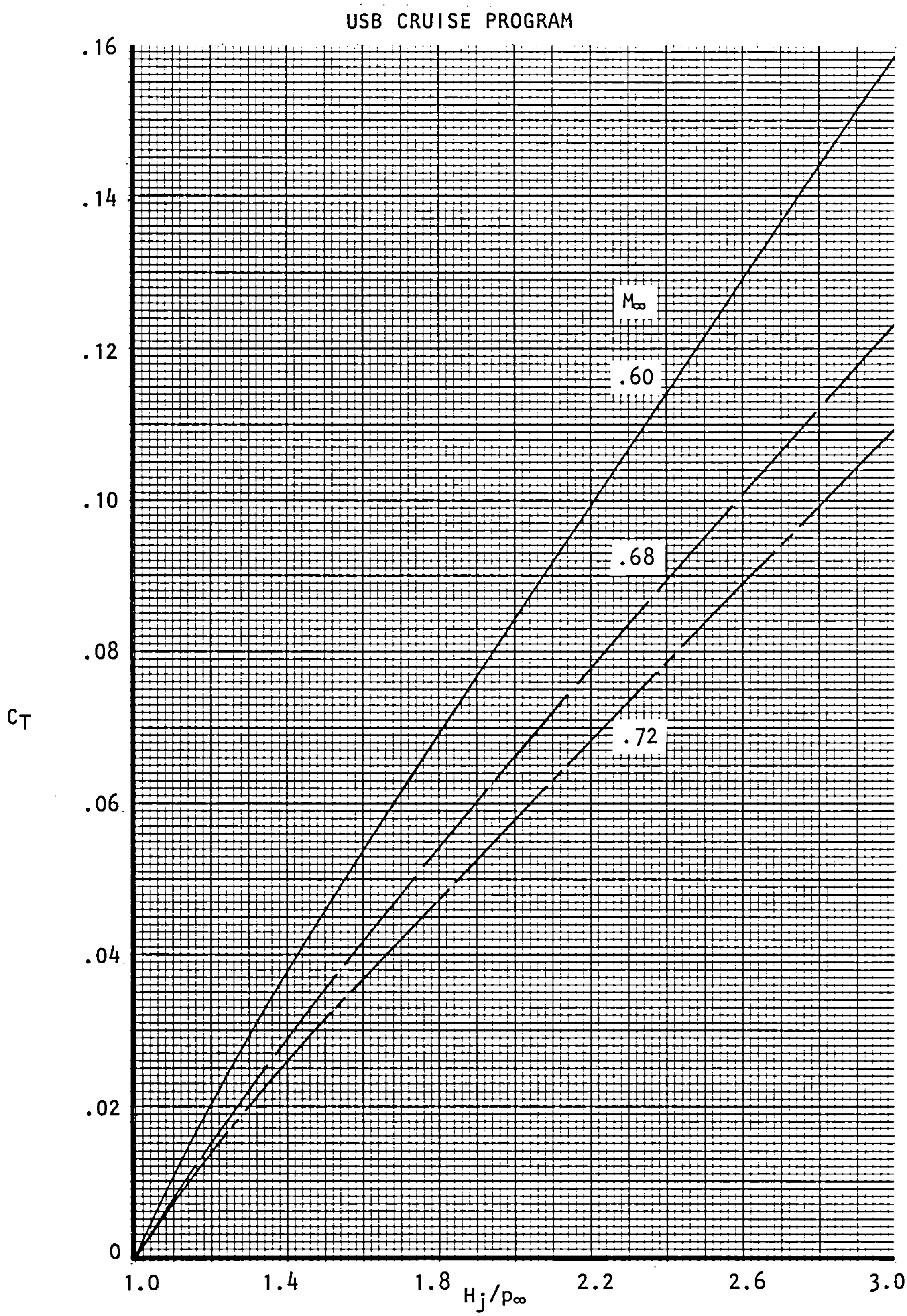

Figure 170. Variation of nozzle gross thrust with Mach No. and pressure ratio, nozzle N_2 (circular).

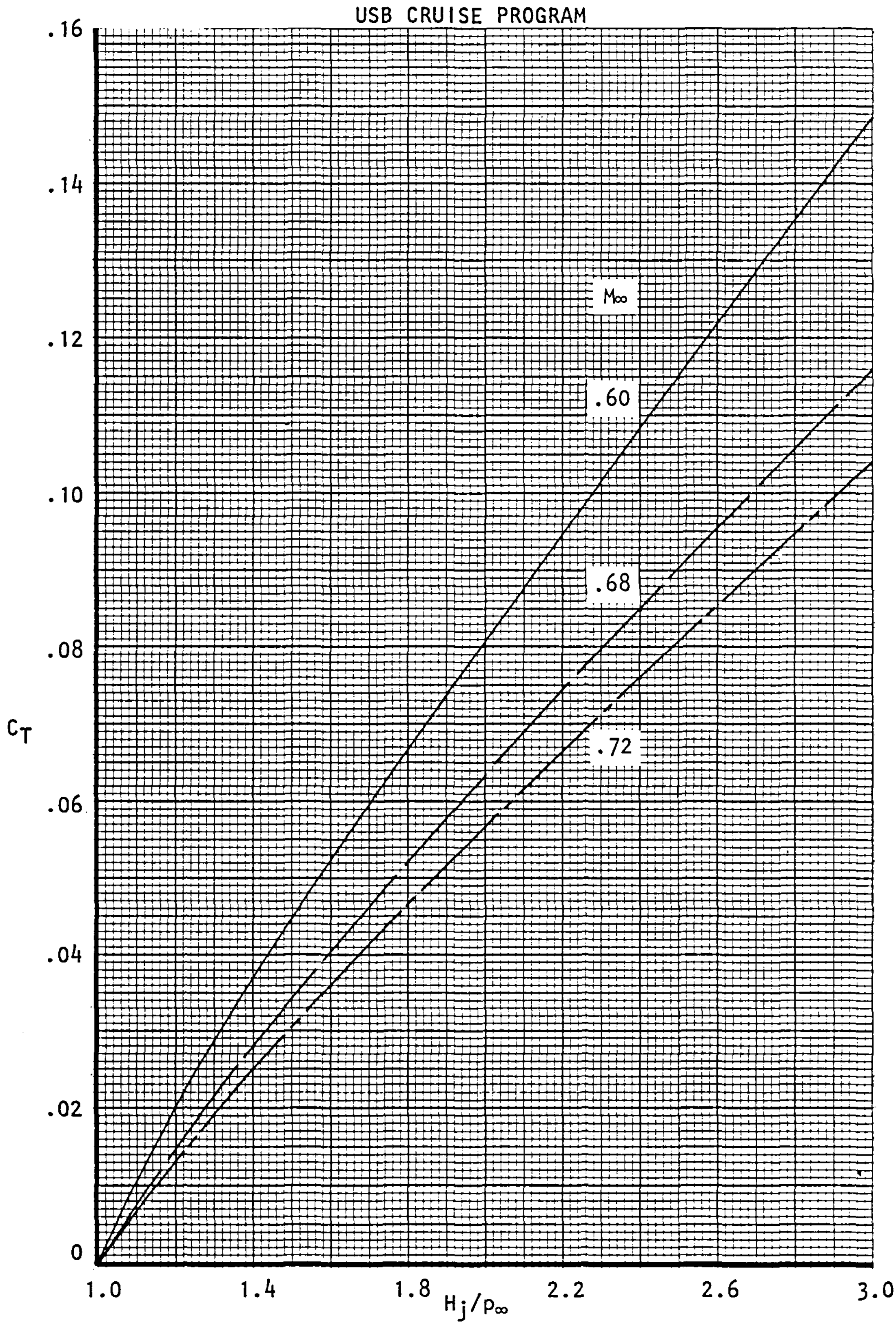

Figure 171 . Variation of nozzle gross thrust with Mach No. and pressure ratio, nozzle N_{3B}.

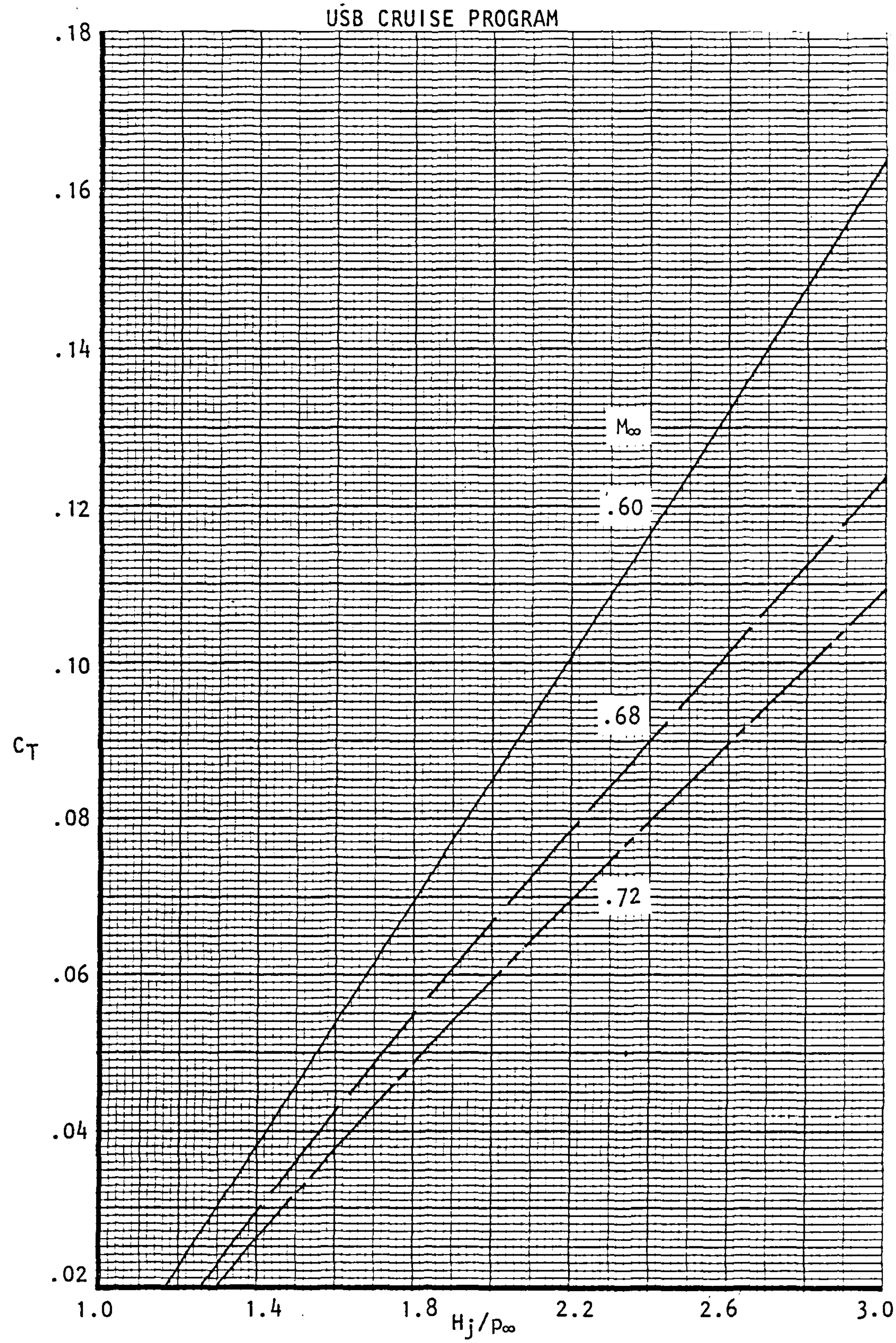

Figure 172 . Variation of nozzle gross thrust with Mach No. and pressure ratio, nozzle N_4.

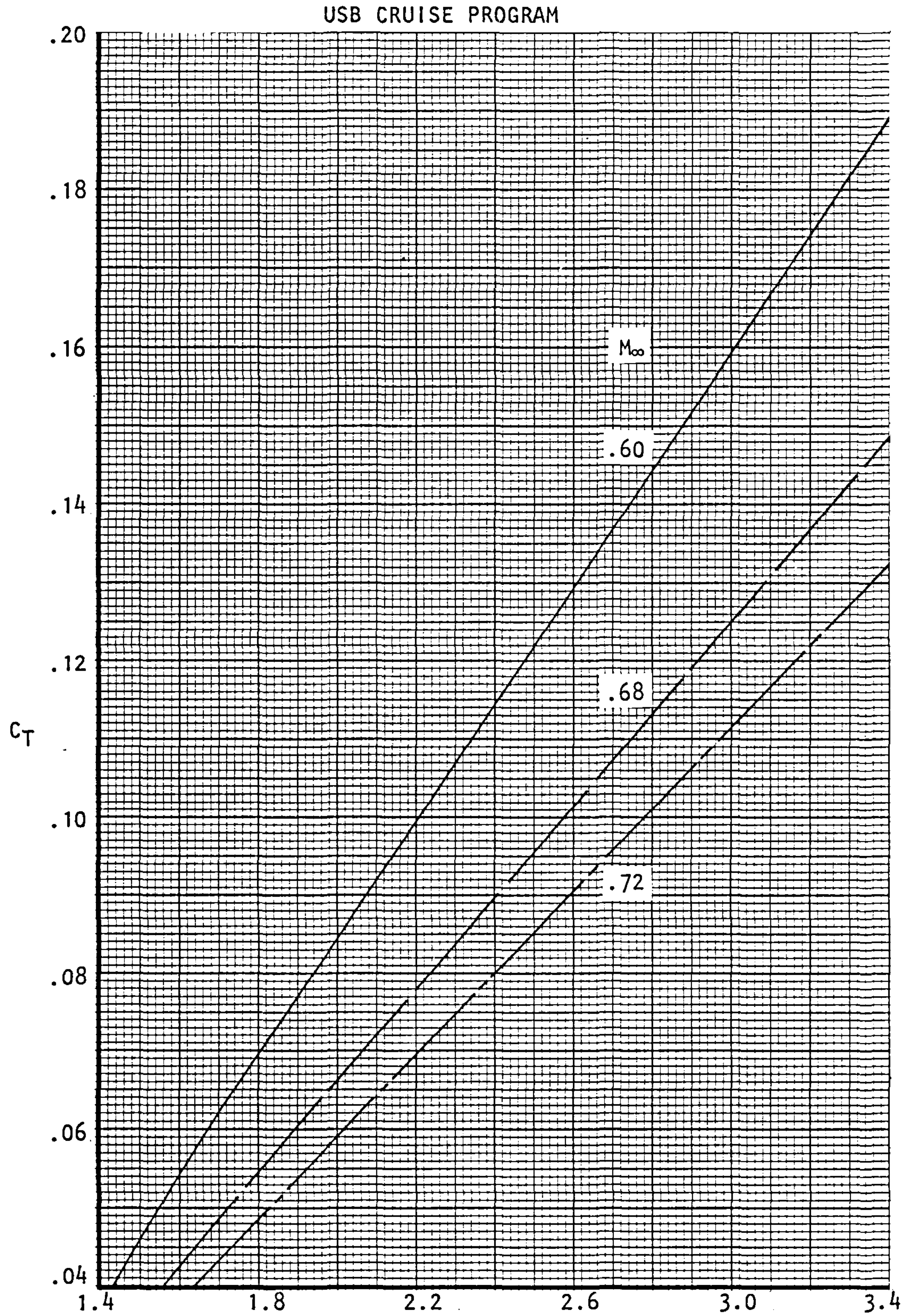

Figure 173 . Variation of nozzle gross thrust with Mach No. and pressure ratio, nozzle N_5.

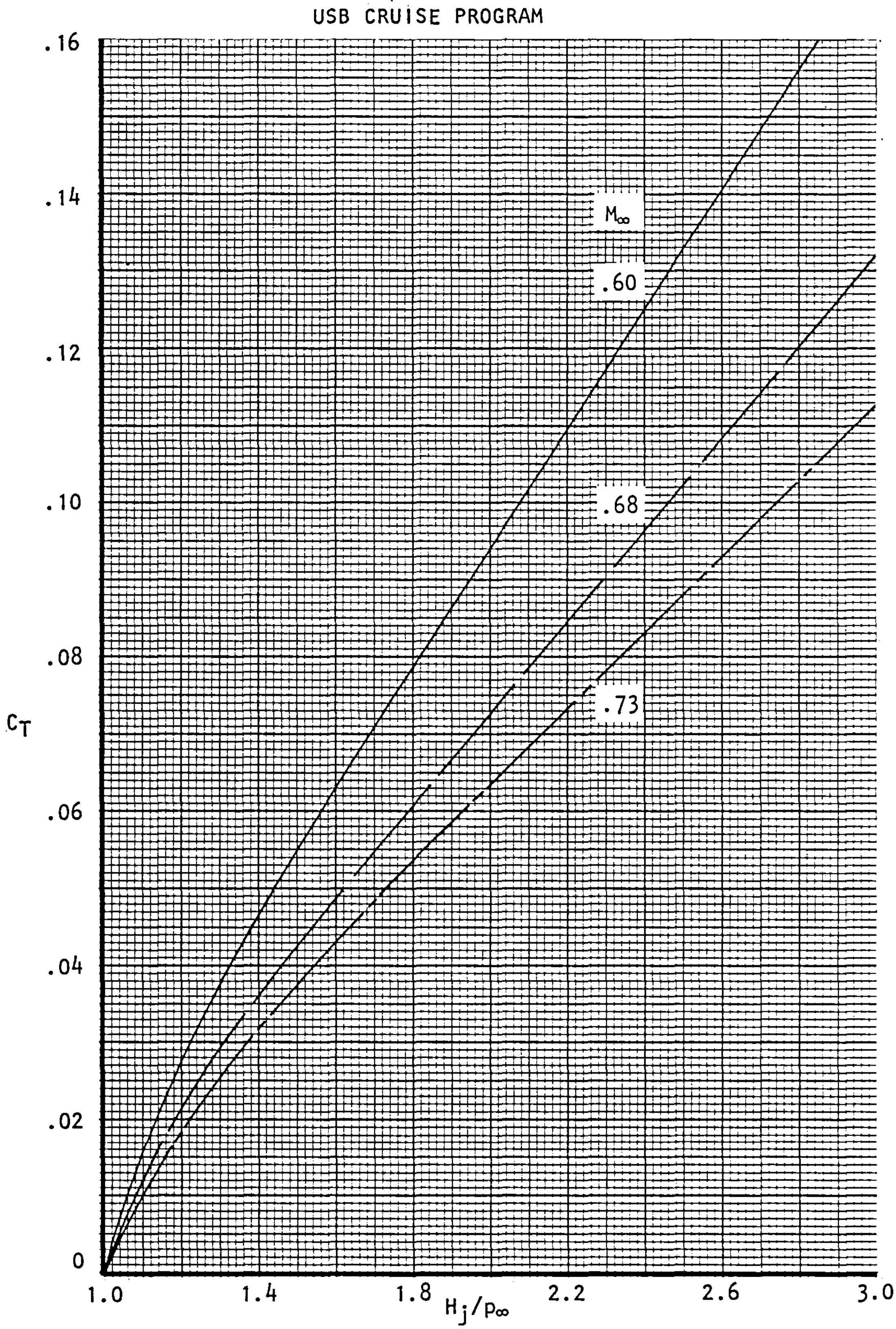

Figure 174. Variation of nozzle gross thrust with Mach No. and pressure ratio, nozzle $N_8^1 + N_8^2$.

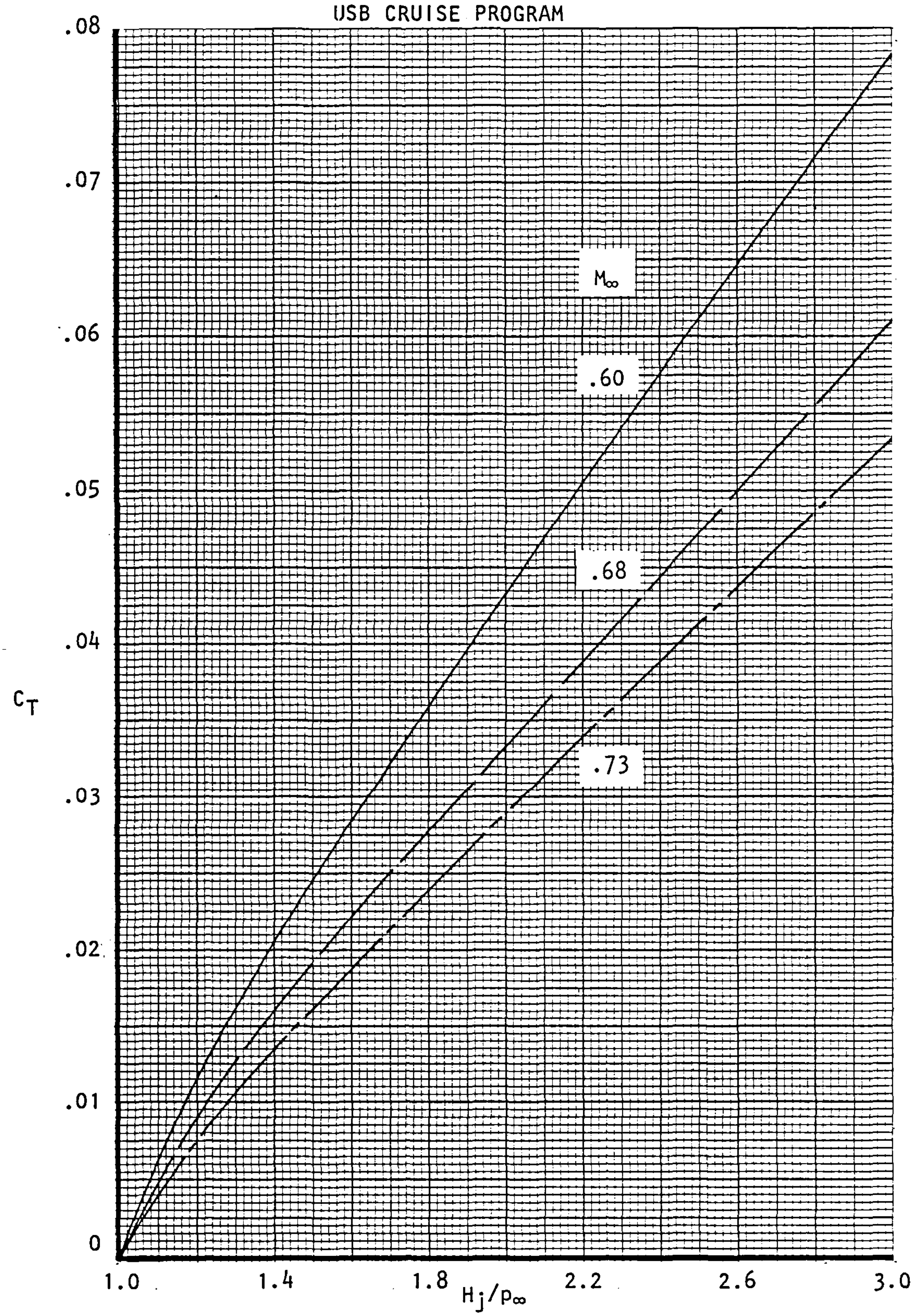

Figure 175 . Variation of nozzle gross thrust with Mach No. and pressure ratio, nozzle $N_8{}^2$.

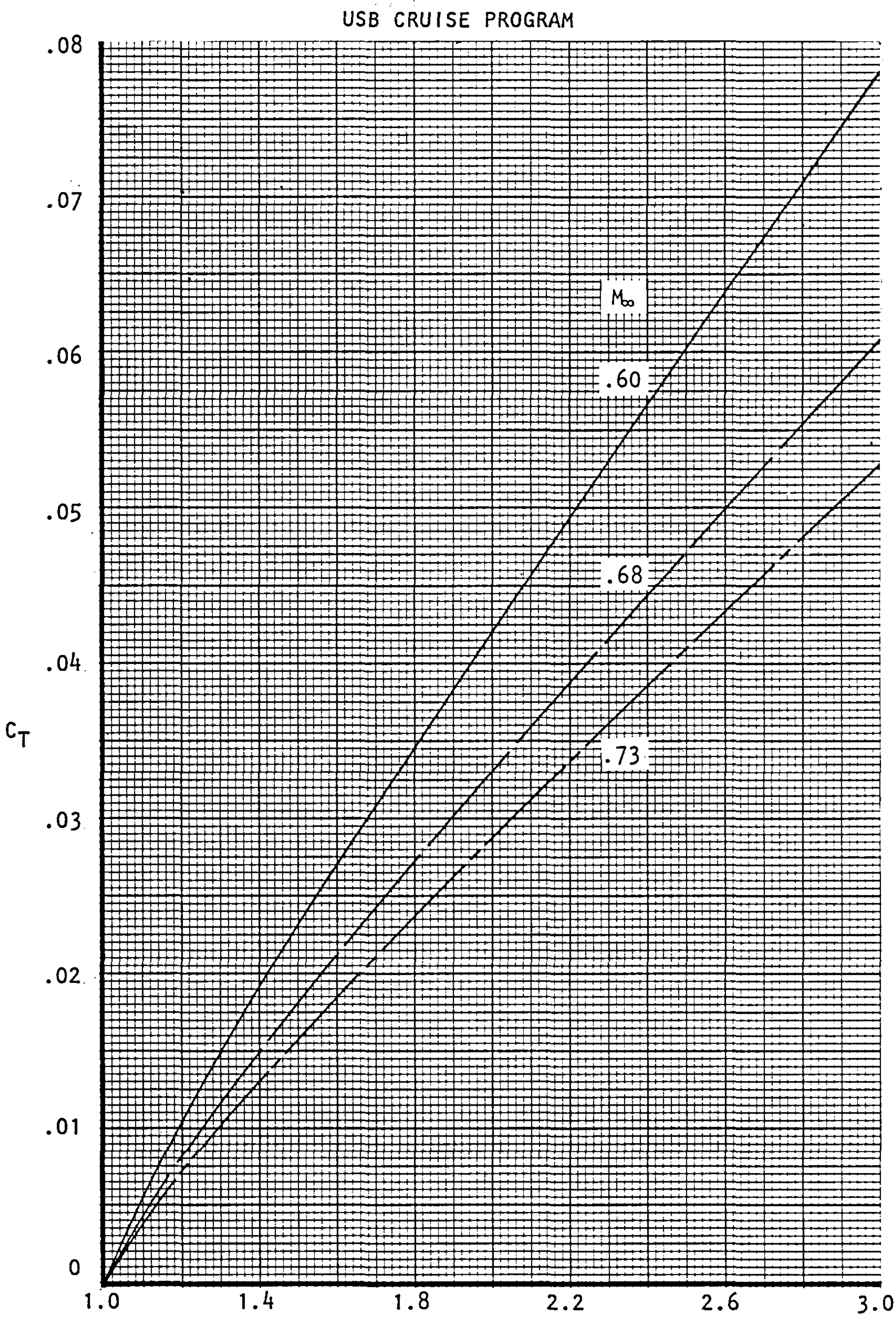

Figure 176 . Variation of nozzle gross thrust with Mach No. and pressure ratio, nozzle N_{11}.

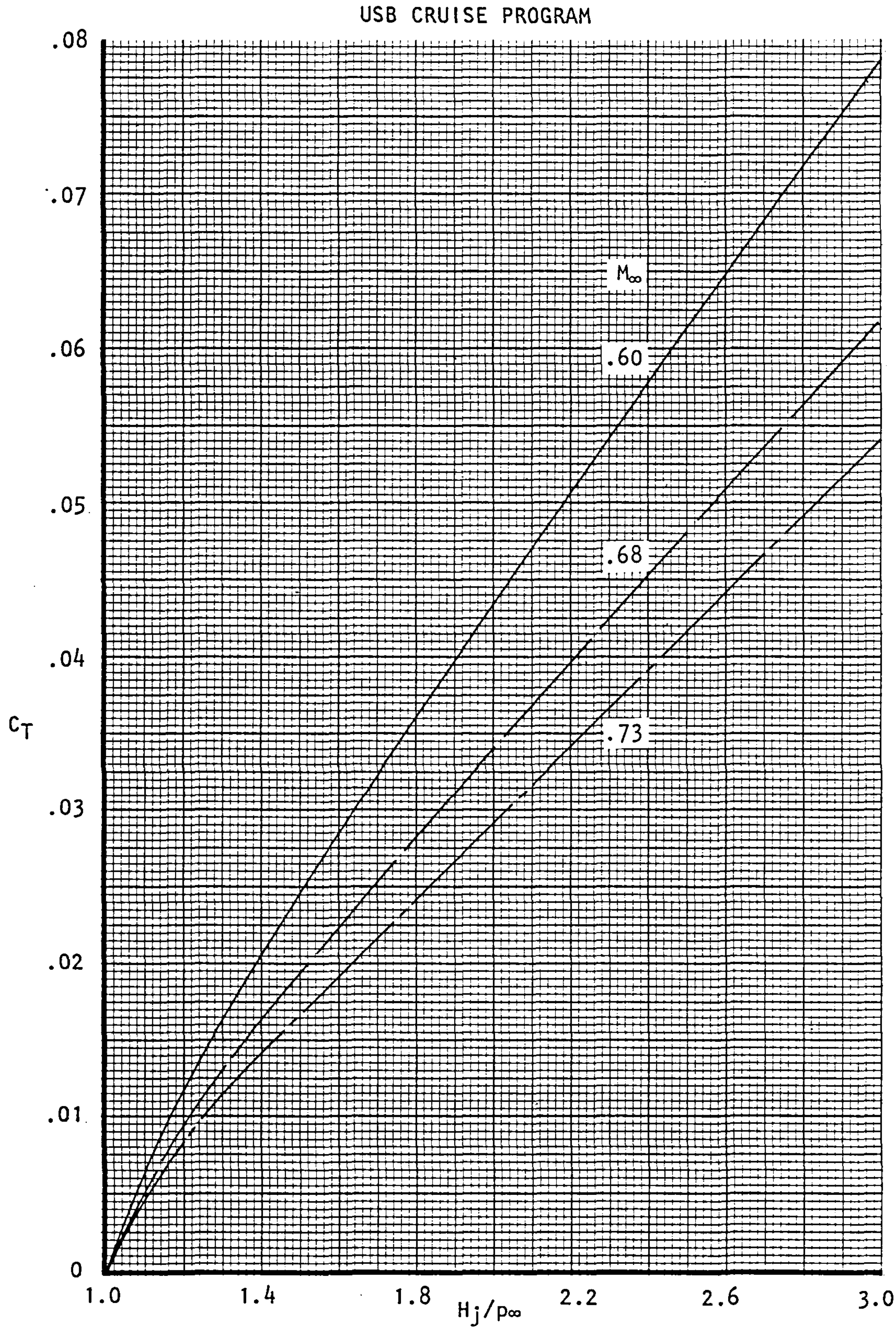

Figure 177 . Variation of nozzle gross thrust with Mach No. and pressure ratio, nozzle N_{12}.

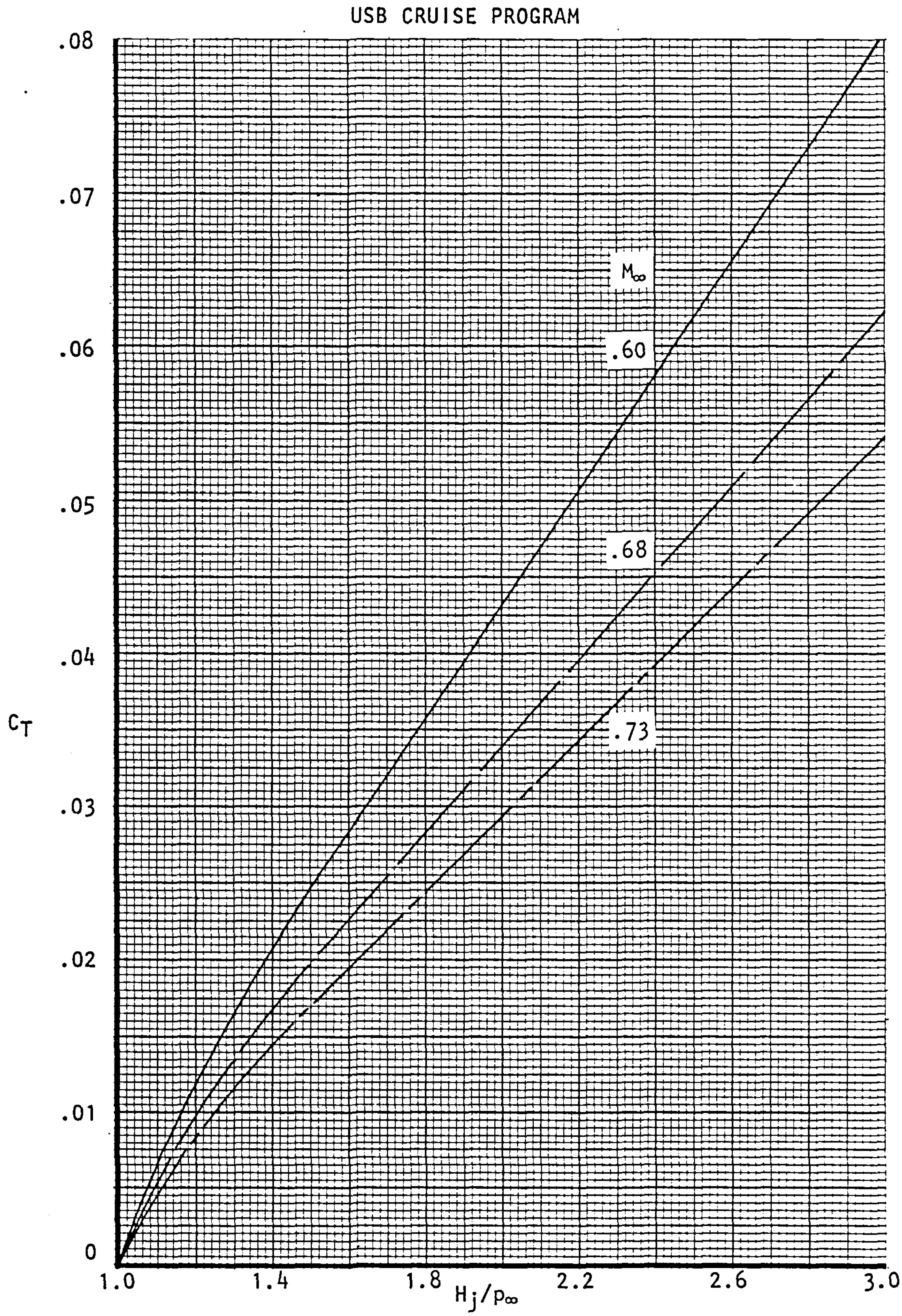

Figure 178 . Variation of nozzle gross thrust with Mach No. and pressure ratio, nozzle N_{13}.

8.0 OIL FLOW PHOTOGRAPHS

In order to visually understand the complex flow phenomena which occur on the surfaces of the nacelle-wing interference regions, oil flow photographs were taken of most of the test configurations after the completion of each configuration series. The more interesting examples of these photos are presented in Figures 179 through 190.

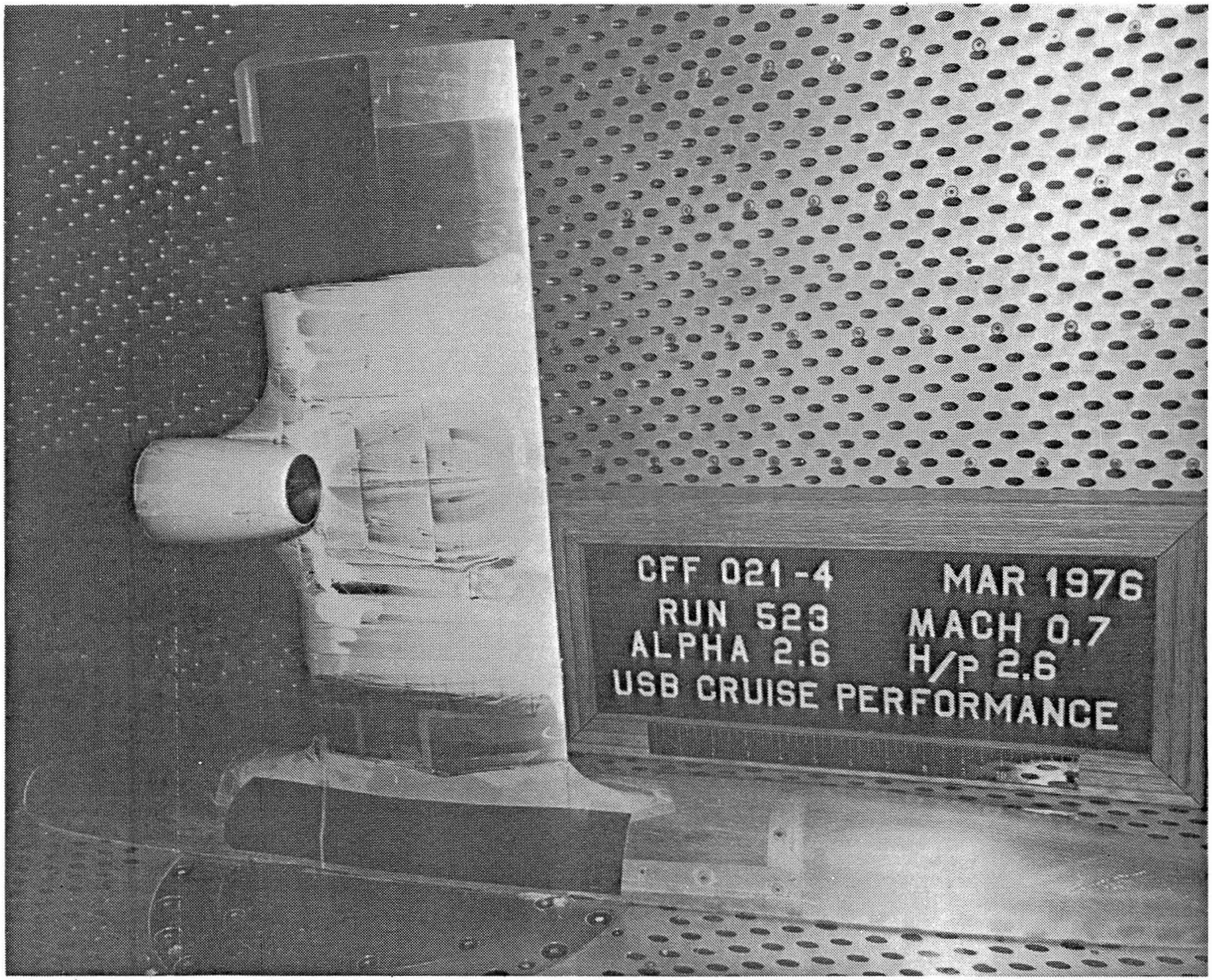

Figure 179. Oil flow pattern, nozzle N_{1E}, $M_\infty = 0.70$, $H_j/p_\infty = 2.6$, $\alpha = 2.6°$.

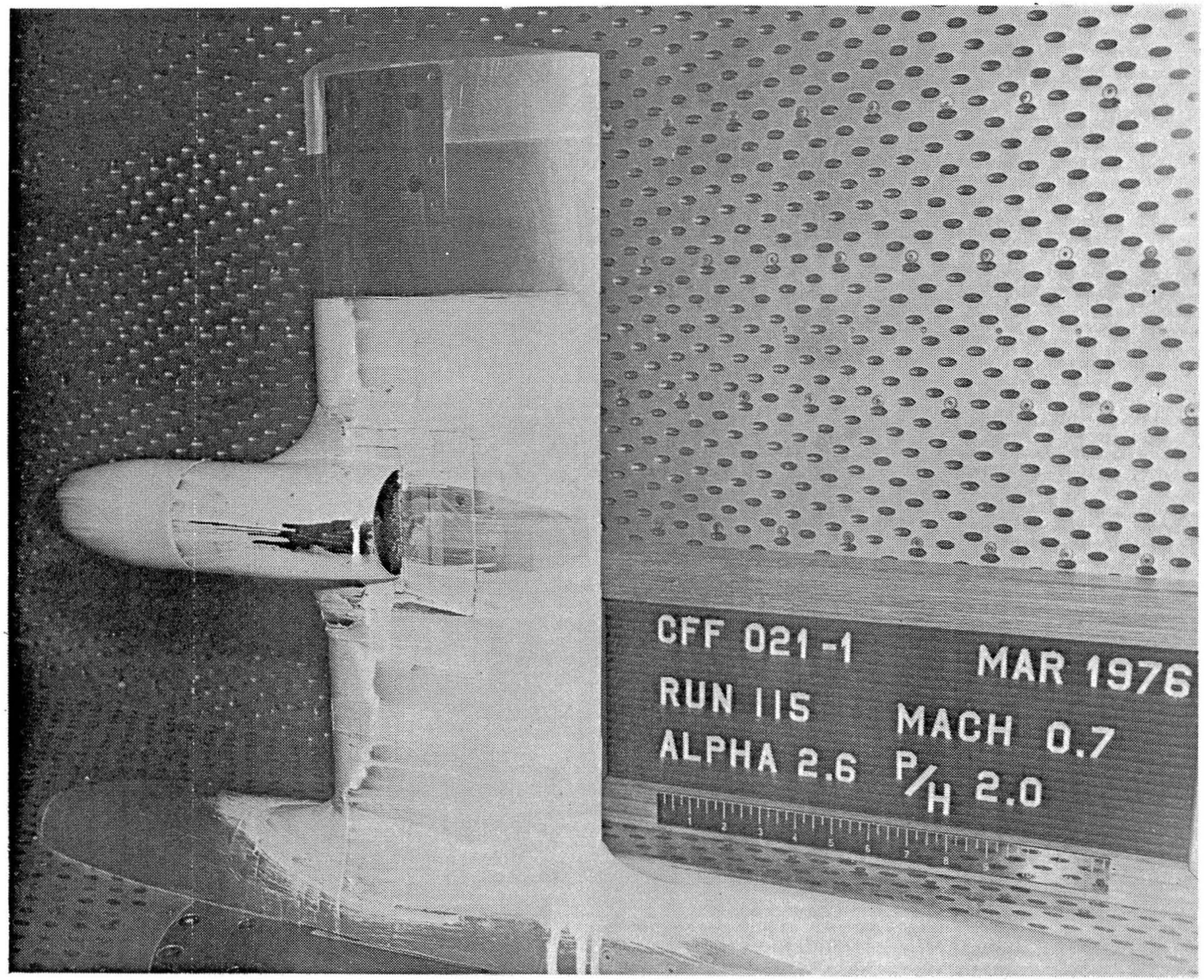

Figure 180. Oil flow pattern, nozzle N_{3E}, $M_\infty = 0.70$, $H_j/p_\infty \doteq 2.0$, $\alpha = 2.6°$.

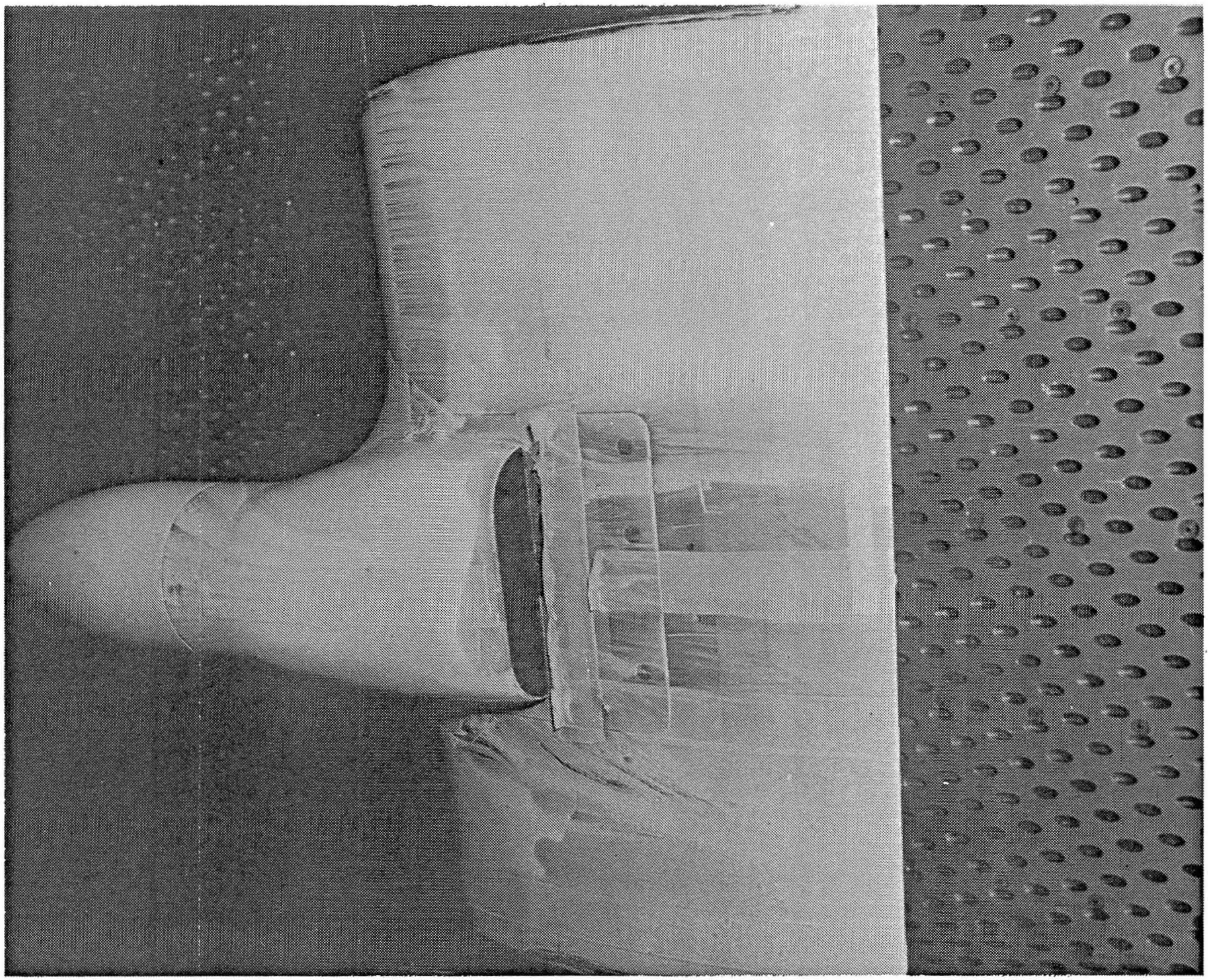

Figure 181. Oil flow pattern, nozzle N_{4E}, $M_\infty = 0.70$, $H_j/p_\infty = 2.6$, $\alpha = 2.6°$.

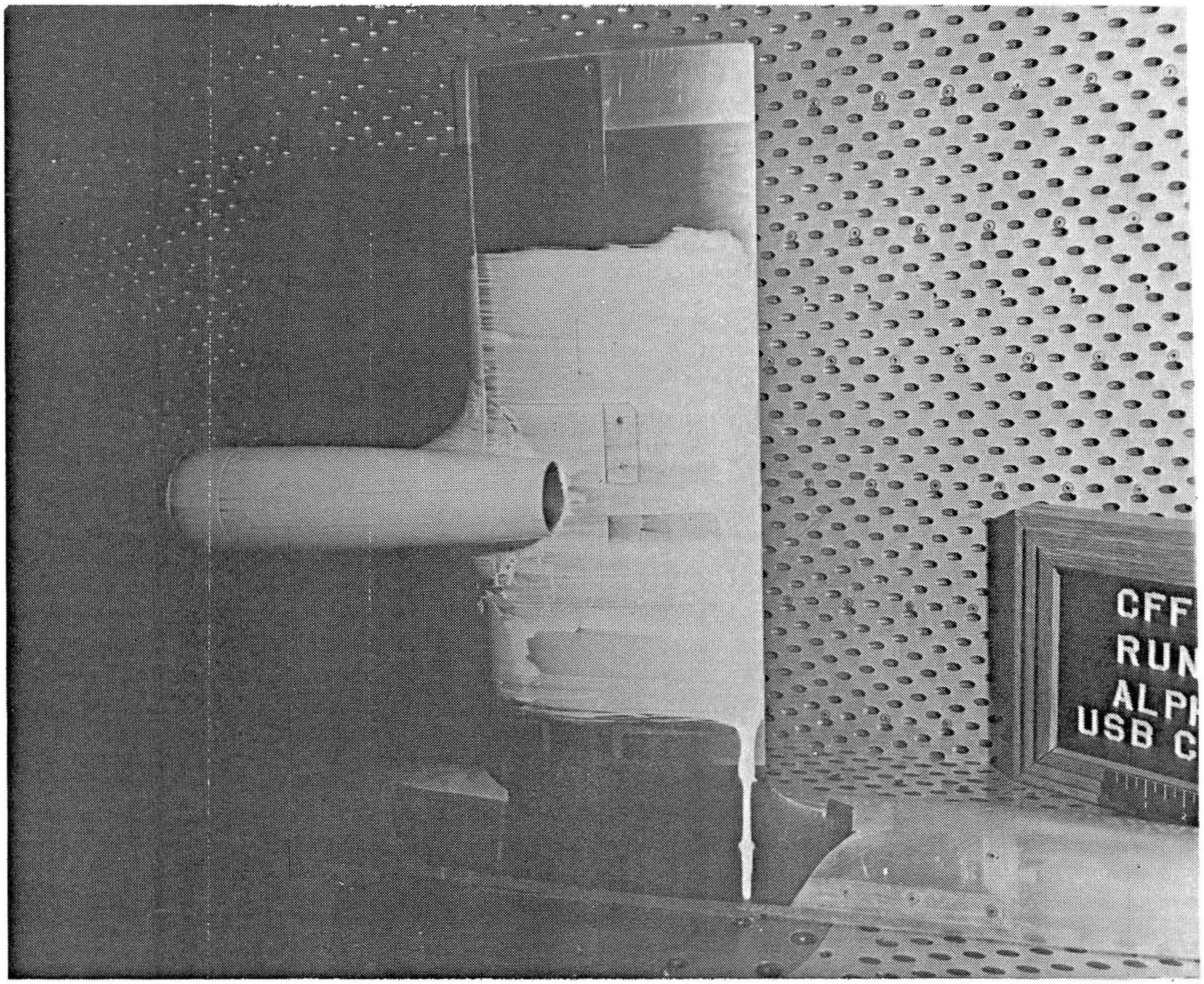

Figure 182. Oil flow pattern, nozzle N_2, $M_\infty = 0.68$, H_j/p_∞ = RPR, $\alpha = 3°$.

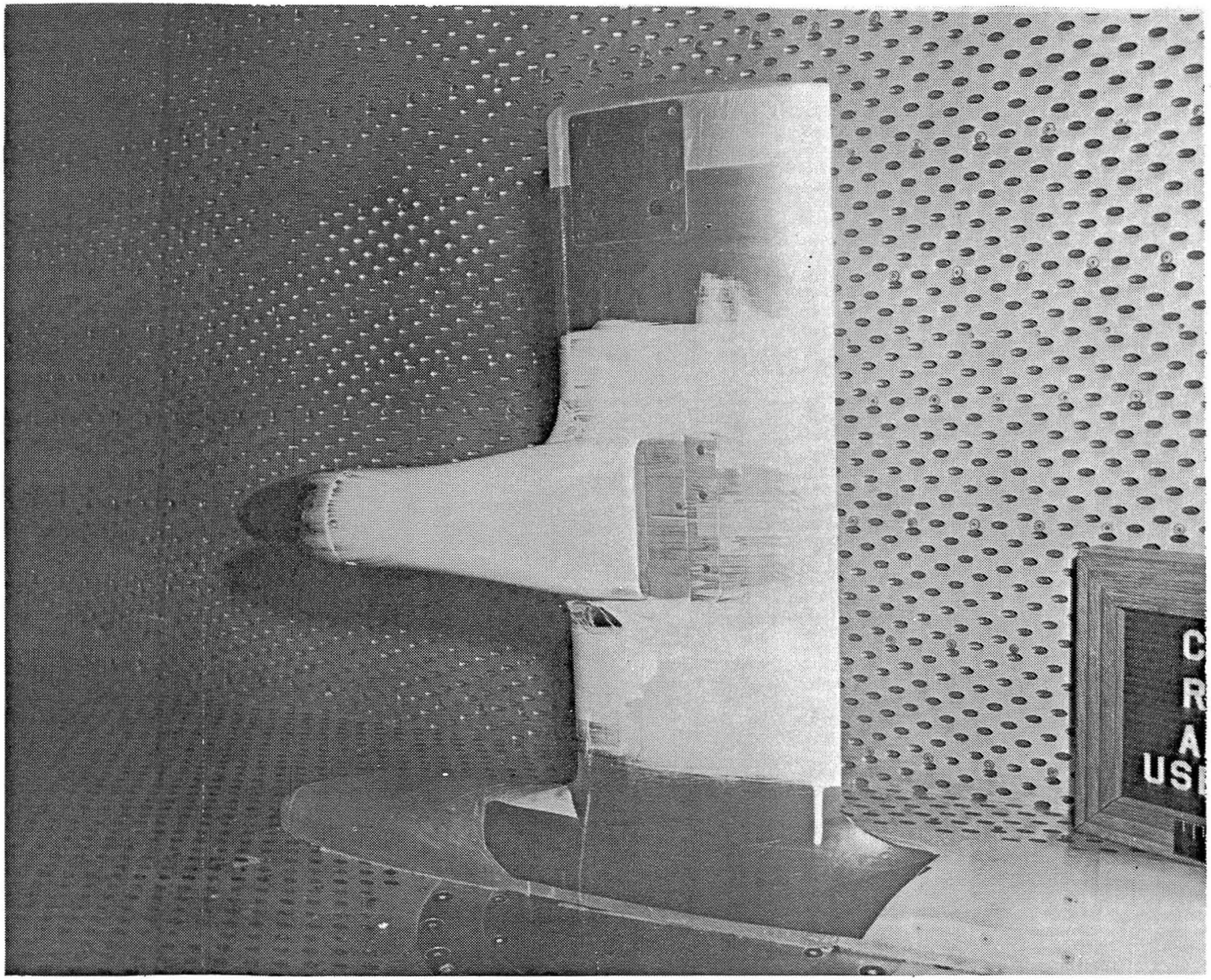

Figure 183. Oil flow pattern, nozzle N_5, $M_\infty = 0.70$, $H_j/p_\infty = 2.6$, $\alpha = 2.6°$.

Figure 184. Oil flow pattern, clean swept wing, $M_\infty = 0.75$, $\alpha = 3°$.

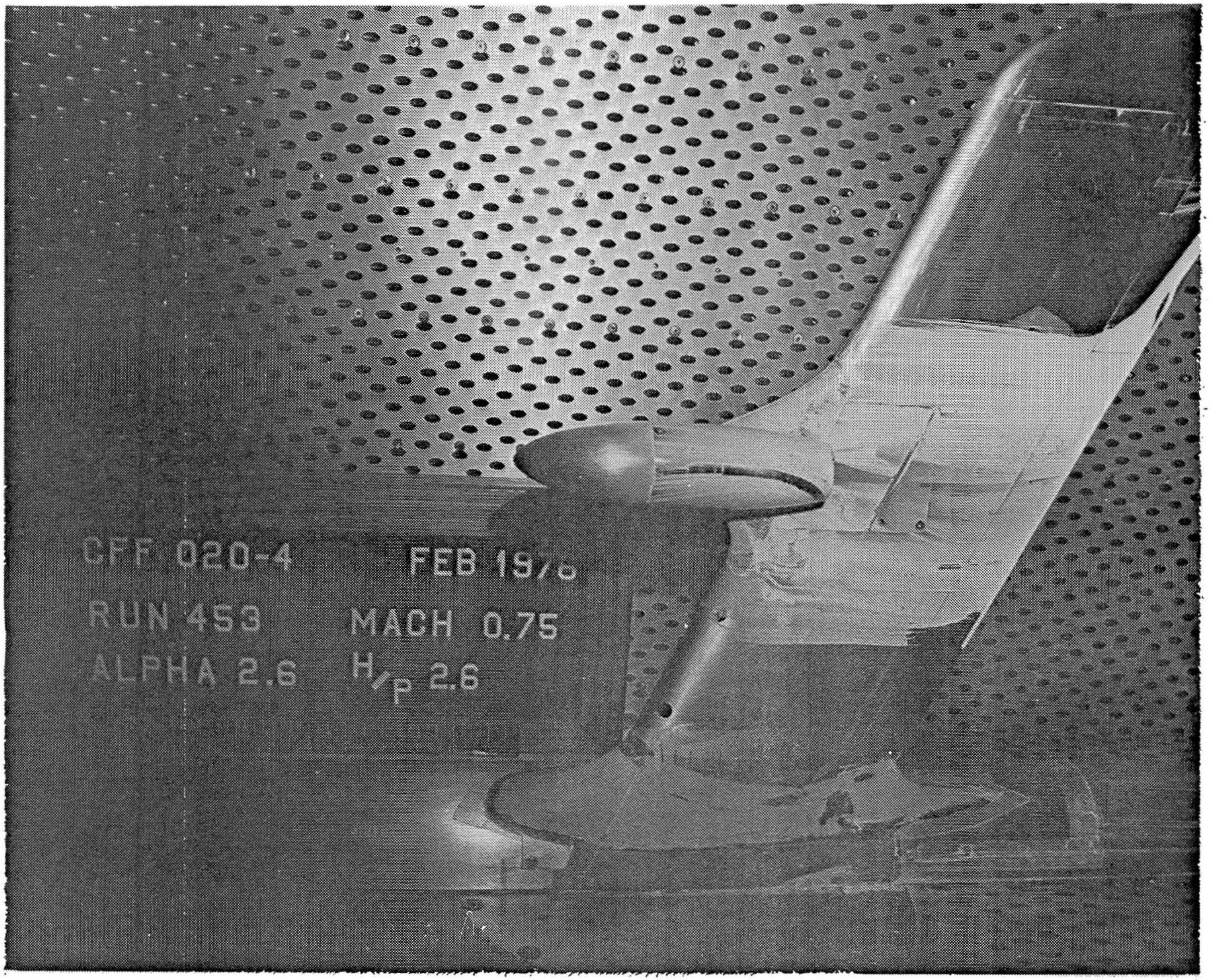

Figure 185. Oil flow pattern, nozzle N_{11}, $M_\infty = 0.75$, $H_j/p_\infty = 2.6$, $\alpha = 2.6°$.

Figure 186. Oil flow pattern, nozzle $N_8{}^1$, $M_\infty = 0.75$, $H_j/p_\infty = 2.6$, $\alpha = 2.6°$.

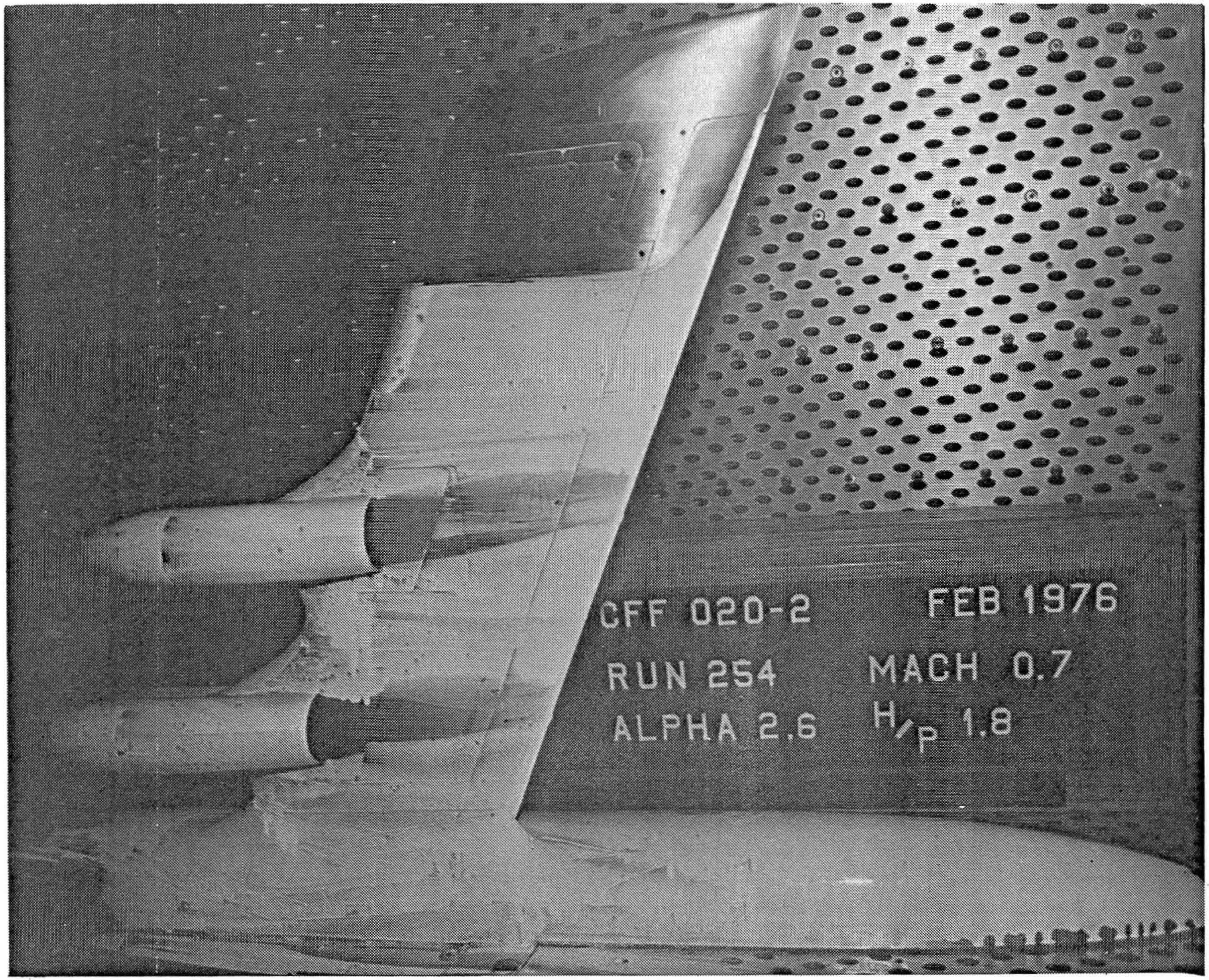

Figure 187. Oil flow pattern, nozzles N_8^1 & N_8^2, $M_\infty = 0.70$, $H_j/p_\infty = 1.8$, $\alpha = 2.6°$.

USB CRUISE PROGRAM

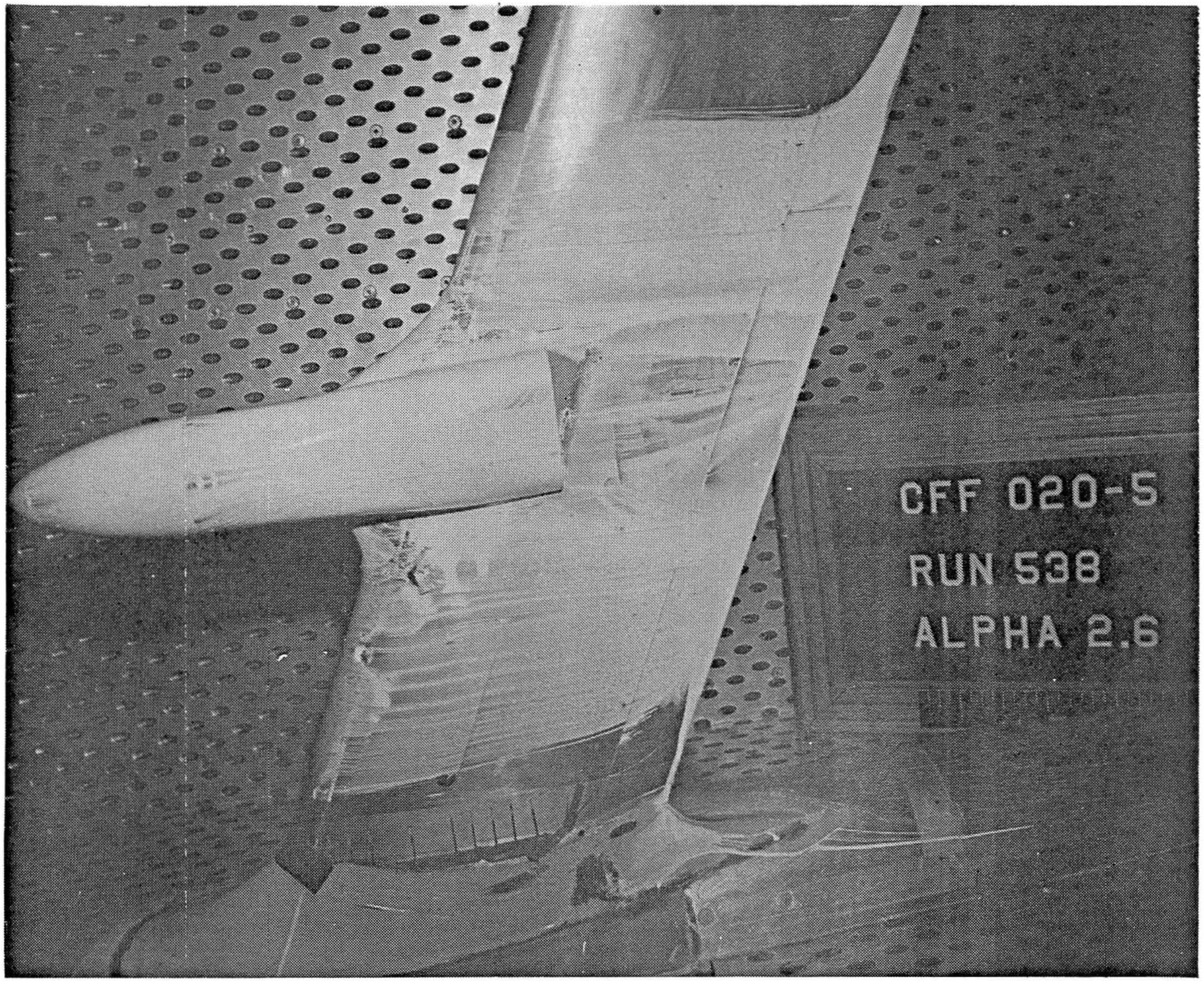

Figure 188. Oil flow pattern, nozzle N_{12}, $M_\infty = 0.75$, $H_j/p_\infty = 2.6$, $\alpha = 2.6°$.

Figure 189. Oil flow pattern, nozzle N_{13}, M_∞ = 0.75, H_j/p_∞ = 2.6, α = 2.6°.

Figure 190. Oil flow pattern, pylon mounted nacelle with nozzle N_2, $M_\infty = 0.75$, H_j/p_∞ = RPR, $\alpha = 2.6°$.

9.0 REFERENCES

1. Braden, J. A., Hancock, J. P., Burdges, K. P., and Hackett, J. E. "Exploratory Studies of the Cruise Performance of Upper Surface Blown Configuration, Experimental Program - Test Facilities, Model Design, Instrumentation and Low-Speed High-Lift Tests." NASA CR-3192, 1979.

3. Braden, J. A., Hancock, J. P., Burdges, K. P., and Hackett, J. E., "Exploratory Studies of the Cruise Performance of Upper Surface Blown Configuration, Program Analysis and Conclusions," NASA CR-159136, 1979.

1. Report No.	2. Government Accession No.	3. Recipient's Catalog No.
CR-159134		

4. Title and Subtitle	5. Report Date
EXPLORATCRY STUDIES OF THE CRUISE PERFORMANCE OF UPPER-SURFACE BLOWN CONFIGURATIONS — Experimental Program — High-Speed Force Tests	October 1979
	6. Performing Organization Code
7. Author(s)	8. Performing Organization Report No.
J. A. Braden, J. P. Hancock, J. E. Hackett, V. Lyman	LG77ER0028
	10. Work Unit No.
9. Performing Organization Name and Address	
Lockheed-Georgia Company 86 South Cobb Drive Marietta, Georgia 30063	11. Contract or Grant No. NAS1-13871
	13. Type of Report and Period Covered
12. Sponsoring Agency Name and Address	Contractor Report
National Aeronautics and Space Administration Langley Research Center Hampton, Virginia 23665	14. Sponsoring Agency Code

15. Supplementary Notes

Part of a Series of Reports Covering Various Phases of the USB Program:
CR-3193, CR-3192, CR-159134, CR-159135, CR-159136

16. Abstract

The present report provides basic force data obtained from an experimental/analytical study of upper-surface blown (USB) configurations at cruise. The high-speed (subsonic) experimental work, studying the aerodynamic effects of wing-nacelle geometric variations, was conducted around semi-span model configurations composed of diversified, interchangeable components. Power simulation was provided by high-pressure air ducted through closed forebody nacelles. Nozzle geometry was varied across size, exit aspect ratio, exit position and boattail angle. Both 3-D force and 2-D pressure measurements were obtained at cruise Mach numbers from 0.5 to 0.8 and at nozzle pressure ratios up to about 3.0. The experimental investigation was supported by an analytical synthesis of the system using a vortex lattice representation with first-order power effects. Results are also presented from a compatibility study in which a short-haul transport is designed on the basis of the aerodynamic findings in the experimental study as well as acoustical data obtained in a concurrent program. High-lift test data are used to substantiate the projected performance of the selected transport design.

17. Key Words (Suggested by Author(s))	18. Distribution Statement
Subsonic cruise performance Propulsion integration High-lift Transport design	Unclassified - Unlimited

19. Security Classif. (of this report)	20. Security Classif. (of this page)	21. No. of Pages	22. Price*
UNCLASSIFIED	UNCLASSIFIED	212	

*For sale by the National Technical Information Service, Springfield, Virginia 22161